



EMANUEL AMORER HERNÁNDEZ

**ESPECTROSCOPIA DE REFLETÂNCIA E EMISSIVIDADE DE ROCHAS
FOSFÁTICAS ÍGNEAS E SEDIMENTARES DO CENTRO-OESTE DO BRASIL:
ESTUDOS DE CASO NOS DEPÓSITOS DE CATALÃO I (GO), TAPIRA (MG),
ROCINHA E LAGAMAR (MG)**

***REFLECTANCE AND EMISSIVITY SPECTROSCOPY OF IGNEOUS AND
SEDIMENTARY PHOSPHATE ROCKS FROM MIDWESTERN BRAZIL: CASE
STUDY OF THE CATALÃO I (GO), TAPIRA (MG), ROCINHA E LAGAMAR (MG)
DEPOSITS***

CAMPINAS

2013



NÚMERO: 469/2013

UNIVERSIDADE ESTADUAL DE CAMPINAS
INSTITUTO DE GEOCIÊNCIAS

EMANUEL AMORER HERNÁNDEZ

ESPECTROSCOPIA DE REFLETÂNCIA E EMISSIVIDADE DE ROCHAS
FOSFÁTICAS ÍGNEAS E SEDIMENTARES DO CENTRO-OESTE DO BRASIL:
ESTUDOS DE CASO NOS DEPÓSITOS DE CATALÃO I (GO), TAPIRA (MG),
ROCINHA E LAGAMAR (MG)

*REFLECTANCE AND EMISSIVITY SPECTROSCOPY OF IGNEOUS AND
SEDIMENTARY PHOSPHATE ROCKS FROM MIDWESTERN BRAZIL: CASE STUDY
OF THE CATALÃO I (GO), TAPIRA (MG), ROCINHA E LAGAMAR (MG) DEPOSITS*

ORIENTADOR: PROF. DR. CARLOS ROBERTO DE SOUZA FILHO

MASTERS DISSERTATION PRESENTED TO THE INSTITUTE OF GEOSCIENCES OF
THE UNIVERSITY OF CAMPINAS TO OBTAIN MASTERS DEGREE IN
GEOCIENCES AREA GEOLOGY AND NATURAL RESOURCES

*DISSERTAÇÃO DE MESTRADO APRESENTADA AO INSTITUTO DE GEOCIÊNCIAS
DA UNICAMP PARA OBTENÇÃO DO TÍTULO DE MESTRE EM GEOCIÊNCIAS NA
ÁREA DE GEOLOGIA E RECURSOS NATURAIS*

ESTE EXEMPLAR CORRESPONDE À VERSÃO FINAL DA TESE
DEFENDIDA PELO ALUNO EMANUEL AMORER HERNÁNDEZ E
ORIENTADO PELO PROF. DR. CARLOS ROBERTO DE SOUZA
FILHO

CAMPINAS

2013

Ficha catalográfica
Universidade Estadual de Campinas
Biblioteca do Instituto de Geociências
Cássia Raquel da Silva - CRB 8/5752

Am68r Amorer Hernández, Emanuel, 1981-
Reflectance and emissivity spectroscopy of igneous and sedimentary rocks from Midwest Brazil : case study of the Catalão I (GO), Tapira (MG), Rocinha and Lagamar deposits / Emanuel Amorer Hernández. – Campinas, SP : [s.n.], 2013.

Orientador: Carlos Roberto de Souza Filho.
Dissertação (mestrado) – Universidade Estadual de Campinas, Instituto de Geociências.

1. Fosfatos. 2. Sensoriamento remoto. 3. Refletância. 4. Emissividade. I. Souza Filho, Carlos Roberto de, 1965-. II. Universidade Estadual de Campinas. Instituto de Geociências. III. Título.

Informações para Biblioteca Digital

Título em outro idioma: Espectroscopia de refletância e emissividade de rochas fosfáticas ígneas e sedimentares do centro-oeste do Brasil : estudos de caso nos depósitos de Catalão I (GO), Tapira (MG), Rocinha e Lagamar (MG)

Palavras-chave em inglês:

Phosphates

Remote sensing

Reflectance

Emissivity

Área de concentração: Geologia e Recursos Naturais

Titulação: Mestre em Geociências

Banca examinadora:

Carlos Roberto de Souza Filho [Orientador]

Lena Virginia Soares Monteiro

Lênio Soares Galvão

Data de defesa: 05-07-2013

Programa de Pós-Graduação: Geociências



UNICAMP

**UNIVERSIDADE ESTADUAL DE CAMPINAS
INSTITUTO DE GEOCIÊNCIAS
PÓS-GRADUAÇÃO EM GEOCIÊNCIAS NA
ÁREA DE GEOLOGIA E RECURSOS NATURAIS**

AUTOR: Emanuel Amorer Hernández

"Espectroscopia de Refletância e Emissividade de Rochas Fosfáticas Ígneas e Sedimentares do Centro-Oeste do Brasil: Estudos de Caso nos Depósitos de Catalão I (GO), Tapira (MG), Rocinha e Lagamar (MG)."

ORIENTADOR: Prof. Dr. Carlos Roberto de Souza Filho

Aprovado em: 05/ 07 / 2013

EXAMINADORES:

Prof. Dr. Carlos Roberto de Souza Filho

_____ - Presidente

Profa. Dra. Lena Virginia Soares Monteiro

Prof. Dr. Lênio Soares Galvão

Campinas, 05 de julho de 2013

Dedicat3ria

A Tabata, por todo lo bueno que he vivido contigo,
y todas las cosas maravillosas que est1n por venir para nosotros.
A todas aquellas personas que decidieron hacer vida fuera de sus pa3ses de nacimiento,
mi respeto y gratitud.
A la vida, que me ha dado tanto...

“Cambia lo superficial / cambia cambia lo profundo / cambia el modo de pensar / cambia todo
en este mundo / Cambia el clima con los a3os / cambia el pastor su reba3o / y as3 como todo
cambia / que yo cambie no es extra3o /...

Pero no cambia mi amor / por mas lejos que me encuentre / ni el recuerdo ni el dolor / de mi
patria y de mi gente/ Lo que no cambi3 ayer/ tendr1 que cambiar ma3ana/ as3 como cambio yo/
en estas tierras lejanas...”

Mercedes Sosa, *Todo cambia*

Agradecimentos

Neste momento, quando sinto-me obrigado a olhar o caminho andado, não posso mas que dizer obrigado a todas as pessoas e eventos que tem modelado minha vida. Incluir todas as histórias que chegaram até mim de personagens maravilhosos que tem passado na minha vida, precisaria de um tomo especial, que se Deus quiser, será editado em quatro línguas, para demonstrar ao mundo que as pessoas de bem são maioria.

Nestes agradecimentos que tem que ser muito mais restritos pelo espaço, quero agradecer primeiramente a meu orientador, Prof. Carlos Roberto de Souza Filho pela oportunidade, disponibilidade e paciência durante o percurso deste mestrado. Ainda faltam muitas conversas que além da geologia e o sensoriamento remoto, incluirão vinhos, gastronomia, política e lendas geológicas...

Quero agradecer ainda aos professores da UNICAMP e da USP que compartilharam comigo seus conhecimentos. Aos professores Lena Monteiro, Emilson Leite (muito obrigado pelas valiosas correções na qualificação), Elson Oliveira, Álvaro Crósta, Rómulo Angélica (UFPA), Wanilson Silva, Roberto Xavier, Jacinta Enzweiler, Teodoro Almeida, Francisco Ferreira (UFPR), Excelso Ruberti e com grande estima aos professores Silvio Roberto Farias Vlach e Piero Comin-Chiaramonti pelo grande aprendizado acadêmico e de vida que os senhores têm me proporcionado.

A ciência é feita de pessoas, e com certeza as coisas funcionam muito melhor quando as pessoas colaboram entre si. Eu quero agradecer aos geólogos Joyce da Cruz, Carlos Peters, Bruno Milanezzi e Aldo Ferrari do Grupo Anglo American-Catalão pela grande colaboração e discussões geológicas durante esta pesquisa. Agradeço também ao Geólogo Thiago da Silva da VALE Fertilizantes-Unidade Tapira, Geraldo Magella de VALE Fertilizantes-Unidade Patos de Minas e aos Srs. Roberto Pedrosi e Almir Pereira de Souza “Miro”, do Grupo Galvani- Unidade Lagamar, pelo grande apoio durante as campanhas de campo. Cumpre destacar também o apoio incondicional proporcionado ao projeto pela CPRM, na pessoa da Geóloga Maisa Abram.

Meu mais sincero agradecimento aos funcionários encarregados de nos levar no ar para que nós Pós-graduandos consigamos focar nas nossas pesquisas: Valdirene Pinotti, Gorete Bernardelli e o pessoal da Secretaria de Pós-graduação do IG-UNICAMP, Sra. Edinalva e Sr. Guerreiro do SIOM, Lúcia Carvalho e Aparecida Vendemiatto do Laboratório de Geoquímica do IG-UNICAMP pela paciência e parceria. Dailto Silva pela ajuda durante as DRX.

Graças a Deus eu consegui amizades muito valiosas neste tempo de pesquisa: Ethianne Agnoletto, Rebecca Scafutto, Alice Bosco, Mariana Velcic, Rosa Correa, Lucíola Magalhães, Carol Stolfi, Helena Malásquez, Danilo Barbuena, José Henrique Matos, Paulo Locatelli, Eric Gonçalves, Adelsom Soares, Sam Murphy, Juliano Senna, Renan Leonel, Brunão e muitos outros!

Agradeço ao CNPq pela concessão da bolsa de estudos.

E por último lugar mas nunca deixando nesse ordem, eu quero agradecer e dedicar tudo o bom mérito que esta dissertação gere para a energia final que me trouxe até aqui... a Entropia que desbalanceou meu universo e me faz ser uma melhor pessoa. As 34.361 palavras nesta tese são poucas para dizer quanto te amo e quanto dou graças á vida de ter você do meu lado, Te amo Tabata.

Súmula Curricular

Emanuel Amorér Hernández

É Engenheiro Geólogo (2007) formado pela Universidad de Los Andes (Mérida, Venezuela). Trabalhou, no começo da carreira, entre 2007 e 2010, como Engenheiro de Minas em depósitos de feldspato sódico e *ball-clays* para a indústria cerâmica na Venezuela. Desde 2011, é aluno de pós-graduação na Universidade Estadual de Campinas.

Durante o período de mestrado publicou trabalhos nos principais eventos nacionais na área de Geociências e Sensoriamento Remoto (46º. Congresso Geológico Brasileiro e XV Simpósio Brasileiro de Sensoriamento Remoto). Desenvolveu seu projeto de Mestrado com bolsa do CNPq.

Tem como interesse científico a avaliação e quantificação de recursos minerais com base no uso de técnicas de sensoriamento remoto, assim como a integração de técnicas analíticas para caracterização de materiais geológicos com aplicações na indústria da mineração, fiscalização ambiental e exploração mineral.



**UNIVERSITY OF CAMPINAS
INSTITUTE OF GEOSCIENCE**

**REFLECTANCE AND EMISSIVITY SPECTROSCOPY OF IGNEOUS AND
SEDIMENTARY PHOSPHATE ROCKS FROM MIDWESTERN BRAZIL: CASE
STUDY OF THE CATALÃO I (GO), TAPIRA (MG), ROCINHA E LAGAMAR (MG)
DEPOSITS**

ABSTRACT

Master of Geoscience's Dissertation

Emanuel Amorer Hernández

In order to aid phosphate exploration programs, this research comprises a reflectance and emission spectroscopy study of phosphate-bearing igneous carbonatites and phosphoritic rocks from the Catalão-I (GO), Tapira, Rocinha and Lagamar (MG) deposits, located in Midwestern Brazil. The ultimate goal of the study was to identify mineral and lithotype endmembers that can be detected through ASTER multispectral remote sensing. Reflectance, diffuse reflectance (0.4-2.5 μm range) and emission (8-12 μm range) data were used in combination with X-ray fluorescence (XRF) and X-ray diffraction (XRD) data, providing a more thoroughly understanding of the chemistry and mineralogy of the studied sites.

The igneous carbonatitic phosphate deposits of Catalão-I and Tapira are comprised in the cretacic Alto Paranaíba Igneous Province (PIAP). Monazite, fluorapatite and apatite-(Cl) were distinguished through full-resolution visible (V), near infrared (NIR) and shortwave infrared (SWIR) reflectance spectroscopy (0.4-2.5 μm). REE inclusions present in these phosphates show diagnostic absorption features around 0.75 μm , which helped defining the phosphate type. Main mineral assemblages observed are fluorapatite-ajóite-vermiculite, fluorapatite-vermiculite-calcite and fluorapatite-calcite-monazite. It was also possible to recognize vermiculite, phlogopite, calcite, dolomite, kaolinite and ajoite-corvusite using their intrinsic absorption features, particularly where phosphate concentration is high. The metasedimentary phosphate deposits of Rocinha and Lagamar are comprised in the neoproterozoic Brasília Fold Belt. The ore is rich in sedimentary fluorapatite. Here, REEs spectral absorption features are absent in apatite, probably due to weathering and natural changes on the crystal structure that occurred during the P cycle. In both deposits, clays provide alternative footprints that can indicate high and low phosphate yield. XRD-checked spectral mineralogy shows that mineral assemblages associated to Rocinha and Lagamar ores are illite-fluorapatite-quartz, fluorapatite-kaolinite-quartz, and fluorapatite-illite-muscovite. Chlorite and calcite are also present, as indicated by their SWIR absorption features.

Considering the spectral signatures yielded through close range spectroscopy, spectral libraries were composed and used for processing ASTER imagery acquired over Catalão-I/Tapira and Rocinha/Lagamar mines. Spectral Angle Mapper (SAM) and Mixture Tuned Matched Filtering (MTMF) processing techniques were applied to the imagery. In the Catalão-I deposit, it was possible to map the spatial distribution of ASTER pixels with spectral signatures similar to those of monazite, vermiculite, magnetitic phoscorite and P-poor isalteritic soils. Ajoite-corvusite, secondary phosphates, vermiculite and picritic carbonatite was discriminated for the Tapira deposit and adjacent areas, indicating previously unmapped occurrences. In the Rocinha and Lagamar deposits, it was possible to discriminate wall rocks from host rocks using clay minerals spectral signatures. These results encourage further exploration of the data with current (Hyperion, ProSpecTIR, HyMap) and future (EnMap, PRISMA, HISUI, HypSIRI) hyperspectral data in order to fully quantify phosphate favorability in phosphate exploration programs.

Keywords: Phosphate; remote sensing; reflectance; emissivity



UNIVERSIDADE ESTADUAL DE CAMPINAS
INSTITUTO DE GEOCIÊNCIAS

**ESPECTROSCOPIA DE REFLETÂNCIA E EMISSIVIDADE DE ROCHAS
FOSFÁTICAS ÍGNEAS E SEDIMENTARES DO CENTRO-OESTE DO BRASIL:
ESTUDOS DE CASO NOS DEPÓSITOS DE CATALÃO I (GO), TAPIRA (MG),
ROCINHA E LAGAMAR (MG)**

RESUMO

Dissertação de Mestrado

Emanuel Amorer Hernández

A pesquisa compreende estudos sobre a assinatura ultraespectral e multiespectral de fosfatos de origem ígnea e sedimentar contidos, respectivamente, nos depósitos de Catalão-I (GO), Tapira (MG) e Rocinha-Lagamar (MG), centro-oeste do Brasil. Medidas de reflectância (faixa de 0.4-2.5 μ m) e emissividade (na faixa de 8-12 μ m) foram analisadas em conjunto com dados de Difração e Fluorescência de Raios X visando a determinação da mineralogia e quimismo das rochas envolvidas nas áreas de estudo.

Os fosfatos ígneos de Catalão-I e Tapira, inseridos na Província Ígnea do Alto Paranaíba, encontram-se hospedados em complexos carbonatíticos. Apresentam Elementos de Terras Raras (ETR) em sua composição e feições de absorção intrínsecas em espectros de reflectância em torno de 0,75 μ m. A profundidade e forma dessas feições auxiliaram na identificação e qualificação de monazita, fluoroapatita e cloroapatita como minerais de minério. Associações comuns nas zonas mineralizadas e que apresentam assinaturas espectrais características incluem fluoroapatita-ajoita-vermiculita; fluoroapatita-vermiculita-calcita e fluoroapatita-calcita-monazita. Teores anômalos de fosfato ocorrem na presença de vermiculita, flogopita, calcita, dolomita, caulinita e ajoita-corvusita, todos passíveis de identificação através de espectros de reflectância. Os fosfatos metassedimentares de Rocinha e Lagamar, inseridos na Faixa de Dobramentos Brasília, encontram-se hospedados em fosfoarenitos do Grupo Bambuí. Correspondem a fluorapatitas, onde o intemperismo, além de mudanças próprias da apatita durante o ciclo do P sedimentar, removeram seu conteúdo de ETR. As argilas presentes nesses depósitos podem ser utilizadas como indicadores indiretos da presença de teores anômalos de fosfatos. As assembléias minerais observadas incluem illita-fluoroapatita-quartzo; fluoroapatita-caulinita-quartzo; fluoroapatita-illita-muscovita. Clorita e calcita são minerais subordinados.

As análises espectro-mineralógica, difratométrica e geoquímica de rochas desses depósitos permitiram a constituição de bibliotecas espectrais que foram utilizadas para subsidiar a classificação espectral de dados do sensor ASTER adquiridos sobre as áreas de estudo. As técnicas Spectral Angle Mapper (SAM) e Mixture Tuned Matched Filtering (MTMF) foram testadas. No complexo de Catalão I foi possível separar, nas imagens, zonas ricas em monazita, vermiculita, foscorito magnetítico e solos isalteríticos com baixo teor de fosfatos. No complexo de Tapira e adjacências, foi possível distinguir ajoita-corvusita, isalteritos com fosfatos secundários, vermiculita e carbonatitos picríticos. Nas minas de Rocinha e Lagamar foi possível discriminar as rochas encaixantes das rochas hospedeiras nas imagens com base em feições de argilas. Em Rocinha, fosfoarenitos apatíticos com illita, fosfoarenitos calcareos com illita e muscovita, arenitos calcáreos e solos transportados foram discriminados. Estes resultados reforçam a potencialidade de qualificar e quantificar minerais-índices relacionadas à depósitos de fosfato a partir de sensores hiperespectrais orbitais (Hyperion) e aerotransportados (ProspecTIR; HyMap) atualmente em operação, além de sensores previstos para lançamento futuro (EnMap, PRISMA, HISUI, HypSIPI), com desdobramentos importantes para programas de exploração mineral.

Palavras chaves:Fosfato; sensoriamento remoto; reflectância; emissividade

Sumário

DEDICATÓRIA	VII
REFLECTANCE AND EMISSIVITY SPECTROSCOPY OF IGNEOUS AND SEDIMENTARY PHOSPHATE ROCKS FROM MIDWESTERN BRAZIL: CASE STUDY OF THE CATALÃO I (GO), TAPIRA (GO), ROCINHA E LAGAMAR (MG) DEPOSITS	XIII
ABSTRACT	XIII
RESUMO	XV
SUMÁRIO	XVII
LISTA DE FIGURAS	XXI
LISTA DE TABELAS	XXV
CAPITULO I: INTRODUÇÃO AO TEMA	1
1.1 INTRODUÇÃO	1
1.2 ESTRUTURA DA DISSERTAÇÃO	2
1.3 LOCALIZAÇÃO DAS ÁREAS DE ESTUDO	3
1.4 SÍNTESE DOS MÉTODOS UTILIZADOS NA PESQUISA	4
1.4.1 ESPECTROSCOPIA DE REFLECTÂNCIA	5
1.4.2 ESPECTROSCOPIA DE EMISSIVIDADE	5
1.4.3 MINIMUM NOISE FRACTION (MNF)	5
1.4.4 SPECTRAL ANGLE MAPPER (SAM)	6
1.4.5 MATCHED FILTERING (MF) E MIXTURE TUNED MATCHED FILTERING (MTMF)	6
CAPITULO II: CONTEXTO GEOLÓGICO	17
2.1 INTRODUÇÃO	17
2.2 OS CARBONATITOS: GENERALIDADES E CLASSIFICAÇÃO	18
2.2.1 CLASSIFICAÇÃO DOS CARBONATITOS: NOÇÕES BÁSICAS E NOMENCLATURA	19
2.3 CONTEXTO GEOLÓGICO	22
2.3.1 PROVÍNCIA ÍGNEA DO ALTO PARANAÍBA (APIP)	22
2.3.1.1 Complexos Carbonatíticos da APIP	24
2.3.1.2 Complexo Carbonatítico Alcalino de Catalão I	25
2.3.1.2 Complexo Carbonatítico Alcalino de Tapira	28
2.3.2 FAIXA DE DOBRAMENTOS BRASÍLIA (FDB)	29
2.3.2.1 GRUPO VAZANTE	30
2.3.2.2 GRUPO BAMBUÍ	32
2.4 REFERÊNCIAS BIBLIOGRÁFICAS	34

<u>CAPITULO III: REFLECTANCE AND EMISSIVITY SPECTROSCOPY OF BRAZILIAN MAGMATIC PHOSPHATES: CATALÃO I (GO) AND TAPIRA (MG) CARBONATITIC COMPLEXES</u>		37
3.1	INTRODUCTION	37
3.2	GEOLOGICAL SETTING	38
3.2.1	CATALÃO I CARBONATITIC ALKALINE COMPLEX	38
3.2.2	TAPIRA ALKALINE CARBONATITIC COMPLEX	43
3.3	MATERIALS AND METHODS	49
3.4	RESULTS	50
3.4.1	SAMPLE DESCRIPTIONS:	50
3.4.2	X-RAY FLUORESCENCE:	50
3.4.3	REFLECTANCE SPECTROSCOPY:	53
3.4.3.1	Catalão I Carbonatitic Alkaline Complex (C1CAC)	53
3.4.3.2	Tapira Carbonatitic Alkaline Complex	66
3.4.4	EMISSIVITY SPECTROSCOPY	70
3.5	DISCUSSION	74
3.6	CONCLUSIONS	76
3.7	REFERENCES	78

<u>CAPITULO IV: REFLECTANCE AND EMISSION SPECTROSCOPY OF BRAZILIAN SEDIMENTARY PHOSPHATES: LAGAMAR AND ROCINHA MINES (MINAS GERAIS STATE)</u>		81
4.1	INTRODUCTION	81
4.2	GEOLOGIC SETTING	82
4.3	MATERIALS AND METHODS	84
4.4	RESULTS	85
4.4.1	SAMPLE DESCRIPTION	85
4.4.2	X RAY FLUORESCENCE	87
4.4.3	REFLECTANCE SPECTROSCOPY	88
4.4.4	EMISSION SPECTROSCOPY AND X-RAY DIFFRACTION	92
4.5	DISCUSSION	96
4.6	CONCLUSIONS	97
4.7	REFERENCES	99

<u>CAPITULO V: REMOTE SENSING OF PHOSPHATIC ROCKS FROM IGNEOUS AND SEDIMENTARY SOURCES: CATALÃO I (GO), TAPIRA, LAGAMAR AND ROCINHA MINES (MG)</u>		101
5.1	INTRODUCTION	101
5.2	MATERIAL AND METHODS	102
5.3	RESULTS	104
5.3.1	TAPIRA CARBONATITIC ALKALINE COMPLEX AND ARAXÁ-BARREIRO CARBONATITIC ALKALINE COMPLEX	106
5.3.1.1	<i>IMAGE ENDMEMBERS:</i>	107
5.3.1.2	<i>SPECTRAL ANGLE MAPPER (SAM):</i>	109
5.3.1.3	<i>MIXTURE TUNED MATCHED FILTERING (MTMF)</i>	112
5.3.2	CATALÃO I ALKALINE CARBONATITIC COMPLEX:	115
5.3.2.1	<i>IMAGE ENDMEMBERS:</i>	115
5.3.2.2	<i>SPECTRAL ANGLE MAPPER RESULTS:</i>	116
5.3.3	LAGAMAR AND ROCINHA MINES	120
5.3.3.1	<i>IMAGE ENDMEMBERS:</i>	120
5.3.3.2	<i>SPECTRAL ANGLE MAPPER RESULTS</i>	120
5.4.	DISCUSSION	124
5.5.	CONCLUSIONS	126
6.	REFERENCES	128

Lista de Figuras

CAPITULO I: INTRODUÇÃO AO TEMA

FIG. 1. 1 LOCALIZAÇÃO DAS ÁREAS DE ESTUDO	4
---	---

CAPITULO II: REVISÃO CONCEITUAL

FIG. 2. 1 OCORRÊNCIAS CARBONATÍTIAS MUNDIAIS SEGUNDO WOOLLEY & KJARSGAARD (2008)	18
FIG. 2. 2: ESBOÇO GEOLÓGICO DA PIAP, SEGUNDO BARBOSA <i>ET AL.</i> (2012).	23
FIG. 2. 3 PERFIL DE INTEMPERISMO DO COMPLEXO CARBONATÍTICO ALCALINO DE CATALÃO I (MODIFICADO DE OLIVEIRA & IMBERNON, 1998).	27

CAPITULO III: REFLECTANCE AND EMISSION SPECTROSCOPY OF BRAZILIAN MAGMATIC PHOSPHATES: CATALÃO I (GO) AND TAPIRA (MG) CARBONATITIC COMPLEXES

FIG. 3. 1 EVOLUTION MODEL FOR THE CATALÃO I COMPLEX. MODIFIED FROM HIRANO (1987) AND LAPIN (1982, APUD RIBEIRO 2008)	40
FIG. 3. 2 A) WEATHERING PROFILE MODEL FOR THE CATALÃO I CARBONATITIC ALKALINE COMPLEX (BASED ON OLIVEIRA & IMBERNON 1998) AND (B) COMPARABLE FIELD PHOTOGRAPH. (C) MINE FACE COMPOSED OF ALTERED ROCK WITH ANOMALOUS CONCENTRATION OF P ₂ O ₅ IN APATITES (GREEN POLYGONS).....	42
FIG. 3. 5. C1CAC REFLECTANCE SPECTRA OF MONAZITE-BARITE INTERGROWTH.....	55
FIG. 3. 6 REFLECTANCE SPECTRA SUBSET OF FLUORAPATITE AND MONAZITE (CLARK <i>ET AL.</i> , 2007).	56
FIG. 3. 7 REFLECTANCE SPECTRA OF P-FREE SOILS AND ROCKS FROM THE C1ACC. A) SILEXITE. B) HAND SPECIMEN OF BROWN ALOTERITE WITH SILEXITE VEIN. C) ALOTERITIC TITANIFEROUS SOIL. D) BROWN ALOTERITE.	57
FIG. 3. 8. XRD OF SAMPLE CA-29 REPRESENTATIVE OF THE ISALTERITIC-ALOTERITIC PROFILE STERILE ROCKS AND SOILS FROM THE C1CAC.....	58
FIG. 3. 9. C1CAC SAMPLES WITH REES-P ABSORPTION FEATURES IN THE VNIR SPECTRA. A) PHOSCORITE WITH MAGNETITE. B) HAND SPECIMEN OF PHOSCORITE. C) PHLOGOPITE-PHOSCORITE. D) PHLOGOPITIC PHOSCORITE.....	59
FIG. 3. 10 SPECTRAL SUBSET (0.65-08.5 MM) FOR SAMPLE CA-20 (C1CAC). THE BLUE SPECTRUM REPRESENTS A SAMPLE FRACTION THAT HAS MORE MAGNETITE, MASKING THE REES+3 ABSORPTION FEATURES. RED AND GREEN SPECTRA WERE MEASURED IN SAMPLES FRACTIONS IN WHICH FLUORAPATITES WERE DOMINANT	60
FIG. 3. 11 REFLECTANCE SPECTRA OF A CARBONATITE-APATITITE OF THE C1CAC.....	61
FIG. 3. 12 SPECTRAL SUBSET (0,55-0,85 MM) FOR SAMPLE CA- CARBONATITE- APATITITE (C1CAC).....	61
FIG. 3. 13 REFLECTANCE SPECTRA OF THE PHOSCORITE-PHLOGOPITITE (C1CAC)	62
FIG. 3. 14 REFLECTANCE OF A GREEN BRECCIA (SAMPLE CA-123) FROM C1CAC.....	63
FIG. 3. 15 REFLECTANCE SPECTRA OF BRECCIATED PHLOGOPITITE (C1CAC). WAVELENGTH IS IN μM.	63
FIG. 3. 16 REFLECTANCE SPECTRA OF ALTERED PHLOGOPITITE (C1CAC).....	64
FIG. 3. 17 REFLECTANCE SPECTRUM OF GREEN BRECCIA WITH CARBONATITIC VEINS (C1CAC)	64

FIG. 3. 19 A) REFLECTANCE SPECTRA AND B) XRD OF A SAMPLE WITH AJOITE-CORVUSITE (TACC).....	67
FIG. 3. 20: SAMPLE TA-219 OF A LAYERED CARBONATITE (TACC)	68
FIG. 3. 21 A) PHOSCORITE-PICRITE-CARBONATITE FROM THE TACC. B) FULL SPECTRUM OF THE PHOSCORITE-PICRITE-CARBONATITE (TACC) C) SUB-SET OF THE 0.55 μ M-0.85 μ M SPECTRUM DISPLAYING REES ABSORPTION FEATURES.....	68
FIG. 3. 22.A) REFLECTANCE SPECTRA OF CARBONATITIC BEBEDOURITE (TACC). GREEN SPECTRUM CORRESPONDS TO A BEBEDOURITE WITH PHLOGOPITE; BLUE SPECTRUM IS A BEBEDOURITE WITH MAGNETITE; RED SPECTRUM IS A BEBEDOURITE SENSU STRICTO. B) PICTURE OF THE ANALYZED SAMPLE. TARGET COLORS CORRESPOND TO SPECTRAL CURVES ILLUSTRATED IN (A).	69
FIG. 3.23: VNIR-SWIR REFLECTANCE SPECTRA OF ISALTERITES WITH SECONDARY PHOSPHATES.	70
FIG. 3. 24 MONAZITE CRYSTALS YIELDED FROM THE C1CAC MEASURED FOR DIFFUSE REFLECTANCE (2.5-25 MM).	71
FIG. 3. 25 EMISSIVITY OF PURE MONAZITE CRYSTALS (C1CAC).	72
FIG. 3. 26 EMISSIVITY OF SAMPLE CA-115 (C1CAC).	73
FIG. 3. 27 EMISSIVITY OF GREEN BRECCIA SAMPLE CA-123 (C1CAC).	73
FIG. 3. 28 EMISSIVITY SPECTRA OF ISALTERITE WITH SECONDARY PHOSPHATES. SAMPLE TA-236 (TACC).....	74

CAPÍTULO IV: REFLECTANCE AND EMISSION SPECTROSCOPY OF BRAZILIAN SEDIMENTARY PHOSPHATES. LAGAMAR AND ROCINHA MINES (MG)

FIG. 4. 1 PANORAMIC VIEWS FROM ROCINHA (A) AND LAGAMAR (B) MINES. PICTURE OF LAGAMAR MINE COURTESY OF GALVANI MINERAÇÃO LTD (2011)	85
FIG. 4. 2 REFLECTANCE SPECTRA OF SELECTED SAMPLES OF THE LAGAMAR MINE	89
FIG. 4. 3 REFLECTANCE SPECTRA FOR ROCINHA MINE SAMPLES. A) RED WEATHERED RYTHMITE; B) PHOSPHORITIC SLATE, WHERE DARK CALCITIC SEDIMENTS HOST CRIPTOCRISTALINE FLUORAPATITE; C) ORIENTATED PHOSPHATIC RYTHMITE; D) KAOLINITE-RICH PHOSPHORITE-SILTITE, MARKEDLY WITH LESS PHOSPHATE CONCENTRATION.	90
FIG. 4. 4 REFLECTANCE SPECTRA OF SELECTED SAMPLES FROM THE ROCINHA MINE. A) FOLDED SLATES WITH KAOLINITE AND REDUCED APATITE CONCENTRATION; B) FOLDED RYTHMITES WITH APATITE; C) P-FREE, STERILE SLATES WITH FEW LEVELS OF RYTHMITES; D) CRYPTOCRYSTALLINE FLUORAPATITE IN SLATE.	91
FIG. 4. 5 REFLECTANCE SPECTRA OF ROCINHA MINE SAMPLES. A) P-FREE, STERILE BLOCK SHOWING FOLDED LAMINATIONS OF KAOLINITE WITH LESS ILLITE AND FLUORAPATITE; B) STERILE SOILS WITH REMNANTS OF FLUORAPATITE CRYPTOCRYSTALLINE SEDIMENTS (DARK GRAINS)	92
FIG. 4. 6 EMISSIVITY OF ROCINHA SAMPLE RO-30.	93
FIG. 4. 7: A) EMISSIVITY AND B) X RAY DIFFRACTION DATA FOR THE ROCINHA APATITIC CONCENTRATE.	94
FIG. 4. 8: A) EMISSIVITY (WAVELENGTH IN μ M) AND B) X-RAY DIFFRACTION DATA FOR LAGAMAR SAMPLE LG-01B	95

CAPÍTULO V: REMOTE SENSING OF PHOSPHATIC ROCKS FROM IGNEOUS AND SEDIMENTARY SOURCES: CATALÃO I (GO), TAPIRA, LAGAMAR AND ROCINHA MINES (MG)

- FIG. 5. 1: GRAPHICAL EXPLANATION OF THE MIXTURE TUNE MATCHED FILTERING TARGET SELECTION. FROM A LARGE CLOUD OF POSSIBLE RESULTS IN MF, THE ALGORITHM LEADS THE USER TO REFINE THE TARGET SELECTION BY USING THE BEST SCORES VS INFEASIBILITY PIXELS (ITT, 2009). 104
- FIG. 5. 2 SPECTRAL ENDMEMBERS FOR THE TAPIRAA ALKALINE CARBONATITICCOMPLEX. TOP SPECTRA REPRESENTS ASTER RESOLUTION SPECTRA AND BOTTOM SPECTRA REPRESENTS LABORATORY SPECTRA. 106
- FIG. 5. 3 AVERAGE IMAGE SPECTRA FROM THE ROI ENDMEMBERS IN THE TAPIRA ALKALINE CARBONATITIC COMPLEX 108
- FIG. 5. 4 LABORATORY AND IMAGE ACQUIRED SPECTRA OF REGIONS OF INTEREST FOR THE TAPIRA ALKALINE CARBONATITIC COMPLEX. A) PHOSCORITIC CARBONATITE, B) BEBEDOURITES WITH SULPHATES, C) BEBEDOURITES WITH SECONDARY PHOSPHATES, D) BEBEDOURITES WITH VERMICULITE. 109
- FIG. 5. 5 SPECTRAL ANGLE MAPPER RESULTS FOR THE TAPIRA AND ARAXÁ PHOSPHATE DEPOSITS. 110
- FIG. 5. 6 MIXTURE TUNED MATCHED FILTERING RESULTS FOR THE TAPIRA CARBONATITIC ALKALINE COMPLEX. 112
- FIG. 5. 7 INFEASIBILITY SCATTERPLOTS FOR THE MTMF CLASSIFICATION OF THE TAPIRA-ARAXÁ ASTER IMAGERY. LOW VALUES OF INFEASIBILITY AND HIGH MF SCORES WERE OBTAINED FOR BEBEDOURITES WITH VERMICULITE (YELLOW CLOUD), BEBEDOURITES WITH SULPHATES (PURPLE CLOUD) AND PHOSCORITIC CARBONATITE (RED CLOUD). BEBEDOURITES WITH SECONDARY PHOSPHATES (BLUE CLOUD) MAY PRESENT FALSE POSITIVES FOR 15% OF THE MAPPED PIXELS. 113
- FIG. 5. 8: ENDMEMBER IMAGE EXTRACTED SPECTRA FROM ASTER VNIR-SWIR 9 SPECTRAL BANDS. A) LABORATORY SPECTRA RESAMPLED TO ASTER RESOLUTIONOF THE ONLY THREE POINTS THAT WERE PROPERLY IDENTIFIED IN THE IMAGE. B) THE RESAMPLED SPECTRA FROM THE IMAGE, EXTRACTED THROUGH THE N-DIMENSIONAL VISUALIZE THAT WERE USED AS ENDMEMBERS FOR CLASSIFICATION OF TARGETS IN THE CATALÃO I DEPOSIT USING THE SAM METHOD 116
- FIG. 5. 9: SPECTRAL ANGLE MAPPER RESULTS FOR THE CATALÃO I CARBONATITIC COMPLEX. 117
- FIG. 5. 10 SPECTRA (IMAGE EXTRACTED AND LABORATORY) FROM LAGAMAR MINE 121
- FIG. 5. 11 ENDMEMBER SPECTRA (IMAGE EXTRACTED AND LABORATORY) OF ROCINHA MINE. 121
- FIG. 5. 12 SPECTRAL ANGLE MAPPER RESULTS FOR LAGAMAR MINE, USING IMAGE EXTRACTED SPECTRA SHOWN ON FIG.5.10 122
- FIG. 5. 13 SPECTRAL ANGLE MAPPER RESULTS FOR ROCINHA MINE, USING IMAGE EXTRACTED SPECTRA SHOWN ON FIG.5.11 123
- FIG. 5. 14. INSET (ZOOM) OF THE RESULTS YIELDED FROM SAM CLASSIFICATION IN ROCINHA AND LAGAMAR MINES. A) ROCINHA MINE. B) LAGAMAR MINE. 123

Lista de Tabelas

CAPITULO II: REVISÃO CONCEITUAL

TAB. 2. 1:CLASSIFICAÇÃO SIMPLIFICADA DE CARBONATITOS, SEGUNDO LE MAITRE (2002).....	21
TAB. 2. 2: INFORMAÇÕES GERAIS DE COMPLEXOS CARBONATÍTIOS SELECIONADOS DA APIP	25

CAPITULO III: REFLECTANCE AND EMISSION SPECTROSCOPY OF BRAZILIAN MAGMATIC PHOSPHATES: CATALÃO I (GO) AND TAPIRA (MG) CARBONATITIC COMPLEXES

TAB. 3. 1 SELECTED SAMPLE DESCRIPTIONS OF THE CA1AC AND TACC	50
TAB. 3. 2 X-RAY FLUORESCENCE DATA FOR SAMPLES COLLECTED IN THE C1CAC AND TACC COMPLEXES	53

CAPÍTULO IV: REFLECTANCE AND EMISSION SPECTROSCOPY OF BRAZILIAN SEDIMENTARY PHOSPHATES. LAGAMAR AND ROCINHA MINES (MG)

TAB. 4. 1: SAMPLE DESCRIPTION OF THE ROCINHA AND LAGAMAR MINE SITES.	86
TAB. 4. 2: X RAY FLUORESCENCE OF THE ROCINHA AND LAGAMAR ROCKS	87

CAPÍTULO V: REMOTE SENSING OF PHOSPHATIC ROCKS FROM IGNEOUS AND SEDIMENTARY SOURCES: CATALÃO I (GO), TAPIRA, LAGAMAR AND ROCINHA MINES (MG)

TAB. 5. 1: SAMPLE COORDINATES AND DESCRIPTION	105
TAB. 5. 2 ROI DESCRIPTION AND PIXEL EXTENT OF THE CHOSEN ENDMEMBERS FOR THE TAPIRA ALKALINE CARBONATITIC COMPLEX	107
TAB. 5. 3: SAM CLASSIFICATION COLORS FOR TARGETS (ENDMEMBERS) IN THE TAPIRA CARBONATITIC ALKALINE COMPLEX	110
TAB. 5. 4: CONFUSION MATRIX FOR THE SAM CLASSIFICATION IN THE TAPIRA CARBONATITIC COMPLEX	111
TAB. 5. 5 CONFUSION MATRIX FOR MTMF CLASSIFICATION. TAPIRA ALKALINE CARBONATITIC COMPLEX	114
TAB. 5. 6. CONFUSION MATRIX FOR THE SAM RESULTS OBTAINED IN CATALÃO I.	119

Capítulo I: Introdução ao tema

1.1 Introdução

Os fosfatos têm sido prospectados desde o século XIX para uso como fertilizantes. Entre os minerais não metálicos, têm tido um papel importante na economia mineral e agropecuária, como insumo básico para as culturas agrícolas e rações animais. Os maiores teores mundiais de fosfatos economicamente aproveitáveis estão concentrados em depósitos fosforíticos. São depósitos de origem marinha, onde o fósforo, não aproveitado pelos macro e microrganismos durante o intemperismo de rochas na crosta continental, é transportado e finalmente depositado em ambientes de plataformas relativamente rasas. A alta atividade biogênica característica desses ambientes faz sua concentração chegar até um milhão de vezes acima do normal, podendo atingir porcentagens entre 16 a 32% em conteúdo de P_2O_5 (FÖLLMI, 1996).

São também de grande relevância, principalmente no Brasil, as reservas econômicas de fosfatos ígneos associados a complexos alcalino-carbonatíticos ultramáficos. Nestes complexos, os teores de fosfato são variáveis, com teores de corte entre 6 e 7% de P_2O_5 em peso, mas que podem alcançar, em determinados depósitos (Catalão I, Tapira, Araxá), concentrações pontuais de até 30% (BIONDI, 2005).

Dada a significância destes minerais para a segurança alimentar do país, é necessário estabelecer as características espectro-químicas, tanto das ocorrências atuais, como de novas reservas, para que possam ser detectadas e estudadas remotamente. Nesse sentido, a espectroscopia de reflectância e emissividade são métodos fundamentais para a avaliação da possibilidade de detecção remota de atributos relacionados à depósitos de fosfato.

Atualmente, faltam informações básicas sobre a assinatura espectral das rochas fosfáticas brasileiras, o que representa um obstáculo para a sua caracterização remota. No caso particular dos fosfatos sedimentares, são raros os estudos mineralógicos detalhados, que possam ajudar na identificação destes alvos. Outro problema para a detecção remota é que as respostas espectrais para os litotipos hospedeiros e encaixantes dos minérios de fosfato também são pouco conhecidas. Na medida em que

seja possível reconhecer indicadores de rochas que contém fosfatos com teores anômalos, poder-se-á estabelecer métodos diretos ou indiretos para sua detecção.

Nesse contexto, almeja-se, nessa pesquisa, avaliar as características espectrais de depósitos de fosfatos ígneos e sedimentares, considerando minas em operação no centro-oeste do Brasil, e constituir bibliotecas espectrais de referência para a detecção remota dos alvos estudados nas faixas do visível e infravermelho próximo (VNIR 0,35-1,0 μm), infravermelho de ondas curtas (1,1-2,5 μm) e infravermelho de ondas longas (2,5-25 μm). A eficácia da espectroscopia de reflectância e emissividade na caracterização desses depósitos será testada mediante comparações qualitativas com outras técnicas analíticas (Difração de Raios X e Fluorescência de Raios X). Adicionalmente, pretende-se investigar a assinatura de alvos selecionados nesses depósitos e a possibilidade de mapeamento remoto dos mesmos a partir de dados multiespectrais do sensor ASTER (*Advanced Spaceborne Thermal Emission and Reflection Radiometer*), proporcionando uma contribuição para a prospecção regional de depósitos de fosfatos no país.

1.2 Estrutura da Dissertação

A dissertação foi elaborada em cinco capítulos auto-consistentes. O Capítulo 1 compreende uma introdução geral e localização das áreas de estudo, uma resenha da geologia geral da Província Ígnea do Alto Paranaíba e da Faixa de Dobramentos Brasília, além de uma revisão sumária dos métodos de espectroscopia e sensoriamento remoto utilizados na pesquisa.

No Capítulo 2 apresenta-se uma revisão da geologia das áreas de estudo que compreendem os fosfatos ígneos e sedimentares abordados. Apresenta-se, além disso, a classificação dos carbonatitos, visando proporcionar ao leitor informações básicas sobre esses litotipos diferenciados.

O Capítulo 3 aborda estudos espectroscópicos realizados nas rochas fosfáticas ígneas dos complexos alcalinos carbonatíticos de Catalão I (GO) e Tapira (MG), incluindo resultados da espectroscopia de reflectância e a relação entre as respostas espectrais obtidas com as determinações por Difratometria de Raios X (DRX) e Fluorescência de Raios X (FRX).

O Capítulo 4 compreende estudos espectroscópicos realizados nas rochas fosfáticas sedimentares das Formações Lagamar e Rocinha, inseridos na Faixa de Dobramentos Brasília. São apresentadas as descrições espectroscópicas de reflectância e emissividade dos calcários fosfáticos de Rocinha e dos fosfoarenitos de Lagamar. Estes dados são também comparados com a informação obtida a partir da DRX e FRX.

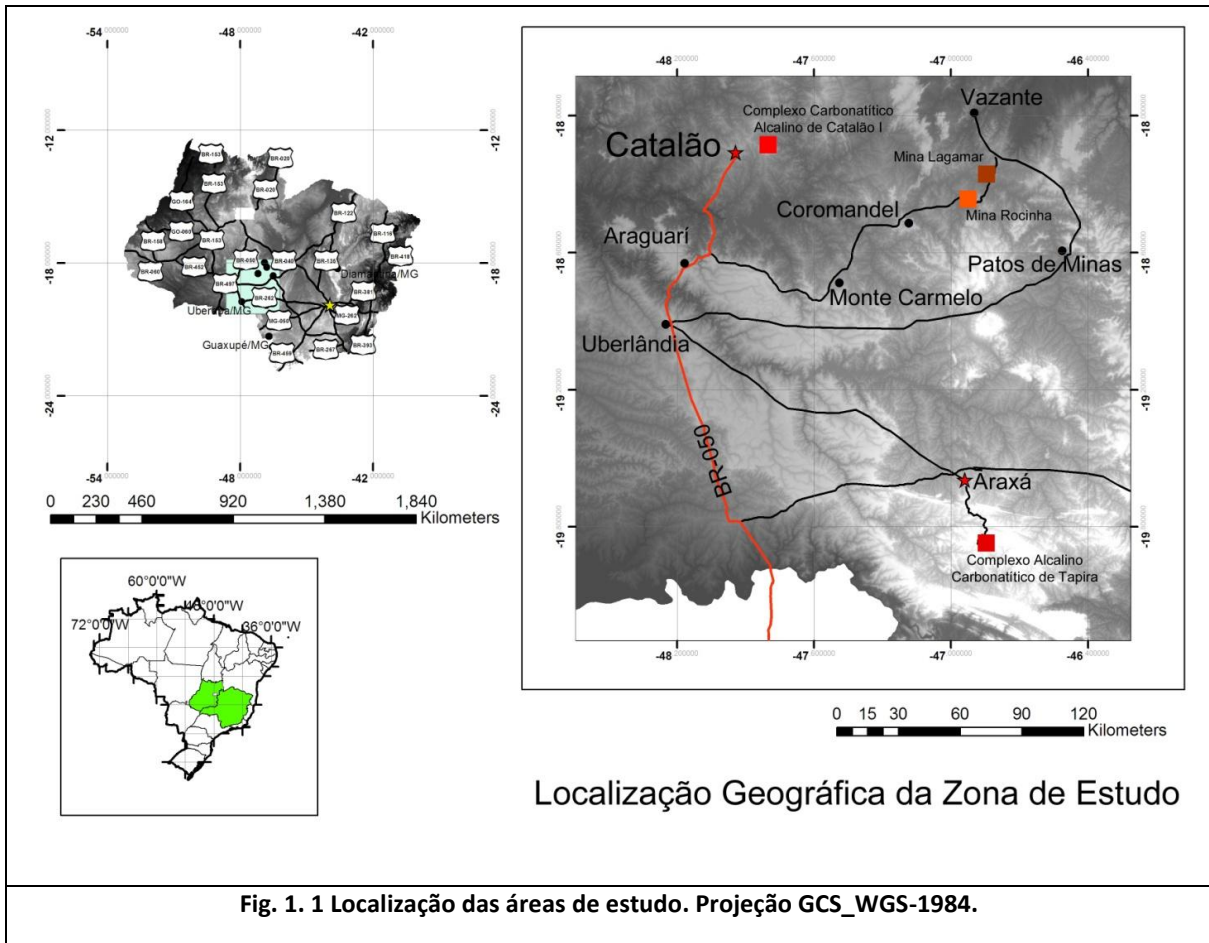
O Capítulo 5 engloba a apresentação dos resultados oriundos do processamento digital de imagens ASTER visando a detecção de alvos identificados como importantes guias para a prospecção de fosfatos ígneos e sedimentares através de métodos de sensoriamento remoto.

1.3 Localização das áreas de estudo

As ocorrências fosfáticas abordadas nessa pesquisa estão localizadas nos Estados de Goiás (GO) e Minas Gerais (MG). A via de acesso principal é a Rodovia BR-050, vindo de Uberlândia (MG), tal como indicado na Fig. 1.1.

O Complexo Foscorítico Alcalino de Catalão I situa-se na porção sudeste do Estado de Goiás, a 216 km da cidade de Goiânia. O Complexo Alcalino Carbonatítico de Tapira situa-se a 35 km da cidade de Araxá (MG). Ambos complexos fazem parte da Província Ígnea do Alto Paranaíba (GIBSON *et al.* 1995). O Complexo de Tapira, atualmente operado pela empresa Vale Fertilizantes, é acessado a partir da Rodovia BR-146. O Complexo de Catalão I, particularmente no sítio da mineração Ouvidor, operado pela empresa Copebrás Ltda. (Grupo Anglo American), é acessado pela rodovia GO-210.

Os depósitos sedimentares de Rocinha e Lagamar (DA ROCHA ARAUJO *et al.*, 1992; DARDENNE & CAMPOS NETO, 1976; DARDENNE *et al.* 1986; NOGUEIRA, 1993) encontram-se situados no segmento centro-oeste do Estado de Minas Gerais. O acesso aos depósitos é feito a partir de Uberaba, no sentido a Brasília, tomando-se a rodovia MG-223 com sentido a Monte Carmelo – Coromandel. Em Coromandel, pega-se a rodovia BR-352 com sentido a Lagamar-Vazante. A entrada ao Complexo Minerador de Patos de Minas (Mina Rocinha-Vale Fertilizantes) fica na mesma rodovia. Já o acesso à Mina Lagamar (Operado pela Mineração Galvani) fica 18 km à nordeste do Complexo Minerador Patos de Minas.



1.4 Síntese dos Métodos Utilizados na Pesquisa

O desenvolvimento do projeto englobou estudos bibliográficos, atividades de campo, análises laboratoriais e trabalhos de gabinete. Os trabalhos de campo visaram a coleta de uma grande quantidade de amostras, representativas das principais variações de litotipos e minérios observados nos depósitos. Informações de campo também serviram para a calibração e verificação da validade dos resultados obtidos a partir das imagens de sensoriamento remoto.

As atividades laboratoriais principais consistiram em medidas de espectroscopia no espectro refletivo e emissivo e a elaboração de bibliotecas espectrais dos depósitos de fosfatos ígneos e sedimentares. As atividades de gabinete mais importantes consistiram no Processamento Digital de imagens multiespectrais ASTER, através de um conjunto de métodos e procedimentos, que incluíram correção atmosférica, re-amostragem dos dados espectroscópicos para a resolução espectral do sensor ASTER, remoção do contínuo dos

dados, análise das imagens com algoritmos de classificação e avaliação da incerteza da classificação mediante matrizes de confusão.

A seguir, explica-se brevemente os fundamentos dos métodos utilizados.

1.4.1 Espectroscopia de Reflectância

A espectroscopia de reflectância é o estudo da relação entre a luz incidente e sua componente refletida por sólidos, líquidos e gases, segundo comprimentos de onda entre 0,35-2,5 μm . É um método capaz de identificar as ligações químicas que absorvem a luz em determinados comprimentos de onda. A sua principal vantagem é a possibilidade de ser usada tanto em pequena escala (laboratório) até escalas astronômicas (CLARK, 1999).

Visto sua sensibilidade, a técnica tem grande utilidade na caracterização composicional de vários materiais terrestres, tais como argilas (e.g. SENNA, 2008), hidrocarbonetos (e.g. LAMMOGLIA & DE SOUZA FILHO, 2011; PABÓN & DE SOUZA FILHO, 2011) e vegetação (e.g., KOKALY & CLARK, 1999; ALMEIDA & DE SOUZA FILHO, 2004).

1.4.2 Espectroscopia de Emissividade

A espectroscopia de emissividade é o estudo da emissão de energia por sólidos, líquidos e gases, segundo comprimentos de onda $> 3\mu\text{m}$ e $< 1\text{mm}$, em função de sua temperatura. A diferença em relação à espectroscopia de reflectância é que essa técnica se baseia nas propriedades de emissão dos materiais. Medidas de reflectância bidirecional podem ser convertidas para emissividade a partir da aproximação de Kirchoff (Eq.1):

$$\varepsilon = 1 - \rho \quad (\text{Eq. 1})$$

onde ε é a emissividade e ρ é a reflectância difusa medida do material analisado.

1.4.3 Minimum Noise Fraction (MNF)

Este método funciona como uma transformada linear baseada em Principais Componentes (PC) para determinar os pixels com ruído nos dados e discriminar as regiões com respostas espectrais mais específicas (GREEN *et al.*, 1988).

O método consiste em duas fases. A primeira fase tem cinco passos: 1) determinação do ruído na imagem, 2) cálculo matriz de covariância de ruído na imagem e

decomposição subsequente dos autovalores, 3) correção da média da imagem, 4) decorrelação do ruído na imagem e, 5) normalização do ruído linear nos dados (redução de ruído). Este procedimento gera imagens com três características principais: bandas decorrelacionadas, com média zero e variância unitária de ruído, o que permite separar as zonas da imagem que tem respostas espectrais mais puras (MUNDT *et al.*, 2007).

1.4.4 Spectral Angle Mapper (SAM)

O método *Spectral Angle Mapper*, definido por KRUSE *et al.* (1993), é um método de classificação espectral que mede a variação do ângulo n-D de espectros desconhecidos com espectros de referência de alguma biblioteca espectral conhecida. O algoritmo determina a semelhança espectral entre o espectro medido e o espectro de referência com base no ângulo que os separa na sua representação na forma de vetores no espaço de atributos. A vantagem da técnica é a insensibilidade às variações de iluminação (albedo) das cenas.

1.4.5 Matched Filtering (MF) e Mixture Tuned Matched Filtering (MTMF)

Estes métodos funcionam como ferramentas para identificar respostas espectrais específicas, obscurecidas pela sua semelhança com o albedo da imagem. O *Matched Filtering* (MF) extrai a abundância de *endmembers* (definidos pelo usuário, a partir de uma biblioteca ou pixels da própria imagem), usando um algoritmo de desmistura espectral parcial. Esta técnica maximiza a resposta do *endmember* conhecido e suprime a resposta do *background* desconhecido. O *Mixture Tuned* adiciona uma informação de erro aos resultados, denominada de imagem *Infeasibility* ou infactibilidade, usada para reduzir o número de falsos positivos que são comuns aos resultados obtidos exclusivamente com o MF.

Os valores de MF são calculados para cada pixel projetando-se os dados MNF a um vetor MF. Este vetor, por sua vez, é derivado do espectro alvo no espaço MNF, projetado sobre os dados de covariância inversa do MNF e normalizado ao intervalo de 0-1, o que resulta também em componentes vetoriais que são quantificadas de 0 a 100%. A definição matemática do vetor MF, simplificada por MUNDT *et al.* (2007), é apresentada na Eq. 2:

$$\vec{v} = \frac{[C_{MNF}]^{-1} \times \vec{t}_{MNF}}{(\vec{t}_{MNF})^T \times [C_{MNF}]^{-1} \times \vec{t}_{MNF}} \quad (\text{Eq.2})$$

onde $[C_{MNF}]^{-1}$ é o inverso da matriz de covariância MNF e t_{MNF} é o vetor do espectro alvo no espaço MNF. Os valores de MF são, subsequentemente, calculados em um espaço vetorial (o que cria uma imagem de abundância $i \times j$), conforme expresso na eq. 3

$$[MF] = \vec{v} \times [MNF] \quad (\text{Eq.3})$$

Os resultados do MF são distribuídos segundo uma normal e tem média zero, onde a grandeza do valor MF representa a solução linear da projeção MF. Se os valores de MF são iguais ou menores a zero, representam valores do *background*; valores acima de zero representam proximidade ao espectro alvo, equivalente ao valor MF.

O MT avalia a probabilidade de um erro de estimação para cada pixel da imagem baseado no conceito de factibilidade. A factibilidade é calculada em três etapas: i) determinação do componente vetorial do alvo no pixel; ii) interpolação dos auto-valores de variância relativos a componente vetorial do alvo; e iii) cálculo da separação padronizada entre o pixel e seu componente vetorial ideal. O componente vetorial do espectro alvo é o produto escalar do valor MF pelo vetor do alvo (Eq. 4).

$$\vec{c}_i = MF_i \bullet \vec{t} \quad (\text{Eq. 4})$$

onde MF_i é o valor do pixel de MF e C_i o componente vetorial do alvo para o pixel i . O valor ideal que contém a direção do pixel reside na mesma direção do vetor alvo, porém, na maioria dos casos, existe uma variação dada pelo ruído e mistura com o *background*. A proximidade de cada pixel a sua localização ideal sobre o vetor alvo é a medida de infactibilidade.

Referencias Bibliográficas:

ALKMIM, F. F.; BRITO NEVES, B. B.; ALVES, J. A. C. Arcabouço tectônico do Cráton do São Francisco - uma revisão. In: DOMINGUEZ, J. M. L.; MISI, A. (Eds.). **O Cráton de São Francisco**. Salvador: SBG, 1993. p. 45–62.

ALMEIDA, F. F. . Relações tectônicas das rochas alcalinas da região meridional da Plataforma Sul-Americana. **Revista Brasileira de Geociências**, v. 13, n. 3, p. 139–158, 1983.

ALMEIDA, F. F. M. **Observações sobre o Pre-Cambriano da região central de Goiás**. 21 Congresso Brasileiro de Geologia. **Anais...** Curitiba: [s.n.], 1967

ALMEIDA, F. F. M.; HASUI, Y.; NEVES, B. B. B. The upper Precambrian of South America. **Boletim do Instituto de Geociências USP**, v. 7, p. 45–80, 1976.

ALMEIDA, T. I. R.; SOUZA FILHO, C. R. DE. Principal component analysis applied to feature oriented band ratios of hyperspectral data: A tool for vegetation studies. **International Journal of Remote Sensing**, v. 25, n. 22, p. 5005–5023, 2004.

AMARAL, G.; BUSHEE, J.; CORDANI, U. G.; KAWASHITA, K.; REYNOLDS, J. H. Potassium-argon ages of alkaline rocks from southern Brazil. **Geochimica et Cosmochimica Acta**, v. 31, p. 117–142, 1967.

ARAÚJO, D. P. **Metassomatismo no complexo carbonatítico Catalão I: implicações para a composição do magma carbonatítico e para o metassomatismo carbonatítico no manto superior**. [S.l.]: Universidade de Brasília, 1996.

BAECKER, M. L. **A mineralização de nióbio do solo residual laterítico e petrografia das rochas ultramáfica alcalinas do domo de Catalão I, Goiás**. [S.l.]: Universidade de Brasília, 1983.

BARBOSA, E. S. R.; BROD, J. A.; JUNQUEIRA-BROD, T. C.; *et al.* Bebedourite from its type area (Salitre I complex): A key petrogenetic series in the Late-Cretaceous Alto Paranaíba kamafugite–carbonatite–phoscorite association, Central Brazil. **Lithos**, v. 144-145, p. 56–72, jul 2012.

BIONDI, J. C. Brazilian mineral deposits associated with alkaline and alkaline-carbonatite complexes. In: COMIN-CHIARAMONTI, P.; GOMES, C. B. (Eds.). **Mesozoic to Cenozoic Alkaline Magmatism in the Brazilian Platform**. São Paulo: Edusp/Fapesp, 2005. p. 707–755.

BISHOP, J. L.; DARBY DYAR, M.; LANE, M. D.; BANFIELD, J. F. Spectral identification of hydrated sulfates on Mars and comparison with acidic environments on Earth. **International Journal of Astrobiology**, v. 3, n. 4, p. 275–285, 10 jun 2005.

BIZZI, L. A.; ARAÚJO, A. L. N. Dynamics of Mantle-Derived magmatism in the southwestern São Francisco Craton, Brazil. In: COMIN-CHIARAMONTI, P.; GOMES, C. B. (Eds.). **Mesozoic to Cenozoic Alkaline Magmatism in the Brazilian Platform**. São Paulo: Edusp/Fapesp, 2005. p. 341–365.

BORN, H.; LENHARO, S. L. R.; KAHN, H. Mineralogical characterization of apatites from Brazilian phosphate deposits with reference to flotation behaviour. **Transactions of the Institute of Mining and Metallurgy**, v. 105, p. 117–126, 1996.

BRIGATTI, M. F.; Malferrari, D.; Medici, L.; Ottolini, L.; Poppi, L. Crystal chemistry of apatites from the Tapira carbonatite complex, Brazil. **European Journal of Mineralogy**, v. 16, n. 4, p. 677–685, 1 ago 2004.

Brod, J. A. **Petrology and geochemistry of the Tapira alkaline complex, Minas Gerais State, Brazil**. [S.l.]: University of Durham, 1999.

Brod, J. A.; Gaspar, J. C.; Araújo, D. P. DE; *et al.* Phlogopite and tetra-ferriphlogopite from Brazilian carbonatite complexes : petrogenetic constraints and implications for mineral-chemistry systematics. **Journal of Asian Earth Sciences**, v. 19, p. 265–296, 2001.

Brod, J. A.; Gaspar, J. C.; Diniz-Pinto, H. S.; Junqueira-Brod, T. C. Spinel chemistry and petrogenetic processes in the Tapira Alkaline-Carbonatite Complex , Minas Gerais , BRAZIL. **Revista Brasileira de Geociências**, v. 35, n. 1, p. 23–32, 2005.

Brod, J. A.; Gibson, S. A.; Thompson, R. .; *et al.* The Kamafugite-Carbonatite association in the Alto Paranaíba Igneous Province (APIP) Southeastern Brazil. **Revista Brasileira de Geociências**, v. 30, n. 3, p. 404–408, 2000.

Brod, J. A.; Junqueira-Brod, T. C.; Gaspar, J. C.; Gibson, S. A.; Robert, N. **Ti-rich and Ti-poor garnet from the Tapira Carbonatite Complex, SE BRAZIL: Fingerprinting fractional crystallisation and liquid immiscibility**. Proceedings of the 8th International Kimberlite Conference. **Anais...** [S.l.: s.n.]. , 1999

Brod, J. A.; Ribeiro, C. C.; Gaspar, J. C.; *et al.* **Geologia e mineralizações dos complexos alcalino-carbonatíticos da Província Ignea do Alto Paranaíba**. 42 Congresso Geológico Brasileiro. **Anais...** [S.l.: s.n.]. , 2004

Carranza, E. J. M.; Saeghi, M. Predictive mapping of prospectivity and quantitative estimation of undiscovered VMS deposits in Skellefte district (Sweden). **Ore Geology Reviews**, v. 38, n. 3, p. 219–241, nov 2010.

Christensen, P. R.; Bandfield, J. L.; Hamilton, V. E.; *et al.* A thermal emission spectral library of rock-forming minerals. **Journal of Geophysical Research**, v. 105, n. E4, p. 9735–9739, 2000.

Clark, R. N. Spectroscopy of Rocks and Minerals and Principles of Spectroscopy. **Manual of Remote Sensing**. New York: John Wiley and Sons, 1999. p. 3–58.

Clark, R. N.; Swayze, G. .; Wise, R.; *et al.* **USGS digital spectral library splib06a**. . [S.l.: s.n.]. Disponível em: <<http://speclab.cr.usgs.gov/spectral-lib.html>>. , 2007

Comin-Chiaramonti, P.; Gomes, C. B.; Censi, P.; Speziale, S. Carbonatites from southeastern Brazil: a model for the carbon and oxygen isotope variations. In: Comin-Chiaramonti, P.; Gomes, C. B. (Eds.). **Mesozoic to Cenozoic Alkaline Magmatism in the Brazilian Platform**. São Paulo: [s.n.], 2005. p. 629–650.

Cordeiro, P. F. DE O. **Petrologia e Metalogenia do Depósito primário de Nióbio do Complexo Carbonatítico-Foscorítico de Catalão I, GO**. [S.l.]: Universidade de Brasília, 2009.

Costa, M. T.; Branco, J. J. R. **Roteiro para a excursão Belo Horizonte-Brasília**. 14 Congresso Brasileiro de Geologia. **Anais...** Belo Horizonte: UFMG. , 1961

CRÓSTA, A. P.; SOUZA FILHO, C. R. DE; AZEVEDO, F.; BRODIE, C. Targeting key alteration minerals in epithermal deposits in Patagonia, Argentina, using ASTER imagery and principal component analysis. **International Journal of Remote Sensing**, v. 24, n. 21, p. 4233–4240, 1 nov 2003.

CRUZ, J. R. **Dados e Métodos de Sensoriamento Remoto Aplicados ao Estudo do Depósito de Fosfato de Araxá á , Minas Gerais**. [S.l.]: Universidade Estadual de Campinas (UNICAMP), 2011.

CRUZ, J. R.; SOUZA FILHO, C. R. DE; ABRAM, M. B.; MARCON, R. **Caracterização espectral do depósito de fosfato de Araxá (MG)**. Anais XV Simpósio Brasileiro de Sensoriamento Remoto. **Anais...** Curitiba: INPE. , 2011

DAASCH, L.; SMITH, D. Infrared Spectra of Phosphorus Compounds. **Analytical Chemistry**, v. 23, n. 6, p. 853–868, 1 jun 1951.

DARDENNE, M. A. **Síntese sobre a estratigrafia do Grupo Bambuí no Brasil Central**. 30 Congresso Brasileiro de Geologia. **Anais...** Recife: SBG. Disponível em: <<http://www.scribd.com/doc/91113300/Dardenne-1978-Sintese-Sobre-A-Estratigrafia-do-Grupo-Bambui-No-Brasil-Central>>. , 1978

DARDENNE, M. A. The Brasilia Fold Belt. In: CORDANI, U. G.; MILANI, E. J.; THOMAZ-FILHO, A.; CAMPOS, D. A. (Eds.). **Tectonic Evolution of South America**. Rio de Janeiro: 31st International Geological Congress Rio de Janeiro, 2000. p. 231–263.

DARDENNE, M. A. **Lithostratigraphic sedimentary sequences of the Vazante Group**. (A. Misi & J. B. G. Teixeira, Eds.)Base Metal Deposits of Africa and South America, IGCP 450. **Anais...** Belo Horizonte-Paracatú: [s.n.]. , 2001

DARDENNE, M. A.; CAMPOS NETO, M. C. **Geologia da região de Lagamar, Minas Gerais**. 29 Congresso Brasileiro de Geologia. **Anais...** Ouro Preto: [s.n.]. , 1976

DARDENNE, M. A.; FREITAS-SILVA, F. H.; NOGUEIRA, G. M. DOS S.; SOUZA, J. F. C. Depósitos de fosfato de Rocinha e Lagamar, Minas Gerais. **Principais Depósitos Minerais do Brasil, Volumen 4,Parte C**. [S.l.]: Companhia de Pesquisa e Recursos Minerais do Brasil, 1997. p. 634.

DARDENNE, M. A.; SCHOBENHAUS, C. **Metalogênese do Brasil**. [S.l: s.n.], 2001. p. 392

DARDENNE, M. A.; TROMPETTE, R.; MAGALHÃES, L. F.; SOARES, L. A. Proterozoic and Cambrian phosphorites - regional review: Brazil. In: COOK, P. J.; SHERGOLD, J. H. (Eds.). **Phosphate Deposits of the world Volume 1**. [S.l.]: University of Cambridge, 1986. p. 116–131.

FERRARI, V. C.; TOLEDO, M. C. M. DE; ATENCIO, D. Gorceixite from Catalão, Goiás, Brazil: Rietveld Crystal Structure Refinement. **Geologia USP Serie Científica**, v. 7, n. 2, p. 25–36, 2007.

FILIPPELLI, G. M. The Global Phosphorus Cycle. In: RAKOVAN, J.; HUGHES, J. M.; KOHN, M. J. (Eds.). **PHOSPHATES Geochemical, geobiological, and materials importance**. [S.l: s.n.], 2002. p. 391–425.

FILIPPELLI, G. M. The Global Phosphorus Cycle: Past, Present, and Future. **Elements**, v. 4, p. 89–95, 2008.

FLICOUTEAUX, R.; LUCAS, J. Weathering of Phosphate Minerals. **Phosphates Minerals**. Berlin: Springer-Verlag, 1984. p. 292–317.

FÖLLMI, K. B. The phosphorus cycle , phosphogenesis phosphate-rich deposits. **Earth-Science Reviews**, v. 40, p. 55–124, 1996.

FUCK, R. A.; SÁ, E. F. J. DE; PIMENTEL, M. M.; DARDENNE, M. A.; SOARES, A. C. P. As faixas de dobramentos marginais do cráton do São Francisco: síntese de conhecimentos. **O Cráton de São Francisco**. [S.l: s.n.], 1993. p. 161–185.

FUJISADA, H. **Design and performance of ASTER instrument**. Proceedings of SPIE the International Society for Optical Engineering. **Anais...** [S.l: s.n.], 1995

GIBSON, S. A.; THOMPSON, R. N.; LEONARDOS, O. H.; DICKIN, A. P.; MITCHELL, J. G. The Late Cretaceous Impact of the Trindade Mantle Plume : Evidence from Magmatism in SE Brazil. **Journal of Petrology**, v. 36, n. 1, p. 189–229, 1995.

GIERTH, E.; BAECKER, M. L. A mineralização de nióbio e as rochas alcalinas associadas no complexo Catalão I, Goiás. In: SCHOBENHAUS, C. (Ed.). **Principais Depósitos Mineraiis do Brasil, Volumen 2**. MME/DNPM ed. Brasília: [s.n.], 1986. p. p456–462.

GIRARD, J.-P.; FLICOUTEAUX, R.; WALTER, A.-V.; SAVIN, S. M.; NAHON, D. Oxygen and carbon isotope composition of structural carbonate in weathering apatites from laterites, southern Brazil and western Senegal. **Applied Geochemistry**, v. 8, n. 6, p. 617–632, nov 1993.

GOMES, C. B.; RUBERTI, E.; MORBIDELLI, L. Carbonatite complexes from Brazil : A review. **Journal of South American Earth Sciences**, v. 3, n. 1, p. 51–63, 1990.

GRASSO, C. B. **Petrologia do Complexo Alcalino-Carbonatítico de Serra Negra, MG**. [S.l.]: Universidade de Brasília, 2010.

GREEN, A. A.; BERMAN, M.; SWITZER, P.; CRAIG, M. D. A transformation for ordering multispectral data in terms of image quality with implications for noise removal. **Transactions on Geoscience and Remote Sensing**, v. 26, n. 1, p. 65–74, 1988.

HAIDER, S. Z. Identification of phosphate anions in Niobium and Tantalum phosphates by means of infra-red spectra. **Analytica Chimica Acta**, v. 24, p. 250–253, 1961.

HASUI, Y.; ALMEIDA, F. F. M. Geocronologia do Centro-Oeste Brasileiro. **Boletim da Sociedade Brasileira de Geologia**, v. 1, p. 7–26, 1970.

HEINRICH, E. W. **The Geology of Carbonatites**. Chicago: Rand McNally, 1967. p. 601

HEZEL, A.; ROSS, S. D. Forbidden transitions in the infra-red spectra of tetrahedral anions m_{rn} , Spectra-structure correlations in perchlorates , sulphates and phosphates of the formula MXO_4 . **Spectrochimica Acta**, v. 22, n. 1962, p. 1949–1961, 1966.

HUNT, G. H.; SALISBURY, J. W. Visible and Near Infrared Spectra of Minerals and Rocks: XI. Sedimentary Rocks. **Modern Geology**, v. 5, p. 211–217, 1976.

HUNT, G.; SALISBURY, J.; LENHOFF, C. Visible and near-infrared spectra of minerals and rocks. V. Halides, phosphates, arsenates, vanadates, and borates. **Modern Geology**, v. 3, p. 121–132, 1972.

KNUDSEN, A. C.; GUNTER, M. E. Sedimentary Phosphorites - An Example: Phosphoria Formation, Southeastern Idaho, U.S.A. In: RAKOVAN, J.; HUGHES, J. M.; KOHN, M. J. (Eds.). **PHOSPHATES Geochemical, geobiological, and materials importance**. [S.l: s.n.], 2002. p. 363–389.

KOKALY, R. **PRISM : Processing Routines in IDL for Spectroscopic Measurements (Installation Manual and User ' s Guide , Version 1 . 0)** . [S.l: s.n.] , 2011

KOKALY, R.; CLARK, R. N. Spectroscopic determination of leaf biochemistry using band-depth analysis of absorption features and stepwise multiple linear regression. **Remote Sensing of Environment**, v. 67, n. 3, p. 267–287, 1999.

KRUSE, F. A.; LEFKOFF, A. B.; BOARDMAN, J. B.; *et al.* The Spectral Image Processing System (SIPS)- Interactive Visualization and Analysis of Imaging spectrometer Data. **Remote Sensing of Environment**, v. 44, p. 145–163, 1993.

LAMMOGLIA, T.; SOUZA FILHO, C. R. DE. Spectroscopic characterization of oils yielded from Brazilian offshore basins: Potential applications of remote sensing. **Remote Sensing of Environment**, v. 115, p. 2525–2535, 2011.

LANE, M. D.; BISHOP, J. L.; DARBY DYAR, M.; *et al.* Identifying the phosphate and ferric sulfate minerals in the Paso Robles soils (Gusev Crater, Mars) using an integrated spectral approach. **Lunar and Planetary Science**, v. XXXVIII, p. 2–3, 2007.

LANE, M. D.; BISHOP, J. L.; DARBY DYAR, M.; *et al.* Mineralogy of the Paso Robles soils on Mars. **American Mineralogist**, v. 93, n. 5-6, p. 728–739, 1 maio 2008.

LANE, M. D.; DARBY DYAR, M.; BISHOP, J. L. Spectra of phosphate minerals as obtained by Visible-Near Infrared Reflectance, Thermal Infrared Emission, and Mössbauer laboratory analyses. **Lunar and Planetary Science**, v. 4, n. XXXVIII, p. 1–2, 2007.

LAPIN, A. V. Carbonatite differentiation process. **International Geological Review**, v. 21, p. 1243–1252, 1982.

LEBAS, M. J. Nephelinites and Carbonatites. **Journal of the Geological Society of London**, v. 30, p. 53–83, 1987.

LIMA, O. N. DE. **Estratigrafia isotópica e evolução sedimentar do Grupo Bambuí na borda ocidental do Cráton do São Francisco : implicação tectônica e paleo-ambiental**. [S.l.]: Universidade de Brasília, 2011.

LUCAS, J.; FLICOUTEAUX, R.; NATHAN, Y.; PRÉVOT, L.; SHAHAR, Y. **Different aspects of phosphorite weathering**. SEPM Special Publication. **Anais...** Tulsa: [s.n.] , 1980

MAITRE, R. W. LE (ED.). **Igneous rocks- A classification and glossary of terms**. Cambridge: Cambridge University Press, 2002. p. 236

MARS, J. C.; ROWAN, L. C. ASTER spectral analysis and lithologic mapping of the Khanneshin carbonatite volcano, Afghanistan. **Geosphere**, v. 7, n. 1, p. 276–289, 31 jan 2011.

MISI, A.; KAUFMAN, A. J.; AZMY, K.; *et al.* Neoproterozoic successions of the Sao Francisco Craton, Brazil: the Bambui, Una, Vazante and Vaza Barris/Miaba groups and their glaciogenic deposits. **Geological Society, London, Memoirs**, v. 36, n. 1, p. 509–522, 30 nov 2011.

MORBIDELLI, L.; GOMES, C. B.; BECCALUVA, L.; *et al.* Mineralogical , petrological and geochemical aspects of alkaline and alkaline-carbonatite associations from Brazil. **Earth-Science Reviews**, v. 39, p. 135–168, 1995.

MUNDT, J. T.; STREUKER, D. R.; GLENN, N. F. **Partial Unmixing of Hyperspectral Imagery: Theory and Methods**. ASPRS Annual Conference. **Anais...** Tampa: [s.n.] , 2007

NOGUEIRA, G. M. DOS S. **Enquadramento Litoestratigráfico, Sedimentologia e Evolução Geoquímica do Depósito Fosfático de Lagamar, MG-Formação Vazante - Proterozoico Médio**. [S.I.]: Universidade de Brasília, 1993.

OLIVEIRA, S. M. B. DE; IMBERNON, R. A. L. Weathering alteration and related REE concentration in the Catalão I carbonatite complex , central Brazil. **Journal of South American Earth Sciences**, v. 11, n. 4, p. 379–388, 1998.

PABÓN, R. E. C.; SOUZA FILHO, C. R. DE. **Identificação de solos impregnados com hidrocarbonetos a partir da espectroscopia de reflectancia e espectroscopia de imageamento**. Anais XV Simpósio Brasileiro de Sensoriamento Remoto2. **Anais...** Curitiba: INPE. , 2011

PAN, Y.; FLEET, M. E. Compositions of the Apatite Minerals. In: HUGHES, J. M.; RAKOVAN, J.; KOHN, M. J. (Eds.). **PHOSPHATES Geochemical, geobiological, and materials importance**. [S.I: s.n.], 2002. p. 13–49.

PEREIRA, V. P. **Alteração no Maciço Alcalino-Carbonatítico de Catalão I**. [S.I.]: Unversidade Federal do Rio Grande do Sul, 1995.

PICCOLI, P. M.; CANDELA, P. A. Apatite in Igneous Systems. In: RAKOVAN, J.; HUGHES, J. M.; KOHN, M. J. (Eds.). **PHOSPHATES Geochemical, geobiological, and materials importance**. [S.I: s.n.], 2002. p. 257–292.

PIMENTEL, M. M.; JOST, H.; FUCK, R. A. O embasamento da Faixa Brasília e o Arco Magmático de Goiás. **Geologia do Continente Sul-Americano: Evolução da obra de Fernando Flávio Marquez de Almeida2**. [S.I: s.n.], 2004. p. 355–370.

REDDY, B. J.; FROST, R. L.; PALMER, S. J. A near-infrared spectroscopic study of the phosphate mineral pyromorphite $Pb_5(PO_4)_3Cl$. **Spectrochimica acta. Part A, Molecular and biomolecular spectroscopy**, v. 71, n. 2, p. 430–5, 15 nov 2008.

RIBEIRO, C. C. **Geologia, Geometalurgia, Controles e Gênese dos depósitos de fósforo, terras raras e titânio do Complexo Carbonatítico Catalão I, GO**. [S.I.]: Universidade de Brasília, 2008.

RIBEIRO, C. C.; GASPAR, J. C.; BROD, J. A. **Controle e Gênese dos depósitos de monazita no Complexo Carbonatítico Catalão I**. I Simpósio Brasileiro de Metalogenia. **Anais...** Gramado: [s.n.] , 2005

ROCHA ARAUJO, P. R. DA. **Les phosphorites d'âge protérozoïque moyen de Rocinha (Minas Gerais, Bresil). Genèse et evolution d'un gisement de phosphate tectonisé et metamorphisé au Brésilien (~600 Ma)**. [S.I.]: Université Aix-Marseille III, 1988.

ROCHA ARAUJO, P. R. DA; FLICOTEAUX, R.; PARRON, C.; TROMPETTE, R. Phosphorites of Rocinha Mine Patos de Minas (Minas Gerais , Brazil) : Genesis and Evolution of a Middle

Proterozoic Deposit Tectonized by the Brasiliano Orogeny. **Economic Geology**, v. 87, p. 332–351, 1992.

ROWAN, L. C.; BOWERS, T. L.; CROWLEY, J. K.; *et al.* Analysis of Airborne Visible-Infrared Imaging Spectrometer (AVIRIS) Data of the Iron Hill, Colorado, Carbonatite-Alkalic Igneous Complex. **Economic Geology**, v. 90, p. 1966–1982, 1995.

ROWAN, L. C.; KINGSTON, M. J.; CROWLEY, J. K. Spectral Reflectance of Carbonatites and Related Alkalic Igneous Rocks: Selected Samples from Four North American Localities. **Economic Geology**, v. 81, p. 857–871, 1986.

ROY, R.; CASSARD, D.; COBBOLD, P. R.; *et al.* Predictive mapping for copper–gold magmatic-hydrothermal systems in NW Argentina: Use of a regional-scale GIS, application of an expert-guided data-driven approach, and comparison with results from a continental-scale GIS. **Ore Geology Reviews**, v. 29, n. 3-4, p. 260–286, nov 2006.

RUFF, S. W.; CHRISTENSEN, P. R.; BARBERA, P. W.; ANDERSON, D. L. Quantitative thermal emission spectroscopy of mineral: A laboratory technique for measurement and calibration. **Journal of Geophysical Research**, v. 102, n. B7, p. 14899–14913, 1997.

SANCHES, A. L.; MISI, A.; KAUFMAN, A. J.; AZMY, K. As sucessões carbonáticas neoproterozóicas do Cráton do São Francisco e os depósitos de fosfato: correlações e fosfogênese. **Revista Brasileira de Geociências**, v. 37, p. 182–194, 2007.

SANTANA, R. O. **Estratigrafia, geoquímica e isótopos de C, O, e Sr do Grupo Bambuí a leste da Falha de São Domingos, NE de Minas Gerais**. [S.l.]: Universidade de Brasília, 2011.

SENNA, J. **Caracterização de Argilas de Utilização na Indústria Cerâmica por Espectroscopia de Reflectância**. [S.l.]: Universidade Estadual de Campinas, 2003.

SENNA, J. **Caracterização Espectro-Mineralógica e Aspectos sobre a Gênese de Matérias-Primas Cerâmicas Clássicas do Brasil: Estudos de Caso em Depósitos de Pirofilita, Talco e Caulinita**. [S.l.]: Universidade Estadual de Campinas, 2008.

SONOKI, I. K.; GARDA, G. M. Idades K-Ar de rochas alcalinas do Brasil Meridional e Paraguai Oriental. Compilação e adaptação às novas constantes de decaimento. **Boletim Instituto de Geociencias Universidade de São Paulo**, v. 19, p. 63–85, 1988.

SOUBIÈS, F.; MELFI, A. J.; AUTEFAGE, F. Comportamento Geoquímico dos Elementos Terras Raras nos alteritos da jazida de fosfato e titânio de Tapira (Minas Gerais, Brasil): a importância dos fosfatos. **Revista Brasileira de Geociências**, v. 21, n. 1, p. 3–16, 1991.

SOUZA, N. P. DE. **Espectrorradiometria em Depósito de fosfato magmatogenico: aplicação para o Depósito de Catalão I - GO**. [S.l.]: Universidade Federal da Bahia, 2009.

TASSINARI, M. M. L.; KAHN, H.; RATTI, G. Process mineralogy studies of Corrego do Garimpo REE ore, catalao-I alkaline complex, Goiás, Brazil. **Minerals Engineering**, v. 14, n. 12, p. 1609–1617, dez 2001.

TEXEIRA, R. DE A. **Avaliação espectral de Depósitos de Fosfatos utilizando imagens ASTER nas regiões de Campos Belos e Catalão (GO)**. [S.l.]: Universidade de Brasília, 2011.

TOLEDO, M. C. M. DE. **Mineralogia dos principais fosfatos do maciço alcalino carbonatítico de Catalão I (GO) e sua evolução no perfil laterítico**. [S.l.]: Universidade de São Paulo, 1999.

TOLEDO, M. C. M. DE; FERRARI, V. C.; NETO, A. A.; *et al.* Fosfatos aluminosos com Ferro do Grupo da Crandallita nas coberturas lateríticas de Catalão I, Juquiá e Tapira (Brasil) e Chirigué (Paraguai). **Revista Brasileira de Geociências**, v. 32, n. 4, p. 393–406, 2002.

TOLEDO, M. C. M. DE; LENHARO, S. L. R.; FERRARI, V. C.; *et al.* The compositional evolution of apatite in the weathering profile of the Catalão I Alkaline-Carbonatitic Complex, Goiás, Brazil. **The Canadian Mineralogist**, v. 42, p. 1139–1158, 2004.

TOLEDO, M. C. M. DE; OLIVEIRA, S. M. B. DE; FONTAN, F.; FERRARI, V. C.; PARSEVAL, P. DE. Mineralogia, Morfologia e Cristalquímica da Monazita de Catalão I (GO, Brasil). **Revista Brasileira de Geociências**, v. 34, n. 1, p. 135–146, 2004.

TORRES, M. G. **Composição química superficial e nanotopográfica da apatita do Proto-minério da Mina do Barreiro**. [S.l.]: Universidade de Brasília, 2008.

U.S. GEOLOGICAL SURVEY (USGS). **Mineral Commodity Summaries 2010. Office**. [S.l.: s.n.], 2010

VALARELLI, J. V. **O minério de Nb,Ti e terras raras de Catalão, GO**. [S.l.]: Universidade de São Paulo, 1971.

VALERIANO, C. DE M.; DARDENNE, M. A.; FONSECA, M. A.; SIMÕES, L. S. A.; SEER, H. J. A. Evolução Tectônica da Faixa Brasília. **Geologia do Continente Sul-Americano: Evolução da obra de Fernando Flávio Marquez de Almeida**. [S.l.: s.n.], 2004. p. 575–592.

VAZ DE MELLO, M. T. **Depósitos minerais associados ao complexo alcalino carbonático de Tapira (MG)**. . Belo Horizonte: [s.n.], 1983

WOOLLEY, A. R.; KEMPE, D. R. C. Carbonatites: nomenclature, average chemical compositions, and element distribution. In: BELL, K. (Ed.). **Carbonatites. Genesis and evolution**. London: Unwin-Hyman, 1989. p. 1–14.

WOOLLEY, A. R.; KJARSGAARD, B. A. Paragenetic Types of Carbonatite As Indicated By the Diversity and Relative Abundances of Associated Silicate Rocks: Evidence From a Global Database. **The Canadian Mineralogist**, v. 46, n. 4, p. 741–752, 1 ago 2008.

YEGOROV, L. S. Phoscorites from the Maymecha-Kotuy ijolite-carbonatite association. **International Geological Review**, v. 35, p. 346–358, 1993.

Capítulo II: Contexto Geológico

2.1 Introdução

Os diversos usos dos fosfatos como insumo na indústria de fertilizantes, na indústria biomédica, nas aplicações em cerâmicas de alta tecnologia e como mineral de interesse científico (pelas relações geocronológicas e geoquímicas inerentes a sua formação), são tópicos extensivamente abordados na literatura.

O papel do fósforo nos ciclos geoquímicos dos elementos biófilos tem sido discutido e analisado em revisões especiais (FILIPPELLI, 2002, 2008), destacando-se a importância e delicado balanço entre a formação natural de fosfatos primários e a complexidade dos processos que permitem que os fosfatos não catalisados sejam depositados em sequências marinhas (FÖLLMI, 1996).

É amplamente aceito na literatura que a estrutura básica do principal fosfato, a apatita ($A_5(XO_4)_3Z$ (onde $A=[Ca^{2+}, Sr^{2+}, Pb^{2+}, Ba^{2+}, Mg^{2+}, Mn^{2+}, Fe^{2+}, ETR^{3+}, Eu^{2+}, Cd^{2+}, Na^+]$; $X=[P^{5+}, Si^{4+}, S^{6+}, As^{5+}, V^{5+}]$ e $Z=[Cl^-, F^-, OH^-]$) (PICCOLI & CANDELA, 2002), originada primariamente em rochas ígneas, sofre várias mudanças composicionais até chegar as bacias marinhas e depositar-se nas sequências fosforíticas sedimentares (KNUDSEN & GUNTER, 2002).

As rochas com grande afinidade pelos carbonatos (sejam biogênicas, sedimentares, metamórficas ou ígneas) são responsáveis por importantes acúmulos anômalos de fósforo. Porém, as assembléias minerais nas quais se hospedam os fosfatos mudam substancialmente, dependendo do ambiente geológico de concentração. Assim, o contexto geológico das rochas hospedeiras de mineralizações de fosfatos deve ser explicado separadamente para melhor entendimento sobre quais minerais podem ser tomados como guias em programas prospectivos.

Neste capítulo são definidos os contextos geológicos dos depósitos de Catalão I (GO), Tapira, Rocinha e Lagamar (MG). Apresenta-se, primeiramente, uma síntese do sistema de classificação dos carbonatitos, visando proporcionar ao leitor informações sobre esses litotipos no cenário mundial de recursos fosfáticos. Em seguida, aborda-se

aspectos gerais da geologia da Província Ígnea Alto Paranaíba (APIP) e da Faixa de Dobramentos Brasília (FDB), onde estão contidos os depósitos estudados nesta pesquisa.

2.2 Os carbonatitos: Generalidades e classificação

Os carbonatitos são rochas ígneas ricas em minerais carbonáticos (>50% do total modal; STRECKEISEN, 1980). São de grande importância econômica devido às concentrações de Nb, P, ETR, Ti, F, entre outros elementos.

O interesse mundial nos carbonatitos tem aumentado desde a década de 80, visto a crescente demanda por elementos raros hospedados nessas rochas. Os carbonatitos estão entre as rochas terrestres que contém o maior enriquecimento em ETR(WOOLLEY & KEMPE, 1989).

A ocorrência de carbonatitos no mundo é pouco expressiva quando comparada com outros litotipos mais comuns (e.g., rochas basálticas, graníticas ou sedimentares). Estimativas atuais colocam o volume de carbonatitos em torno de 3% da cobertura litosférica terrestre (WOOLLEY & KJARSGAARD, 2008). Embora seu volume seja pouco expressivo, acredita-se que as composições químicas próprias destes corpos ígneos, ricos em elementos incompatíveis e ETR, reflitam características particulares do manto litosférico.

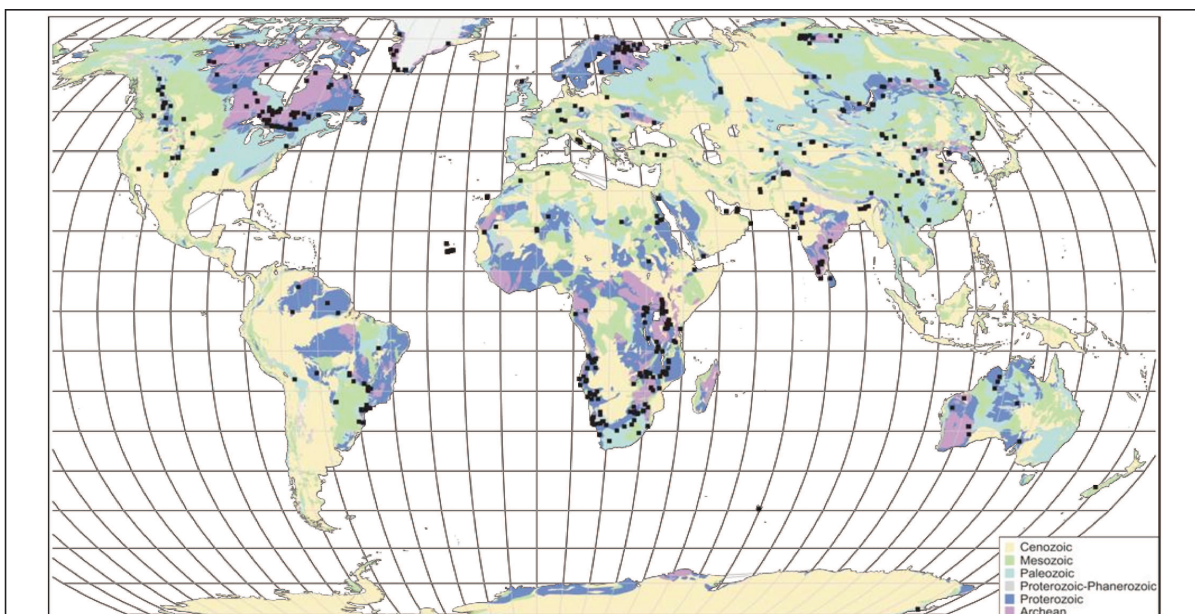


Fig. 2. 1 Ocorrências carbonatíticas mundiais segundo WOOLLEY & KJARSGAARD(2008)

Vários complexos carbonatíticos são considerados depósitos de classe mundial para diversas *commodities*. As províncias de Kola, Alto Paranaíba e Phalaborwa contêm importantes reservas de fosfatos magmáticos. A Província Ígnea do Alto Paranaíba, por sua vez, contêm reservas de Nb consideradas inexauríveis (BARBOSA *et al.*, 2012). Os complexos de Bayan Obo (China) e Mountain Pass (EUA) são os principais provedores mundiais de minérios de ETR provenientes de carbonatitos.

A maior parte dos carbonatitos do mundo encontra-se relacionado à grandes estruturas tectônicas intracontinentais (e.g. Província Carbonatítica de Ontario, Canadá; Província ígnea do Alto Paranaíba, Brasil; Distrito Powderhorn, Estados Unidos; Distrito Mountain Pass Estados Unidos, Província Kola, Rússia-Finlândia). Os complexos carbonatíticos podem estar relacionados a magmatismo potássico e/ou alcalino (LEBAS, 1987), incluindo rochas ultramáficas e kamafugitos (BARBOSA *et al.*, 2012; BROD *et al.*, 2004; BROD *et al.*, 2005). A mais recente classificação proposta para os carbonatitos (WOOLLEY & KJARSGAARD, 2008) os relaciona às rochas silicáticas ou sem série magmática definida.

O Brasil concentra grande parte dos carbonatitos presentes na América do Sul. Exemplos amplamente citados na literatura são os complexos de Araxá (MG), Salitre I (MG), Jacupiranga (SP), Anitápolis (SC), Ángico dos Dias (BA) e Mutum (AM). Um dos problemas para a geologia brasileira são as controvérsias geradas pela adoção de uma classificação relacionada à natureza química dos carbonatitos. Os complexos da Província Ígnea do Alto Paranaíba possuem séries foscoríticas associadas e há dificuldade de classificá-los no esquema proposto por WOOLLEY & KJARSGAARD (2008).

2.2.1 Classificação dos Carbonatitos: Noções básicas e nomenclatura

A primeira classificação universal dos carbonatitos, proposta por HEINRICH (1967), foi baseada principalmente na presença majoritária de carbonatos calcínicos, magnesianos ou férricos e o tamanho de grão dos carbonatos. Tal classificação mostrava problemas para inclusão de rochas extrusivas. WOOLLEY & KEMPE (1989) modificaram uma proposta de STREICKEISEN (1980) e estabeleceram o seguinte:

- Os carbonatitos são rochas ígneas que podem ser extrusivas ou intrusivas e que tem mais de 50% em volume de minerais carbonáticos.
- Distinguem-se as seguintes classes de carbonatitos:

- Carbonatitos calcíticos (sovitos, de granulação grossa; alvikito, de granulação média a fina)
 - Carbonatito dolomítico (beforsito)
 - Ferrocarbonatito (composto essencialmente de carbonatos ricos em Fe)
 - Natrocarbonatito (essencialmente composta de carbonatos de Na-K-Ca)
- Carbonatitos contendo vários tipos de minerais carbonáticos (e.g., calcita e dolomita) são indicados por prefixos de acordo com as regras estabelecidas para composição de rochas nos limites 10%-50%-90%.
 - Rochas ígneas com porcentagem inferior a 10% de minerais carbonáticos podem ser chamadas ijolitos portadores de calcita, peridotitos portadores de dolomita, etc.
 - Rochas ígneas com porcentagem de carbonatos entre 10-50% são chamadas de ijolito calcítico, peridotito dolomítico, etc.
 - Os termos melanocrático e/ou leucocrático devem ser descartados.
 - Conteúdos característicos de outros minerais devem ser mencionados como sufixos, p.e. carbonatito apatítico-piroclórico, carbonatito magnetítico-dolomítico, etc.

A classificação descrita em epígrafe teve o mérito de unificar e clarificar lacunas de conhecimento. Entretanto, apresenta as seguintes dificuldades :

- Muitos carbonatitos contêm pelo menos duas espécies de carbonatos que nem sempre são de fácil distinção por mostrarem texturas de exsolução (*cf.* HEINRICH 1966).
- Ainda não existem evidências sobre a existência de uma série de solução sólida que envolva a dolomita, a dolomita com ferro e a ankerita, com amplos intervalos de razões Fe:Mg (WOLLEY & KEMPE, 1989).
- Siderita e siderita magnésiana (breunnerita) têm sido reportadas em carbonatitos ricos em ferro (SAMOILOV 1977- KAPUSTIN 1980 apud WOLLEY & KEMPE (1989).
- Texturas em vários carbonatitos ricos em Fe parecem indicar a presença prévia de carbonatos ricos em Fe, os quais foram alterados a carbonatos

empobrecidos em Fe + óxidos de Fe durante o processo de assimilação magmática.

- A magnesita também tem sido reportada em carbonatitos (KAPUSTIN, 1980 apud WOLLEY & KEMPE, 1989).

LEMAITRE (2002) propõe uma classificação simplificada, também baseada no conteúdo de carbonatos predominantes, mas que exclui carbonatitos com teores de SiO₂ superiores a 20%. Segundo o autor, acima desse limiar, a rocha deve ser denominada de sílico-carbonatito. A classificação é apresentada na Tabela 2.1.

Tab. 2. 1 Classificação Simplificada de Carbonatitos, segundo LE MAITRE (2002)

Carbonato principal	Nome da Rocha	Nome tradicional
Calcita	Calcita-Carbonatito	Sovito (Grão grosso) Alvikito (grão fino)
Dolomita	Dolomita-carbonatito	Beforsito
Carbonatos ricos em Fe (ankerita, siderita)	Ferro-carbonatito	
Carbonatos de Na, K e Ca	Natrocronatito	

WOLLEY & KJARSGAARD (2008) propõem uma classificação paragenética dos complexos carbonatíticos com as rochas magmáticas associadas com base em 477 ocorrências das 527 conhecidas mundialmente:

- Carbonatitos associados a melilito (ou melilitolito)
- Carbonatitos associados a nefelinito (ou ijolito)
- Carbonatitos associados a basanitos (ou gabro alcalino)
- Carbonatitos associados a fonolito (ou feldspatóide sienito)
- Carbonatitos associados a traquito (sienito)
- Carbonatitos associados a kimberlito
- Carbonatitos associados a lamprófiros (aikilito, alnoito)
- Carbonatitos isolados.

Mesmo considerando um acervo mundial de carbonatitos e associando-os à rochas alcalinas, esta classificação tem restrições para ser usada na Província Ígnea Alto Paranaíba (APIP). GRASSO (2010) menciona vários problemas decorrentes do seu uso, entre os quais (i) a desconsideração da afinidade geoquímica dos magmas; (ii) a ausência dos kamafugitos e foscritos da classificação elimina litotipos de importância do ponto de vista econômico, tanto no caso brasileiro como no cenário mundial.

Pelo exposto, a classificação que melhor se adapta a APIP é a definida por LE MAITRE (2002), pois engloba litotipos de simples descrição e terminologia.

2.3 Contexto Geológico

As Unidades abordadas neste projeto estão incluídas na Província Ígnea do Alto Paranaíba (APIP; GIBSON *et al.*, 1995) e na Faixa de Dobramentos Brasília (FDB; DARDENNE, 2000; PIMENTEL *et al.*, 2004). Nos tópicos seguintes é apresentada uma síntese das características geológicas mais relevantes da APIP e da FDB.

2.3.1 Província Ígnea do Alto Paranaíba (APIP)

A Província Ígnea do Alto Paranaíba (APIP; ALMEIDA, 1983; GIBSON *et al.*, 1995, Figura 2.2), localiza-se na região do triângulo mineiro em Minas Gerais e no sudeste de Goiás. É limitada a NE pela Bacia do Paraná e a SE pelo Cráton do São Francisco. Inclui rochas alcalinas (kamafugíticas, kimberlíticas e carbonatíticas) que ocorrem sob a forma de diques, pipes, plugs, diatremas, derrames de lavas, depósitos piroclásticos e grandes complexos plutônicos (ALMEIDA, 1983).

A APIP estende-se por aproximadamente 250 Km no sentido NW-SE, desde o sul de Goiás até o sul de Minas Gerais, incluindo os complexos carbonatíticos alcalinos de Catalão I e II (OLIVEIRA & IMBERNON, 1998; TOLEDO *et al* 2004; CORDEIRO, 2009; RIBEIRO, 2008), Serra Negra e Salitre (GRASSO, 2010; BARBOSA *et al*, 2012), Araxá (TORRES, 2008) e Tapira (BROD, 1999; VAZ DE MELLO, 1983). É considerada uma das maiores províncias alcalinas do mundo (GRASSO 2010), contendo concentrações de P, Nb, ETR, e Ti (BROD *et al*, 2004). Vermiculita e magnetita também são frequentes nos complexos. Os corpos da APIP intrudem rochas metassedimentares neoproterozoicas da Faixa Brasília Meridional (VALERIANO *et al.*, 2004).

A origem do magmatismo predominante na província é motivo de controvérsias na literatura. GIBSON *et al.* (1995) defendem a teoria de que o magmatismo alcalino seria produto da atividade da Pluma Trindade, e que os magmas alcalinos da província refletem características da astenosfera. VANDECAR *et al* (1995), com base em estudos geofísicos, atribuem o magmatismo da província aos efeitos da Pluma Tristão da Cunha, relatando que a pluma ainda estaria em atividade a 600 Km de profundidade.

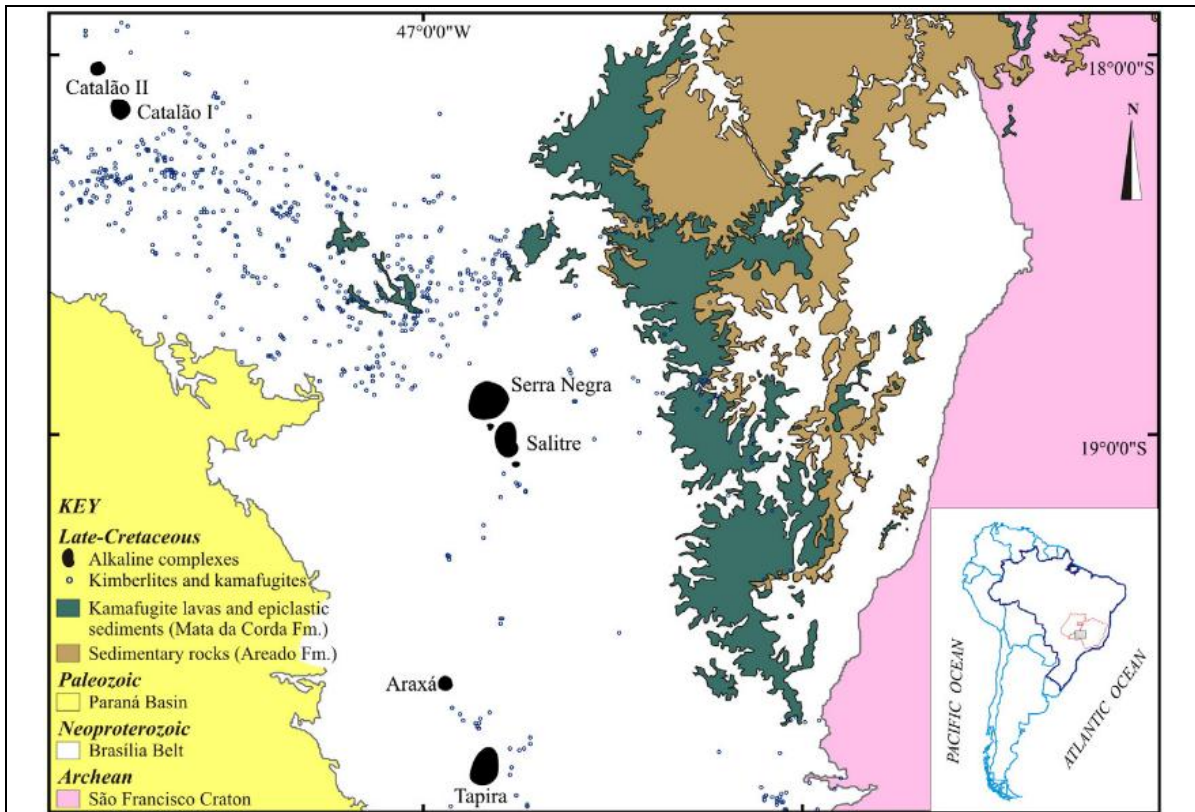


Fig. 2. 2: Esboço geológico da PIAP, segundo Barbosa *et al.* (2012).

COMIN-CHIARAMONTI & GOMES (2004), baseados em informações geoquímicas e isótopos Sm-Nd, Pb-Pb, estabelecem diferenças entre os magmas da APIP com a Pluma Trindade e magmas N-MORB. Estas diferenças indicam fontes magmáticas provenientes de fusão parcial do manto litosférico. Os autores também demonstraram as semelhanças dos complexos carbonatíticos quanto ao conteúdo e tipos de ETR, o que constituiu um referencial importante para a prospecção mineral.

Os complexos carbonatíticos da APIP, sob ação do intemperismo, desenvolveram profundos perfis lateríticos. Processos supergênicos foram responsáveis pela concentração de quantidades excepcionais de P e Nb (OLIVEIRA & IMBERNON, 1998; BROD *et al.*, 2004). Fluoroapatita, vermiculita, magnetita, pirocloro e titanita são minerais comuns a todos os corpos. Já concentrações econômicas diferenciadas correspondem a Ti em Tapira (VAZ DE MELLO, 1997) e Nb e Monazita em Catalão I (TASSINARI *et al.*, 1999; CORDEIRO, 2009).

A APIP hospeda a localidade tipo da série bebedourítica (TRÖGGER 1928, *apud* BROD *et al.*, 2004; BARBOSA *et al.*, 2012) nos complexos de Salitre I e Tapira. A série bebedourítica varia entre *endmembers* de perovskita+magnetita, apatita e diopsídio+olivina. Os complexos de Tapira e Salitre-Serra Negra são considerados equivalentes, com a diferença de que em Serra Negra as intrusões sieníticas são pouco relevantes.

Outras séries importantes são a foscorítica (YEGOROV, 1993), a série carbonatítica (LE MAITRE, 2002), a série kamafugítica (BROD *et al.*, 2005) e a série ijolítica, relacionada a eventos explosivos e de pipes kimberlíticos, abundantes na região.

As rochas da série foscorítica têm variações modais baseadas na apatita, magnetita e olivina (YEGOROV, 1993). Apresenta-se como diques e veios que cortam rochas ultramáficas (clinopiroxenitos, piroxenitos e dunitos) dos complexos pertencentes à APIP. Os foscoritos no Complexo de Catalão I têm um sólido enriquecimento em ETR leves a médios (RIBEIRO, 2008). O mesmo é observado em Araxá (TORRES 2008), com implicações sobre uma possível equivalência desses complexos na APIP. Contudo, os complexos tem suas particularidades. Araxá foi afetado de forma mais pervasiva por eventos hidrotermais (GOMES *et al.*, 1990). Catalão I apresenta efeitos produzidos pelo metassomatismo e auto-metassomatismo que ocorreram no período de mistura de magmas e imiscibilidade magmática (LAPIN, 1982; Hirano (1983) *apud* RIBEIRO, 2008).

2.3.1.1 Complexos Carbonatíticos da APIP

A Província Ígnea do Alto Paranaíba inclui os complexos Catalão I e II, Serra Negra, Salitre I, II e III, Araxá e Tapira, cujas características gerais são apresentadas na tabela 2.1. Dos complexos da APIP, três estão sendo operados para extração de P (Catalão I, Araxá, Tapira), Nb (Catalão I e II, Araxá) e Ti (Tapira). Os complexos Salitre e Serra Negra devem iniciar atividades de aproveitamento e extração econômica a partir de 2014.

Tab. 2. 2: Informações Gerais de Complexos Carbonatíticos selecionados na APIP

Complexo	Forma	Idade (método)	Litotipos	Mineralizações
Serra Negra	Dômica circular de 10 km de diâmetro	(K/Ar) 83.4-83.72 ²	Dunitos Calcita carbonatitos, dolomita carbonatito, bebedouritos, flogopititos ⁴ .	P, Nb, magnetita
Salitre I II III	Distorcida em forma de rin (Salitre I) plugs irregulares (Salitre II e III)	(K/Ar) 86.3 ±6.9 Ma ²	Bebedouritos e rochas feldspáticas, nelsonitos, calcita carbonatitos e dolomita carbonatitos ³	P, Ti, Nb
Araxá	Dômica circular, 5 km de diâmetro	(K/Ar) 88.4±4 Ma ¹	Calcita-carbonatitos e foscoritos que intruem dunitos e piroxenitos. Alta influencia hidrotermal ⁵	P, Nb, ETR,
Tapira	Dômica elipsoidal, 7 km de diâmetro	(K/Ar) 71.2±5.1 Ma ²	Bebedouritos e clinopiroxenitos, carbonatitos, sienitos e wehrlitos ⁶	P, Ti, vermiculita e magnetita
Catalão I	Dômica circular, 6,5 km de diâmetro	(K/Ar) 85±6.9 Ma ¹ 84±4 Ma ²	Dunitos e piroxenitos intrudidos por calcita carbonatitos, foscoritos e flogopititos, nelsonitos, apatititos ⁷	P, Nb, ETR, monazita, magnetita, vermiculita e Ti.

Referências ¹: EBY & MARIANO (1986); ²: SONOKI & GARDA (1988); ³: BROD *et al*, 2004; ⁴: GRASSO (2010); ⁵: TORRES (2008); ⁶: BROD (1999); ⁷: RIBEIRO (2008)

Os complexos de Catalão e Tapira foram objeto deste estudo e serão descritos em maior detalhe a seguir.

2.3.1.2 Complexo Carbonatítico Alcalino de Catalão I

Situa-se a 10 km da cidade de Catalão, sul do estado de Goiás. É acessado pela Rodovia BR-050, a partir de Uberaba. O complexo representa um alto topográfico na planície goiana, com drenagem centrípeta que, junto ao clima tropical, favoreceu a formação de um espesso perfil laterítico. Concentrações de P, Nb, vermiculita e fosfatos secundários aumentam da base para o topo nesse perfil (OLIVEIRA & IMBERNON 1998).

Trata-se de uma intrusão sub-circular, com cerca de 6 km na direção N-S e 5.5 km na direção E-W. É composto por rochas duniticas e piroxenitos que são cortadas por veios e *stocks* calcítico-carbonatíticos, dolomita-carbonatíticos e flogopititos (RIBEIRO, 2008). A cobertura laterítica atinge profundidades de até 200 metros (BROD *et al*, 2004).

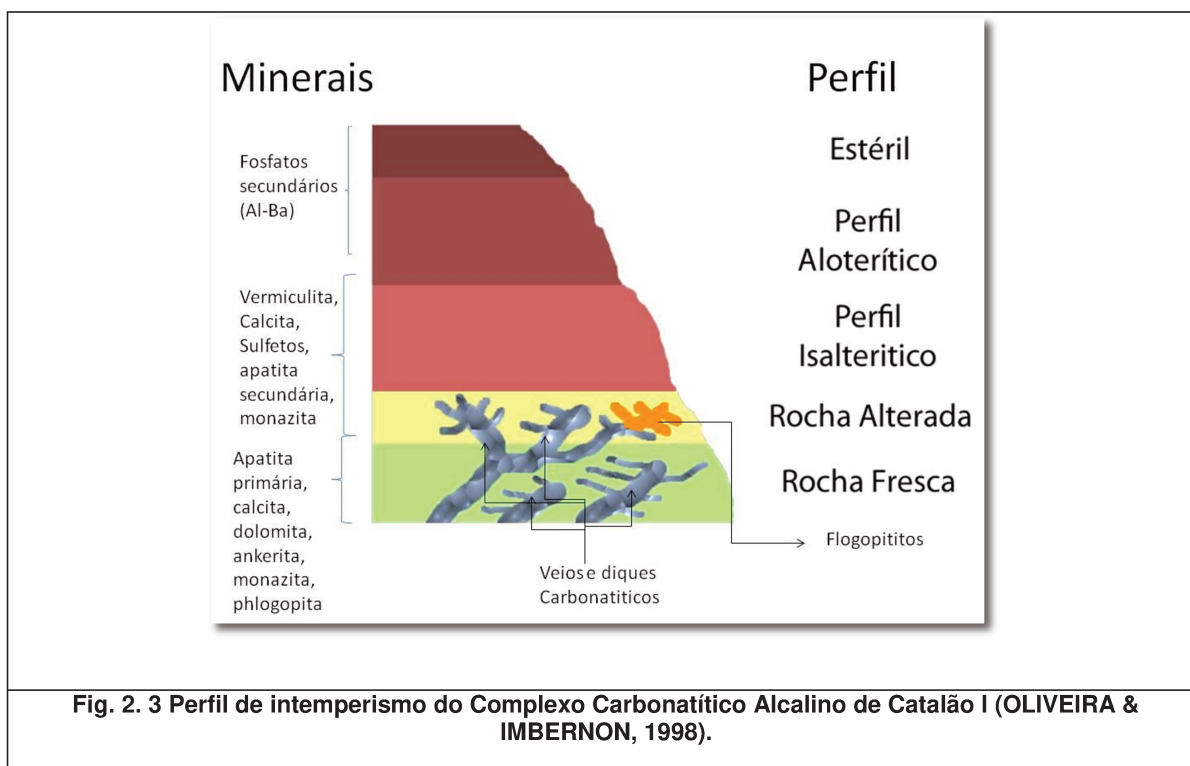
O complexo intrude quartzitos e xistos micáceos do Grupo Araxá (VALERIANO *et al.*, 2011), os quais foram fenitizados, enriquecendo-se em K, Na e Al, com perda de sílica (CARVALHO, 1974).

O primeiro estudo do complexo foi feito por HUSSAK (1894; *apud* RIBEIRO 2008). O autor indicou a afinidade das rochas do complexo com os jacupirangitos e com rochas do Complexo de Ipanema em São Paulo. VALARELLI (1971) constatou a presença de rhabdofânio (baseado em petrografia óptica), monazita e outros fosfatos (usando DRX). CARVALHO (1974) explicou que a estrutura do complexo é a de um núcleo de rochas ígneas, rodeadas por rochas metamórficas do Grupo Araxá, que encontram-se dobradas numa estrutura dômica (o que é corroborado pelo padrão radial da drenagem). O mesmo autor gerou um mapa radiométrico e demonstrou que valores anômalos de Nb, P e Ti apresentam correlação espacial com altos radiométricos; a abundância de monazita nas rochas, por sua vez, apresenta tendência contrária (CARVALHO, 1974).

Devido à importância econômica das concentrações de P, Nb e ETR presentes nas coberturas lateríticas, vários trabalhos foram dedicados ao estudo do comportamento destes elementos no perfil de intemperismo (OLIVEIRA & IMBERNON, 1998; TOLEDO *et al.*, 2004; TOLEDO, 1999). OLIVEIRA & IMBERNON (1998) definem o perfil de intemperismo em cinco horizontes, do topo para base, da seguinte forma:

- Coberturas alóctones: solos transportados de cores vermelha e rosa, com aproximadamente 25 metros de espessura.
- Horizonte aloterítico: material argilo-arenoso amarelo a avermelhado. A homogeneização não permite identificar estruturas rochosas.
- Horizonte isalterítico: nesse horizonte, de 25 m de espessura, é possível reconhecer relictos da estruturas original da rocha, mas a aparência geral é a de um solo homogêneo.
- Rocha alterada: neste horizonte, a estrutura da rocha está quase totalmente preservada. Alterações metassomáticas podem enriquecer os flogopititos em apatita e monazita (TOLEDO, 1999).
- Rocha Fresca: dunitos, piroxenitos, foscoritós e flogopititos, intrudidos por abundantes veios carbonatíticos.

Um esquema do perfil de intemperismo é apresentado na fig. 2.3, na qual são representados horizontes do perfil, os veios e diques que cortam a rocha fresca e parte das rochas alteradas do complexo de Catalão I.



A evolução da apatita no perfil intempérico foi o foco do trabalho de TOLEDO (1999). A autora estabeleceu que a apatita primária do complexo foi transportada hidrotermalmente através dos veios carbonatíticos e foscoríticos, formando bolsões de apatita na rocha alterada que podem atingir concentrações pontuais de até 30% de P_2O_5 . Segundo a autora, a monazita formou-se tardiamente à colocação dos carbonatitos, e de forma contemporânea aos silexitos do perfil isalterítico, com baixa “cristalinidade”, porém sem fugir dos padrões de cela unitária da monazita estudada por HEZEL & ROSS (1966).

Uma comparação entre fosfatos secundários aluminosos dos complexos de Catalão I, Tapira, Juquiá e Chiriguelo (Paraguai), feita por TOLEDO *et al.*, (2002), indicou que o Ba predomina na formação de fosfatos secundários sobre os outros possíveis *endmembers* (Ca, Sr, ETR para a série crandallítica). Nos depósitos de Catalão I e Tapira, os fosfatos secundários, embora enriquecidos em ETR, não conseguem hospedá-los estavelmente em sua estrutura cristalina.

A monazita do complexo de Catalão I foi estudada com o intuito de ser recuperada industrialmente por TASSINARI *et al.* (2001). Os autores mencionam a dificuldade de manter estável a estrutura da monazita no processo industrial durante o processo de *leaching*, dificultando a concentração industrial do mineral em granulometria grossa. Porém, quando o minério monazítico (seja silexítico, nelsonítico, intermediário ou apatítico) é finamente moído, até atingir tamanhos de grão finos, pode-se concentrar cristais monazíticos. Esses cristais, por sua vez, podem conter até 20% de óxidos de ETR.

2.3.1.2 Complexo Carbonatítico Alcalino de Tapira

É o mais meridional de todos os complexos da APIP. Cobre uma área de aproximadamente 35 km². Intrude rochas do Grupo Canastra (BROD *et al.*, 2004). O complexo contém bebedouritos, clinopiroxenitos, carbonatitos, wehrlitos, flogopita picritos e, subordinadamente, melilitolitos e flogopita picritos (BROD *et al.*, 1999).

VAZ DE MELLO (1983) identificou várias zonas lateríticas, do topo para base:

- Um zona estéril também chamada latossólica, que atinge até vinte metros de profundidade. Apresenta caulinita, gibbsita, goethita, hematita e fosfatos aluminosos secundários como minerais principais.
- A zona subjacente correspondente a zona rica em Ti, tem uma profundidade aproximada de 40 metros. As estruturas rochosas podem ser parcialmente identificadas nesse horizonte. Os minerais principais são os mesmos do horizonte latossólico, porém o anatásio é mais amarelo e os minerais em geral tem maior tamanho de grão. A maioria das micas desta zona foram transformadas em vermiculita. Alguma perovskita é também observada.
- A terceira zona é rica em Ti-P. Compreende rochas com texturas e estruturas bem preservadas. Bolsões de apatita primária, com dissolução parcial, podem ser identificados, usualmente ao lado de perovskita alterada a anatásio verde. As micas aparecem alteradas para vermiculita e a magnetita rica em Ti é alterada para maghemita e hematita. Desta zona provém a maioria do minério do complexo.
- A zona laterítica mais rica em P possui 80 metros, até atingir a rocha fresca. Nessa zona são observados piroxenitos e peridotitos pouco

alterados por intemperismo químico, contendo cristais de perovskita sem alteração. A apatita é o mineral principal. Magnetita rica em Ti, diopsídio, olivina e flogopita são os minerais subordinados.

BROD (1999) e BROD *et al.* (2004) definem duas unidades de bebedouritos. Os bebedouritos propriamente ditos (B1) são rochas com quantidades variáveis de diopsídio, flogopita, perovskita, apatita, magnetita, melanita e titanita. A segunda classe de bebedouritos definidos (B2) são apatita-clinopiroxenitos de grão mais fino que os bebedouritos B1 (BROD, 1999).

Os carbonatitos do Complexo de Tapira apresentam-se em cinco corpos intrusivos e podem variar de composição de calcita-carbonatitos a calcita-dolomita-carbonatitos. Segundo BROD (1999) e BROD *et al.* (2005) essas variações representam estágios de evolução do magma carbonatítico. Os minerais acessórios observados nesses carbonatitos são apatita, magnetita, flogopita e barita.

SOUBIÈS *et al.*, (1991) definiram o comportamento geoquímico dos ETR dos fosfatos secundários do complexo. Identificaram a perovskita como a principal fonte de ETR no perfil intempérico e que esses elementos são reabsorvidos por fosfatos aluminosos. BRIGATTI *et al.* (2004) indicaram a afinidade das apatitas em favorecer substituições de ETR (principalmente La e Ce) por Ca. BROD *et al.* (2005) exploraram dados petrológicos de minerais do grupo do espinélio presentes em três das cinco possíveis intrusões carbonatíticas do complexo.

2.3.2 Faixa de Dobramentos Brasília (FDB)

A FDB representa a acreção de terrenos neoproterozoicos em escamas de empurrões, orientados em duas vergências principais: uma mais setentrional, de orientação NE (Faixa Brasília Setentrional, FBS) e outra meridional, de orientação NW (Faixa Brasília Meridional, FBM). Essas faixas se estendem por aproximadamente 1100 Km (VALERIANO *et al.*, 2004) e são divididas pela Megaflexura dos Pireneus (COSTA & ANGIERAS, 1971 *apud* Valeriano *et al.*, 2004).

A FDB foi estruturada pela Orogênese Brasileira, durante o Neoproteróico, comprimindo pacotes rochosos metamorfisados no fácies xisto verde (Fuck, 1994; Dardenne, 2000). Concentra em seu registro estratigráfico uma série de jazidas importantes, principalmente de Zn-Pb (Morro Agudo), Au (Morro de Ouro) e P (Rocinha, Lagamar) (DARDENNE & SCHOBENHAUS, 2001). Na FBM ocorrem depósitos de

fosforitos metassedimentares, cuja posição estratigráfica é controversa. Alguns autores os relacionam ao Grupo Vazante (DARDENNE & SCHOBENHAUS, 2001); outros na parte superior do Grupo Bambuí (DE LIMA, 2011; SANCHES, 2012)

2.3.2.1 Grupo Vazante

O Grupo Vazante compreende sequências estromatolíticas com presença de argilas e ritmitos, estendidos por quase 300 Km na direção N-S, sobrepostos a oeste da FBM entre as cidades de Unaí e Coromandel (DARDENNE, 2000). As rochas do grupo localizadas na porção leste experimentaram metamorfismo de fácies xisto verde, estando bem preservadas. Porém, a oeste, ocorrem pacotes fortemente deformados sob fácies anfíbolito ou granulito (MISI *et al.* 2011).

As correlações baseadas em estromatolitos colunares favorecem uma equivalência com o Grupo Paranoá, enquanto os diamictitos da base indicam uma correlação com o Grupo Bambuí ou o Grupo Jequitai (SANCHES *et al.*, 2007).

A litoestratigrafia dos fosforitos foi especificada por DARDENNE (1997), que descreveu sete unidades dentro do Grupo Vazante:

- **Formação Santo Antônio do Bonito:** considerada como basal, é constituída por bancos de quartzitos brancos, por vezes conglomeráticos, intercalados com níveis pelíticos ardosianos. Gonzaga & Thompkins (1991; *apud* DARDENNE *et al.*, 1997) descrevem para a região de Coromandel, perto dos rios Santo Antônio do Bonito e Santo Inácio, a presença de diamictitos com matriz pelítica ligeiramente fosfatada. Os intervalos fosfáticos são compostos de sequências argilosas e finos níveis de fosfarenitos ricos em intraclastos e *pellets*, sendo denominados intervalos fosfáticos inferiores.
- **Formação Rocinha:** é composta por três sequências. Uma primeira, basal, consiste de pacotes de metarritmitos representados por intercalações centimétricas e decimétricas de quartzitos e ardósias, com coloração amarelada e avermelhada. Tem contato transicional com a Formação Santo Antônio do Bonito. Uma segunda sequência, intermediária, compreende um espesso pacote de ardósias e metassiltitos regularmente intercalados, com coloração amarelada e avermelhada. Em direção ao contato com a unidade fosfatada superior, observa-se uma zona de transição representada por ardósias cinza escuro carbonáticas, piritosas, com finas laminações fosfáticas. Sondagens da CPRM registraram,

adicionalmente, a presença de lentes de dolomitos rosados e de paraconglomerados. A mina Rocinha é desenvolvida nessa unidade. A sequência superior exibe rochas com cor essencialmente amarelada, apresenta um aspecto bandado característico, evidenciado pela presença de níveis de material cinza escuro, maciço e resistente, rico em fosfato, alternado com níveis pelíticos amarelados. Esta sequência fosfatada, intensamente microdobrada, é relativamente contínua, principalmente na base, com espessura aflorante aproximada de 250m no depósito de Rocinha. Para o topo, a rocha fosfática encontra-se na forma de lentes nas ardósias amareladas estéreis ou pobres em fosfato ($P_2O_5 < 5\%$), caracterizadas pela presença de glauconita (DA ROCHA ARAÚJO, 1988; DA ROCHA ARAÚJO *et al.*, 1992). Este intervalo fosfatado é explorado na mina de Lagamar (DARDENNE, 1998).

- **Formação Lagamar - Membro Arrependido:** foi subdividida em duas sub-unidades, E₁ e E₂, em função das variações laterais de fácies observadas entre os depósitos de Rocinha e Lagamar. A E₁ ocorre na área de Rocinha, onde o depósito de fosfato é sobreposto por um espesso pacote de ardósias vermelhas, argilosas, totalmente estéreis, mostrando um aspecto relativamente homogêneo nos afloramentos visíveis no campo. A E₂ distribui-se lateralmente em direção a jazida de Lagamar, sendo caracterizada por uma sedimentação rítmica de fosfarenitos cinza escuro e pelitos amarelados.
- **Formação Lagamar -Membro Sumidouro:** composta por metarritmitos, onde alternam-se níveis de ardósias, metassiltitos e quartzitos. Em direção ao topo, intercalam-se níveis de conglomerados, descritos sob a denominação “Conglomerado do Córrego Arrependido” (DARDENNE *et al.*, 1989). Os seixos dentro do conglomerado são de quartzitos, metassiltitos, quartzo e calcário preto.
- **Formação Serra do Garrote:** sobrepõe-se a unidade anterior, tendo sido descrita sob a denominação de Membro Lagamar (DARDENNE *et al.*, 1989). É caracterizada pela sedimentação carbonática na forma de calcário preto, dolomito cinza, doloarenito, dolorudito e, principalmente, biohermas cor de rosa e bege claro (com esteiras plano-paralelas), oncolitos e estromatolitos colunares (com laminações convexas e cônicas) pertencentes aos gêneros *Kussiella*, *Colonnella*, *Conophyton* e *Jacutophyton*. Esses biohermas interdigitam-se lateralmente e verticalmente à espessa sequência pelítica denominada Membro Serra do Garrote, que se sotopõe aos dolomitos da região de Vazante-Paracatu. É representada por

ardósias cinza escuro, às vezes carbonosas e/ou carbonáticas, alternando-se para cores amareladas e avermelhadas em superfície.

2.3.2.2 Grupo Bambuí

O Grupo Bambuí sempre atraiu interesse da comunidade geológica brasileira visto seu potencial para depósitos de Zn-Pb e P. Foi definido formalmente por COSTA & BRANCO(1961) e reformulado por DARDENNE (1978). Continua sendo objeto de pesquisa visando um melhor estabelecimento dos seus limites com o Grupo Vazante, sua relação com os depósitos de P das jazidas de Lagamar e Rocinha (MISI *et al.*, 2011), assim como a determinação de suas idades máximas e mínimas de deposição ao longo da margem ocidental do Cráton São Francisco (LIMA, 2011; SANTANA, 2011).

O Grupo Bambuí consiste, da base para o topo, das Formações Jequitaí, Sete Lagoas, Serra de Santa Helena, Lagoa de Jacaré, Serra da Saudade e Três Marias. O Grupo foi depositado em uma bacia antepaís (ALKMIM *et al.*, 1993), envolvendo uma série de eventos glaciais que favoreceram a sedimentação de material fosfático de margens plataformais (LIMA, 2011).

Adotando-se a divisão de DARDENNE (1978), combinada às atualizações de LIMA (2005; 2011), as unidades do Grupo podem ser definidas da seguinte forma:

- **Formação Jequitaí:** representa uma série glacial graodecrescente, iniciada por diamictitos e paraconglomerados na base e arenitos e pelitos no topo.
- **Formação Sete Lagoas:** consiste de uma unidade pelito-carbonática, que varia de siltitos, calcários estromatólitos e dolomitos formados em ambientes intramaré, inframaré e plataformas carbonáticas.
- **Formação Serra de Santa Helena:** composta por seqüências siliciclásticas, silte-argilosas, associadas a fluxos gravitacionais (LIMA, 2005).
- **Formação Lagoa de Jacaré:** exhibe depósitos carbonáticos retrabalhados, com calcarenitos oolíticos e oncolíticos, calcirruditos e dolorruditos e, subordinadamente, carbonatos bioconstruídos (LIMA, 2005).
- **Formação Serra da Saudade:** unidade com ocorrência restrita, formada por rochas siliciclásticas com seqüências finas de siltitos, arenitos-grauvacas e pelitos esverdeados (LIMA, 2011).

- **Formação Três Marias:** representa a transição dos sistemas marinho a continental do Grupo, com fácies prodeltaica e fluvial. É composta por arenitos arcossianos médios a finos, com estratificações cruzadas *hummocky*, siltitos e ritmitos interlaminados, além de conglomerados dispersos na coluna estratigráfica (LIMA, 2011)

2.4 Referências Bibliográficas

- ALKMIM, F. F.; BRITO NEVES, B. B.; ALVES, J. A. C. Arcabouço tectônico do Cráton do São Francisco - uma revisão. In: DOMINGUEZ, J. M. L.; MISI, A. (Eds.). **O Cráton de São Francisco**. Salvador: SBG, 1993. p. 45–62.
- ALMEIDA, F. F. . Relações tectônicas das rochas alcalinas da região meridional da Plataforma Sul-Americana. **Revista Brasileira de Geociências**, v. 13, n. 3, p. 139–158, 1983.
- BARBOSA, E. S. R.; BROD, J. A.; JUNQUEIRA-BROD, T. C., DANTAS, E.L., CORDEIRO, P.F DE O., GOMIDE, C. S.: Bebedourite from its type area (Salitre I complex): A key petrogenetic series in the Late-Cretaceous Alto Paranaíba kamafugite–carbonatite–phoscorite association, Central Brazil. **Lithos**, v. 144-145, p. 56–72, jul 2012.
- BRIGATTI, M. F.; Malferrari, D.; Medici, L.; OTTOLINI, L.; POPPI, L. Crystal chemistry of apatites from the Tapira carbonatite complex, Brazil. **European Journal of Mineralogy**, v. 16, n. 4, p. 677–685, 1 ago 2004.
- BROD, J. A.; GASPAR, J. C.; DINIZ-PINTO, H. S.; JUNQUEIRA-BROD, T. C. Spinel chemistry and petrogenetic processes in the Tapira Alkaline-Carbonatite Complex , Minas Gerais , Brazil. **Revista Brasileira de Geociências**, v. 35, n. 1, p. 23–32, 2005.
- BROD, J. A.; RIBEIRO, C. C.; GASPAR, J. C., JUNQUEIRA-BROD, T.C., BARBOSA, E.S.R., RIFFEL, B.F., SILVA, J. F., Ferrari, A.J. D: Geologia e mineralizações dos complexos alcalino-carbonatíticos da Província Ignea do Alto Paranaíba. **Anais 42 Congresso Geológico Brasileiro, Araxá, p1-29**, 2004
- CORDEIRO, P. F. DE O. Petrologia e Metalogenia do Depósito primario de Niobio do Complexo Carbonatítico-Foscorítico de Catalão I, GO. Tese de Doutorado: Universidade de Brasília, 2009.
- COSTA, M. T.& BRANCO, J. J. R. **Roteiro para a excursão Belo Horizonte-Brasília**. 14 Congresso Brasileiro de Geologia. **Anais...** Belo Horizonte: UFMG. , 1961
- DARDENNE, M. A. **Síntese sobre a estratigrafia do Grupo Bambuí no Brasil Central**. 30 Congresso Brasileiro de Geologia. **Anais...** Recife: SBG. Disponível em: <<http://www.scribd.com/doc/91113300/Dardenne-1978-Sintese-Sobre-A-Estratigrafia-do-Grupo-Bambui-No-Brasil-Central>>. , 1978
- DARDENNE, M. A. The Brasilia Fold Belt. In: CORDANI, U. G.; MILANI, E. J.; THOMAZ-FILHO, A.; CAMPOS, D. A. (Eds.). **Tectonic Evolution of South America**. Rio de Janeiro: 31st International Geological Congress Rio de Janeiro, 2000. p. 231–263.
- DARDENNE, M. A.; SCHOBENHAUS, C. **Metalogênese do Brasil**. [S.l: s.n.], 2001. p. 392
- FILIPPELLI, G. M. The Global Phosphorus Cycle. In: RAKOVAN, J.; HUGHES, J. M.; KOHN, M. J. (Eds.). **PHOSPHATES Geochemical, geobiological, and materials importance**. [S.l: s.n.], 2002. p. 391–425.
- FILIPPELLI, G. M. The Global Phosphorus Cycle: Past, Present, and Future. **Elements**, v. 4, p. 89–95, 2008.
- FÖLLMI, K. B. The phosphorus cycle , phosphogenesis phosphate-rich deposits. **Earth-Science Reviews**, v. 40, p. 55–124, 1996.
- GRASSO, C. B. **Petrologia do Complexo Alcalino-Carbonatítico de Serra Negra, MG**. [S.l.]: Universidade de Brasília, 2010.
- HEINRICH, E. W. **The Geology of Carbonatites**. Chicago: Rand McNally, 1967. p. 601

HEZEL, A.; ROSS, S. D. Forbidden transitions in the infra-red spectra of tetrahedral anions, Spectra-structure correlations in perchlorates, sulphates and phosphates of the formula MX₀₄. **Spectrochimica Acta**, v. 22, n. 1962, p. 1949–1961, 1966.

KNUDSEN, A. C.; GUNTER, M. E. Sedimentary Phosphorites - An Example: Phosphoria Formation, Southeastern Idaho, U.S.A. In: RAKOVAN, J.; HUGHES, J. M.; KOHN, M. J. (Eds.). **PHOSPHATES Geochemical, geobiological, and materials importance**. [S.l.: s.n.], 2002. p. 363–389.

LAPIN, A. V. Carbonatite differentiation process. **International Geological Review**, v. 21, p. 1243–1252, 1982.

LEBAS, M. J. Nephelinites and Carbonatites. **Journal of the Geological Society of London**, v. 30, p. 53–83, 1987.

LIMA, O. N. DE. **Estratigrafia isotópica e evolução sedimentar do Grupo Bambuí na borda ocidental do Cráton do São Francisco: implicação tectônica e paleo-ambiental**. Tese de Doutorado. Universidade de Brasília, 2011.

MAITRE, R. W. LE (ED.). **Igneous rocks- A classification and glossary of terms**. Cambridge: Cambridge University Press, 2002. p. 236

MISI, A.; KAUFMAN, A. J.; AZMY, K.; DARDENNE, M.A., SIAL, A. N., OLIVIERA, T. F.: Neoproterozoic successions of the Sao Francisco Craton, Brazil: the Bambui, Una, Vazante and Vaza Barris/Miaba groups and their glaciogenic deposits. **Geological Society, London, Memoirs**, v. 36, n. 1, p. 509–522, 30 nov 2011.

MISI, A.; KYLE, J. R. Upper Proterozoic Carbonate Stratigraphy, diagenesis and stromatolitic phosphorite formation, Irece Basin, Bahia, Brazil. **Journal of Sedimentary Research**, v. A64, n. 2, p. 299–310, 1994.

MONTEIRO, L. V. S. **Estudo metalogenético das mineralizações de Zinco e Chumbo dos depósitos de Vazante, Ambrósia e Fagundes, Faixa Vazante - Paracatu, Minas Gerais**. Tese de Doutorado. Universidade de Sao Paulo, 2002.

OLIVEIRA, S. M. B. DE; IMBERNON, R. A. L. Weathering alteration and related REE concentration in the Catalão I carbonatite complex, central Brazil. **Journal of South American Earth Sciences**, v. 11, n. 4, p. 379–388, 1998.

PICCOLI, P. M.; CANDELA, P. A. Apatite in Igneous Systems. In: RAKOVAN, J.; HUGHES, J. M.; KOHN, M. J. (Eds.). **PHOSPHATES Geochemical, geobiological, and materials importance**. [S.l.: s.n.], 2002. p. 257–292.

PIMENTEL, M. M.; JOST, H.; FUCK, R. A. O embasamento da Faixa Brasília e o Arco Magmático de Goiás. **Geologia do Continente Sul-Americano: Evolução da obra de Fernando Flávio Marquez de Almeida**. [S.l.: s.n.], 2004. p. 355–370.

RIBEIRO, C. C. **Geologia, Geometalurgia, Controles e Gênese dos depósitos de fósforo, terras raras e titânio do Complexo Carbonatítico Catalão I, GO**. [S.l.]: Universidade de Brasília, 2008.

SANCHES, A. L.; MISI, A.; KAUFMAN, A. J.; AZMY, K. As sucessões carbonáticas neoproterozóicas do Cráton do São Francisco e os depósitos de fosfato: correlações e fosfogênese. **Revista Brasileira de Geociências**, v. 37, p. 182–194, 2007.

SANTANA, R. O. **Estratigrafia, geoquímica e isótopos de C, O, e Sr do Grupo Bambuí a leste da Falha de São Domingos, NE de Minas Gerais**. [S.l.]: Universidade de Brasília, 2011.

SOUBIÈS, F.; MELFI, A. J.; AUTEFAGE, F. Comportamento Geoquímico dos Elementos Terras Raras nos alteritos da jazida de fosfato e titânio de Tapira (Minas Gerais, Brasil): a importância dos fosfatos. **Revista Brasileira de Geociências**, v. 21, n. 1, p. 3–16, 1991.

- TASSINARI, M. M. L.; KAHN, H.; RATTI, G. Process mineralogy studies of Corrego do Garimpo REE ore, catalao-I alkaline complex, Goias, Brazil. **Minerals Engineering**, v. 14, n. 12, p. 1609–1617, dez 2001.
- TOLEDO, M. C. M. DE. **Mineralogia dos principais fosfatos do maciço alcalino carbonatítico de Catalão I (GO) e sua evolução no perfil laterítico**. [S.l.]: Universidade de São Paulo, 1999.
- TOLEDO, M. C. M. DE; FERRARI, V. C.; NETO, A. A, FONTAN, F., MARTIN, F., DOS SANTOS, C. N., CARVALHO, F.M.DE: . Fosfatos aluminosos com Ferro do Grupo da Crandallita nas coberturas lateríticas de Catalão I, Juquiá e Tapira (Brasil) e Chiriguelo (Paraguai). **Revista Brasileira de Geociências**, v. 32, n. 4, p. 393–406, 2002.
- TOLEDO, M. C. M. DE; LENHARO, S. L. R.; FERRARI, V. C., FONTAN, F., PARSEVAL, P. DE, LEROY, G.:.The compositional evolution of apatite in the weathering profile of the Catalão I Alkaline-Carbonatitic Complex, Goiás, Brazil. **The Canadian Mineralogist**, v. 42, p. 1139–1158, 2004.
- TORRES, M. G. **Composição química superficial e nanotopográfica da apatita do Proto-minério da Mina do Barreiro**. [S.l.]: Universidade de Brasília, 2008.
- VALARELLI, J. V. **O minério de Nb,Ti e terras raras de Catalão, GO**. [S.l.]: Universidade de São Paulo, 1971.
- VALERIANO, C. DE M.; DARDENNE, M. A.; FONSECA, M. A.; SIMÕES, L. S. A.; SEER, H. J. A Evolução Tectonica da Faixa Brasília. **Geologia do Continente Sul-Americano: Evolução da obra de Fernando Flávio Marquez de Almeida**. [S.l.: s.n.], 2004. p. 575–592.
- WOOLLEY, A. R.; KEMPE, D. R. C. Carbonatites: nomenclature, average chemical compositions, and element distribution. In: BELL, K. (Ed.). **Carbonatites. Genesis and evolution**. London: Unwin-Hyman, 1989. p. 1–14.
- WOOLLEY, A. R.; KJARSGAARD, B. A. Paragenetic Types of Carbonatite As Indicated By the Diversity and Relative Abundances of Associated Silicate Rocks: Evidence From a Global Database. **The Canadian Mineralogist**, v. 46, n. 4, p. 741–752, 1 ago 2008.
- YEGOROV, L. S. Phoscorites from the Maymecha-Kotuy ijolite-carbonatite association. **International Geological Review**, v. 35, p. 346–358, 1993.

Capítulo III: Reflectance and Emissivity Spectroscopy of Brazilian Magmatic Phosphates: Catalão I (GO) and Tapira (MG) Carbonatitic Complexes

3.1 Introduction

The Alto Paranaíba Igneous Province (APIP), defined by GIBSON *et al.* (1995), hosts a series of alkaline carbonatitic complexes and plutons of kamafugitic-toleitic affinity. In this region, alkaline magmatism was a key event in the formation of magmatogenic phosphate deposits, most of them aligned along a 125° azimuth regional structure (BIZZI & ARAÚJO 2005).

This regional structure holds several carbonatitic alkaline complexes (e.g.: Catalão I and II, Araxá, Salitre-Serra Negra and Tapira). Catalão I is currently under mining by Copebrás Ltd, Mineração Catalão and VALE, whereas Tapira is being mined exclusively by VALE.

Whereas there are many discussions about petrological aspects of the Province, given its metalogenic importance (BROD *et al.*, 2000; COMIN-CHIARAMONTI *et al.*, 2005; GIBSON *et al.*, 1995; MORBIDELLI *et al.*, 1995), remote sensing studies are still scarce. Previous work were focused only on reflectance spectroscopy of rocks/soils from the Catalão I and Araxá complexes (e.g. SOUZA 2009; CRUZ *et al.* 2011; CRUZ 2011; TEXEIRA 2011).

This lack of information justifies a full VNIR-SWIR-TIR reflectance and emissivity spectroscopy characterization of the Alto Paranaíba Igneous Province (APIP) rock assemblages. To date, there are no mineralogical associations or distinguished lithotypes that could be used as mineral guides for the remote sensing of phosphates. In addition, band depth and location of phosphates spectral features have not been fully explored in order to use that information as a mineralogical identifier.

The remote sensing of carbonatitic rocks has been approached since the early stages of hyperspectral remote sensing (Mars & Rowan, 2011; Rowan et al., 1995; Rowan, Kingston, & Crowley, 1986). Using reflectance spectroscopy it is possible to infer relevant chemical bonds related to carbonatite occurrence, especially carbonates (calcite, magnetite, ankerite), micas (biotite, phlogopite, vermiculite), and REEs minerals or oxides (REEs phosphates or REEs inclusion in apatites and Al-U-phosphates). The calibration of these results with other analytical approaches (i.e., X Ray Diffraction and X Ray Fluorescence) helps reducing qualitative uncertainty of the measurements. A calibration dataset coupled with extensive Diffuse Reflectance and Emissivity data should provide better mineralogical information that can be resampled to match hyperspectral (e.g., Hyperion) and multispectral (e.g., ASTER) resolution and be used as prospective endmembers in regional remote sensing exploration programs.

In this context, this research aims to define the reflectance and emission spectroscopy characteristics of the phosphatic rocks from the Catalão I and Tapira carbonatitic alkaline complexes, identifying the mineralogical associations that can be separated and used as mineralogical endmembers for detection of phosphates using remote sensing instruments.

3.2 Geological Setting

3.2.1 Catalão I Carbonatitic Alkaline Complex

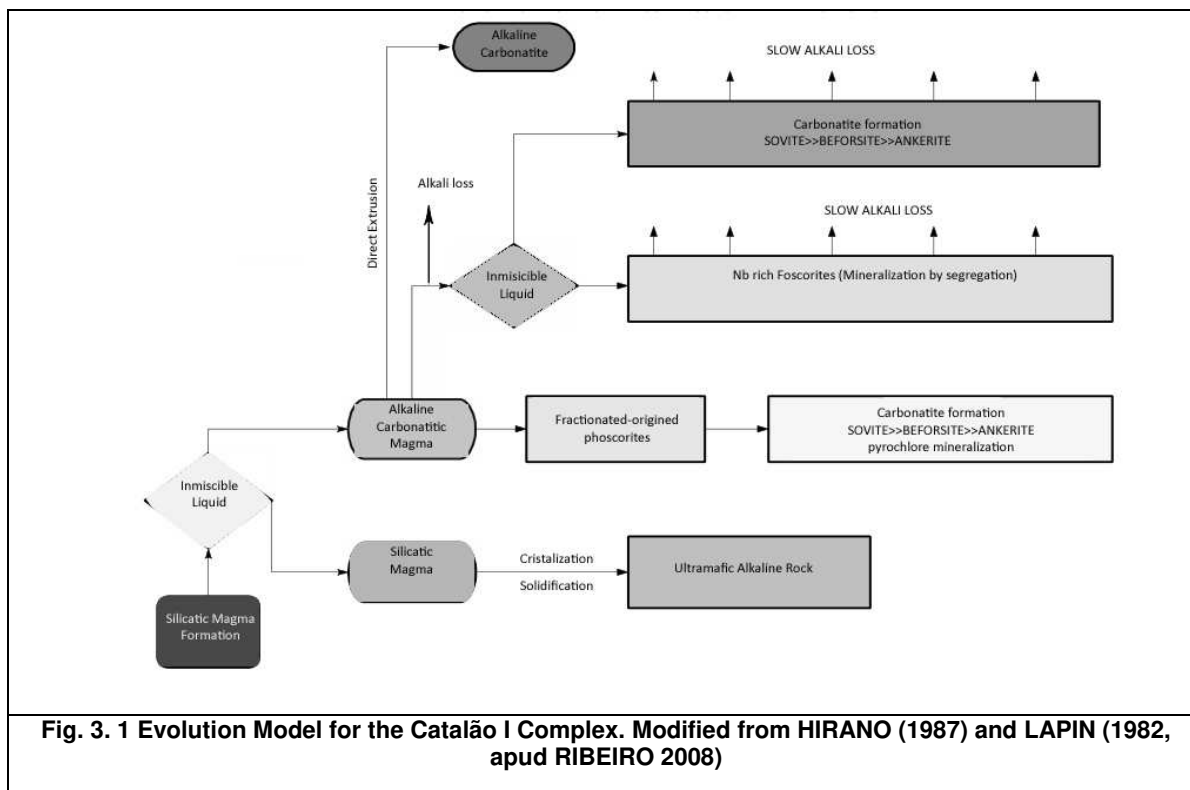
The Catalão I Carbonatitic Alkaline Complex (C1CAC) is located in the Alto Paranaíba Igneous Province (GIBSON *et al.* 1995), along with several other carbonatitic alkaline complexes (Serra Negra, Salitre I-II-III, Araxá, Tapira). All these bodies are associated to a major 125° Azimuth tectonic structure (BIZZI & ARAÚJO 2005). These complexes were emplaced along deep, northwest-trending faults (GOMES *et al.*, 1990). The C1CAC has an age of 85.0 ± 0.9 Ma (K/Ar) (AMARAL *et al.* 1967; SONOKI & GARDA 1988).

The C1CAC stands as a topographic high in the Goiás plainlands, surrounded by a ring of fenitized quartzite and mica schists of the Araxá Group. A ~100 m thick weathered profile was developed over the complex. It host P, Nb and Fe mineralizations that have been detailed as regards their mineralogy by numerous authors (e.g., OLIVEIRA & IMBERNON 1998; TOLEDO *et al.*, 2002; TOLEDO *et al.*, 2004; TOLEDO *et al.* 2004; FERRARI *et al.*, 2007; RIBEIRO *et al.*, 2005).

BAECKER (1983) proposed a magmatic evolution model for the C1CAC where a set of silicic ultramafic alkaline rocks and a set of carbonatitic rocks show a spatial and temporal relationship in three stages: (i) a first stage, comprising an ultramafic intrusion; (ii) a second stage of auto-metasomatism, which favors fenitization of the host rock and alters the ultramafic rocks previously emplaced; and (iii) a final stage of carbonatization, which can be subdivided into five rock forming events: magmatic foscrites, sovites, silicosovites, beforsites, late veins.

GIERTH & BAECKER (1986) studied the evolution stages of the C1CAC. The authors proposed a model of mineral occurrences with an initial ultramafic stage, a later carbonatic stage, followed by a hydrothermal stage and final weathering. The initial ultramafic stage is characterized by phlogopite, apatite, oxides and carbonates and phlogopitization of the serpentine. The third stage is characterized by sulphides, chlorite, barite, quartz and carbonate remobilizations. The last stage was responsible for alteration, remobilization and concentration of apatite along the weathering profile.

LAPIN (1982) and HIRANO *et al.*(1987) (apud RIBEIRO 2008) proposed an evolutionary scheme for the Catalão I magmatism, which involved liquid immiscibility, as illustrated in Fig. 3.1. From silicic magmas and a liquid fluid immiscibility process, silicatic magmas and carbonatitic alkaline magmas were generated. The silicic magmas crystallized, creating the ultramafic rocks of the C1CAC. In contrast, the alkaline magma underwent three processes: fractionation, which yielded phoscrites; direct extrusion into alkaline carbonatites and a second phase of liquid immiscibility, in which Nb-rich carbonatites and sovite>>beforsite>>ankerite-bearing carbonatites were generated.



ARAÚJO (1996) made a petrographic and mineral chemistry study in the C1CAC, analyzing numerous rocks, including dunite, pyroxenite, phoscorite, phlogopite, carbonatite and carbonatitic breccias. The author suggested that phlogopites originated by the transformation of dunites, foscrites and clinopyroxenites. The author also recognized two evolutional phases: an ultramafic magmatic phase and a carbonatic phase, proposing that the metasomatism described in the complex is related to the carbonatitic intrusions.

BAECKER (1983) and DANNI *et al.*(1991) (apud RIBEIRO 2008) suggested that metasomatic process enriched the magnetite-bearing olivinites and clinopyroxenites with magnetite, phlogopite, calcite and apatite by addition of CO₂, Ca, P, K, Al and Na and removal of Si, Mg, Fe and Ti. PEREIRA (1995) exposed a petrologic evolution model that involved firstly a magmatic phase that created the phoscorites and pyroxenites. Later, a metasomatic phase induced the transformation of olivine into phlogopite and brought the pyrochlore mineralization into the rock. The later phases, almost exclusively hydrothermal, created the carbonatitic, the apatite mineralization and transformed olivine into serpentine and perovskite into anatase.

Several other studies conducted in the C1CAC were focused on its weathering mantle. The work of OLIVEIRA & IMBERNON (1998); TOLEDO *et al.* (2002); TOLEDO *et al.* (2004a) and TOLEDO *et al.* (2004b) defined the weathering mantle classification, the possible mineralogical phases within it and the mining products favored in several stages. OLIVEIRA & IMBERNON (1998) defined five horizons of the weathered mantle from top to bottom (Fig. 3.2):

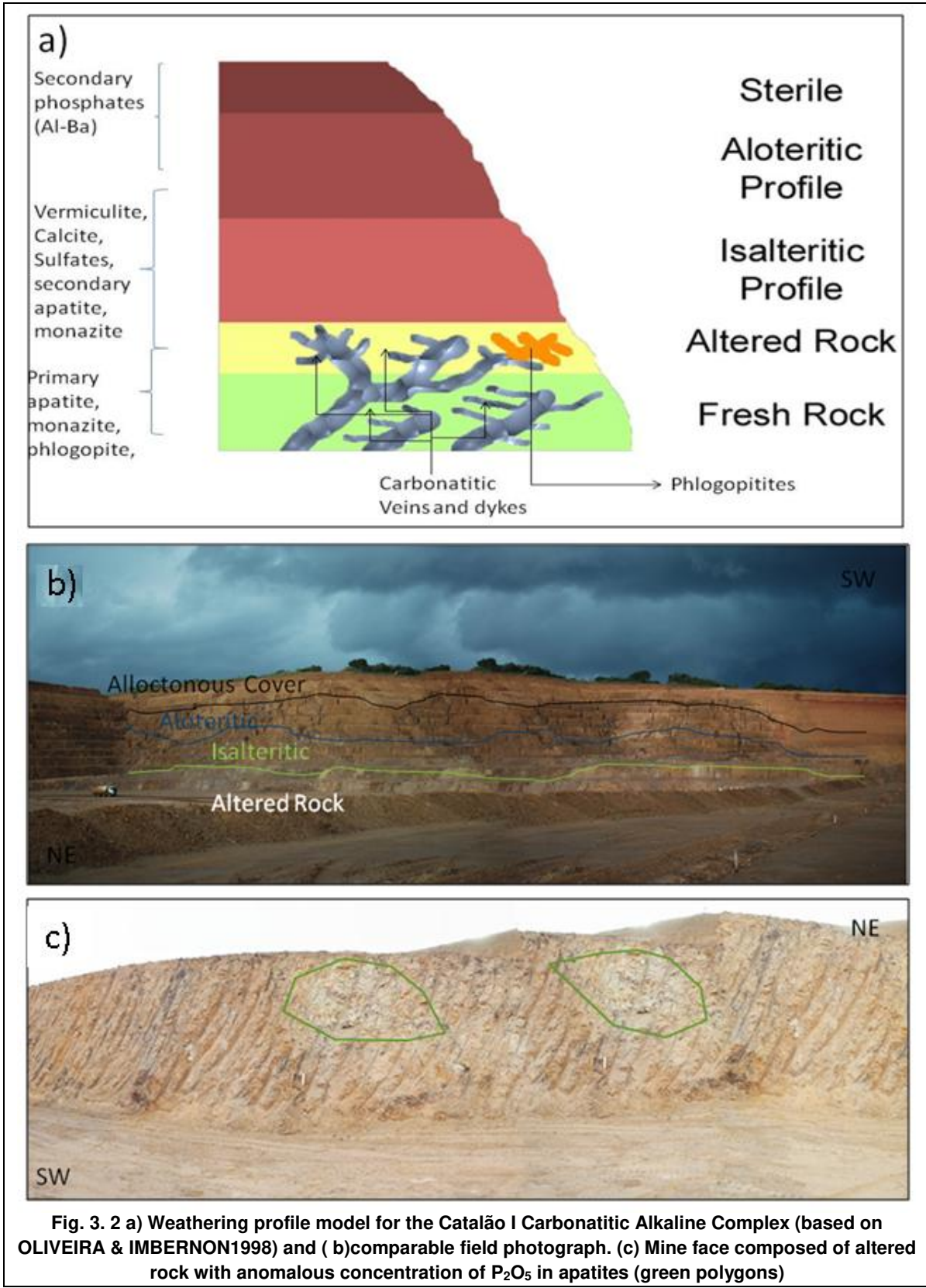
Allocthonous covers: the top layer consists of reddish to pink allocthonous soils.

Isalteritic saprolite: another 25m deep profile. It has clayish-sandy material that can be yellow to reddish. Homogenization of mineral phases does not allow identifying rock structures.

Aloteritic Saprolite: a 25m deep profile, resulting from advanced weathering of the altered rock horizon. Some primary rock structures can still be observed, but the overall appearance is that of a homogenous altered soil. Vermiculite is the main mineral in this section.

Altered rock: in this horizon, rock structure is almost completely preserved. Metasomatic alteration can enrich phlogopitites with hydrothermally transported apatite (TOLEDO, 1999), creating green breccias (where dunites are intruded) or apatite pockets (where nelsonites are intruded by phoscorites).

Fresh rock: phoscorites and phlogopitites, intruded by abundant carbonatite veins.



Although this weathering profile model has been admitted for the whole complex, the authors acknowledge that the model does not relate directly to the original rock lithologies. They pinpoint the isalteritic saprolite as the most interesting economic target for P. They also note that most phosphate minerals have degraded from apatite into hydrated phosphates that may have Ba, Al or Fe. TOLEDO *et al.* (2004) showed that apatite grains still present in the aloteritic saprolite show dissolution marks when examined through SEM and EMP analyses

Chemically, the aloteritic saprolites are dominated by Fe_2O_3 and TiO_2 . They present phosphates when apatite is dissolved and altered into goerceiveite and other aluminous phosphates of the crandallite group. TOLEDO (1999), TOLEDO *et al.* (2004), TOLEDO *et al.* (2002) and FERRARI *et al.* (2007) showed that a variation on this group was dominated by Ba (goerceiveite) > Al (crandallite) > goyazite (Sr) >> REEs-bearing phosphate (florencite).

The monazite deposits were studied in more detail by TOLEDO *et al.* (2004) and TASSINARI (2001). The authors tried to provide mineralogical background information for industrial recovery. The results obtained made clear that crystallization of monazite in the complex was hardly developed. Commercial tryouts to enrich monazite and make it profitable as an economic commodity are being executed since 1995.

3.2.2 Tapira Alkaline Carbonatitic Complex

The Tapira Alkaline Carbonatitic Complex (TACC) is located in the southern part of a late Cretaceous, carbonatite-bearing complex in the Alto Paranaíba Igneous Province (GIBSON *et al.*, 1995). Bebedourites are common, primarily composed of diopsidic pyroxene and variable amounts of phlogopite, perovskite, apatite, magnetite, Ti-garnet and sphene (BRIGATTI *et al.*, 2004).

The geologic and petrologic characteristics of the Tapira complex were detailed by BROD (1999) and BROD *et al.* (2001). The crystal chemistry of the micas from this pluton and the relative proportion of endmembers (phlogopite, annite and tetra-ferriflogopite) were used both to discriminate between different alkaline rock types and to establish evolution trends (BRIGATTI *et al.*, 2004)

Lithologically, the TACC was classified by BROD (1999) and BROD *et al.* (2005) based on the petrography of drill cores. Resuming the lithotype classification, there are two

types of Bebedourites (B1 and B2), five types of carbonatites (C1 to C5), wehrlites and other olivine-bearing cumulates, phlogopite picrites and bebedouritic dykes.

The bebedourites are defined by TRÖGER (1928; *apud* BROD *et al.* 2005) as clinopyroxenites rich in diopside, biotite, perovskite and opaque minerals with accessory apatite, K-feldspar and olivine. The type locality for bebedourites is located on the Salitre Alkaline complex in the Alto Paranaíba Igneous Province (GIBSON *et al.*, 1995). The B1 bebedourites comprise essential diopside, perovskite, apatite, phlogopite and magnetite. Olivine and chromium-rich spinel are typically absent. Melanite, carbonate and rare zirconolite may occur in accessory amounts. According to BROD *et al.* (2005), abundant perovskite are strong indicators of silica-undersaturation in the magma that produced these rocks. The opaque minerals crystallized either after or as the same time than phlogopite. This resulted in the opaque minerals forming anhedral and interstitial phases. The crystallization order defined by BROD (1999) for the least evolved magmatic rocks are apatite>perovskite>diopside>phlogopite+magnetite. For the more evolved rocks the trend is diopside>perovskite>apatite>magnetite+phlogopite.

The B2 bebedourites are usually finer-grained and have higher clinopyroxene content than those of B1. Densely packed diopside crystals with intercumulus phlogopite are common, with apatite, perovskite, melanite and titanite present as accessories. An initial crystallization order at the early stages proposed by BROD *et al.* (2005) is the following: apatite + perovskite > diopside > phlogopite + magnetite > garnet > titanite. Later on, this sequence is replaced by diopside > ±perovskite > apatite > phlogopite + magnetite > garnet > titanite > ±K-feldspar.

B2 bebedourites appears to be more evolved than the B1 bebedourites, given its higher silica content. However, as BROD *et al.* (2005) pointed out, this evolution was not swift due to the presence of Ti-rich garnet in the less differentiated wehrlites. The same authors indicate that this process might have been controlled by any of three alternative events: (i) preferential removal of silicate (olivine, clinopyroxene) or non-silicates (apatite, perovskite, oxides) phases; (ii) assimilation of the quartzitic country rock given the high Sr and Nd amounts in some ultramafic dykes and rounded quartz xenocrysts in carbonatite dykes (BROD, 1999) or (iii) involvement of Tapira magmas into one or more episodes of carbonate-silicate liquid immiscibility.

Carbonatites (C1 to C5) are dispersed throughout the whole complex, having differentiated mineralogy according to the evolution of the bebedourites. C1 carbonatites encompass the largest carbonatite area in Tapira, and consists of Ca carbonatites and dolomite-Ca carbonatites intruding the ultramafic rocks of the B1 unit, near the center of the complex. They are granular, medium-grained, and vary from homogeneous to locally banded. The essential minerals are calcite, phlogopite, magnetite and apatite, whereas dolomite, sulphides, barite and pyrochlore occur subordinately.

C2 carbonatites occurs either as an independent intrusion, spatially associated with syenites in the center-northern region of the complex; either as dykes and diatreme-facies breccias elsewhere in the complex. C2 carbonatites are associated with the syenites, usually appear more fine-grained than C1 carbonatites and are composed of carbonate, with accessory magnetite.

C3 carbonatites occur in the northern extremity of the complex and are geographically associated to B2 bebedourites. They are usually found intruding at the contact between B2 and B1 bebedourites. This unit consists of isotropic, granular, medium- to coarse-grained calcite-carbonatites, with subordinate rounded crystals of apatite. Magnetite is common, and xenocrysts of diopside and phlogopite are conspicuous (BROD 1999).

C4 carbonatites are very similar to C3, but lack diopside xenocrysts. It outcrops where no contact with country rocks is observed. C5 carbonatite comprises a number of late-stage, thin dykes and veins scattered throughout the complex. C5 carbonatites are usually fine-grained and equigranular, composed of dolomite or mixtures of dolomite and calcite. Magnetite and barite are common. Apatite and xenocrystic phlogopite are rare (BROD *et al.*, 2005).

Phlogopite picrites are composed of subhedral to euhedral olivine phenocrysts set in a fine-grained groundmass rich in phlogopite, carbonate, apatite, perovskite and opaque minerals. It is also possible to find phlogopite, apatite, clinopyroxene or perovskite as xenocrysts.

The bebedouritic rocks typically contain phenocrysts of one or several pyroxenes, apatite, garnet and phlogopite. With the magmatic evolution of these dykes, the carbonate content progressively increases in the groundmass, often leading to the formation of

carbonate globules or ocelli textures, which are interpreted as evidence of liquid immiscibility, in the same way as with the phlogopite picrites (BROD *et al.*, 2005).

The P mineralization is associated with Ti in the weathering cover of the whole weathering profile. Chemical alteration depths are varied, reaching at points more than 200 meters. The weathering profile has been characterized in four different zones from top to bottom: sterile, Ti-rich, P-Ti-rich and mineralized in P (Vaz de Mello, 1983)

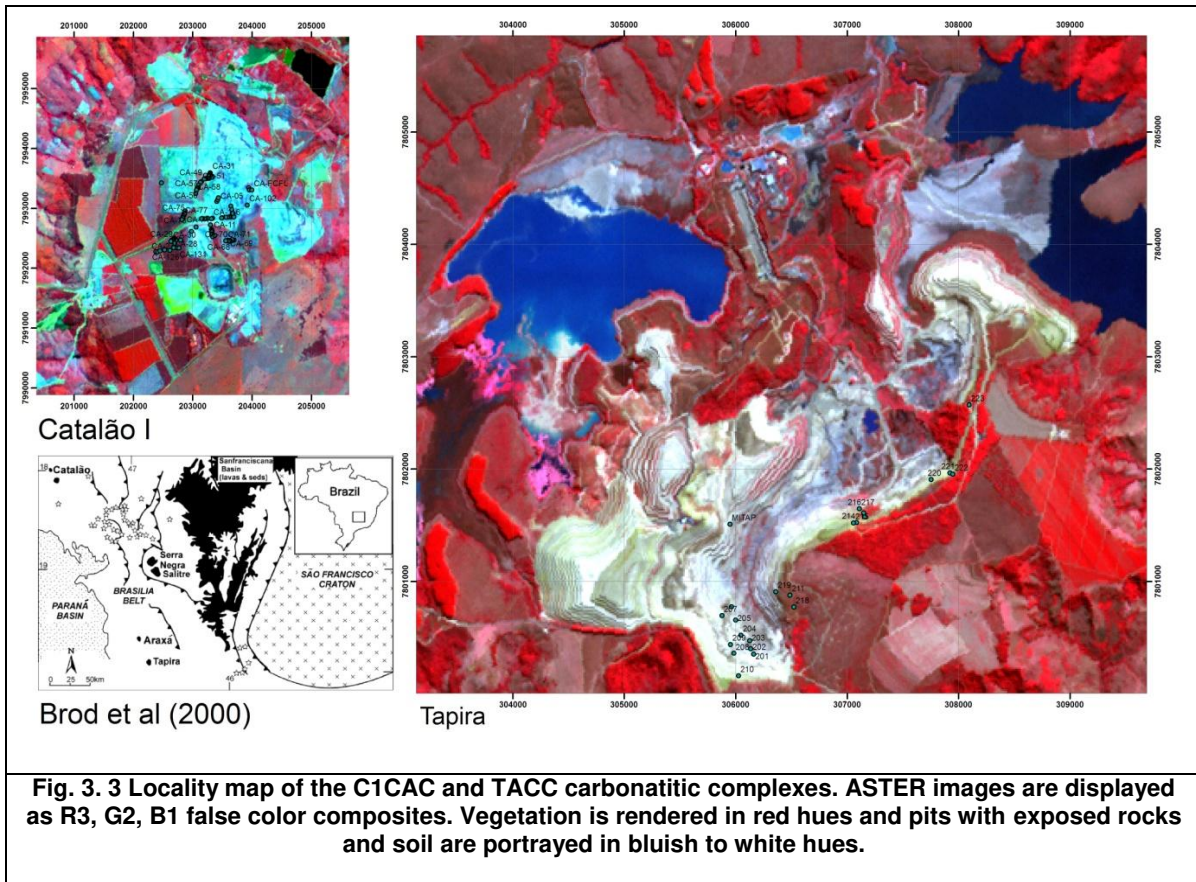
The **sterile zone**, also called latosolic, can cover 20 meters deep. The main minerals described by VAZ DE MELLO (1983) in this zone are kaolinite, gibbsite, goethite, hematite, secondary aluminum phosphates and anatase. Eventually, concretionary nodules with quartz sediments of the Araxá Group are also observed in this zone.

The underlying, **Ti-rich zone** has an approximate depth of 40 meters. Rock structure at this zone can be partially identified. Main minerals are the same than those observed in the latosolic zone, but anatase is more yellow and fine grain size minerals are less abundant. Most of the micas in this zone are transformed into vermiculite and some perovskite is apparent.

Down below, the **Ti-P-rich zone** has well preserved rock structure. Substantial amounts of primary apatite that has undergone partial dissolution can be identified with perovskite altered to green anatase. The micas are altered to vermiculite; Ti-rich magnetite is altered to maghemite and hematite. This zone corresponds to the most sought-after rock product of the mine.

The **P-rich zone** is an 80 meters thick layer formed above the fresh bedrock. It is composed of piroxenites and peridotites less altered by chemical weathering. Fresh perovskite is ubiquitous and apatite becomes the main mineral. Ti-rich magnetite, diopside, ferruginized olivine and fresh phlogopite are secondary minerals.

A locality map of the Tapira and Catalão I complex is shown in fig. 3.3. Figs. 3.4a and 3.4b display a simplified geological map of both complexes, as well as a sites visited in the field.



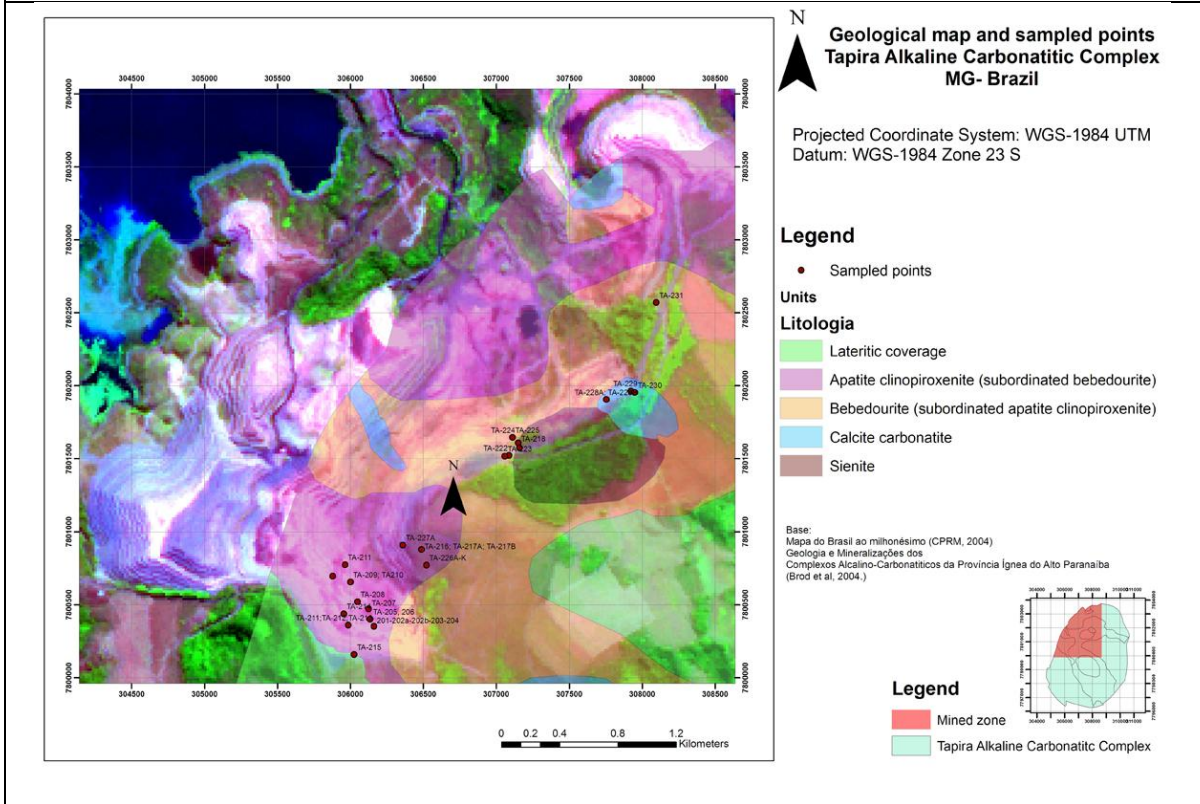
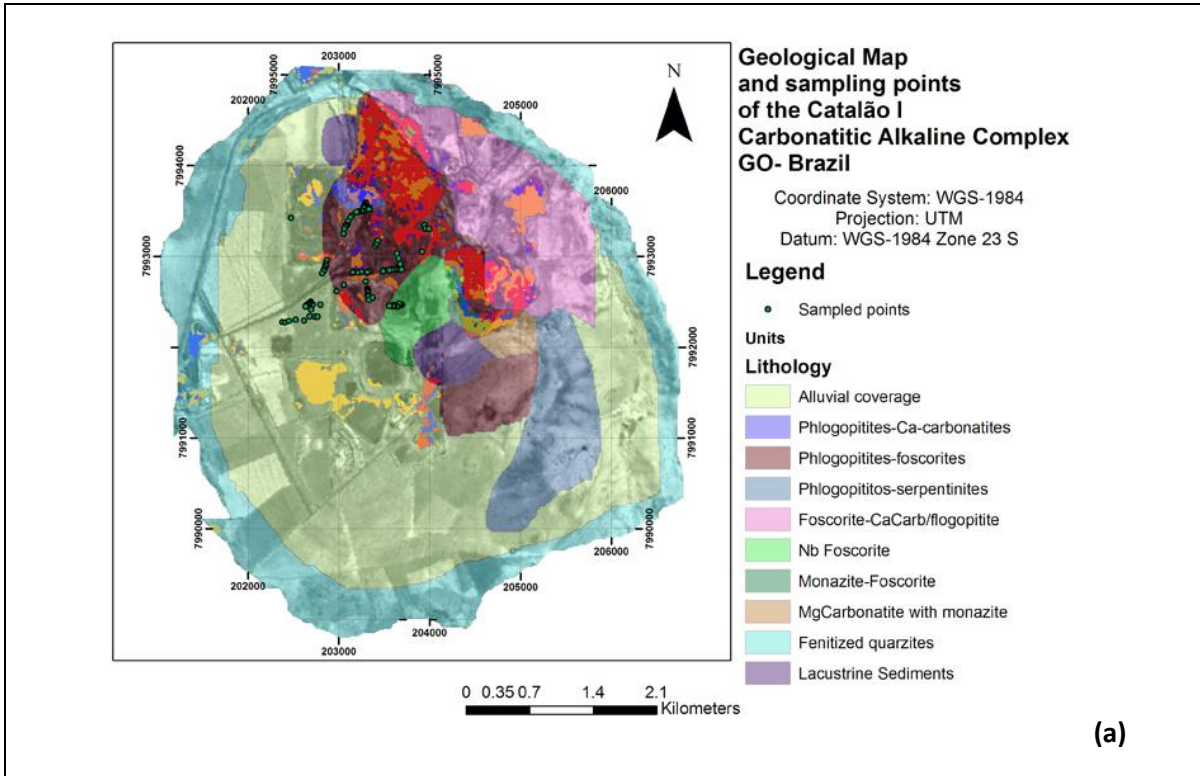


Fig. 3. 4. C1CAC (a) and TACC (b) geological maps. Sampling points are marked by circles. Background images correspond to a ASTER R6, G3, B2 false colour composite.

3.3 Materials and Methods

Rock and soil samples were collected in the horizons in which phosphatic rocks and minerals occurred in economic concentration in the C1CAC and TACC. Samples were collected from vertical and horizontal profiles when possible to determine if changes in topography could help integrate the location of the weathering mantle, the main mineral phases of the studied horizon and the spatial distribution of the phosphate minerals.

Sample processing followed four main steps:

1. Raw Samples were dried at 50°C for over 24 hours to eliminate excess humidity and avoid carbonatic recrystallization.
2. A first measurement of reflectance was conducted on the samples.
3. Samples were crushed on jaw steel crushers, grinded in ball planetary mills and their 200 mesh finer fraction separated.
4. Grinded samples smaller than 200 meshes were analyzed by reflectance spectroscopy, XRD, XRF and Fourier Transformed Infrared spectroscopy (FTIR).

Reflectance measurements were performed with a Portable ASD® FieldSpec 3 Hi Resolution Field Spectrometer coupled to a Mineral Probe. This proximal sensor records 2151 channels/bands in the VIS-NIR-SWIR region of the electromagnetic spectrum. The mineral probe allows measurements to be made almost in direct contact with the sample. Spectra collection was set to 75 counts for white reference and dark current standards, using a measurement time of 5 seconds per spectra and a Spectralon (calibration) panel.

In order to properly estimate absorption features, reflectance values were normalized through Continuum Removal in the 0.35-2.5µm range to locate prominent absorption features in the VNIR-SWIR range. For detailed spectral comparison, especially in the 0.75µm, the continuum removal was performed using the PRISM plugin application for ENVI(KOKALY, 2011).

Emission spectroscopy (RUFF et al. 1997) analysis were conducted in the Infrared Spectroscopy Laboratory of the State University of Campinas. Diffuse Reflectance (r) measurements of finely grinded sampled material were taken on a Nicolet 6700 FTIR spectrometer, with a DRIFT Chamber (Diffuse Reflectance Infrared Fourier Transformed measure) at 20°C. This measurement was then conversed to emissivity using Kirchoff's Law, as shown in equation 1:

$$\varepsilon = 1 - r \quad (1)$$

where ε stands for emissivity and r stands for diffuse reflectance.

X Ray Diffraction was made using a Bruker AXS D2 phaser diffractometer. The current was set to $\text{CuK}\alpha = 1.546$; 2θ angles varied from 6° to 60° with step times of 1 second. The resulting diffraction file was processed using the Phillips X'pert HighScore 1.0b software for mineral phase recognition.

X Ray Fluorescence was made using glass discs, with lithium tetraborate, using 5 g of fundent and 1.2 g of calcinated sample for major elements and pressed powder pellets for trace and minor elements. Seventeen samples were analyzed at the Geochemistry Laboratory of the State University of Campinas. The Standard Reference Material used for P were BCR[®]-032 (Natural Moroccan phosphate Rock), SRM-120c (Florida Phosphate Rock) and SRM-694 (Western Phosphate Rock).

3.4 Results

Reflectance and emissivity spectroscopic charts, plus XRD and XRF results, are displayed below to show the behavior of primary and secondary phosphates phases. Reflectance spectra are presented from $0,35\mu\text{m}$ to $2,5\mu\text{m}$. Emissivity spectra are presented from $2,5\mu\text{m}$ to $25\mu\text{m}$.

3.4.1 Sample descriptions:

Samples from the C1CAC were mostly taken from the isalteritic and altered rock horizons. Fewer samples were collected in the aloteritic and in the fresh rock horizons. Weathering in the TACC, although present, is not as expressive as in C1CAC, so it was possible to collect data from fresher rocks. A resumed list indicating the classification of the collected samples and their location in UTM coordinates is given in table 3.1.

3.4.2 X-Ray Fluorescence:

X Ray Fluorescence data was obtained in order to see how chemical content could influence the reflectance and emissivity spectroscopy features. It was preferred over other analytical techniques (for example ICP-MS) for its wide range of element detection, preparation procedures similar to those used for the spectroscopic analyses, availability and reduced analytical costs. X Ray Fluorescence data is presented in table 3.2.

Economically relevant phosphates in both complexes are marked by $\geq 7\%$ wt of P_2O_5 . This information was here used as a chemical discriminator in the selection of phosphate rock targets.

Interesting results yielded from chemical associations may explain the P_2O_5 percentages found in the phosphatic rocks. Primary and secondary apatites sampled from fresh rock or altered rock horizons show a CaO/P_2O_5 ratio $> 1,5$. Apatites that have undergone weathering process and lost structural Ca display a CaO/P_2O_5 ratio between 1,5 and 1.

Tab. 3. 1 Selected sample descriptions of the CA1AC and TACC

		X	Y	Sample	Sample Description
Catalão I	Aloteritic Horizon	203321	7992628	CA-09	Brown Aloterite
	Isalteritic Horizon	203327	7992558	CA-16	Isalteritic phosphatic soil
		203373	7992546	CA-18D	Phlogopite phoscorite
		202714	7992466	CA-20	Phoscorite with magnetite
		203298	7993583	CA-32	Silexite
		203284	7993567	CA-33	Isalteritic titaniferous soil
		203276	7993550	CA-35	Isalteritic Phoscorite soil with magnetite
		203278	7993534	CA-37	Isalteritic ferric soil
		Altered Rock Horizon	203331	7993520	CA-39, CA-42
	203078		7993341	CA-55	Saprolite with Apatite and magnetite
	202411		7992272	CA-123	Green Breccia with magnetite
	202798		7992471	CA-127	Brecciated Phlogopitite
	202678		7992341	CA-129	Silexite-dolomite carbonatite contact
	203463		7992849	CA-VERCA2	Vermiculite
	202738		7992339	CA-130	Phlogopitite with magnetite
	202767		7992339	CA-131	Brecciated Phlogopitite
	Fresh Rock Horizon	203943	7993343	CA-Monazite-Barite	Monazite intergrown with Barite
		203652	7992866	CA-103	Cumulatic Carbonatite
		203943	7993343	CA-APCA	Carbonatite-apatitite
	Tapira	Ti Zone	307160	7801575	TA-219-220-221
307754			7801906	TA-228A; TA-228B	Altered B2 bebedourite with goethite
308096			7802571	TA-236	Isalterite with secondary phosphates
P Zone		305999	7800656	TA-209; TA210	Vermiculite; Bebedourite with vermiculite
		307150	7801610	TA-218	Flux-mineral banding, carbonatite-picrite
Fresh Rock Zone		306161	7800354	TA201-202a-202b-203-204	Altered B1 bebedourite ; Pegmatoid B1 bebedourite
		306135	7800402	TA-205	Possible monazite; Monazite B1- Bebedourite

Tab. 3. 2 X-Ray Fluorescence data for samples collected in the C1CAC and TACC complexes

Sample	Nb ₂ O ₅	P ₂ O ₅	Fe ₂ O ₃	TiO ₂	MnO ₂	SiO ₂	Ta ₂ O ₅	BaO	PbO	ThO ₂	U ₃ O ₈	Al ₂ O ₃	CaO	MgO	Oxides	CaO/P ₂ O ₅	Others	TOTAL
CA-09	0.84	5.89	43.06	0.05	6.37	10.9	0.04	6.88	0.09	0	0	13.76	0	0.17	88.05	0.00	11.95	100
CA-16	0.38	28.7	8.48	0.54	0.5	7.38	0.08	0.34	0.09	0.48	0.31	0.13	34.39	0	81.8	1.20	18.2	100
CA-180	0.35	22.52	23.21	3.09	0.58	10.81	0.09	0.17	0.04	0.38	0.17	0.67	30.44	1.95	94.47	1.35	5.53	100
CA-20	0.37	28.66	17.67	3.63	0.47	4.73	0.1	0.22	0.05	0.46	0.22	0.72	36.56	0.22	94.08	1.28	5.92	100
CA-32	0.49	5.25	21.57	3.65	1.36	46.86	0.07	0.45	0.1	0.03	0.05	4.44	5.89	2.16	92.37	1.12	7.63	100
CA-33	0.1	3.55	23.8	10.75	0.42	34.22	0.07	0.54	0.08	0.07	0.04	3.76	6.84	7.87	92.11	1.93	7.89	100
CA-35	0.21	11.29	33.22	9.59	0.58	20.35	0.06	1.48	0.07	0.15	0.07	2.83	13.94	2.23	96.07	1.23	3.93	100
CA-37	0.35	0.76	45.99	4.63	2.84	24.15	0.06	0.57	0.09	0	0.01	5.88	0.16	3.29	88.78	0.21	11.22	100
CA-39	0.15	22.66	31.49	0.72	0.45	10.69	0.05	0.03	0.08	0.26	0.16	0	31.26	0.3	98.3	1.38	1.7	100
CA-42	0.16	28.53	23.74	0.97	0.27	4.03	0.06	0.04	0.08	0.35	0.22	0	37.99	0.02	96.46	1.33	3.54	100
CA-55	0.28	17.19	51.75	2.26	0.49	1.98	0.06	0.01	0.05	0.18	0.1	0	24.64	0.77	99.76	1.43	0.24	100
CA-115	0.0964	24.19	2.634	0.439	0.007	27.29	0.012	0	1.99	0	0.003	9.415	29.2	0.8	96.078	1.21	3.9219	100
CA-123	0.127	18.81	6.315	0.613	0.08	30.57	0.005	0	1.77	0.01	0.003	17.66	10.41	0.87	87.233	0.55	12.767	100
CA-129	0.045	11.46	12.1	1.818	0.259	32.5	9E-04	0	5.45	0	0	9.543	14.56	7.83	95.572	1.27	4.4285	100
CA-130	0.164	7.785	11.2	54.47	0.166	6.81	0.009	0	0.64	0.01	0.006	1.729	7.911	1.89	92.797	1.02	7.203	100
TA-235	0.0043	11.46	12.1	1.818	0.259	32.5	0	0.24	0	0	0	9.543	14.56	7.83	90.314	1.27	9.6856	100
TA-236	1.04	7.785	11.2	54.47	0.166	6.81	0.045	0.25	0	0.07	0.018	1.729	7.911	1.89	93.387	1.02	6.6128	100

3.4.3 Reflectance Spectroscopy:

In both TACC and C1CAC complexes, main absorption features of fluorapatite and/or monazite were identifiable in whole rock samples, as described by HUNT *et al.* (1972), when P₂O₅ wt% reaches ≥10% and rock structure is somewhat preserved. The absorption bands of the REEs in phosphates are doublets located at 0.57µm and 0.75µm and a single absorption band located at 0.8µm. It was not possible to determine precisely yet to which REEs the features correspond. It was observed that the double absorption feature at 0.57µm might not appear at all times that phosphates are detected by reflectance spectroscopy, considering other wavelengths. This is attributed to weathering and loss of the REEs from the crystal lattice. When present in samples, igneous phosphates always display absorption features centered at 0.75µm and 0.8µm.

The spectroscopic charts shown in Figs. 3.5 to 3.23 indicate clear absorption features for monazite, carbonates, phlogopite, vermiculite and kaolinite. Maximum reflectance features for goethite are in the same bands where the REEs absorption features are located. However, as detailed by XRF, absorption features of REEs in apatite and monazite prevail over Fe absorption features when P₂O₅ wt% is ≥15%, regardless of Fe content.

3.4.3.1 Catalão I Carbonatitic Alkaline Complex (C1CAC)

Samples extracted from fresh rock horizons (sample CA-Monazite-Barite) of the C1CAC showed a crystal twinning of monazite with barite. These samples were measured for reflectance and emission spectroscopy (fig. 3.5), considering different proportions

between these two minerals. The spectrum displays weak absorption bands due to REE ion charge transfers at 0,565 μm , 0,75 μm and 0,8 μm , similarly as reported by HUNT *et al.* (1972), ROWAN *et al.* (1986), ROWAN *et al.* (1995) and MARS & ROWAN (2011) for apatite and carbonatites from the Oka Carbonatitic Complex, Iron Hill, Gem Park and Mountain Pass in the US and Kaneshinn in Afghanistan. Hydroxyl and water absorption features are present at 1.4 μm and 1.9 μm and a well-defined calcite band is marked around 2.34 μm .

The region around 0.565 μm , 0.75 μm and 0.8 μm helps to determine to which phosphate mineral corresponds those absorption features, based on the shape imprinted by the REEs present as inclusions in the phosphate minerals. A more detailed spectrum on this region, extracted from the United States Geological Survey Spectral library, is presented in fig. 3.5 for comparison.

A zoom in the 0.5-0.95 spectral range (figs. 3.5 b,d,f) shows that a double absorption feature, commonly observed when monazite is abundant in the samples, appears around 0.75 μm . Such feature is due to the charge transfer of ions of REEs present in the mineral, either by La (HUNT *et al.*, 1972) or Nd (ROWAN *et al.*, 1986; 1995). Fluorapatite has a relatively poorly-resolved double feature, both in band depth and shape, with a small displacement of the band center towards 0.754 μm (fig. 3.6, CLARK *et al.*, 2007). These attributes can be used to identify the mineralogy of phosphates and REEs-bearing phases directly. A comparison between the monazite present in the USGS Spectral Library and the C1CAC monazite shows that the later has a doublet feature around 0.8 μm , instead of a single feature, as observed in the reference library spectrum.

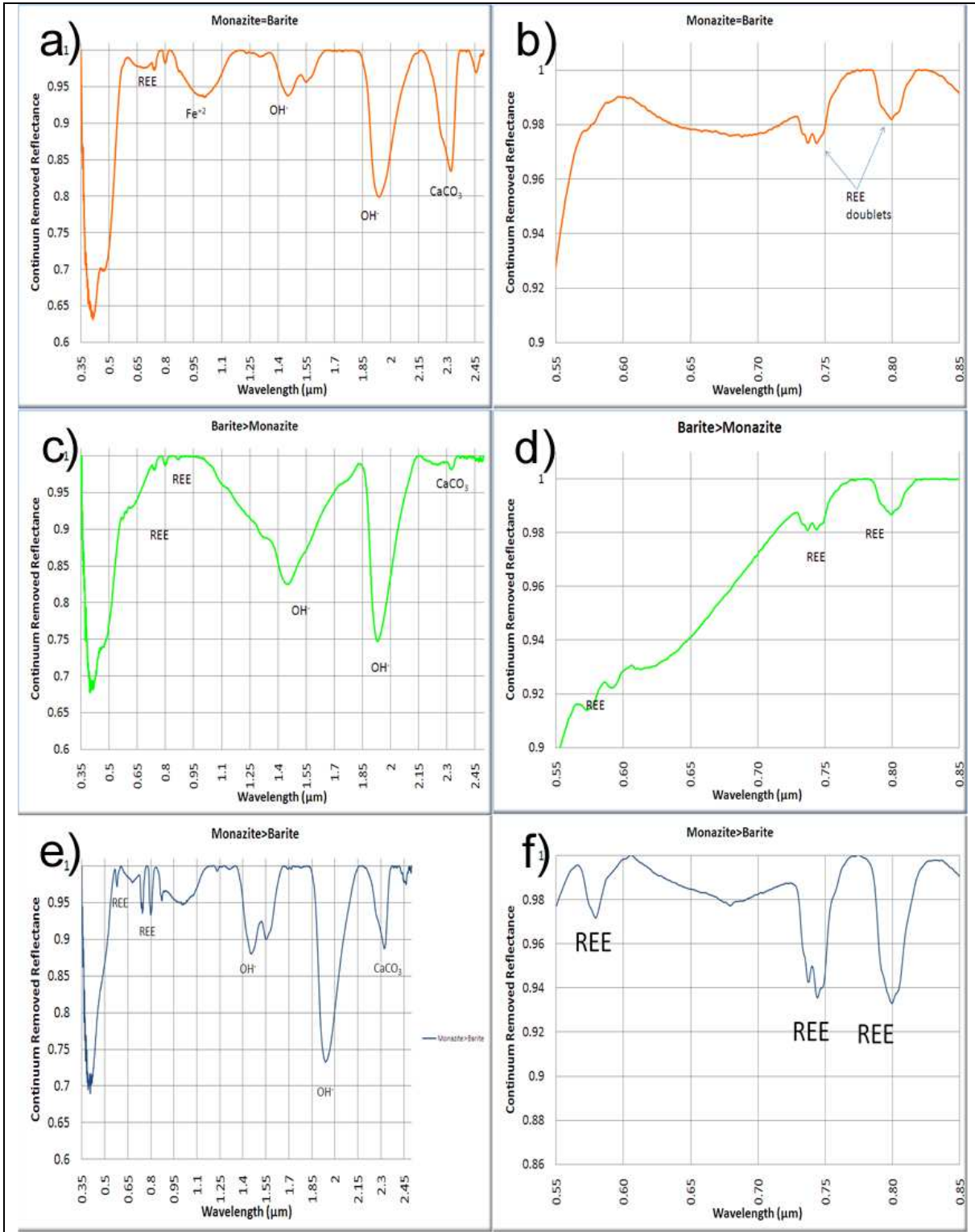
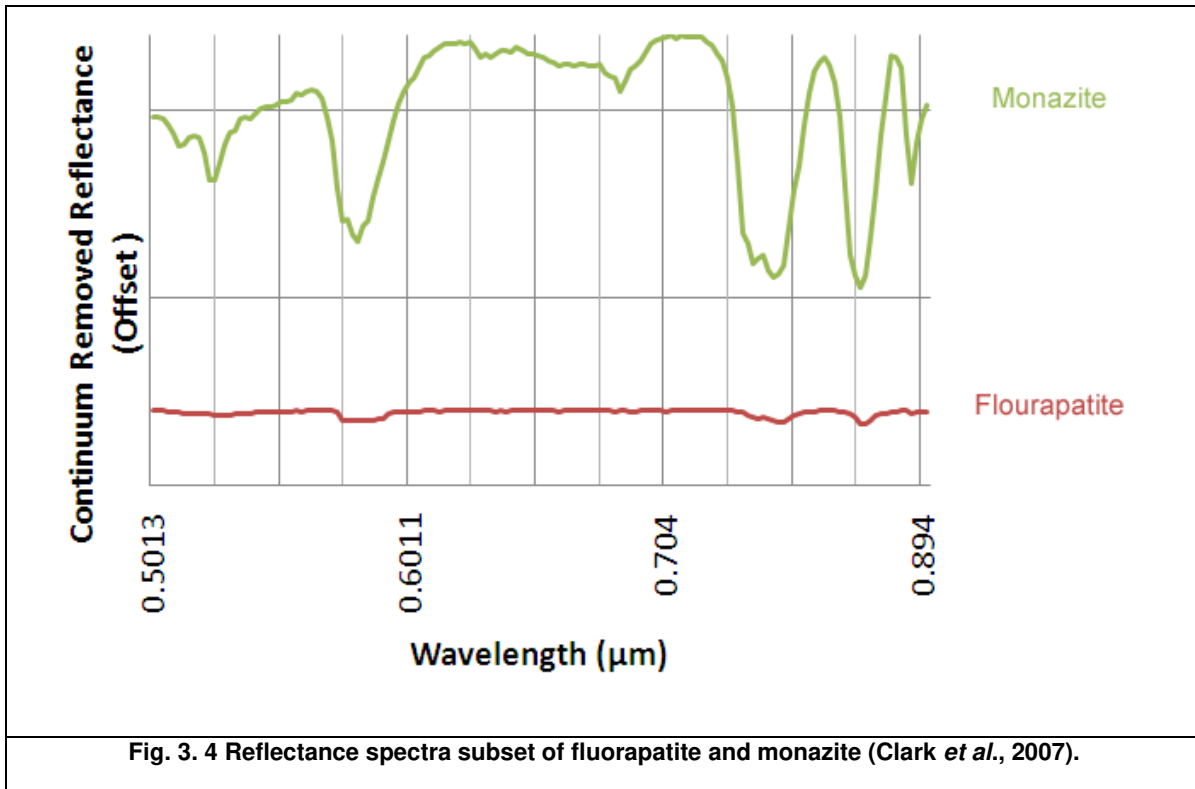


Fig. 3. 3. C1CAC Reflectance spectra of monazite-barite intergrowth.



A selected cluster of soil and rock samples collected above and within the isalteritic and aloteritic horizons (OLIVEIRA & IMBERNON 1998), which particularly bear low P_2O_5 content (as revealed by XRF), show well developed features for goethite (Fe_2O_3), magnetite (FeO), muscovite and dolomite (fig. 3.7).

XRD analysis of sample CA-29 (fig. 3.8), representative of sterile samples from the aloteritic and isalteritic horizons, shows the presence of secondary Al phosphates and secondary Ca phosphates (ernstite, aldermanite, paramendozavilite and carbonate-fluorapatite). These minerals show low intensity and evidences of low “crystallinity” on the diffractograms, given the wide peaks observed. XRF results for these samples yielded a P_2O_5 content of less than 5%, a threshold that makes this material expendable in the industrial recovery of apatite.

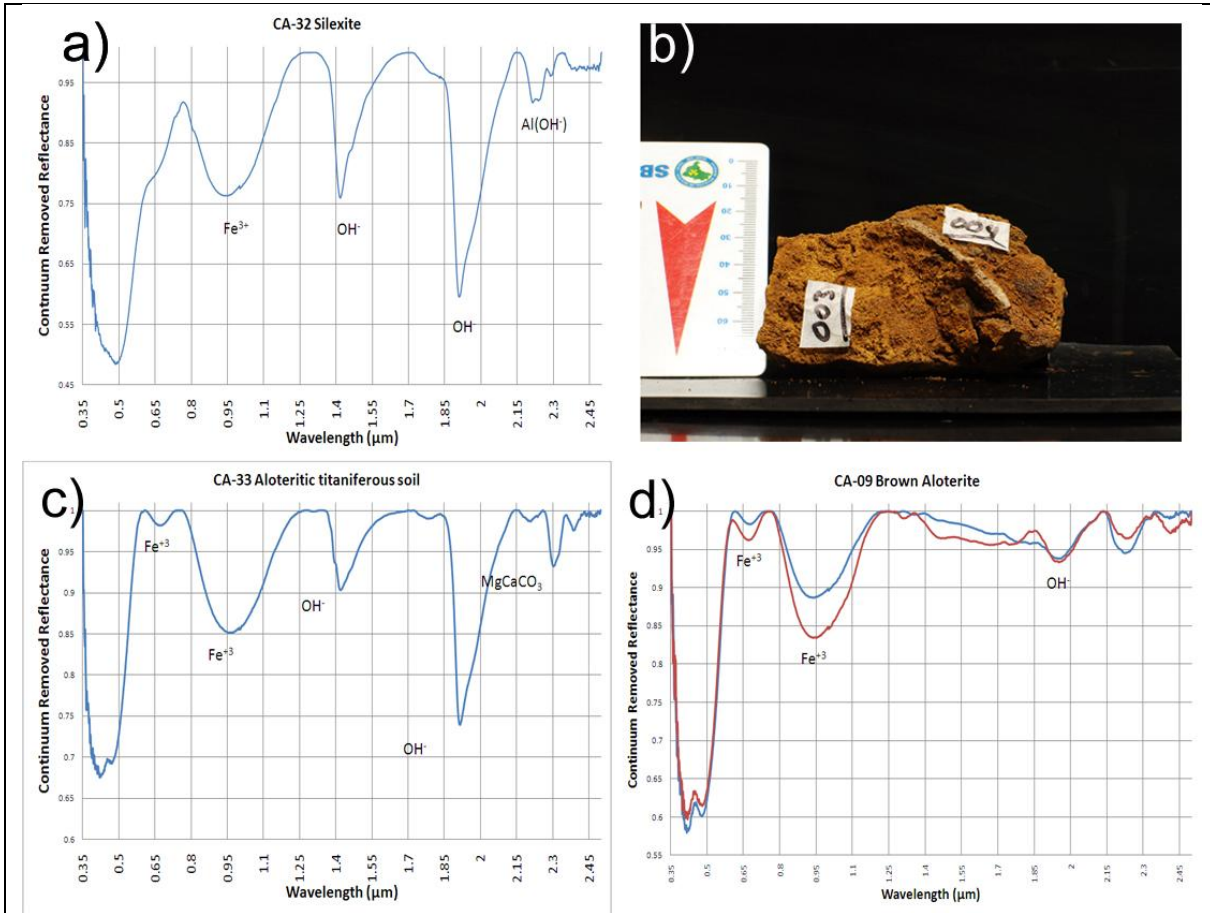
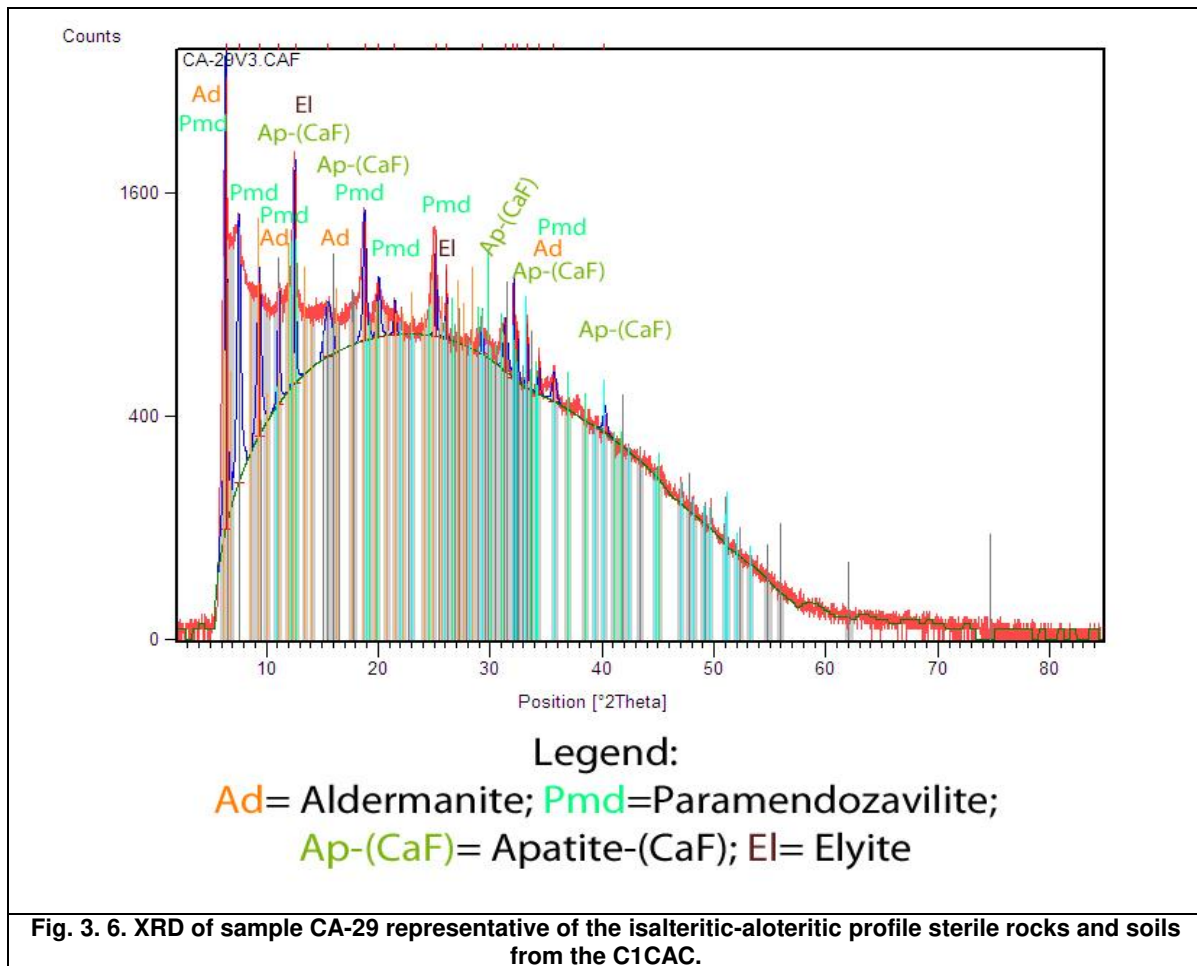
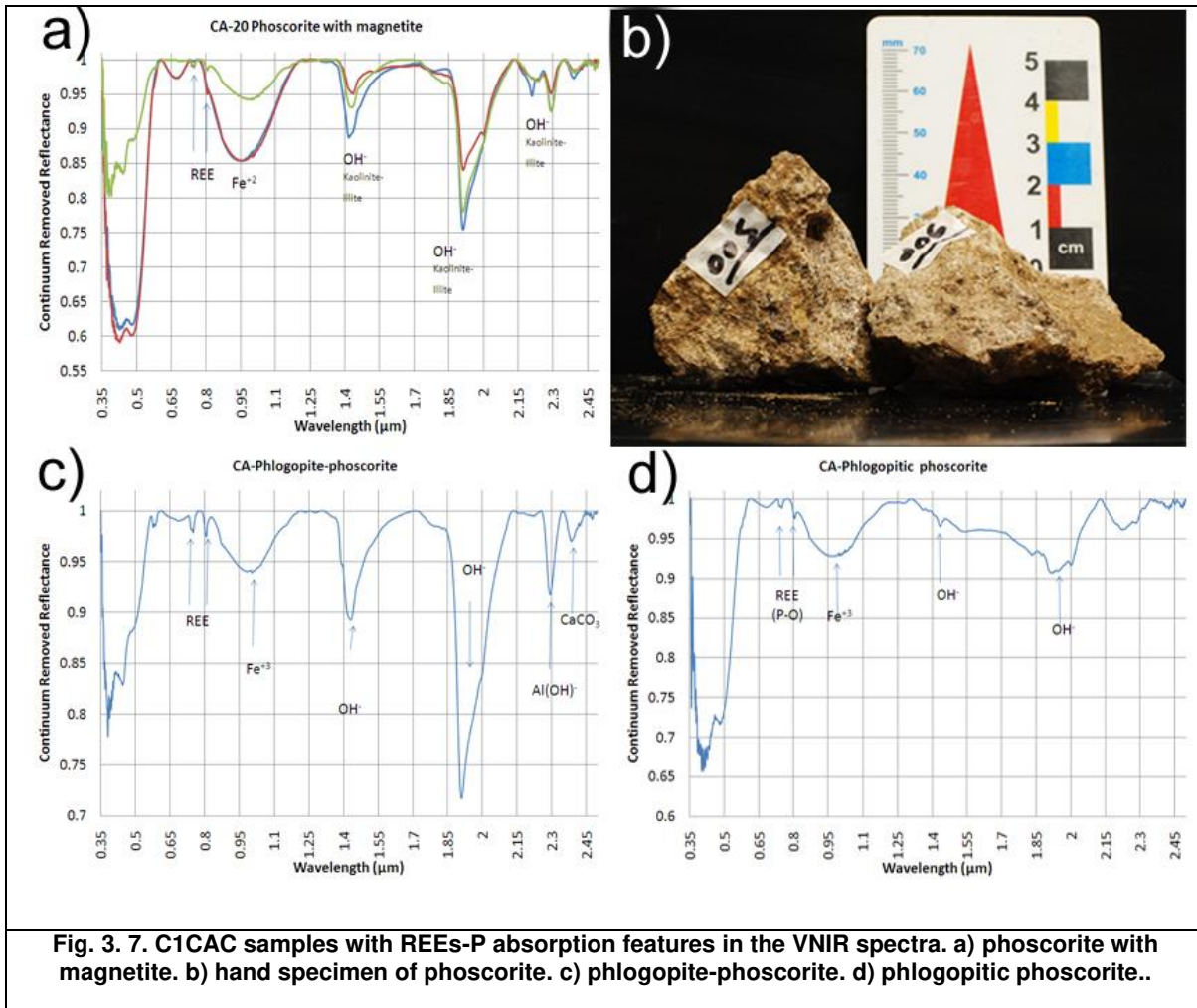


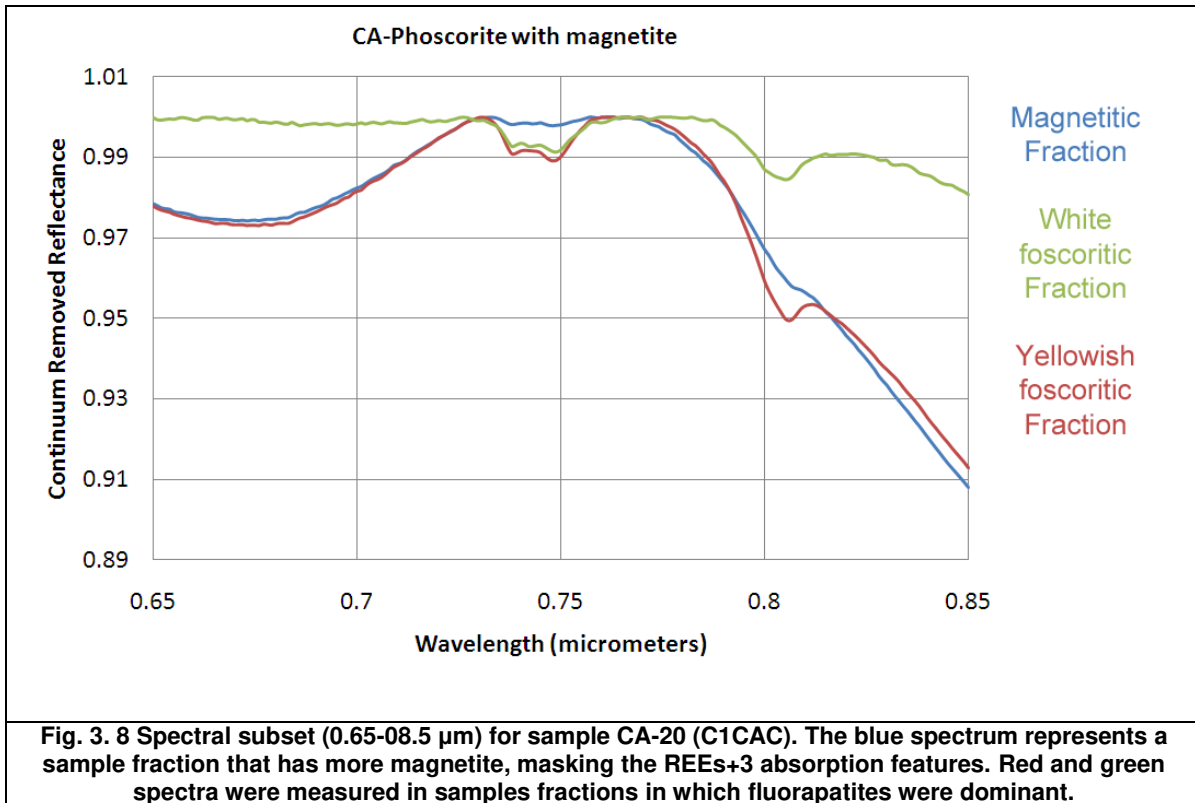
Fig. 3. 5 Reflectance spectra of P-free soils and rocks from the C1ACC. a) silexite. b) hand specimen of brown aloterite with silexite vein. c) aloteritic titaniferous soil. d) brown aloterite.



Samples of carbonatite-apatites, phoscorites, phlogopite-phoscorites and altered phlogopitites form a representative cluster of materials mined in the isalteritic and altered rock profiles (fig. 3.9). They are named specifically as phlogopite-phoscorite (CA-18D), dark magnetitic phoscorite (CA-55), phoscorite with magnetite (CA-20) and magnetitic phoscorite (CA-39). Most samples show typical REEs-bearing phosphate features between 0.5-0.95 μm , although the 0.5 μm feature can be absent when samples are severely weathered. Features of additional mineral phases in these rocks, such as phlogopitite, calcite, dolomite and kaolinite, are identified as secondary markers of the lithotypes.



Detailed analysis of sample CA-20 in the 0.75 μm -0.8 μm range (fig. 3.10) indicates that there is a match between the existence of fluorapatite in the sample and the appearance of REEs absorption features in the spectra. Note in the figure that the doublet feature is ill-defined in the spectra displayed in blue color (reflectance measurement of the magnetitic fraction of the phoscoritic sample). The absorption feature represents the presence of REEs inclusions in the fluorapatite structure, forming a plateau instead of a doublet absorption band. An absorption band centered at 0.754 μm is observed in contrast to the well-defined doublet that monazite usually shows at 0.749 μm . The band absorption at 0.8 μm is also probably linked to the presence of REEs. The difference in the features is attributed to variation of Fe content, forming intimate mixtures in the sample.



Spectra of rocks collected in the altered and fresh rock horizons generally display REEs absorption features that are easily discernable both at mined and wall rocks. A sample of carbonatite-apatite (fig. 3.11) was collected at the fresh rock horizon. It shows a well-defined calcite absorption feature at 2,34μm and absorption features at 0.75-0.8 μm related to the presence of REEs. Some water absorption features are also detected in the water band between 1.90-1.97 μm. This sample shows a good match to previously published spectra of carbonatites studied elsewhere (ROWANet *al.* 1986; ROWANet *al.* 1995; MARS & ROWAN 2011).

A detailed analysis of the REEs absorptions features of fig. 3.10 indicates that the phosphate detected in sample CA-carbonatite-apatite is monazite. This interpretation is based on the depth of the feature and the clear doublet at the 0.75μm band; also the band center matches the monazite band center at 0.749 μm(fig. 3.12).

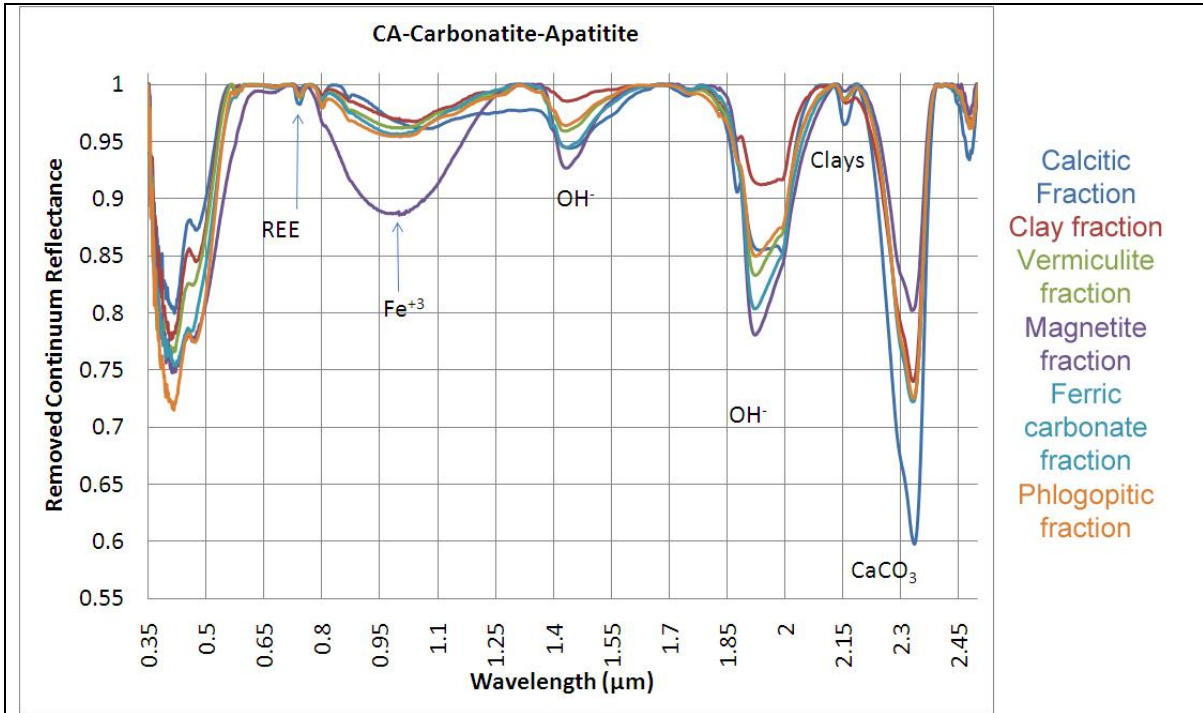


Fig. 3. 9 Reflectance spectra of a Carbonatite-Apatite of the C1CAC.

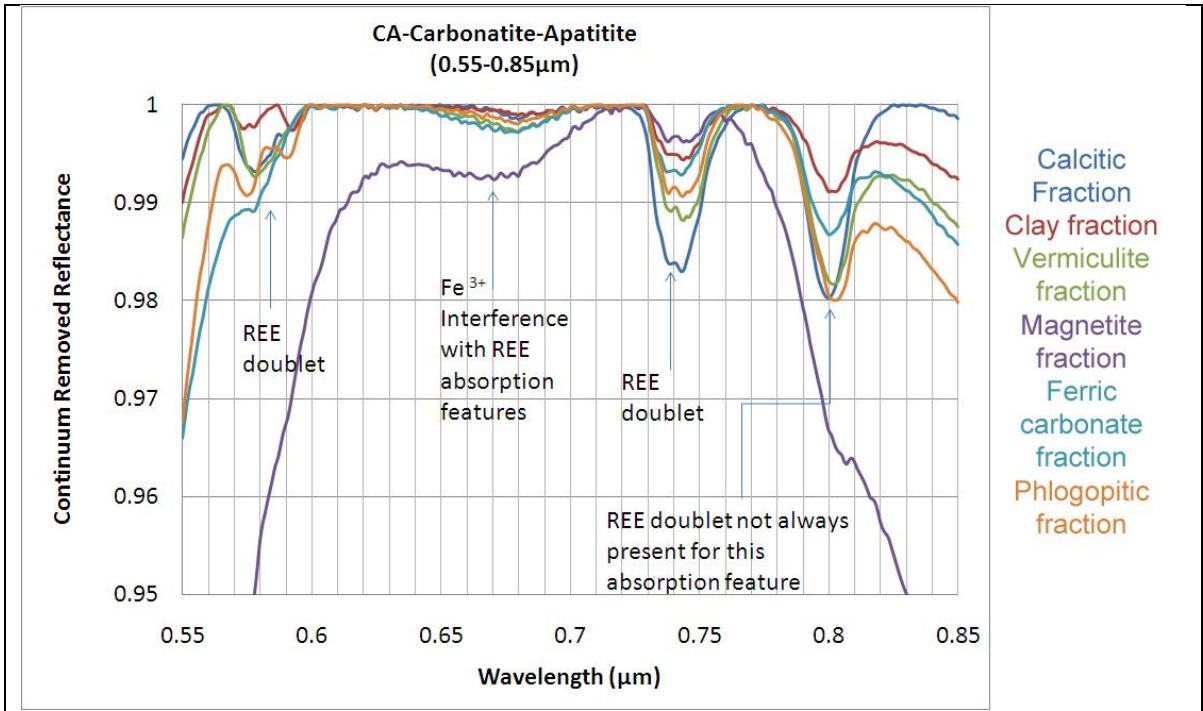


Fig. 3. 10 Spectral subset (0,55-0,85 μm) for sample CA- Carbonatite- Apatite (C1CAC).

The phoscorite-phlogopitite (fig. 3.13) displays ill-defined REE features in the 0.55 μm band. It also show features centered at 1.4 μm , which are diagnostic of phlogopite. Water trapped in the phlogopite structure has a well-defined absorption band at 1.9 μm . A an absorption feature of calcite at 2.34 μm can also be identified and attributed to the carbonate-rich portion of the phoscorite. The rounded slope seen between 0.62 μm and 0.887 μm is attributed to goethite.

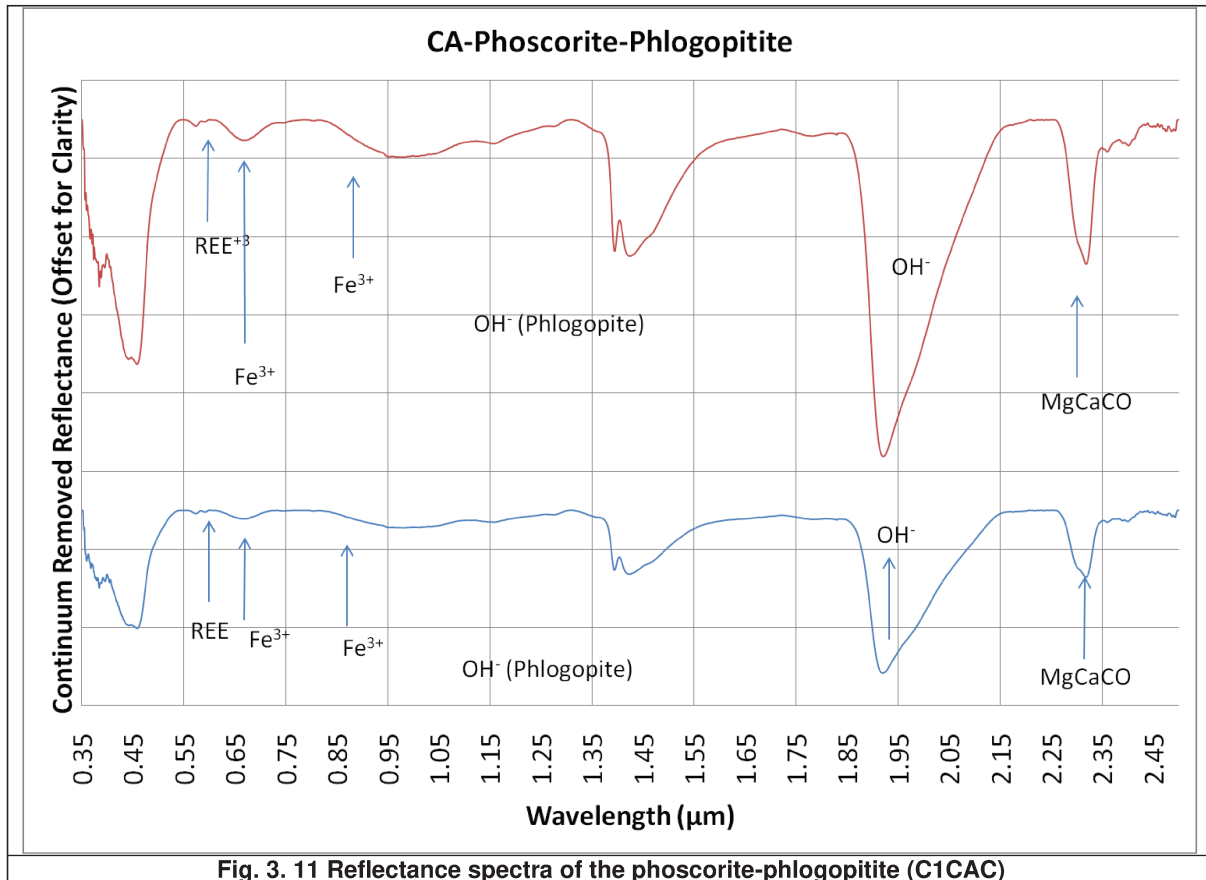
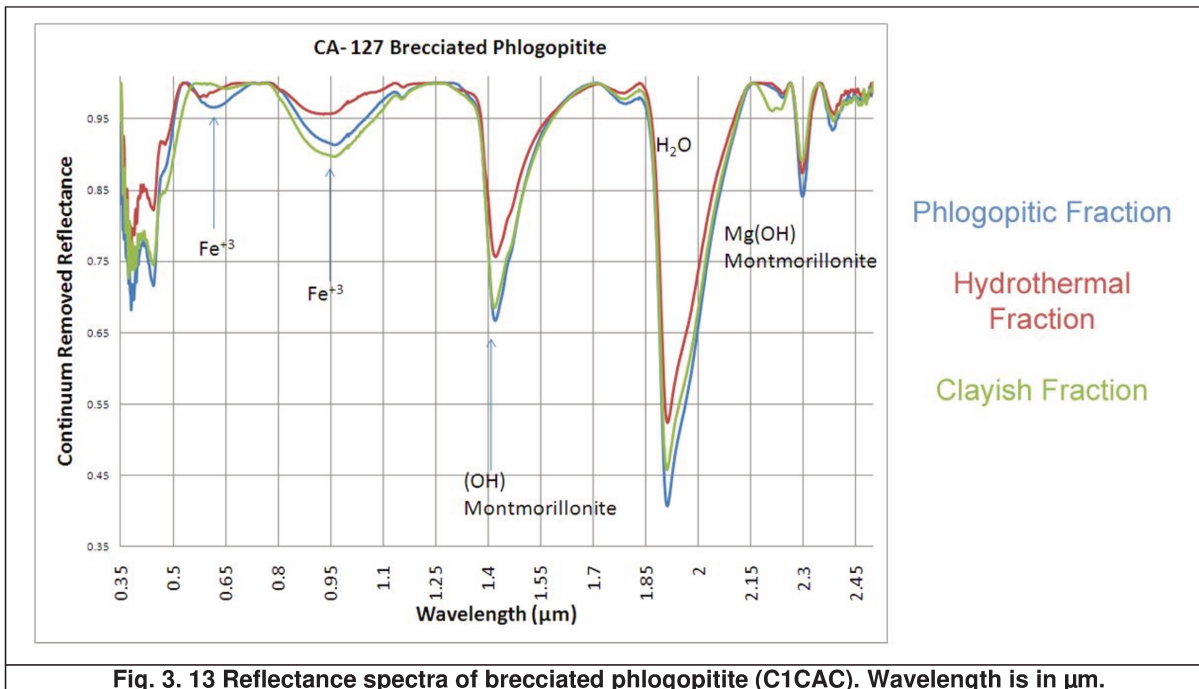
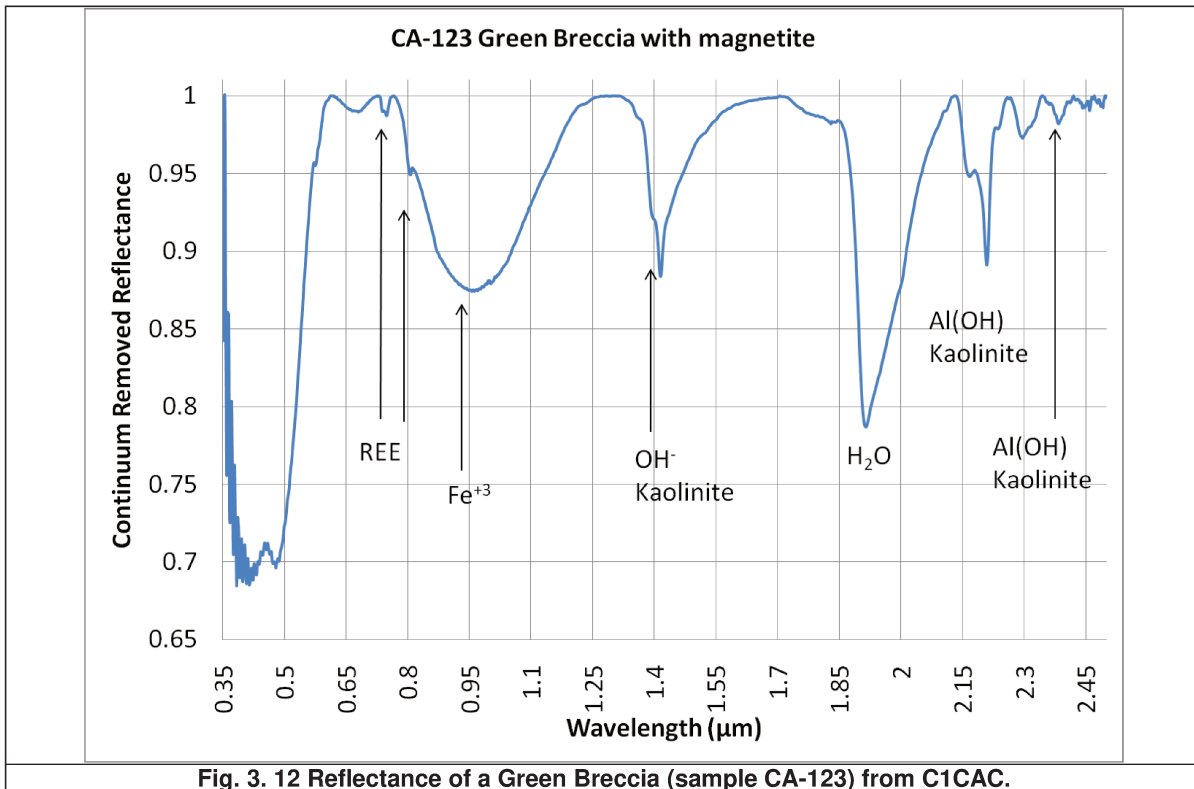


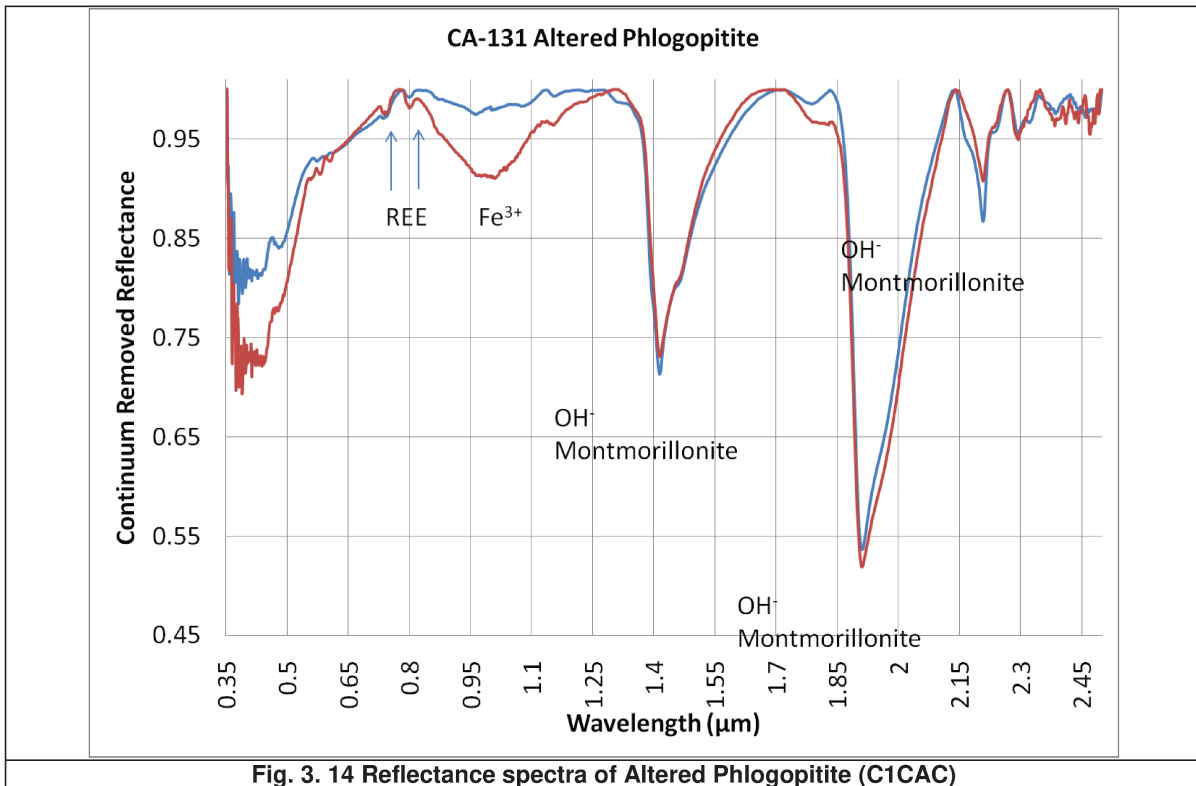
Fig. 3. 11 Reflectance spectra of the phoscorite-phlogopitite (C1CAC)

The green breccia with magnetite shows clear REEs absorption features (fig. 3.14). It also hosts typical features of kaolinite, with absorptions at 2.165 and 2.2 μm . Very weak shoulders that could be attributed to kaolinite are located at 2.28-2.35 μm . Water, probably trapped in the kaolinite chains, is also detected at 1.9 μm .

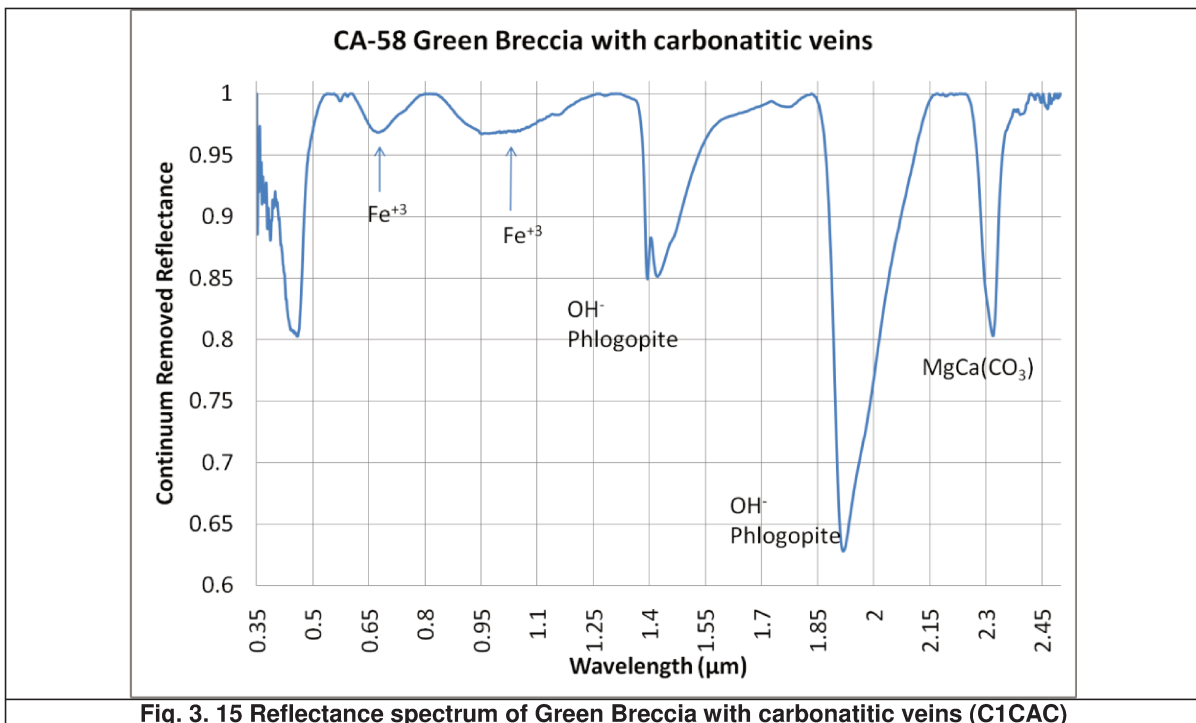
The brecciated phlogopitite (fig. 3.15) displays absorption features at 1.4 μm ; 1.9 μm and 2.1 μm that are diagnostic of montmorillonite. The 2.1 μm absorption feature is enhanced in this particular sample.



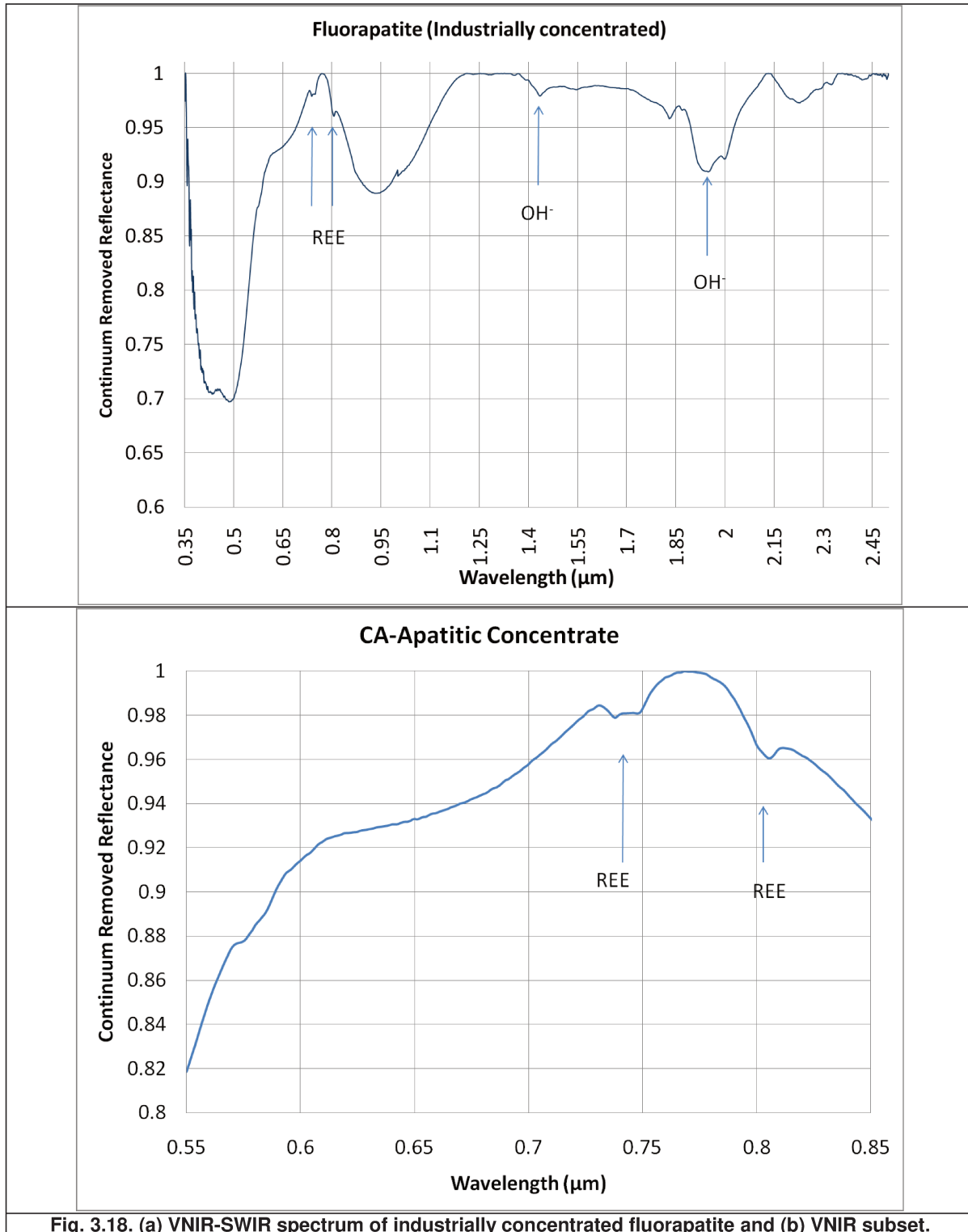
The altered phlogopite (sample CA-131, fig. 3.16) is marked by diagnostic absorption features of REEs (0.75-0.85 μm). Other features at 1.4 μm ; 1.9 μm and 2.1 μm are attributed to montmorillonite.



The green breccia with carbonatitic veins displays a well-defined 1.3 μm absorption feature, characteristic of phlogopite, and a 2.3 μm feature typical of dolomite (fig. 3.17). No REE absorption bands are observed in this sample, which concur with XRF results.



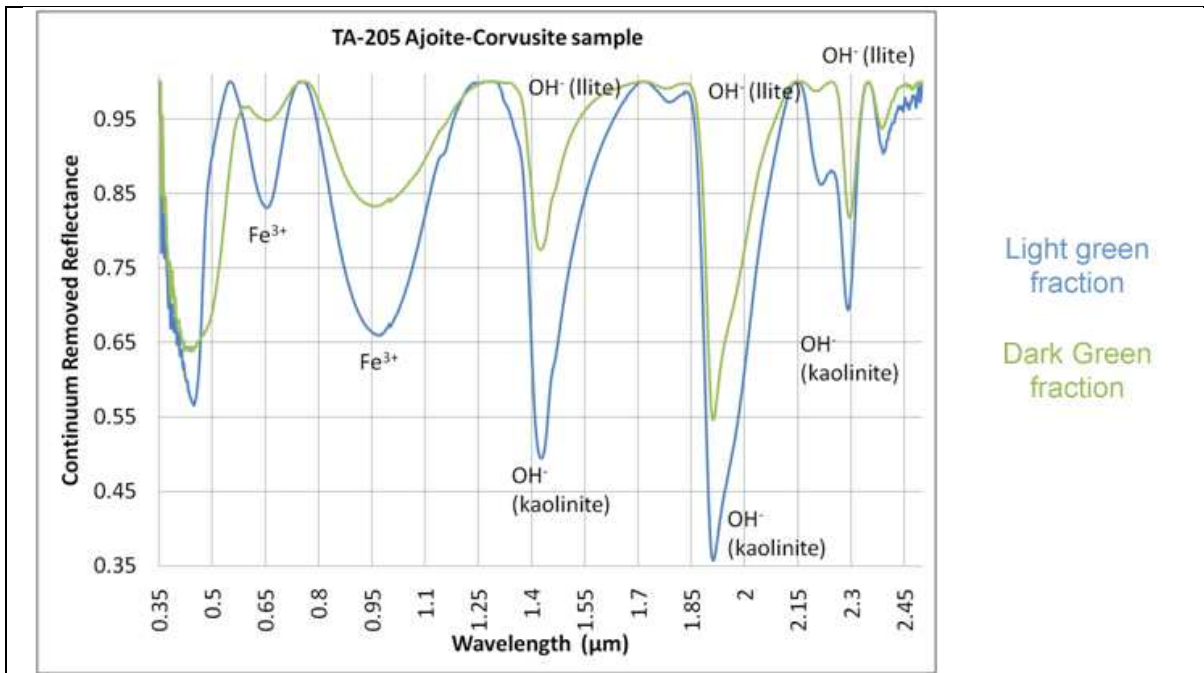
Industrially concentrated apatite extracted from C1CAC rocks displays relatively subtle REE absorption features in the 0.75 μm region (figs. 3.18a and b). These spectra are more characteristic of fluorapatite, which is the main phosphate product of the mine.

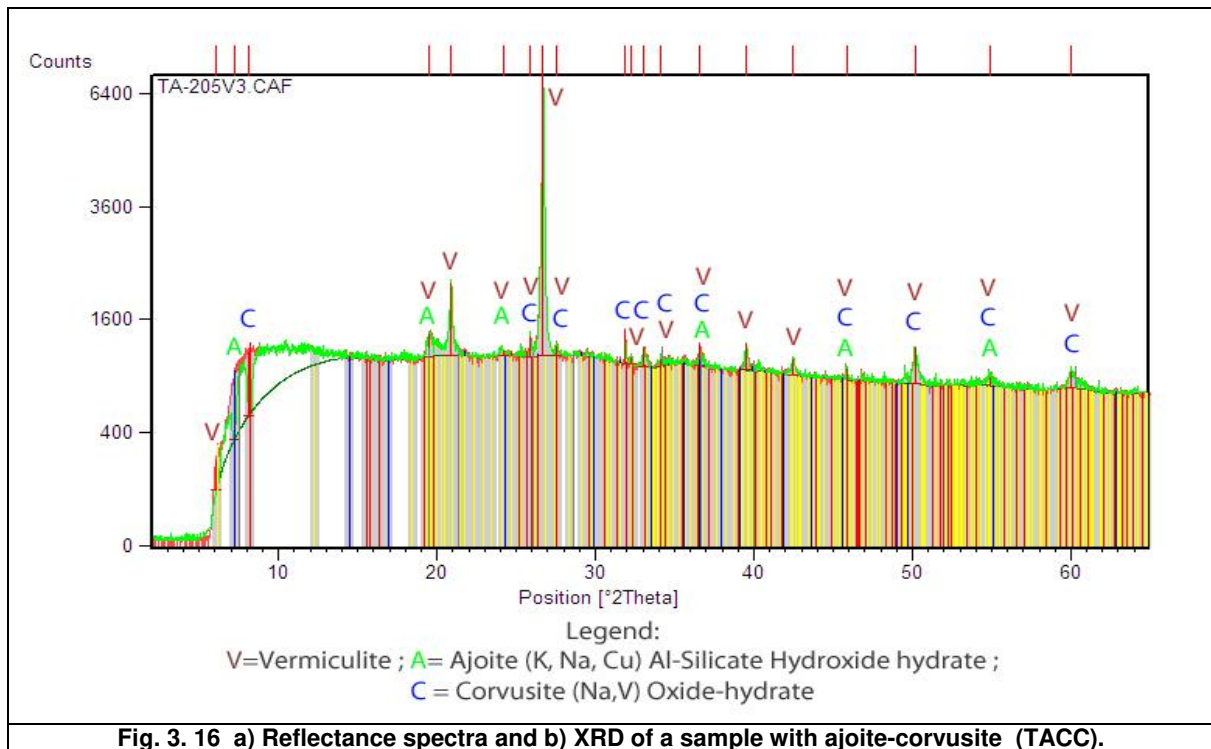


3.4.3.2 Tapira Carbonatitic Alkaline Complex

The Tapira Alkaline Carbonatitic Complex (TACC) spectra are marked by more smoothed absorption features in general. Here, weathering is not as widespread as observed in the C1CAC. REEs absorption features are depicted at 0,52 μm ; 0,75 and 0,8 μm . Micas analyzed through reflectance spectroscopy range from phlogopite, vermiculite and biotite, and can form phenocrysts up to 8 cm in length. Clays are scantier and Fe-O bonds have broader shoulders than those found in the C1CAC samples, probably due to less significant chemical weathering.

Sample TA-205 comprises a green, hard mineral described as monazite by miners in the TACC. Reflectance spectra yielded from this sample are displayed in fig. 3.19a. Vermiculite was also detected. Maximum reflectance spikes are observed around 0.48 μm ; 0.64 μm and 0.82 μm . Vermiculite features appear at 1.4 μm . Al-OH absorption bands are depicted at 2.29 μm and 2.38 μm . The reflectance peak at 0.54 μm is responsible for the vivacious green color of the sample. Using XRD, it was possible to identify three mineral phases in the sample: ajoite, corvusite and vermiculite (fig. 3.19b).





The most prominent REEs absorption features were identified in sample TA-219. The hand specimen was catalogued as a layered phoscoritic-picritic-carbonatite (fig. 3.20). The sample spectra show significant REEs absorption bands (fig. 3.21b, 3.21c). In different parts of the spectrum, calcite, illite and kaolinite features are also observed (Fig. 3.21b). A detailed examination of the pattern of the REEs absorption bands shows that monazite is the dominant phosphate in the sample, considering the sharp doublet centered at 0.75 μ m.



Fig. 3. 17: Sample TA-219 of a layered carbonatite (TACC)

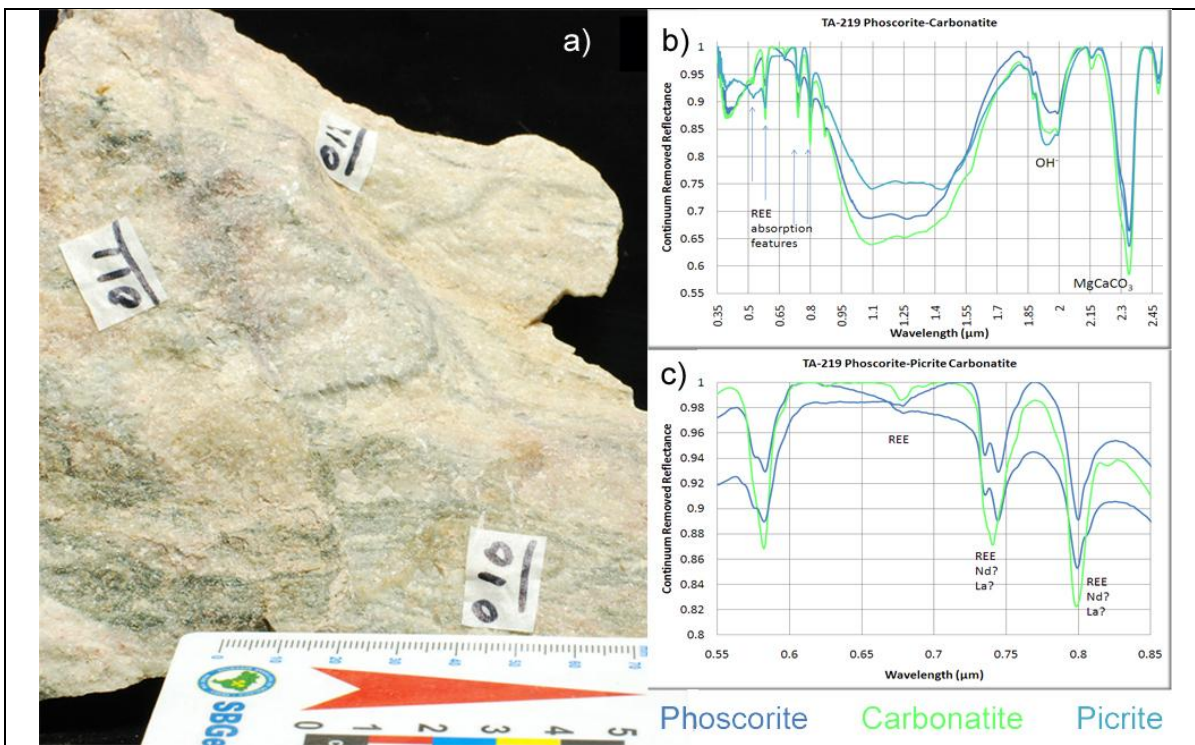


Fig. 3. 18 a) Phoscorite-picrite-carbonatite from the TACC. b) Full spectrum of the phoscorite-picrite-carbonatite (TACC) c) Sub-set of the 0.55μm-0.85μm spectrum displaying REEs absorption features.

The TACC B2 (carbonatitic) bebedourite display a strong Fe^{+3} absorption within isolated REEs absorption features. REEs absorption features are present at 0.55μm; 0.75μm and 0.8μm. Typical phlogopite and dolomite absorption features are also observed

in the sample spectra. Phlogopite features are strong and distinctive, especially at 1.4 μm . The spectra can be seen in fig. 3.22.

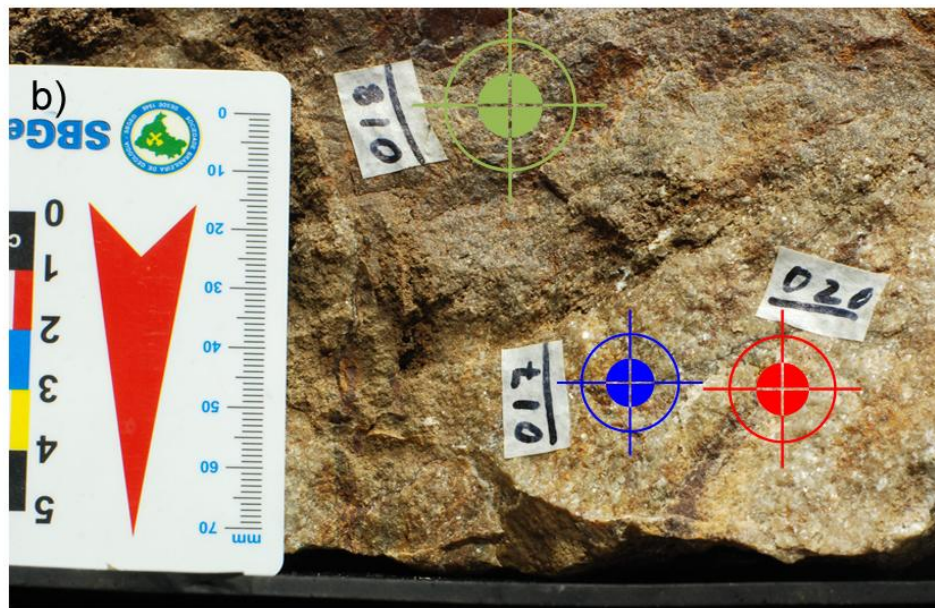
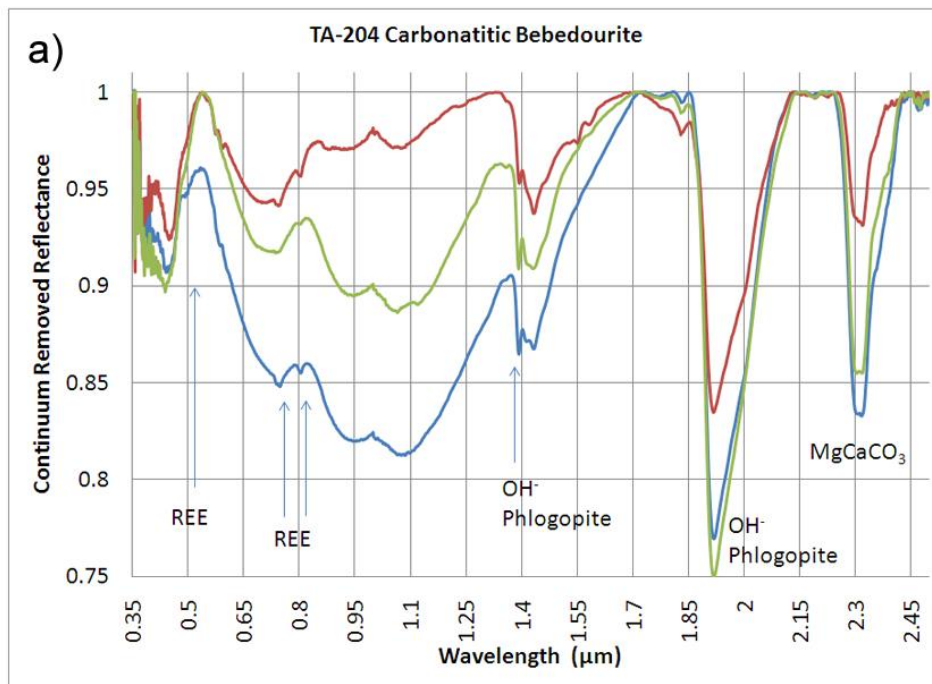


Fig. 3. 19.a) Reflectance Spectra of Carbonatitic Bebedourite (TACC). Green spectrum corresponds to a bebedourite with phlogopite; blue spectrum is a bebedourite with magnetite; red spectrum is a bebedourite sensu stricto. b) Picture of the analyzed sample. Target colors correspond to spectral curves illustrated in (a).

Secondary phosphates show strong REEs features in Tapira, as displayed by sample TA-236, extracted from an isalterite horizon (fig. 3.23). The phosphates detected by XRD in this sample are phuralumite (Al-U-phosphate) and ushkovite (Mg-Fe-phosphate). Vermiculite was also distinguished.

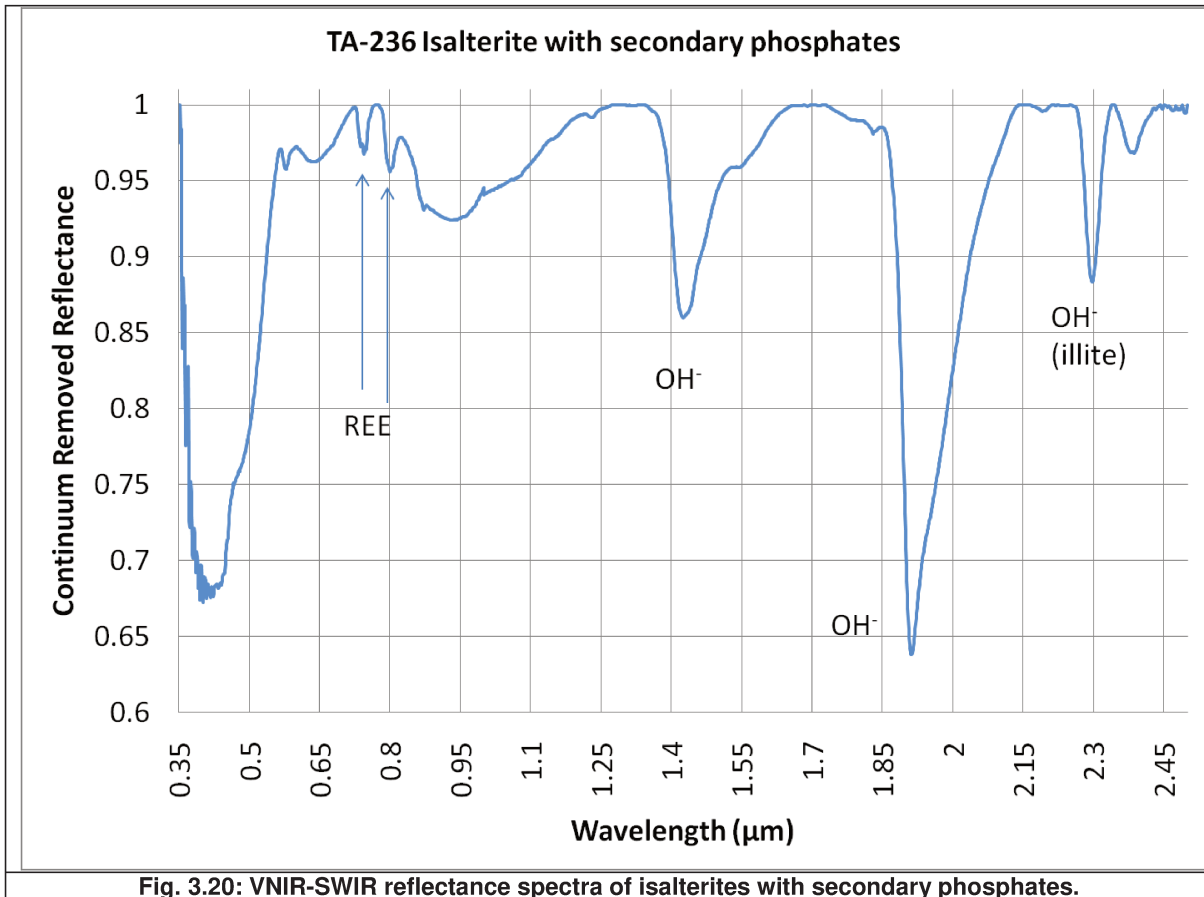


Fig. 3.20: VNIR-SWIR reflectance spectra of isalterites with secondary phosphates.

3.4.4 Emissivity Spectroscopy

For the Emissivity spectroscopy of sample CA-Monazite-Barite, the crystals were separated from the intergrowth using steel tweezers, selecting only the monazite crystals, as shown in fig. 3.24. The collected crystals were not submitted to crushing and grinding to avoid loss of material.



Fig. 3. 21 Monazite crystals yielded from the C1CAC measured for Diffuse Reflectance (2.5-25 μm).

The spectrum, shown in fig. 3.25, is dominated by double absorption features at 3.43-3.54 μm and 4.01-4.08 μm . There is a minimum in emissivity at longer wavelengths (8.81 μm) that is due to P-O bonds. This feature coincides with the phosphate stretching and bending ν_3 region (REDDY *et al.* 2008). The main absorption feature in Emissivity was not observed with the spike doublet as it is reported in other spectral libraries (DAASCH & SMITH 1951; CHRISTENSEN *et al.* 2000; LANE *et al.* 2007a; LANE *et al.* 2007). This may be caused by the crystallizing conditions in Catalão I, which have been reported as non-ideal for apatite and monazite, while goerzeixite is produced when primary apatite goes through Ba replacement. Also, interstitial water has been determined in monazites from Catalão I (TOLEDO *et al.* 2004a; TOLEDO *et al.* 2004b).

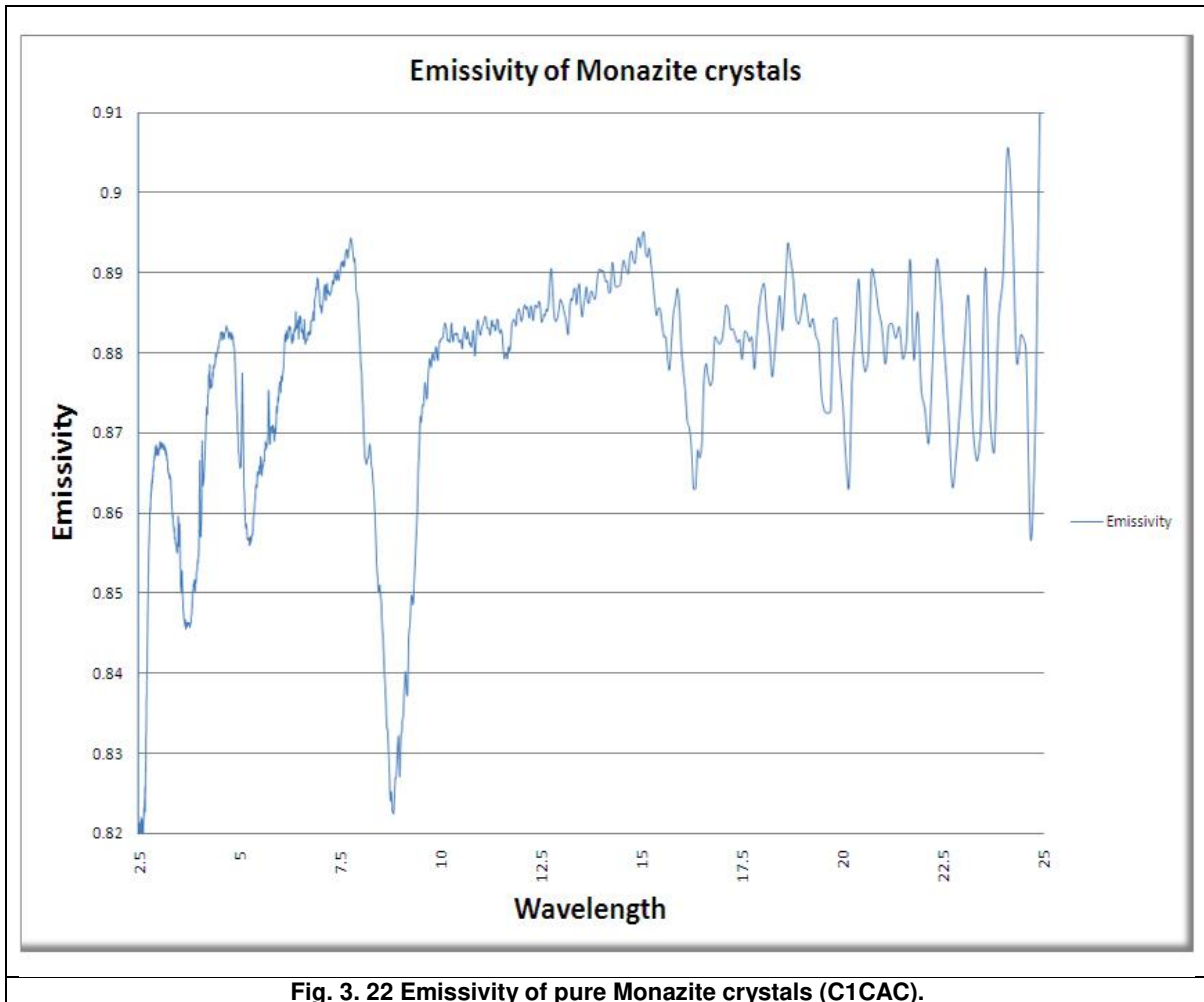


Fig. 3. 22 Emissivity of pure Monazite crystals (C1CAC).

Emissivity characterization of sample CA-115, a phoscorite rich in apatite, yielded a stronger absorption feature in the P-O band, once again without the spike of the P-O double absorption feature (fig. 3.26). XRF data for this sample yielded the highest P_2O_5 %wt measured in this deposit (35%wt P_2O_5).

Sample CA-123 (fig. 3.27) shows absorption features centered at 8,5-9,2 μm related to niobium and apatite, similarly as reported by HAIDER (1961) elsewhere. Double absorption features are less accentuated due to lower phosphate content as indicated by XRF analysis.

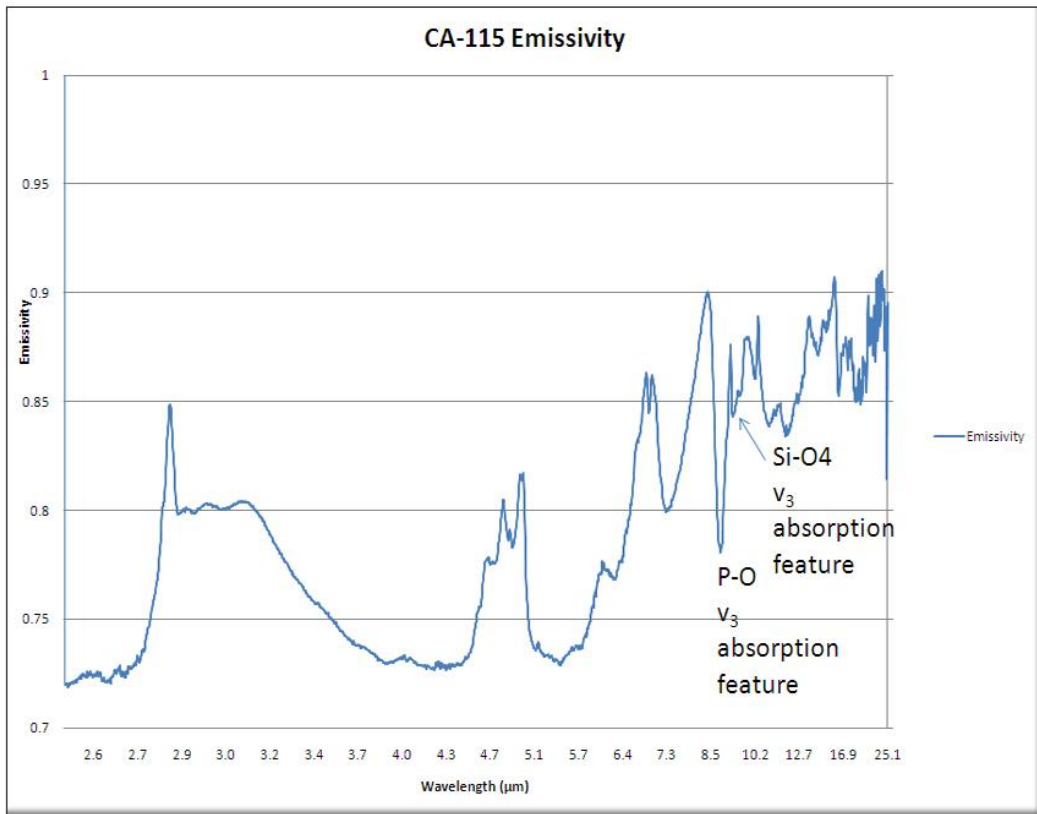


Fig. 3. 23 Emissivity of Sample CA-115 (C1CAC).

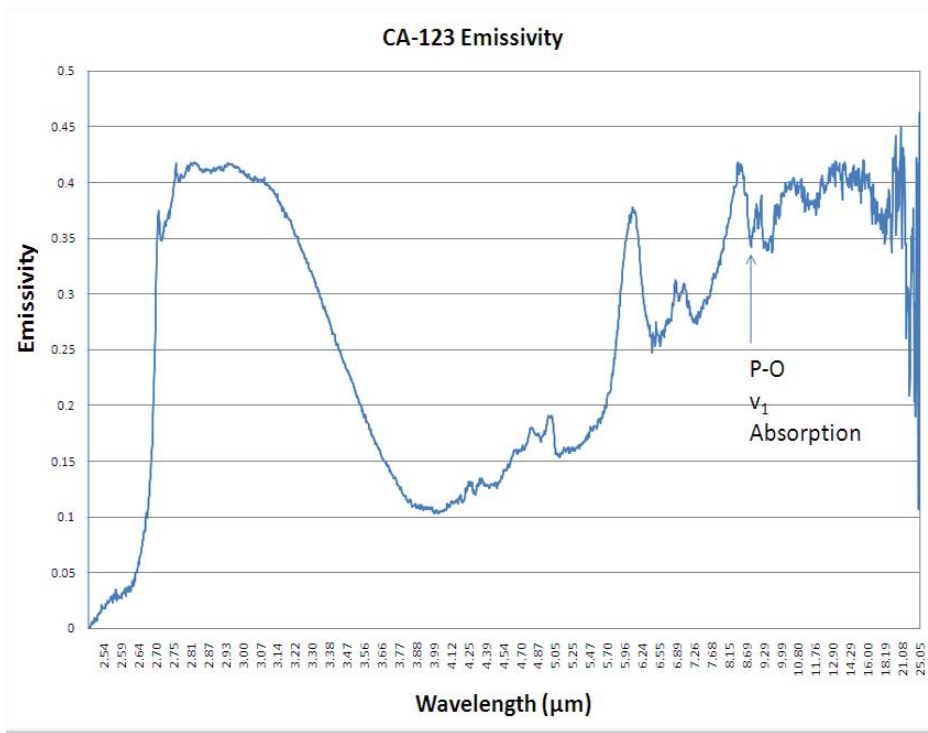


Fig. 3. 24 Emissivity of Green Breccia sample CA-123 (C1CAC).

Sample TA-236 (fig.3.28) hosts P_2O_5 content lower than 7%. It shows a subtle emission peak in the ν_3 region, typical of phosphates minerals. Overtones of the P-O absorption features are observed in the 7.08 μm band.

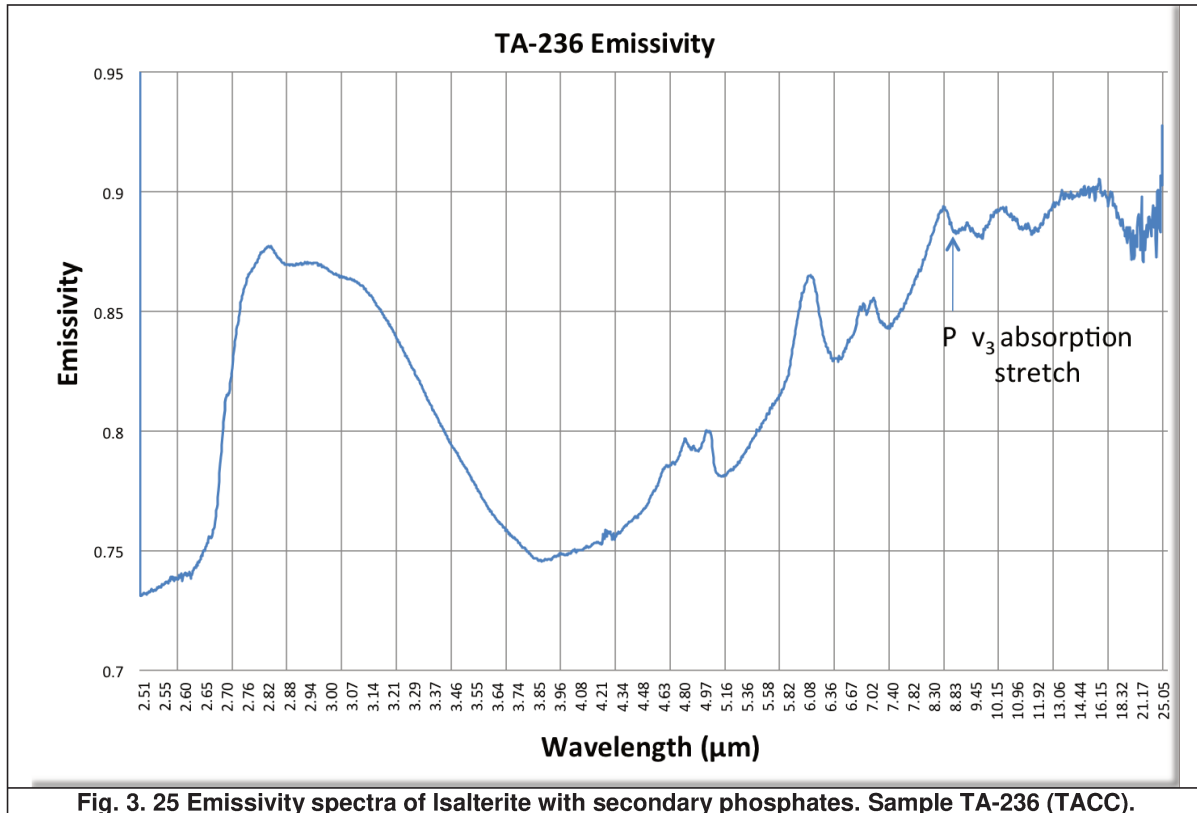


Fig. 3. 25 Emissivity spectra of Isalterite with secondary phosphates. Sample TA-236 (TACC).

3.5 Discussion

It is evident that no exclusive phosphate absorption features can be found in reflectance spectra of the magmatic deposits investigated here, but those due to REEs (e.g., HUNT *et al.* 1972). Specific, well-resolved REEs double absorption features centered at 0.575 μm and 0.75 μm can be used to indirectly diagnose the presence of either fluorapatite or monazite in phosphate samples.

Overall reflectance values for rocks from the Tapira complex are generally higher in reflectance, reflecting the white colors present in most of the mined rocks from the complex. Even though rock features are more preserved in the Tapira complex, absorption features are smoother than those observed for the Catalão I specimens.

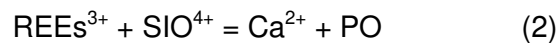
The emission spectroscopy results for the approached lithotypes suggest that relationships for the amount of P_2O_5 detected by the FTIR instrument are non-linear. Other oxides that were detected by XRF could not be distinguished in the emissivity spectra. However, it is noticeable that the emission high centered at $8.2 \mu m$ is consistent in all samples investigated. This suggests that it is possible to characterize phosphates using FTIR techniques and then use this information for remote sensing of igneous phosphates, combined with the spectroscopic information from the REEs absorption bands. Also, the presence of high contents of U on samples from the TACC complex might be responsible for less developed features in the TIR region of the spectra, which gives TACC emission spectra a smoother, less crystalline visual pattern.

It was noted for the majority of studied samples that phosphates are more prone to be identified through their REEs absorption features in the phlogopitite and carbonatite lithotypes, especially when P_2O_5 is above 10%wt. Main mineral phases in these units are phlogopite, vermiculite, biotite, calcite, dolomite, and clays (kaolinite and montmorillonite). The clays are usually present in the areas where phlogopitites are exposed. Phoscorite weathering favors the formation of sandy soils, given the resistance of apatite and magnetite to weathering agents.

REEs absorption bands presented here cannot be pinpointed to a specific REE. While HUNT *et al.*, (1972) attributed the REEs absorption features to the divalent ion of La^{2+} , ROWAN *et al.*, (1986) qualifies the absorption features of 0.75 and $0.8 \mu m$ to Nd_2O_3 . This cannot be confirmed yet, since a detailed REEs study is out of the scope for the moment, but it will be looked on in future research. Another factor that leads to unclear results is the substitution mechanisms in monazite and apatite that can make that fluorapatite features become less prominent.

Substitutions in the fluorapatite structure by REEs are complex and prone to many outcomes (PAN & FLEET, 2002). For the fluorapatite of Catalão I, REEs varies from Sr to Gd (RIBEIRO, 2008), but always as a secondary REE carrier. Monazite acts as the main REEs mineral bearer. The dependence of the partitioning coefficient of REEs on SiO_2 is generally attributed to a decrease in the number of melt sites suitable for $REEs^{3+}$ cations, with increase in the degree of polymerization (WATSON 1976; ELLISON AND HESS 1989, GAETANI AND GROOVE 1995, *apud* PAN & FLEET 2002). In this context, it is very likely that although apatites in the Catalão I complex were being altered due to weathering

and transportation on the weathering profile, they could substitute minerals into the apatite structure following the equation proposed by PAN & FLEET, (2002):



This equation would be consistent with the weathering products in Catalão I, when hydrothermal fluids alter the carbonatitic rocks, lixiviating Ca^{2+} and mobilizing supergene apatite, as established by TOLEDO (1999).

3.6 Conclusions

Spectroscopy of phosphates proved useful for the discrimination of mine targets for the carbonatitic complexes of Catalão I and Tapira. The presence of REEs in the spectra can promptly indicate the sufficient amount of phosphorous that is needed for the mining recovery of apatite. The combined use of X Ray Fluorescence data, X Ray diffraction data, reflectance and emission spectroscopy allowed the classification and identification of mining lithotypes of the Catalão I and Tapira mines, providing data that is helpful for target selection, mine wall mapping and mineral exploration.

For the carbonatitic complexes studied in this research, the lithotypes that can be best-discriminated using spectroscopy are carbonatites and phoscorites. These rocks host high concentration of phosphates both in the C1CAC and TACC. Mineralogical vectors in the APIP can be vermiculite and phlogopite, since these minerals are ubiquitous in the carbonatitic complexes known to date in the region.

REEs play a major role in the identification of phosphate absorption features. We have been able to determine that the small variations in absorption features centered at $0.75\mu\text{m}$ can be used to distinguish monazite from fluorapatite and apatite-(Cl). This can be a possible path to link phosphate occurrences through remote sensing methods using several current multispectral sensors, including ASTER, given that its band 3 covers absorption features within the $0,75\mu\text{m}$ - $0,8\mu\text{m}$ interval.

Being proved in laboratory conditions that reflectance spectroscopy can identify important mineral phases that indicate the presence of phosphates, possible in situ methods can be developed that may measure, in semi-quantitative ways, the mineral phases present at mine sites, creating new and fast information for target selection and ore control at mine faces.

The spectral data presented here will contribute to the remote sensing of phosphates. It is envisaged that through digital image processing techniques it is possible to discriminate areas with phosphate concentrations using multispectral images that cover the visible and near infrared part of the electromagnetic spectrum.

Reflectance and emissivity data applied jointly may provide regional solutions for the mineral prospecting of igneous phosphates. Using this tool as a prospecting technique in appropriate igneous provinces may lead to the discovery of new carbonatitic alkaline complexes and expansion of current phosphate reserves.

3.7 References

- AMARAL, G., BUSHEE, J., CORDANI, U. G., KAWASHITA, K., & REYNOLDS, J. H. (1967). Potassium-argon ages of alkaline rocks from southern Brazil. **Geochimica et Cosmochimica Acta**, 31, 117–142.
- ARAÚJO, D. P. (1996). **Metassomatismo no complexo carbonatítico Catalão I: implicações para a composição do magma carbonatítico e para o metassomatismo carbonatítico no manto superior**. Dissertação de Mestrado. Universidade de Brasília.
- BAECKER, M. L. (1983). **A mineralização de nióbio do solo residual laterítico e petrografia das rochas ultramáfica alcalinas do domo de Catalão I, Goiás**. Tese de Mestrado. Universidade de Brasília.
- BIZZI, L. A., & ARAÚJO, A. L. N. (2005). Dynamics of Mantle-Derived magmatism in the southwestern São Francisco Craton, Brazil. In P. Comin-Chiaramonti & C. B. Gomes (Eds.), **Mesozoic to Cenozoic Alkaline Magmatism in the Brazilian Platform**(pp. 341–365). São Paulo: Edusp/Fapesp.
- BORN, H., LENHARO, S. L. R., & KAHN, H. (1996). Mineralogical characterization of apatites from Brazilian phosphate deposits with reference to flotation behaviour. **Transactions of the Institute of Mining and Metallurgy**, 105, 117–126.
- BRIGATTI, M. F., Malferrari, D., Medici, L., Ottolini, L., & Poppi, L. (2004). Crystal chemistry of apatites from the Tapira carbonatite complex, Brazil. **European Journal of Mineralogy**, 16(4), 677–685. doi:10.1127/0935-1221/2004/0016-0677
- BROD, J. A. (1999). **Petrology and geochemistry of the Tapira alkaline complex, Minas Gerais State, Brazil**. University of Durham.
- BROD, J. A., Gaspar, J. C., ARAÚJO, D. P. DE, GIBSON, S. A., THOMPSON, R. N., & JUNQUEIRA-BROD, T. C. (2001). Phlogopite and tetra-ferriphlogopite from Brazilian carbonatite complexes : petrogenetic constraints and implications for mineral-chemistry systematics. **Journal of Asian Earth Sciences**, 19, 265–296.
- BROD, J. A., Gaspar, J. C., Diniz-Pinto, H. S., & JUNQUEIRA-BROD, T. C. (2005). Spinel chemistry and petrogenetic processes in the Tapira Alkaline-Carbonatite Complex , Minas Gerais , Brazil. **Revista Brasileira de Geociências**, 35(1), 23–32.
- BROD, J. A., GIBSON, S. A., THOMPSON, R. ., JUNQUEIRA-BROD, T. C., SEER, H. J., MORAES, L. C. D. E., & BOAVENTURA, G. R. (2000). The Kamafugite-Carbonatite association in the Alto Paranaíba Igneous Province (APIP) Southeastern Brazil. **Revista Brasileira de Geociências**, 30(3), 404–408.
- CHRISTENSEN, P. R., BANDFIELD, J. L., HAMILTON, V. E., HOWARD, D. A., LANE, M. D., PIATEK, J. L., ... STEFANOV, W. L. (2000). A thermal emission spectral library of rock-forming minerals. **Journal of Geophysical Research**, 105(E4), 9735–9739. doi:10.1029/1998JE000624
- COMIN-CHIARAMONTI, P., GOMES, C. B., CENSI, P., & SPEZIALE, S. (2005). Carbonatites from southeastern Brazil: a model for the carbon and oxygen isotope variations. In P. Comin-Chiaramonti & C. B. Gomes (Eds.), **Mesozoic to Cenozoic Alkaline Magmatism in the Brazilian Platform**(pp. 629–650). São Paulo.
- CRUZ, J. R. (2011). **Dados e Métodos de Sensoriamento Remoto Aplicados ao Estudo do Depósito de Fosfato de Araxá á , Minas Gerais**. Trabalho de Formatura. Universidade Estadual de Campinas (UNICAMP).
- CRUZ, J. R., DE SOUZA FILHO, C. R., ABRAM, M. B., & MARCON, R. (2011). Caracterização espectral do depósito de fosfato de Araxá (MG). In **Anais XV Simpósio Brasileiro de Sensoriamento Remoto**(pp. 3530–3537). Curitiba: INPE.

- DAASCH, L., & SMITH, D. (1951). Infrared Spectra of Phosphorus Compounds. **Analytical Chemistry**, 23(6), 853–868. doi:10.1021/ac60054a008
- FERRARI, V. C., TOLEDO, M. C. M. DE, & ATENCIO, D. (2007). Gorceixite from Catalão, Goiás, Brazil: Rietveld Crystal Structure Refinement. **Geologia USP Serie Científica**, 7(2), 25–36.
- GIBSON, S. A., THOMPSON, R. N., LEONARDOS, O. H., DICKIN, A. P., & MITCHELL, J. G. (1995). The Late Cretaceous impact of the Trindade mantle plume - evidence from large-volume mafic, potassic magmatism in SE Brazil. **Journal of Petrology**, 36, 189–229.
- GIERTH, E., & BAECKER, M. L. (1986). A mineralização de nióbio e as rochas alcalinas associadas no complexo Catalão I, Goiás. In C. Schobbenhaus (Ed.), **Principais Depósitos Minerais do Brasil, Volumen 2** (MME/DNPM., pp. p456–462). Brasília.
- GOMES, C. B., RUBERTI, E., & MORBIDELLI, L. (1990). Carbonatite complexes from Brazil : A review. **Journal of South American Earth Sciences**, 3(1), 51–63.
- HAIDER, S. Z. (1961). Identification of phosphate anions in Niobium and Tantalum phosphates by means of infra-red spectra. **Analytica Chimica Acta**, 24, 250–253.
- HUNT, G., SALISBURY, J., & LENHOFF, C. (1972). Visible and near-infrared spectra of minerals and rocks. V. Halides, phosphates, arsenates, vanadates, and borates. **Modern Geology**, 3, 121–132. Retrieved from http://www.oato.inaf.it/biblioteca/OLDv3/oato.only/pdf/ModGeo_3_121.pdf
- KOKALY, R. (2011). **PRISM: Processing Routines in IDL for Spectroscopic Measurements (Installation Manual and User ' s Guide , Version 1 . 0)** (p. 431).
- LANE, M. D., BISHOP, J. L., DARBY DYAR, M., PARENTE, M., KING, P. L., & HYDE, B. C. (2007). Identifying the phosphate and ferric sulfate minerals in the Paso Robles soils (Gusev Crater, Mars) using an integrated spectral approach. **Lunar and Planetary Science**, XXXVIII, 2–3.
- LANE, M. D., DARBY DYAR, M., & BISHOP, J. L. (2007). Spectra of phosphate minerals as obtained by Visible-Near Infrared Reflectance, Thermal Infrared Emission, and Mössbauer laboratory analyses. **Lunar and Planetary Science**, 4(XXXVIII), 1–2.
- LAPIN, A. V. (1982). Carbonatite differentiation process. **International Geological Review**, 21, 1243–1252.
- MARS, J. C., & ROWAN, L. C. (2011). ASTER spectral analysis and lithologic mapping of the Khanneshin carbonatite volcano, Afghanistan. **Geosphere**, 7(1), 276–289. doi:10.1130/GES00630.1
- MORBIDELLI, L., GOMES, C. B., BECCALUVA, L., BROTZU, P., CONTE, A. M., RUBERTI, E., & TRAVERSA, G. (1995). Mineralogical , petrological and geochemical aspects of alkaline and alkaline-carbonatite associations from Brazil. **Earth-Science Reviews**, 39, 135–168.
- OLIVEIRA, S. M. B. DE, & IMBERNON, R. A. L. (1998). Weathering alteration and related REE concentration in the Catalão I carbonatite complex , central Brazil. **Journal of South American Earth Sciences**, 11(4), 379–388.
- PAN, Y., & FLEET, M. E. (2002). Compositions of the Apatite Minerals. In J. M. Hughes, J. Rakovan, & M. J. Kohn (Eds.), **PHOSPHATES Geochemical, geobiological, and materials importance** (pp. 13–49).
- PEREIRA, V. P. (1995). **Alteração no Maciço Alcalino-Carbonatítico de Catalão I**. Tese de Doutorado. Universidade Federal do Rio Grande do Sul.
- REDDY, B. J., FROST, R. L., & PALMER, S. J. (2008). A near-infrared spectroscopic study of the phosphate mineral pyromorphite Pb₅(PO₄)₃Cl. **Spectrochimica acta. Part A, Molecular and biomolecular spectroscopy**, 71(2), 430–5. doi:10.1016/j.saa.2007.12.030

- RIBEIRO, C. C. (2008). **Geologia, Geometalurgia, Controles e Gênese dos depósitos de fósforo, terras raras e titânio do Complexo Carbonatítico Catalão I, GO.** Tese de Doutorado. Universidade de Brasília.
- RIBEIRO, C. C., GASPAR, J. C., & BROD, J. A. (2005). Controle e Gênese dos depósitos de monazita no Complexo Carbonatítico Catalão I. In *I Simpósio Brasileiro de Metalogenia* (p. 4p). Gramado.
- ROWAN, L. C., BOWERS, T. L., CROWLEY, J. K., ANTON-PACHECO, C., GUMIEL, P., & KINGSTON, M. J. (1995). Analysis of Airborne Visible-Infrared Imaging Spectrometer (AVIRIS) Data of the Iron Hill, Colorado, Carbonatite-Alkalic Igneous Complex. **Economic Geology**, *90*, 1966–1982.
- ROWAN, L. C., KINGSTON, M. J., & CROWLEY, J. K. (1986). Spectral Reflectance of Carbonatites and Related Alkalic Igneous Rocks: Selected Samples from Four North American Localities. **Economic Geology**, *81*, 857–871.
- RUFF, S. W., CHRISTENSEN, P. R., BARBERA, P. W., & ANDERSON, D. L. (1997). Quantitative thermal emission spectroscopy of mineral: A laboratory technique for measurement and calibration. **Journal of Geophysical Research**, *102*(B7), 14899–14913.
- SONOKI, I. K., & GARDA, G. M. (1988). Idades K-Ar de rochas alcalinas do Brasil Meridional e Paraguai Oriental. Compilação e adaptação às novas constantes de decaimento. **Boletim Instituto de Geociências Universidade de São Paulo**, *19*, 63–85.
- SOUZA, N. P. DE. (2009). **Espectrorradiometria em Depósito de fosfato magmatogenico: aplicação para o Depósito de Catalão I - GO.** Trabalho de Formatura. Universidade Federal da Bahia.
- TASSINARI, M. M. L., KAHN, H., & RATTI, G. (2001). Process mineralogy studies of Corrego do Garimpo REE ore, catalao-I alkaline complex, Goias, Brazil. **Minerals Engineering**, *14*(12), 1609–1617. doi:10.1016/S0892-6875(01)00179-0
- TEXEIRA, R. DE A. (2011). **Avaliação espectral de Depósitos de Fosfatos utilizando imagens ASTER nas regiões de Campos Belos e Catalão (GO).** Dissertação de Mestrado. Universidade de Brasília.
- TOLEDO, M CRISTINA M DE, DE OLIVEIRA, S. M. B., FONTAN, F., FERRARI, V. C., & PARSEVAL, P. DE. (2004). Mineralogia, Morfologia e Cristalquímica da Monazita de Catalão I (GO, Brasil). **Revista Brasileira de Geociências**, *34*(1), 135–146.
- TOLEDO, M CRISTINA M DE, LENHARO, S. L. R., FERRARI, V. C., FONTAN, F., PARSEVAL, P. DE, & LEROY, G. (2004). The compositional evolution of apatite in the weathering profile of the Catalão I Alkaline-Carbonatitic Complex, Goiás, Brazil. **The Canadian Mineralogist**, *42*, 1139–1158.
- TOLEDO, M. C. M. DE. (1999). **Mineralogia dos principais fosfatos do maciço alcalino carbonatítico de Catalão I (GO) e sua evolução no perfil laterítico.** Tese de Livre Docência. Universidade de São Paulo.
- TOLEDO, M. C. M. DE, FERRARI, V. C., NETO, A. A., FONTAN, F., MARTIN, F., NOGUEIRA, C., ... CARVALHO, D. E. S. (2002). Fosfatos aluminosos com Ferro do Grupo da Crandallita nas coberturas lateríticas de Catalão I, Juquiá e Tapira (Brasil) e Chirigué (Paraguai). **Revista Brasileira de Geociências**, *32*(4), 393–406.
- VAZ DE MELLO, M. T. (1983). **Depósitos minerais associados ao complexo alcalino carbonático de Tapira (MG)** (p. 39p). Belo Horizonte.

Capítulo IV: Reflectance and Emission Spectroscopy of Brazilian Sedimentary Phosphates: Lagamar and Rocinha mines (Minas Gerais State)

4.1 Introduction

Given their use in the fertilizing industry, phosphate rocks have been mined and prospected since the XIX century. Major deposits of the world are separated into three types: (i) guano (biogenic) deposits, that forms over accumulation of bird and/or bat excrement; usually on maritime shorelines or caves; (ii) igneous, that are usually mined in Alkaline Carbonatitic Complexes (e.g. Tapira, Araxá and Catalão I) and (iii) phosphoritic that are sedimentary packages of rocks with P₂O₅ %wt that surpasses up to a million times normal P concentration (FÖLLMI, 1996).

These abnormal concentrations have attracted the attention of the phosphate mining industry since the early XX century. Although the geology of phosphate deposits is well defined, there are yet several features about phosphorite-bearing deposits that are subject of controversy in the scientific community.

The spectroscopy of sedimentary rocks has been approached previously as a part of a series of remote sensing efforts to characterize P-bearing targets, either terrestrial or astronomical. As a result, landmark papers by HUNT & SALISBURY (1976) and HUNT *et al.* (1972) have brought important knowledge to the spectroscopy of sedimentary rocks and alteration minerals that can be detected through remote sensing.

Brazilian sedimentogenic phosphates are less searched for than their magmatogenic counterparts, mostly because their spatial extensions are apparently smaller than the alkaline carbonatitic complexes. Sedimentogenic phosphatic rocks are usually situated along the margin of cratons. This is the case of the Neoproterozoic, Vazante Group phosphate deposits of the São Francisco craton (SANCHES *et al.*, 2007). Such deposits stand as excellent targets to serve as a reference for prospecting sedimentogenic phosphates, in order to increase reserves of this important commodity.

The Vazante Group (DARDENNE, 2001) hosts the Coromandel, Rocinha and Lagamar phosphate deposits. Rocinha and Lagamar are currently operational mines. Despite being the most important sedimentary phosphate mines in Brazil (DA ROCHA ARAUJO *et al.*, 1992), the deposits are scarcely reported in the geological literature (NOGUEIRA, 1993), despite regional correlations of phosphogenesis studies (SANCHES *et al.*, 2007) and local publications from the Brazilian Geological Survey and associates (CPRM; DARDENNE *et al.*, 1997).

This work aims to provide the first reflectance and emission spectroscopy study of the Rocinha and Lagamar mines, in order to determine the possibility of finding absorption features that can indicate the presence of phosphates in the host rocks, using a quick and non-destructive analytical method.

4.2 Geologic Setting

Sedimentogenic phosphate deposits in Brazil range from the Neoproterozoic to recent guano accumulations in the northeastern states of Maranhão and Pernambuco. Also of interest are classic metamorphic phosphorites, although with limited spatial distribution (DA ROCHA ARAUJO *et al.*, 1992; GIRARD *et al.*, 1993; NOGUEIRA, 1993).

The regional phosphogenesis of the Proterozoic phosphates of Brazil have been reviewed by SANCHES *et al.* (2007). They studied $\delta_{18}\text{O}$, $\delta_{13}\text{C}$ and $^{87}\text{Sr}/^{86}\text{Sr}$ ratios, covering the deposits of Irecê (BA), Rocinha and Lagamar (MG), and provided possible connections between the sedimentation of the Vazante, Bambuí and Una groups. These groups have lateral correlations due to tectonic emplacements that took place during the Neoproterozoic, simultaneously to the merging of the Gondwana supercontinent.

The Lagamar and Rocinha deposits are host by the metasedimentary sequences of the Brasília Folding Belt (BFB) (HASUI & ALMEIDA, 1970). This belt its located alongside the western portion of the São Francisco craton (ALMEIDA, 1967; ALMEIDA *et al.*, 1976) crossing the Goiás, Distrito Federal and Minas Gerais states in West-Central Brazil.

The BFB is the remnant scar of collisional processes in the Neoproterozoic that ended in the amalgamation of the west of the Gondwana Supercontinent (FUCK *et al.* 1993; NOGUEIRA 1993). The deformational and metamorphic processes recorded in the

metasediments of the BFB are less intense from West to East, where the horizontal sediments of the São Francisco craton are deposited.

Locally, the Rocinha and Lagamar phosphates are basal formations of the Vazante Group, as defined by DARDENNE (2000). The group comprises thick carbonatic sequences (>3000 m), mainly dolomitic that overlay glacially originated diamictites.

The Rocinha Formation consists of three informal units (DARDENNE 2000). The basal unit is composed of yellow to brownish metamorphic phosphoritic, rhythmic quartzites and slates with a transitional contact with the middle unit. The middle unit has a thick, yellow to reddish package of slates and metamorphic siltstones, regularly interbedded. A transition zone can be observed towards the top with dark gray slates, with carbonates, pyrite and thin apatite-(CaF) laminations. This unit represents the main rock feed of the Rocinha mining complex.

The top unit of the Rocinha Formation is a folded set of dark carbonates, rich in phosphates, alternated with yellow pelitic levels. Towards the top, lenses of slate and glauconite and chlorite are observed. This unit has a wide horizontal distribution and stretches from the Rocinha Mine until the bottom of the Lagamar mine.

Regionally, rocks show evidences of ductile deformation and greenschist facies metamorphism. This event has been recorded in folds that concentrate greater amounts of cryptocrystalline apatite-(CaF). In the phosphoritic quartzites, secondary formation of apatite-(CaF) appears without tectonic imprints (DA ROCHA ARAUJO, 1988; DA ROCHA ARAUJO *et al.*, 1992; NOGUEIRA, 1993). Locally, greater P₂O₅ concentration is related to incipient cataclasis that disaggregated apatite (CaF) beds and generated secondary Ca-enriched fluorapatite (DA ROCHA ARAUJO *et al.*, 1992).

The Lagamar Formation was divided by DARDENNE & SCHOBENHAUS (2001) in two members: Arrependido and Sumidouro. The Arrependido Member has two informal units called E1 and E2 that behave as grade control units for the Lagamar mine operations. The E1 unit is a set of impoverished phosphate beds with red, clayey slates. The E2 unit is composed of a rhythmic sedimentation of phosphoritic, dark grey sandstones and yellow pelitic rocks.

The Sumidouro Member has rhythmic sedimentation of sandstones, limey slates and quartzites. Towards the top, it displays some conglomerates that were described by

DARDENNE *et al.* (1986) as the Córrego Arrependido Conglomerate. Pebbles in this conglomerate correspond to quartzites, metamorphic siltstones and dark limestones.

The chemical composition for both deposits is very similar; CO₂ is particularly low for apatites of phosphoritic environments. DA ROCHA ARAUJO *et al.* (1992) emphasized the low content of CO₂ in the Rocinha primary phosphates and attributed this feature to the simultaneous folding and metamorphism that the rocks suffered during the Brasiliano orogeny.

4.3 Materials and Methods

Rock and soil samples from the Rocinha and Lagamar were collected and catalogued at the mine localities. Firstly, they were dried at 50°C for 24 hours. A first set of reflectance measurements were performed with a FieldSpec 3 Hi Resolution[®] Spectrometer (Analytical Spectral Devices). The samples were then crushed in a steel jaw crusher and grinded on a planetary ball mill until achieving a particle size smaller than 200 mesh. This size fraction was used for a new set of reflectance measurements.

Redundant samples were submitted to X-Ray Fluorescence (XRF) analysis in glass discs (using lithium tetraborate as fundent in a 1:5 proportion) and pressed pellets on a Phillips PW 2404 X- Ray Spectrometer. X-Ray Diffraction (XRD) of powdered samples was made on a Bruker AXS D2 Phaser X Ray Diffractometer, using 2θ angles from 0° to 60°, counting each step in 1 second. Samples were further measured in a Nicolet Nexus 6100 for Fourier Transformed Infrared Spectroscopy (FTIR) to determine diffuse reflectance. Diffuse reflectance data were subsequently transformed to Apparent Emissivity using Kirchoff's Law to look for the corresponding P-O vibration absorption features, according to the equation:

$$\varepsilon = 1 - \rho \quad (1)$$

where ρ stands for diffuse reflectance, measured from 2.5 μm up to 25μm.

VNIR-SWIR-TIR spectra were studied in order to find the proper absorption bands and make the mineralogical description of the samples. For each sample, at least 8 reference spectra were yielded, according to variation in mineral phases. Spectral interpretation was made using the PRISM software (KOKALY, 2011) for identification of

the mineral phases. ENVI® 4.8 software was used for spectral analysis, spectral arithmetic operations and visual comparison.

4.4 Results

4.4.1 Sample description

Twenty-eight (28) representative samples collected from the Rocinha and Lagamar mines are described in table 1. The collected samples were taken from vertical profiles in the mines, looking forward to observe any chemical variations in the rock units that could lead to phosphate recognition. The mine pit at Lagamar is notably deeper than that of Rocinha Mine, having 40 meters deep approximately. The Rocinha mine, although in operation for a longer period of time, display higher ore grades. It has been expanded more horizontally along the open pit, deepening less than the Lagamar mine. Photos of the Rocinha and Lagamar mines are provided in fig. 4.1



Fig. 4. 1 Panoramic views from Rocinha (a) and Lagamar (b) mines. Picture of Lagamar mine courtesy of Galvani Mineração Ltd (2011)

Sample colors vary between yellow to dark grey. Tectonics effects are more evident on the Rocinha mine, where the rocks display features developed under ductile deformation (see sample RO-11B on Fig 4.3). The most representative samples from both mining sites are displayed on table 4.1.

Tab. 4. 1: Sample description of the Rocinha and Lagamar mine sites.

X	Y	Sample	Description
296532	7968347	RO-06	Interstratified sandstone-mudstone with cryptocrystalline apatite veins
296500	7968398	RO-07	Laminated phosphoritic siltite with quartz intraclasts
296494	7968409	RO-10A	Phosphoritic dolostone with oxidation sheets
296490	7968429	RO-11B	Thrust-folded phosphorite
296486	7968440	RO-12	Phosphoritic siltstone, folded
296494	7968458	RO-14D	Siltstone/Dolostone, altered
296510	7968465	RO-15A	Brown limestone with few apatite levels
296472	7968332	RO-19A	Brittle Limestone with chlorite and oxidized bands
296458	7968336	RO-21	Phosphoritic siltstone with green matrix
296439	7968342	RO-22	Phosphoritic siltstone with goethite packs
296441	7968343	RO-23	Phosphoritic limestone. Cryptocrystalline apatite as thin sheets
296444	7968344	RO-24	Calcite veins in PO-poor siltstone with goethite
296476	7968306	RO-25A	Clayey Phosphorite
296476	7968306	RO-25B	Soil above Clayey phosphorite
296466	7968309	RO-26A	Phosphorite
296466	7968309	RO-26B	Soil above sample 26A
296448	7968297	RO-27B	Phosphorite/ weathering mantle contact
296448	7968297	RO-27C	Clayish soil with goethite
296448	7968297	RO-27D	Sterile soil
305637	7981023	LG01 Beto-LG01G LG01H	Silty slates with cryptocrystalline apatite
305625	7981003	LG-02	Silty slates with clay and apatite
305626	7981008	LG-0	Clayey siltstone
305602	7981000	LG-03 – Base of profile	Phosphoritic slate/ limestone contact
305592	7980995	LGPV1	Clayey slate PO-poor
305646	7981010	LGBMI05	Phosphoritic slate
305609	7980981	LGBMI07	Marginal siltstone

4.4.2 X Ray Fluorescence

X Ray Fluorescence measured on fused glasses of five samples for both Rocinha and Lagamar mines is presented in table 4.2. It is noteworthy that CaO/P₂O₅ relationships are close to 1 when the rock has enough apatite content to be considered as phosphate ore. Discrimination between carbonate-fluorapatite and fluorapatite is possible when the F/P₂O₅ ratio is higher than 0,2, meaning that anfluorapatite will have a CaO/P₂O₅ ratio higher than 1. Based on these facts, all samples mentioned in table 4.1, except sample RO-30, were portrayers of fluorapatite.

The X-Ray Fluorescence of trace elements in these same samples show very low concentrations of REEs elements, much in contrast with other values reported for igneous phosphates. It can be inferred that the glacial environment that formed the fluorapatite as described by DA ROCHA ARAUJO *et al.* (1992), NOGUEIRA (1993) and DARDENNE *et al.*(1997), was enough to remobilize the REEs ions in the carbonate-fluorapatite structure of the phosphorites. The high values of Y reported by NOGUEIRA (1993) were confirmed for the studied samples. Samples are also rich in Sr and Ba and depleted in Rb and Sr for the normalized phosphorites, compared with data of NOGUEIRA (1993).

Tab. 4. 2: X Ray Fluorescence of the Rocinha and Lagamar rocks

Sample		LG01X	LG02BIF	RO-Conc Apat	RO-30	RO-27
F	%wt	0.156	0.637	1.560	0.662	0.49
Na ₂ O		0.000	0.000	0.160	0.000	0.00
MgO		1.600	1.030	0.377	1.340	1.08
Al ₂ O ₃		13.350	12.140	3.040	12.850	17.94
SiO ₂		52.440	44.780	18.190	33.830	27.25
P ₂ O ₅		6.840	12.690	30.290	17.360	16.73
S		0.00	0.00	0.00	0.00	0.02
SO ₃		0.00	0.00	0.00	0.00	0.00
Cl		0.003	0.002	0.007	0.003	0.004
K ₂ O		2.42	1.84	0.58	2.34	1.83
CaO		10.30	17.35	41.31	23.63	9.22
Sc ₂ O ₃		0.01	0.01	0.01	0.00	0.01
TiO ₂		0.57	0.50	0.17	0.47	0.62
V ₂ O ₅		0.014	0.014	0.008	0.014	0.022
Cr ₂ O ₃		0.009	0.009	0.004	0.008	0.014
MnO		0.029	0.020	0.030	0.006	0.076
Fe ₂ O ₃		4.160	3.620	1.430	2.620	6.21
Co ₃ O ₄		0.001	0.001	0.000	0.000	0.002
NiO		0.002	0.001	0.00	0.00	0.001

CuO		0.003	0.003	0.003	0.003	0.003
ZnO		0.010	0.013	0.008	0.006	0.005
Ga₂O₃		0.002	0.002	0.001	0.002	0.002
Rb₂O		0.009	0.006	0.001	0.006	0.008
SrO		0.169	0.139	0.457	0.296	0.270
Y₂O₃		0.006	0.004	0.011	0.006	0.010
Nb₂O₅		0.001	0.00	0.00	0.00	0.001
In₂O₃		0.001	0.002	0.002	0.001	0.001
Sb₂O₃		0.00	0.00	0.001	0.001	0.00
BaO		0.103	0.051	0.027	0.05	0.113
La₂O₃		0.005	0.004	0.002	0.004	0.014
WO₃		0.001	0.001	0.001	0.001	0.000
F/P₂O₅		0.023	0.050	0.052	0.038	0.030
CaO/P₂O₅		1.506	1.367	1.364	1.361	0.551

4.4.3 Reflectance Spectroscopy

Reflectance spectra collected from samples of Rocinha and Lagamar mines appear to show an almost linear mixture between mineral phases. The absence of visible or near infrared features are typical of pure sedimentary apatite, as generically noted by HUNT *et al.* (1972). These apatites lack the REEs ion charge transfer absorption features in the 0,5-0,75-0,8 μm range. Hence, it is highly possible that REEs that could provide absorption features in Rocinha and Lagamar were lixiviated.

Common spectral-mineralogical phases in rocks stemmed from these mines are illite, muscovite, kaolinite, chlorite and quartz. These rock spectra is in concordance with the spectra of sandstones, siltstones and limestones published by HUNT & SALISBURY (1976). What becomes apparent after viewing the spectra of the P₂O₅ bearing samples is that clays are markers of higher concentration of phosphates. Illite appears consistently when samples have higher P₂O₅ %wt. Illite and kaolinite occur together when the P₂O₅ %wt is in between 8% to 12%, indicating smaller concentration.

Reflectance spectra for nine samples were produced for the Lagamar deposit (Fig. 4.2). In these rocks illite (2.2 μm), muscovite (1.41 μm) and goethite (0.88 μm) show the most prominent absorption features. Minor absorption features are related to calcite (2.34 μm) and dolomite (2.33 μm) for sample LG01G. As for the Rocinha samples, no REEs absorption features are observed, confirming the sedimentary nature of these phosphates.

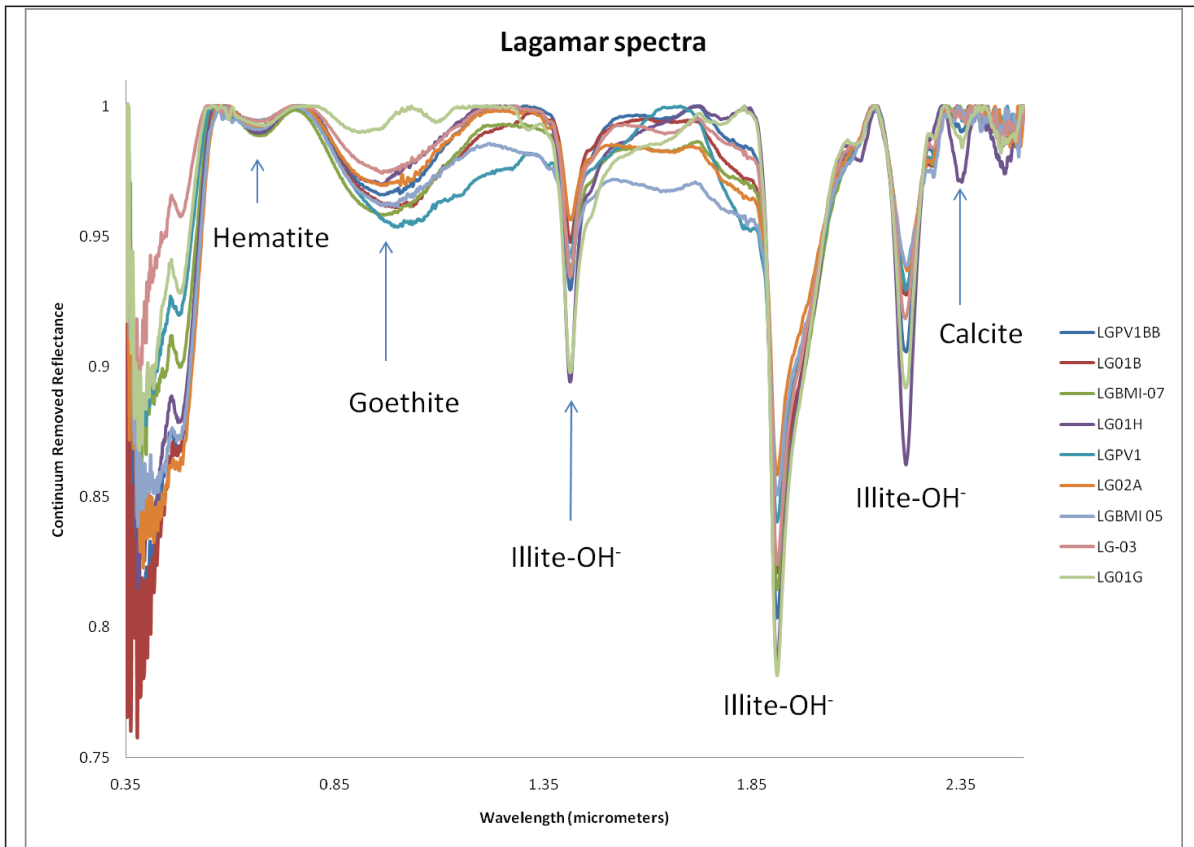


Fig. 4. 2 Reflectance spectra of selected samples of the Lagamar mine

Reflectance spectroscopy of 12 representative samples of the Rocinha Mine are displayed in Figs. 4.3; 4.4 and 4.5. In general, illite, goethite, kaolinite and muscovite absorption features are most relevant.

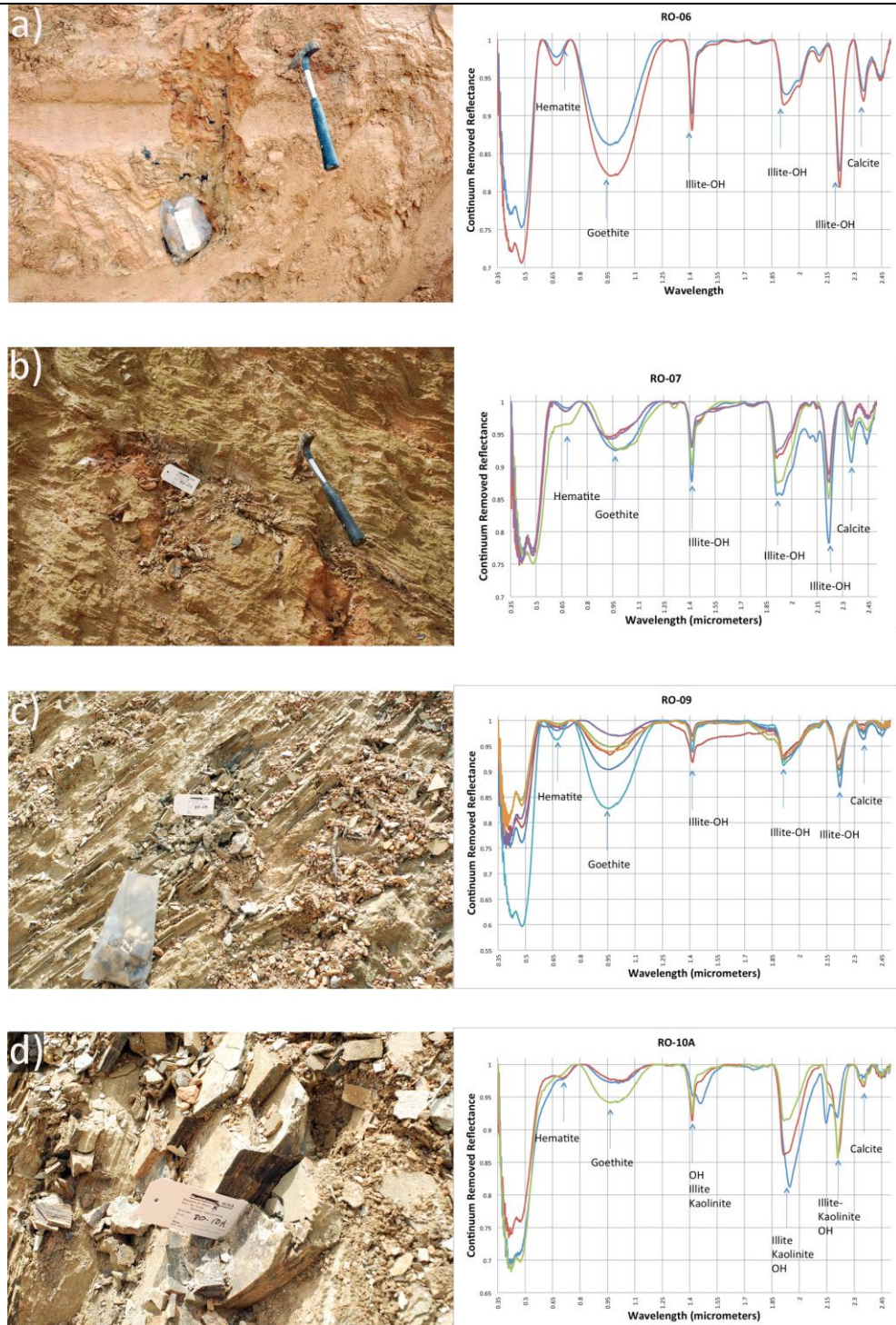


Fig. 4.3 Reflectance spectra for Rocinha mine samples. a) red weathered rythmite; b) phosphoritic slate, where dark calcitic sediments host criptocrystaline fluorapatite; c) orientated phosphatic rythmite; d) kaolinite-rich phosphorite-siltite, markedly with less phosphate concentration.

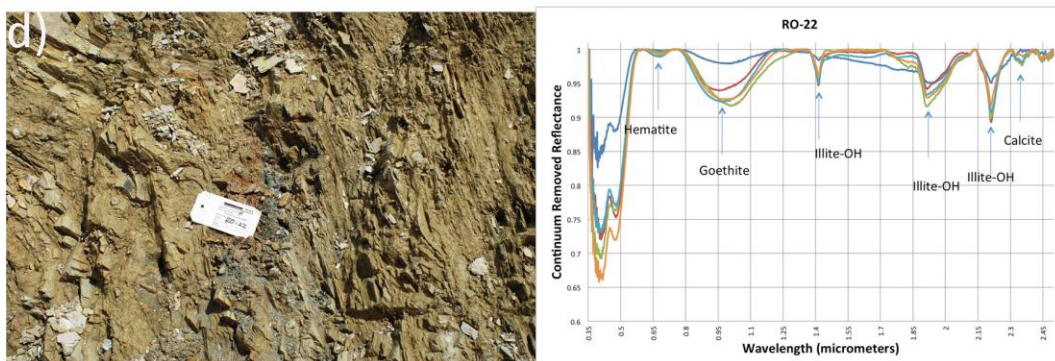
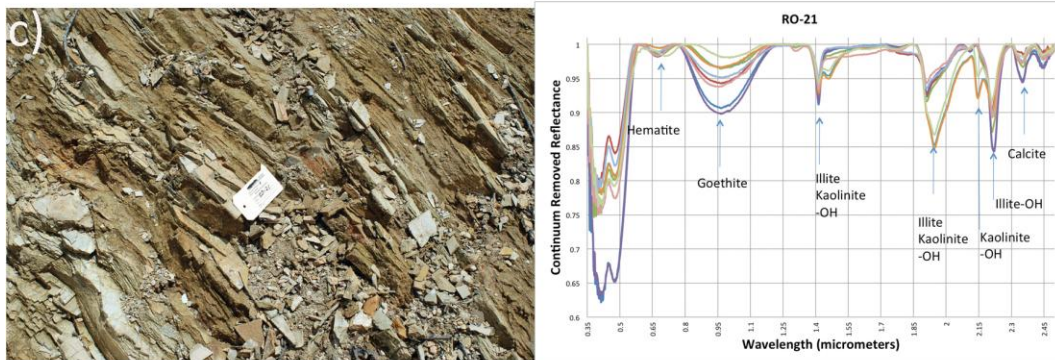
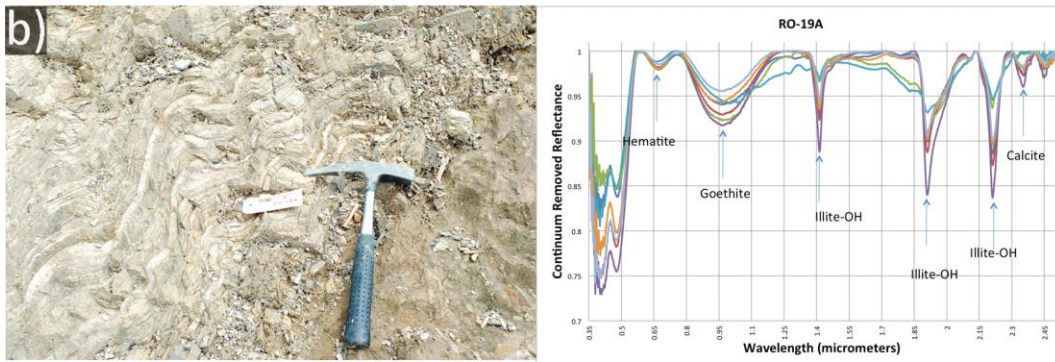
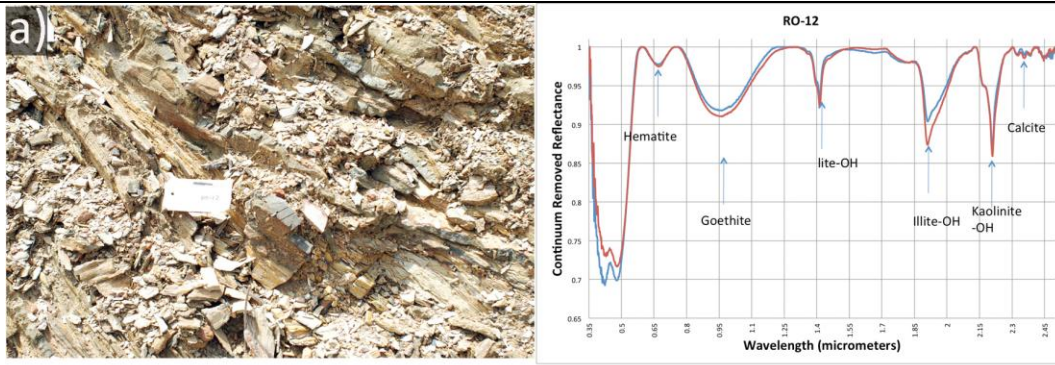
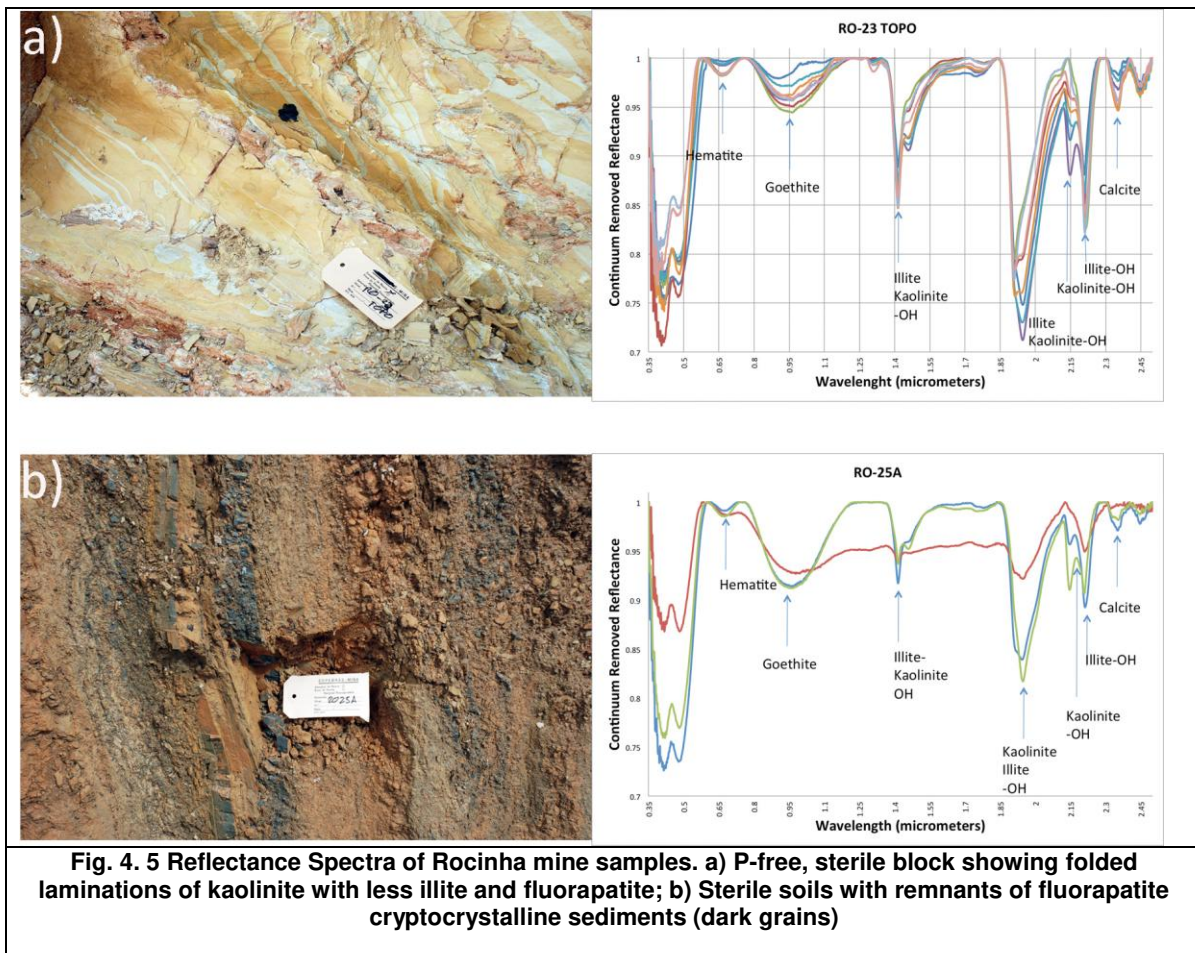


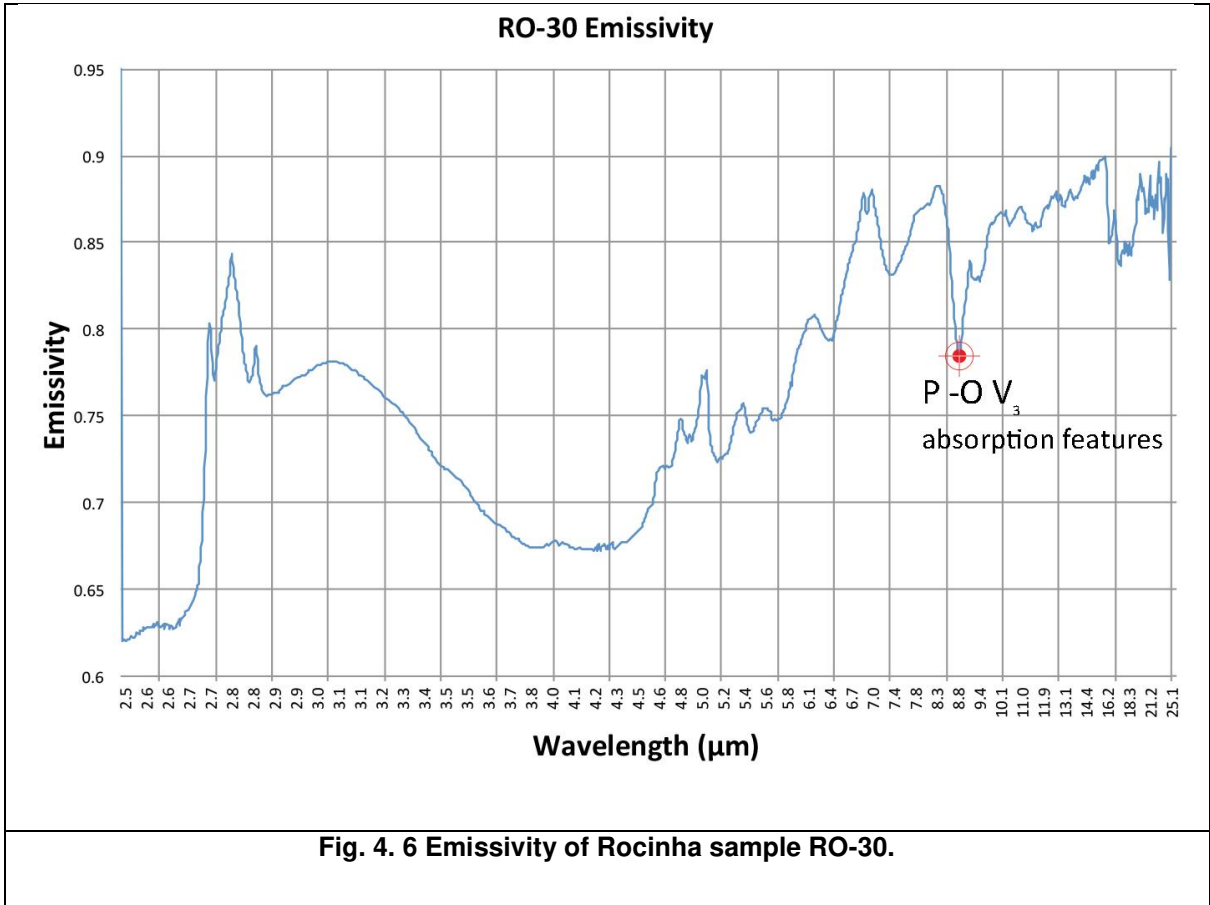
Fig. 4. 4 Reflectance spectra of selected samples from the Rocinha mine. a) folded slates with kaolinite and reduced apatite concentration; b) folded rythmites with apatite; c) P-free, sterile slates with few levels of rythmites; d) cryptocrystalline fluorapatite in slate.

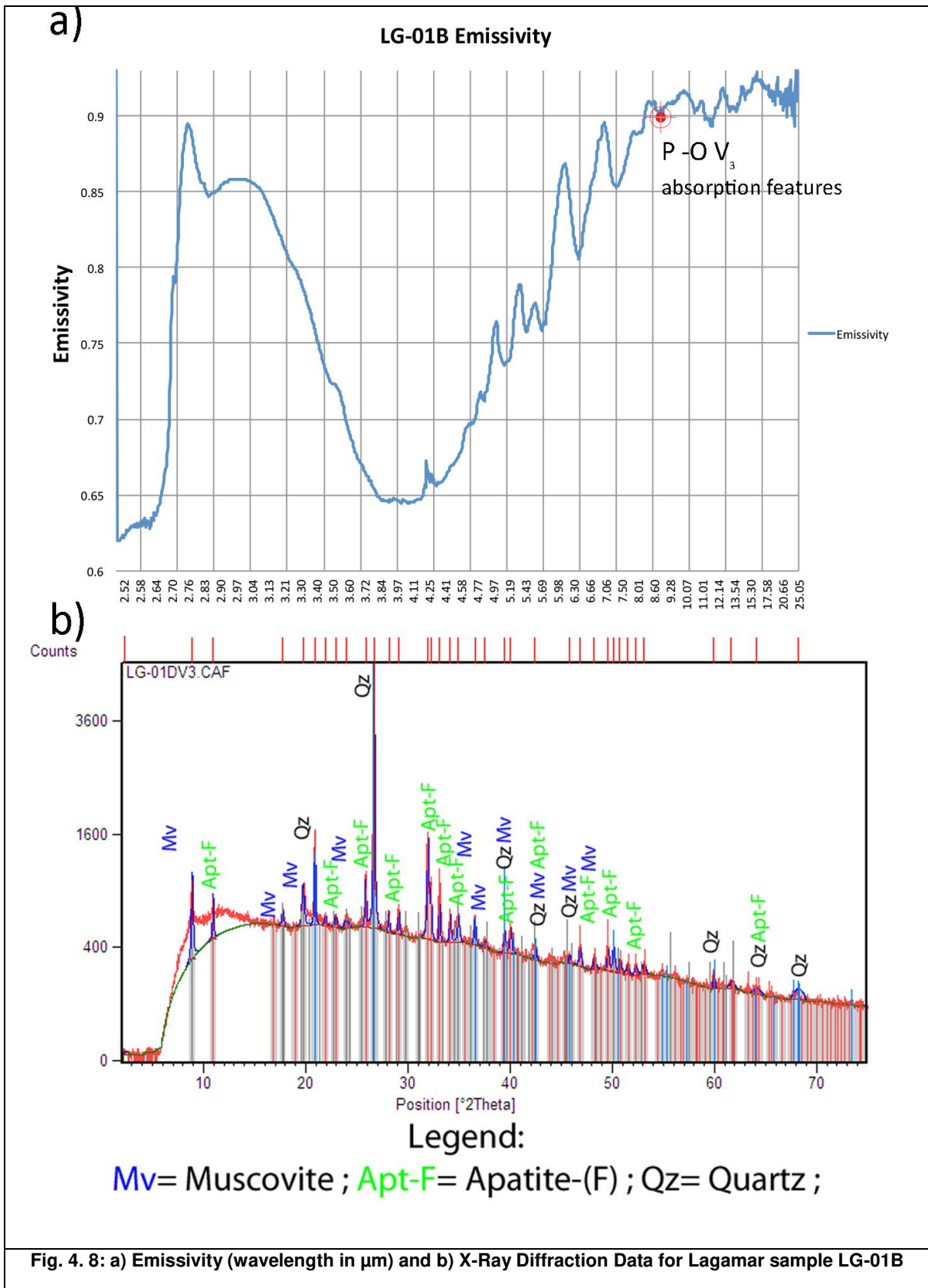


4.4.4 Emission Spectroscopy and X-Ray Diffraction

Emissivity for the Rocinha mine samples showed the ν_3 P-O absorption feature, similar to those described elsewhere (CHRISTENSEN *et al.* 2000; LANE *et al.* 2007; REDDY *et al.* 2008). However, there are differences in the shape and the variety of features observed in the Rocinha and Lagamar phosphatic rocks. The studied samples (e.g., RO-30) do not show the doublet centered at 8.9 μm , whereas an analogous doublet to the ν_3 emissivity maximum is shown at 7.1 μm (see fig. 4.6)

The apatitic concentrate obtained in the Rocinha mine shows a very clear emissivity minimum at 8.56 μm , corresponding to the P-O bonds, as described by DAASCH & SMITH (1951); CHRISTENSEN *et al.* (2000) and REDDY *et al.* (2008). A quartz absorption feature at 8.96 μm is also relevant. Once again, the analogous 7.1 μm doublet maximum features appear in the spectrum, whereas calcite double features are highlighted at 2.81 μm and 4.87 μm . Mineral X Ray Diffraction data confirms the FTIR data interpretation, and also reveal the presence of muscovite in the apatitic concentrate (fig. 4.7).





4.5 Discussion

Although sedimentary phosphates usually tend to concentrate in higher proportions than their igneous counterparts, reflectance spectroscopy does not show a clear trend that can lead to their identification in the VNIR and SWIR region. Even though that spectroscopy standards for fluorapatite exist (see HUNT *et al.*, 1972; CLARK *et al.* 2007), the origin of the sample standard comes from an igneous rock, that still preserve the REEs features in the 0.585 μm , 0,75-0,85 μm range. Emissivity spectroscopy can help to pinpoint phosphate occurrences, given that the 8.2 μm maximum is present in most samples investigated here. However, there are several obstacles to sense phosphates from multispectral and hyperspectral thermal imaging spectrometers. Firstly, the lower signal to noise ratio, typical of thermal scanners. Considering the low spectral (5 bands) and spatial (90m) resolution of ASTER, the first and still the only thermal multispectral sensor currently in operation, chances to discriminate between features of apatites, carbonates and siliceous materials are low. For instance, quartz and phosphate chemical bonds will overlap in ASTER bands 10 and 11. Therefore, mineral mixtures in the pixels will probably mask several key spectral features, diagnostic of these rocks.

Nevertheless, the presence of illite and kaolinite in the weathering profiles show some correlation to the presence or absence of sedimentary phosphates. Spectra extracted from Lagamar and Rocinha rocks show that samples with higher P_2O_5 %wt concentrations (located around the center of the mine), displayed well defined illite absorption features. Besides, portions of the weathering profile containing chlorite or kaolinite concentrations were indicators of smaller concentration of phosphates. Samples that showed mixtures of kaolinite and illite proved to host higher concentration of P_2O_5 too; higher concentrations are found where illite predominates over kaolinite and vice-versa.

Fluorapatite, usually a phosphate of igneous occurrence, is the main phosphate present in Rocinha and Lagamar mines. This was confirmed by XRD in this work, but also previously indicated by DA ROCHA ARAUJO *et al.* (1992) and NOGUEIRA (1993). However, a weathering series for sedimentary phosphates defined by FLICOUTEAUX & LUCAS (1984) place the fluorapatite as a product of weathering of primary carbonate-fluorapatite (the main primary sedimentary apatite).

Chemical criteria for depicting the origin of the sedimentary fluorapatite is based on $\text{CaO}/\text{P}_2\text{O}_5$ and $\text{F}/\text{P}_2\text{O}_5$ ratios (LUCAS *et al.*, 1980). When $\text{CaO}/\text{P}_2\text{O}_5 \geq 1,3$ and $\text{F}/\text{P}_2\text{O}_5 \geq$

0.12, the apatite present in the rock can be described as primary sedimentary specimen (apatite-(CaF)). If the ratio is lower, the apatite present in the sedimentary phosphorite possibly suffered de-carbonization, leading to the fluorapatite structure. This statement suggests that the apatites from the Rocinha and Lagamar mines did experience ionic changes from carbonate-fluorapatite.

The de-carbonization of fluorapatite is not entirely similar to the substitution of REEs elements during weathering. According to DA ROCHA ARAUJO *et al.* (1992) and NOGUEIRA (1993), the Lagamar and Rocinha apatites are impoverished in REEs elements when compared with other world phosphorites normalized to mean phosphorite .

With these insights, it is reasonable to think that the lack of REEs absorption features in the sedimentary apatites will be extensive to most phosphorites in the BFB, given the normal progression of carbonate-fluorapatite to fluorapatite in the weathering of these deposits, and considering the trivalent-divalent substitutions detailed by PAN & FLEET (2002).

4.6 Conclusions

We have found that whereas there are no distinctive ways to identify PO₄ bonds in the reflectance spectroscopy of phosphoritic apatites, mineralogical associations between Illite-calcite-muscovite-kaolinite can be traced to pinpoint zones of favorability to the presence of sedimentogenic phosphates. Therefore, to successfully apply remote-sensing techniques to multispectral imagery for mineral prospecting of phosphates, other minerals found in such deposits, like clays, carbonates and siliceous materials, must be studied and characterized beforehand. This is feasible using ASTER data and spectral mixing analysis (e.g., Senna 2008), and also airborne and orbital hyperspectral data.

Emissivity spectroscopy proved to be a reliable technique to detect the P-O feature centered at 8.2 μm . This absorption closely matches ASTER thermal Band 10 (Fujisada, 1995). According to the spectra shown here, there is enough contrast between the high emissivity of phosphates and low emissivity of quartz to discriminate both in the phosphate deposits of the Brasília Fold Belt. However, ASTER TIR bands pose the problem of a very coarse spatial resolution (90m pixel) and contiguity of PO₄ and SiO₄ maximum absorption regions (8.2 μm and 8.7 μm). So, special care must be considered regarding the spectral

mixtures between adjacent rocks and materials to properly establish mineral mixing models for the BFB.

If remote sensing of the phosphoritic apatites from the Brasília Fold Belt is intended to be successful, it is needed to determine with better certainty the mineral chemistry of the apatites with microanalytical procedures that can give us an idea of the forming conditions and REEs substitutions that underwent during deposition, diagenesis and metamorphism. Also, studies on the mineralogical mixtures and its behavior with temperature and emissivity can help to pinpoint the spectral signatures that are distinctive and exclusive from the sedimentogenic phosphates in the BFB and surroundings of the São Francisco Craton.

4.7 References

- ALMEIDA, F. F. M. (1967). Observações sobre o Pre-Cambriano da região central de Goiás. In **21 Congresso Brasileiro de Geologia** (pp. 19–22). Curitiba.
- ALMEIDA, F. F. M., HASUI, Y., & NEVES, B. B. B. (1976). The upper Precambrian of South America. **Boletim do Instituto de Geociências USP**, 7, 45–80.
- CHRISTENSEN, P. R., BANDFIELD, J. L., HAMILTON, V. E., HOWARD, D. A., LANE, M. D., PIATEK, J. L., ... STEFANOV, W. L. (2000). A thermal emission spectral library of rock-forming minerals. **Journal of Geophysical Research**, 105(E4), 9735–9739. doi:10.1029/1998JE000624
- CLARK, R. N., SWAYZE, G. ., WISE, R., LIVO, E., HOEFEN, T., KOKALY, R., & SUTLEY, S. J. (2007). **USGS digital spectral library splib06a**. Retrieved from <http://speclab.cr.usgs.gov/spectral-lib.html>
- DA ROCHA ARAUJO, P. R. (1988). **Les phosphorites d'âge protérozoïque moyen de Rocinha (Minas Gerais, Brésil). Genèse et evolution d'un gisement de phosphate tectonisé et metamorphisé au Brésilien (~600 Ma)**. Tese de Doutorado. Université Aix-Marseille III.
- DA ROCHA ARAUJO, P. R., FLICOTEAUX, R., PARRON, C., & TROMPETTE, R. (1992). Phosphorites of Rocinha Mine Patos de Minas (Minas Gerais , Brazil): Genesis and Evolution of a Middle Proterozoic Deposit Tectonized by the Brasileiro Orogeny. **Economic Geology**, 87, 332–351.
- Daasch, L., & Smith, D. (1951). Infrared Spectra of Phosphorus Compounds. **Analytical Chemistry**, 23(6), 853–868. doi:10.1021/ac60054a008
- DARDENNE, M. A. (2000). The Brasilia Fold Belt. In U. G. Cordani, E. J. Milani, A. Thomaz-Filho, & D. A. Campos (Eds.), **Tectonic Evolution of South America**(pp. 231–263). Rio de Janeiro: 31st International Geological Congress Rio de Janeiro.
- DARDENNE, M. A. (2001). Lithostratigraphic sedimentary sequences of the Vazante Group. In A. Misi & J. B. G. Teixeira (Eds.), **Base Metal Deposits of Africa and South America, IGCP 450** (pp. 48–50). Belo Horizonte-Paracatú.
- DARDENNE, M. A., FREITAS-SILVA, F. H., NOGUEIRA, G. M. DOS S., & SOUZA, J. F. C. (1997). Depósitos de fosfato de Rocinha e Lagamar, Minas Gerais. In **Principais Depósitos Minerais do Brasil, Volume 4, Parte C**(p. 634). Companhia de Pesquisa e Recursos Minerais do Brasil.
- DARDENNE, M. A., & SCHOBENHAUS, C. (2001). **Metalogênese do Brasil**. (Universidade de Brasília, Ed.) (p. 392).
- DARDENNE, M. A., TROMPETTE, R., MAGALHÃES, L. F., & SOARES, L. A. (1986). Proterozoic and Cambrian phosphorites - regional review: Brazil. In P. J. Cook & J. H. Shergold (Eds.), **Phosphate Deposits of the world Volume 1** (pp. 116–131). University of Cambridge.
- FLICOUTEAUX, R., & LUCAS, J. (1984). Weathering of Phosphate Minerals. In **Phosphates Minerals**(pp. 292–317). Berlin: Springer-Verlag.
- FÖLLMI, K. B. (1996). The phosphorus cycle , phosphogenesis phosphate-rich deposits. **Earth-Science Reviews**, 40, 55–124.
- FUCK, R. A., SÁ, E. F. J. DE, PIMENTEL, M. M., DARDENNE, M. A., & SOARES, A. C. P. (1993). As faixas de dobramentos marginais do cráton do São Francisco: síntese de conhecimentos. In **O Cráton de São Francisco**(pp. 161–185).

- FUJISADA, H. (1995). Design and performance of ASTER instrument. In **Proceedings of SPIE the International Society for Optical Engineering**(pp. 16–25).
- GIRARD, J.-P., FLICOTEAUX, R., WALTER, A.-V., SAVIN, S. M., & NAHON, D. (1993). Oxygen and carbon isotope composition of structural carbonate in weathering apatites from laterites, southern Brazil and western Senegal. **Applied Geochemistry**, 8(6), 617–632. doi:10.1016/0883-2927(93)90017-B
- HASUI, Y., & ALMEIDA, F. F. M. (1970). Geocronologia do Centro-Oeste Brasileiro. **Boletim da Sociedade Brasileira de Geologia**, 1, 7–26.
- HUNT, G. H., & SALISBURY, J. W. (1976). Visible and Near Infrared Spectra of Minerals and Rocks: XI. Sedimentary Rocks. **Modern Geology**,5, 211–217.
- HUNT, G., SALISBURY, J., & LENHOFF, C. (1972). Visible and near-infrared spectra of minerals and rocks. V. Halides, phosphates, arsenates, vanadates, and borates. **Modern Geology**, 3, 121–132. Retrieved from http://www.oato.inaf.it/biblioteca/OLDv3/oato.only/pdf/ModGeo_3_121.pdf
- KOKALY, R. (2011). **PRISM: Processing Routines in IDL for Spectroscopic Measurements (Installation Manual and User ' s Guide , Version 1 . 0)** (p. 431).
- LANE, M. D., BISHOP, J. L., DARBY DYAR, M., PARENTE, M., KING, P. L., & HYDE, B. C. (2007). Identifying the phosphate and ferric sulfate minerals in the Paso Robles soils (Gusev Crater, Mars) using an integrated spectral approach.**Lunar and Planetary Science**,XXXVIII, 2–3.
- LUCAS, J., FLICOUTEAUX, R., NATHAN, Y., PRÉVOT, L., & SHAHAR, Y. (1980). Different aspects of phosphorite weathering. In **SEPM Special Publication** (pp. 41–51). Tulsa.
- NOGUEIRA, G. M. DOS S. (1993). **Enquadramento Litoestratigráfico, Sedimentologia e Evolução Geoquímica do Depósito Fosfático de Lagamar, MG-Formação Vazante - Proterozoico Médio**. Dissertação de Mestrado. Universidade de Brasília.
- PAN, Y., & FLEET, M. E. (2002). Compositions of the Apatite Minerals. In J. M. Hughes, J. Rakovan, & M. J. Kohn (Eds.), **PHOSPHATES Geochemical, geobiological, and materials importance** (pp. 13–49).
- REDDY, B. J., FROST, R. L., & PALMER, S. J. (2008). A near-infrared spectroscopic study of the phosphate mineral pyromorphite $Pb_5(PO_4)_3Cl$. **Spectrochimica acta. Part A, Molecular and biomolecular spectroscopy**, 71(2), 430–5. doi:10.1016/j.saa.2007.12.030
- SANCHES, A. L., MISI, A., KAUFMAN, A. J., & AZMY, K. (2007). As sucessões carbonáticas neoproterozóicas do Cráton do São Francisco e os depósitos de fosfato: correlações e fosfogênese. **Revista Brasileira de Geociências**, 37, 182–194.
- SENNA, J. (2003). **Caracterização de Argilas de Utilização na Indústria Cerâmica por Espectroscopia de Reflectância**. Dissertação de Mestrado. Universidade Estadual de Campinas.
- SENNA, J. (2008). **Caracterização Espectro-Mineralógica e Aspectos sobre a Gênese de Materias-Primas Cerâmicas Clássicas do Brasil: Estudos de Caso em Depósitos de Pirofilita, Talco e Caulinita**. Tese de Doutorado. Universidade Estadual de Campinas.

Capitulo V: Remote Sensing of Phosphatic Rocks from Igneous and Sedimentary Sources: Catalão I (GO), Tapira, Lagamar and Rocinha mines (MG)

5.1 Introduction

Mineral mapping through remote sensing has been a technique well tested for several mineral groups like clays, oxides and hydroxides, as well as carbonates and sulfates. Experiences in remote sensing of minerals have taken place since the 70s, focusing on hydrothermal alteration minerals associated to metallic ore deposits (e.g., CROSTA *et al.*, 2003).

Although remote sensing has played an enormous role in the mineral exploration of precious and base metals, it has not been properly tested yet as a tool for the exploration of phosphate minerals that are of interest for the fertilizer, pharmaceutical and agricultural industry. Given the market push that phosphate prices have had in the last 5 years, only taking a plunge during the world economic crisis of 2008 (U.S. Geological Survey (USGS), 2010), it is reasonable to think that prospecting phosphates is a safe way to maintain control over the food input of states and countries.

While many aspects of the phosphate geology are known in terms of their relevance in the geochemical cycle of phosphor and its link between the organic and inorganic biochemistry, the few papers related to spectroscopy of phosphates are focused on the characterization of the mineralogy (DAASCH & SMITH 1951; HAIDER 1961; REDDY *et al.* 2008). The main reference of spectroscopy of phosphates with applications to remote sensing is the classic work of HUNT *et al.* (1972).

In Brazil, we highlight the work of TEXEIRA (2011). The author tried to establish the spectral behavior of phosphatic rocks of the Catalão I and the Campos Belos deposits, in Goiás State. However, important questions remained unanswered from that work. For

example, mineral assemblages of the main lithotypes were not characterized; the evolution of phosphatic minerals in the weathering profile was not covered; samples were treated as perfect mineral endmembers; and the sampled lithotypes were not directly used with spectral mapping algorithms. This kind of approach isolates responses to a certain band, and it also dismisses responses that reflectance spectroscopy of the VNIR-SWIR can give to identify phosphates and related lithotypes using VNIR and SWIR datasets.

In order to properly characterize the ability of ASTER multispectral images for phosphate prospecting, a full recognition of the VNIR-SWIR spectra of several lithotypes and minerals from the Alto Paranaíba Igneous Province (PIAP) and the Brasília Fold Belt (BFB) can be of great use for national programs, and could be adapted to other Alkaline Igneous Provinces in the world.

In this context, we have used spectral libraries created in laboratory conditions from mineral, rock and soil samples from cretacic alkaline carbonatite complexes and neoproterozoic meta-phosphoritic rocks from Goiás and Minas Gerais states, Midwestern Brazil. The main goal is to use these libraries as endmember spectra and perform attempts to target phosphate minerals and related lithotypes using ASTER imagery.

ASTER reflective spectral bands cover the VNIR-SWIR regions of the electromagnetic spectrum, allowing targeting alteration minerals, carbonates, oxides and hydroxides. The data can be obtained on a regular basis, with little or no cost to the scientific community and mineral exploration companies. Gathering quality data on the alteration mineralogies that phosphates have for the sedimentary and igneous deposits, will give an excellent prospective guide for exploration campaigns of similar wide-reaching deposits.

5.2 Material and Methods

Samples were collected in the phosphate mines, and described and measured for reflectance spectroscopy with a FieldSpec 3 Hi Resolution spectrometer (2151 channels over the VNIR-SWIR) (see Chapters 3 and 4). Illite, kaolinite, muscovite, phlogopite and vermiculite features were analyzed in the 2.1-2.3 μm part of the electromagnetic spectrum; calcite and dolomite in the 2.33-2.34 μm range. REE-bearing phosphates were investigated based on typical absorption features centered around 0.5 μm and between 0.7-0.8 μm .

ASTER scenes were acquired from NASA at Level 1B, corrected for crosstalk effects using the CrossTalk3[®] routine, merged into a single 9 bands dataset at 15m resolution, and atmospherically compensated and converted to reflectance using the ACORN 5[®] software. Once converted to reflectance, images were processed using the ENVI 4.8[®] software.

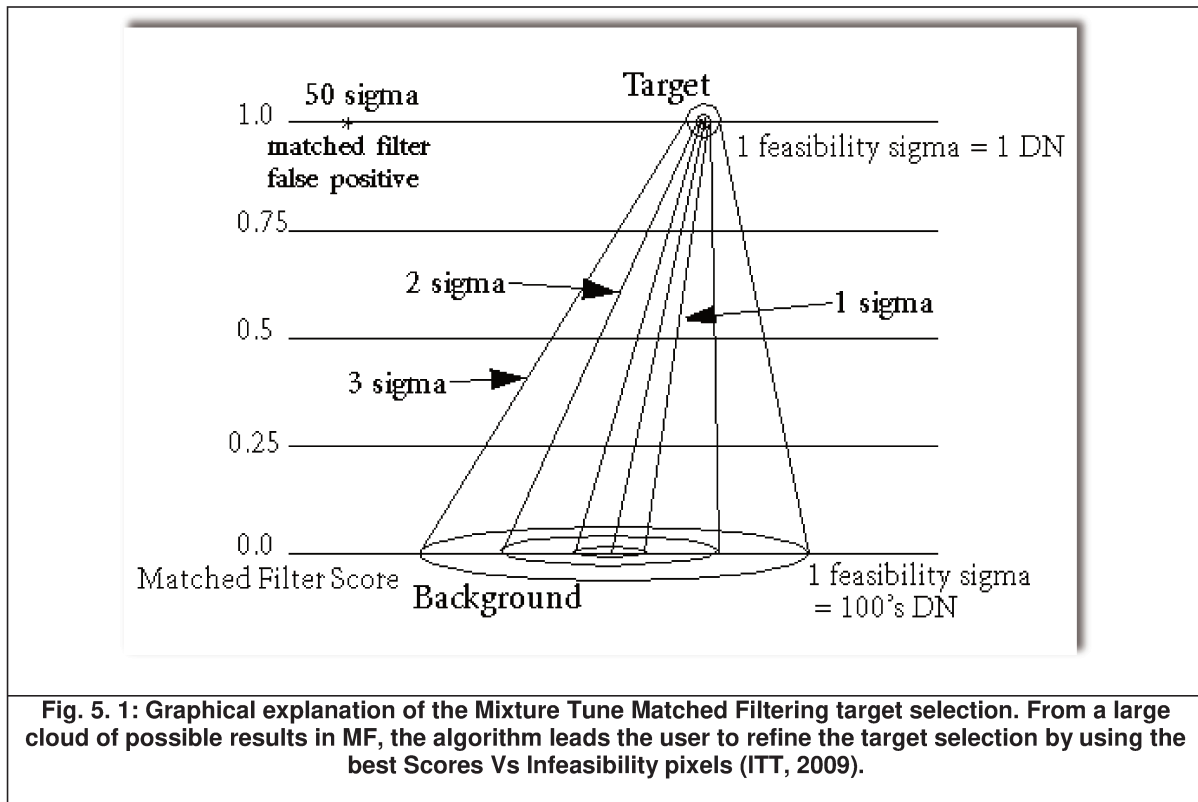
The L1B images were further georeferenced using ground control points (GCPs) measured in the field. Vegetation and agricultural lands were masked. A 3x3-pixel area surrounding a GCP was analyzed when GCPs were located on vegetation-free zones in the imagery, aiming to verify possible variations of the spectral signatures at pixel scale. When GCP were nearby masked zones, the only pixels analyzed were the ones that contained bare soil/rock information.

Spectra obtained from the Image was extracted through the n-Dimensional spectral analyzer provided in the ENVI software when image spectra did not matched in a sufficient way the laboratory spectra. The n-Dimensional selection of endmembers was performed over pixel clouds of 10,000 pixels, restricting n-Dimensional classes to a maximum of five to avoid creating classification additions.

Spectral Angle Mapper (SAM) and Mixture Tuned Matched Filtering (MTMF) classification methods were tested with the VNIR-SWIR ASTER reflectance dataset to map phosphates and related mineral assemblages. The SAM algorithm is a spectral classification that uses an n -D angle to match pixels to an user-defined reference spectra. The algorithm determines the similarity between two spectra by calculating the "spectral angle" between them, treating them as vectors in a space with dimensionality equal to the number of bands (Kruse et al., 1993). Classification maps obtained from SAM processing were later on filtered with a 3x3 median kernel to homogenize the final outputs.

The Mixture Tuned Matched Filtering (MTMF) performs two processes the Matched Filtering algorithm (MF) and the addition for interpretation of an infeasibility image to the results based on a Mixture tune algorithm. The Matched Filtering algorithm allows the user to look for specific endmembers in an image dataset using a partial unmixing of the signals, maximizing the response of the suspected matches to the endmembers and minimizing the background response signal. It is useful to apply when the presence of a mineral endmember is known in the study area. The Mixture Tuned part of the algorithm produces an infeasibility image used to reduce the number of false positives that are

sometimes found when using MF. Pixels with a high infeasibility are likely to be MF false positives. Correctly mapped pixels will have an MF score above the background distribution around zero and a low infeasibility value. The infeasibility values are in noise sigma units that vary in DN scale with an MF score (see fig. 5.1).



Confusion matrices were also computed for the results obtained by SAM and MTMF, in order to evaluate the classification success. They were calculated using ground truth areas that corresponded to sites sampled in the mine.

5.3 Results

The samples investigated here are listed in table 5.1. Using reflectance spectroscopy and XRD data, several mineral assemblages for igneous (vermiculite-goethite-hematite; phlogopite-calcite-dolomite, kaolinite-vermiculite-phlogopite, fluorapatite-monazite-phlogopite; monazite-calcite-dolomite) and sedimentary phosphates (illite-calcite; kaolinite-calcite) were established as positive matches for P_2O_5 presence.

Tab. 5. 1: Sample coordinates and description

X	Y	Sample	Sample Description
203321	7992628	CA-09	Brown Aloterite
203327	7992558	CA-16	Isalteritic phosphatic soil
203373	7992546	CA-18D	Phlogopite phoscorite
202714	7992466	CA-20	Phoscorite with magnetite
203298	7993583	CA-32	Silexite
203284	7993567	CA-33	Isalteritic titaniferous soil
203276	7993550	CA-35	Isalteritic Phoscorite soil with magnetite
203278	7993534	CA-37	Isalteritic ferric soil
203331	7993520	CA-39, CA-42	Magnetite-Calcite Phoscorite; Apatite with magnetite
203943	7993343	CA-Monazite-Barite	Monazite intergrown with Barite
203078	7993341	CA-55	Apatite with magnetite
203652	7992866	CA-103	Cumulatic Carbonatite
202411	7992272	CA-123	Green Breccia with magnetite
202798	7992471	CA-127	Brecciated Phlogopitite
202678	7992341	CA-129	Silexite-dolomite carbonatite contact
203463	7992849	CA-VERCA2	Vermiculite
202738	7992339	CA-130	Phlogopitite with magnetite
202767	7992339	CA-131	Altered Phlogopitite
203943	7993343	CA-APCA	Carbonatite-apatitite
306161	7800354	TA201-202a- 202b-203-204	Altered B1 bebedourite; Pegmatoid B1 bebedourite
306135	7800402	TA-205	Possible monazite; Monazite B1- Bebedourite
305999	7800656	TA-209; TA210	Vermiculite; Bebedourite with vermiculite
307150	7801610	TA-218	Flux-mineral banding, carbonatite-picrite
307160	7801575	TA-219-220-221	Breccia-carbonatite-B2 bebedourite contact
307754	7801906	TA-228A; TA-228B	Altered B2 bebedourite with goethite
308096	7802571	TA-236	Isalterite with secondary phosphates
296532	7968347	RO-03A	Interstratified sandstone-mudstone with cryptocrystalline apatite veins
296500	7968398	RO-09	Laminated phosphoritic siltite with quartz intraclasts
296494	7968409	RO-10A	Phosphoritic dolostone with oxidation sheets
296490	7968429	RO-11B	Thrust-folded phosphorites
296486	7968440	RO-12	Phosphoritic siltstone, folded
296494	7968458	RO-14D	Siltstone/Dolostone, altered
296510	7968465	RO-15A	Brown limestone with few apatite levels
296472	7968332	RO-19A	Brittle Limestone with chlorite and oxidized bands
296458	7968336	RO-21	Phosphoritic siltstone with green matrix
296439	7968342	RO-22	Phosphoritic siltstone with goethite packs
296441	7968343	RO-23	Phosphoritic limestone. Cryptocrystalline apatite as thin sheets
296444	7968344	RO-24	Calcite veins in PO-poor siltstone with goethite
296476	7968306	RO-25A	Clayey Phosphorite
296476	7968306	RO-25B	Soil above Clayey phosphorites
296466	7968309	RO-26A	Phosphorite
296466	7968309	RO-26B	Soil above sample 26A
296448	7968297	RO-27B	Phosphorite/ weathering mantle contact
296448	7968297	RO-27C	Clayish soil with goethite
296448	7968297	RO-27D	Sterile soil
305637	7981023	LG01 Beto-LG01G LG01H	Silty slates with cryptocrystalline apatite
305625	7981003	LG-02	Silty slates with clay and apatite

305626	7981008	LG-02A	Clayey siltstone
305602	7981000	LG-03 Base – Vertical Profile	Phosphoritic slate/ limestone contact
305592	7980995	LGPV1BB	Clayey slate, PO-rich
305646	7981010	LGBMI05	Phosphoritic slate
305609	7980981	LGBMI07	Marginal siltstone

5.3.1 Tapira Carbonatitic Alkaline Complex and Araxá-Barreiro Carbonatitic Alkaline Complex

From the studied set of samples, four endmembers derived from Regions Of Interest (ROI's) in the image were selected. These endmembers matched to sufficient levels the laboratory spectra, which have spectral differences that speak of their diverse ore levels in the Tapira deposit. They correspond to spectra similar to phosphoritic carbonatites, bebedourites with ajoite-corvusite, bebedouritic carbonatites, bebedourites with vermiculites and isalterites with secondary phosphates. These endmembers can be seen in laboratory and in ASTER resolution in Fig. 5.2

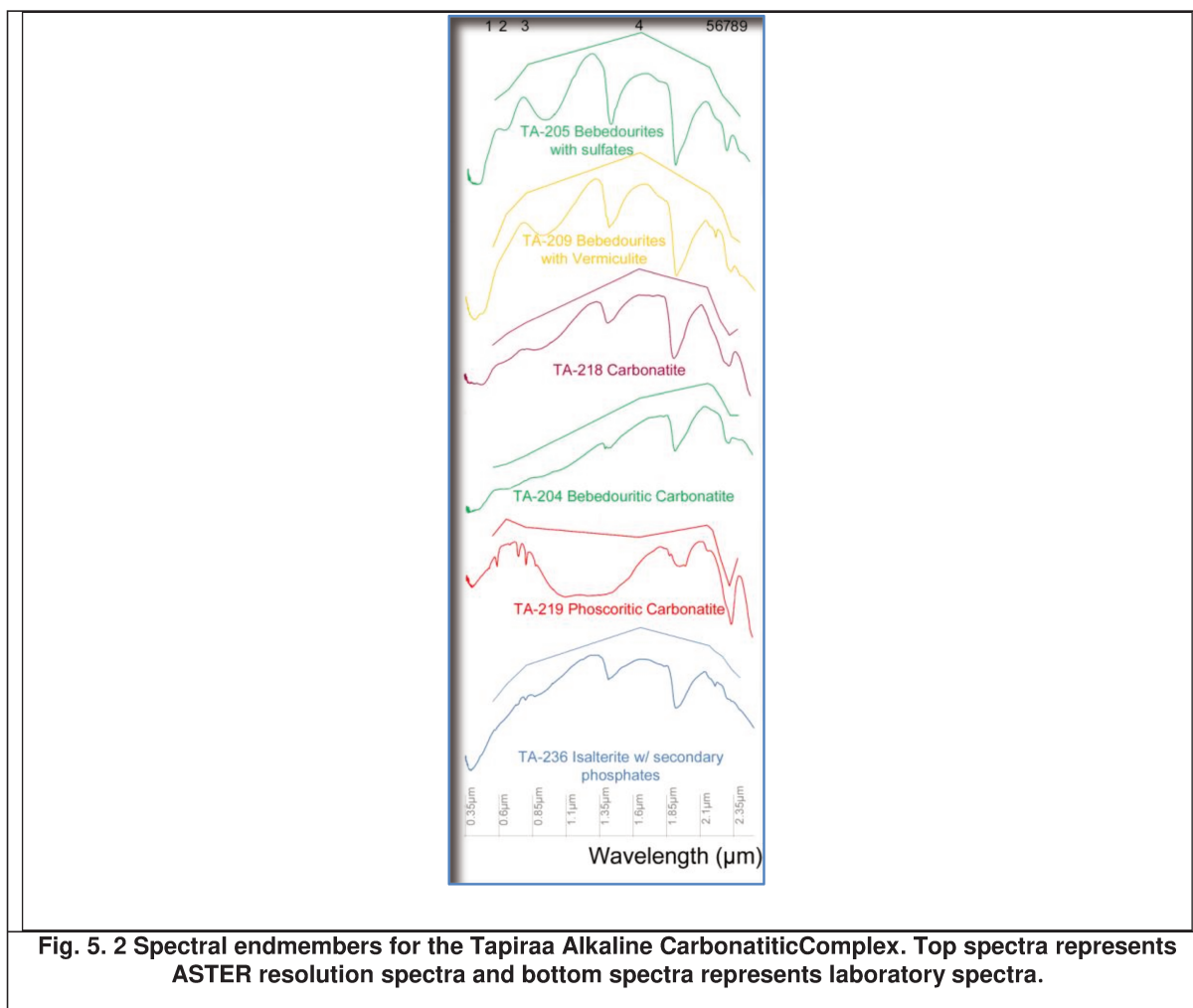


Fig. 5. 2 Spectral endmembers for the Tapira Alkaline Carbonatitic Complex. Top spectra represents ASTER resolution spectra and bottom spectra represents laboratory spectra.

From Fig. 5.2 it can be seen that REE absorption features identified in laboratory resolution (see chapter 3) are lost in ASTER resolution. Therefore, identification of phosphates through ASTER imagery will be limited to the analysis of secondary features from carbonate, clays, mica mineral and Fe content that make up the mineral assemblage of the four endmembers selected.

5.3.1.1 Image Endmembers:

Image endmembers were extracted from Regions Of Interest (ROI) that represent the maximum material mixture from the soils and rocks that outcrops nearby the sampling points. These regions were selected as 3x3 rectangle clusters that contained the sampling point. Given that some samples were taken near vegetation zones, where the sampling point was inside of a masked area in the image, ROI were reduced to the nearest possible pixels to the sampling point, reducing the statistical variation of the spectra from these pixels. The ROI table is shown in Table 5.2. Mean average spectra from these ROI's is displayed on Fig. 5.3

Tab. 5. 2 ROI description and pixel extent of the chosen endmembers for the Tapira Alkaline Carbonatitic Complex

Region of Interest	Color	Pixels
Phoscoritic Carbonatite	Red	16
Clinopyroxenite with secondary phosphates	Cyan	11
Bebedourite with sulfates	Blue	17
Bebedourite with vermiculite	Orange	13

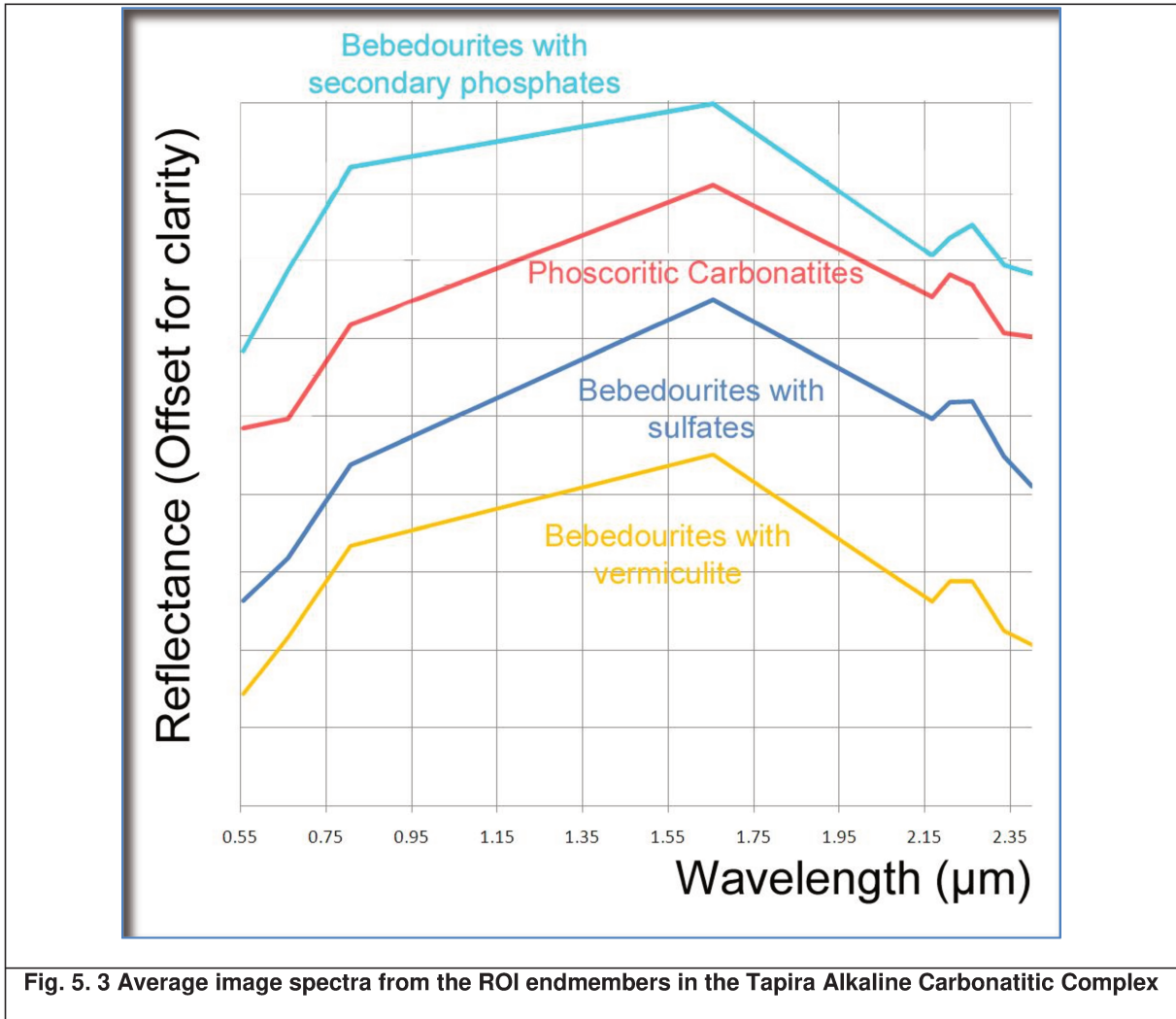
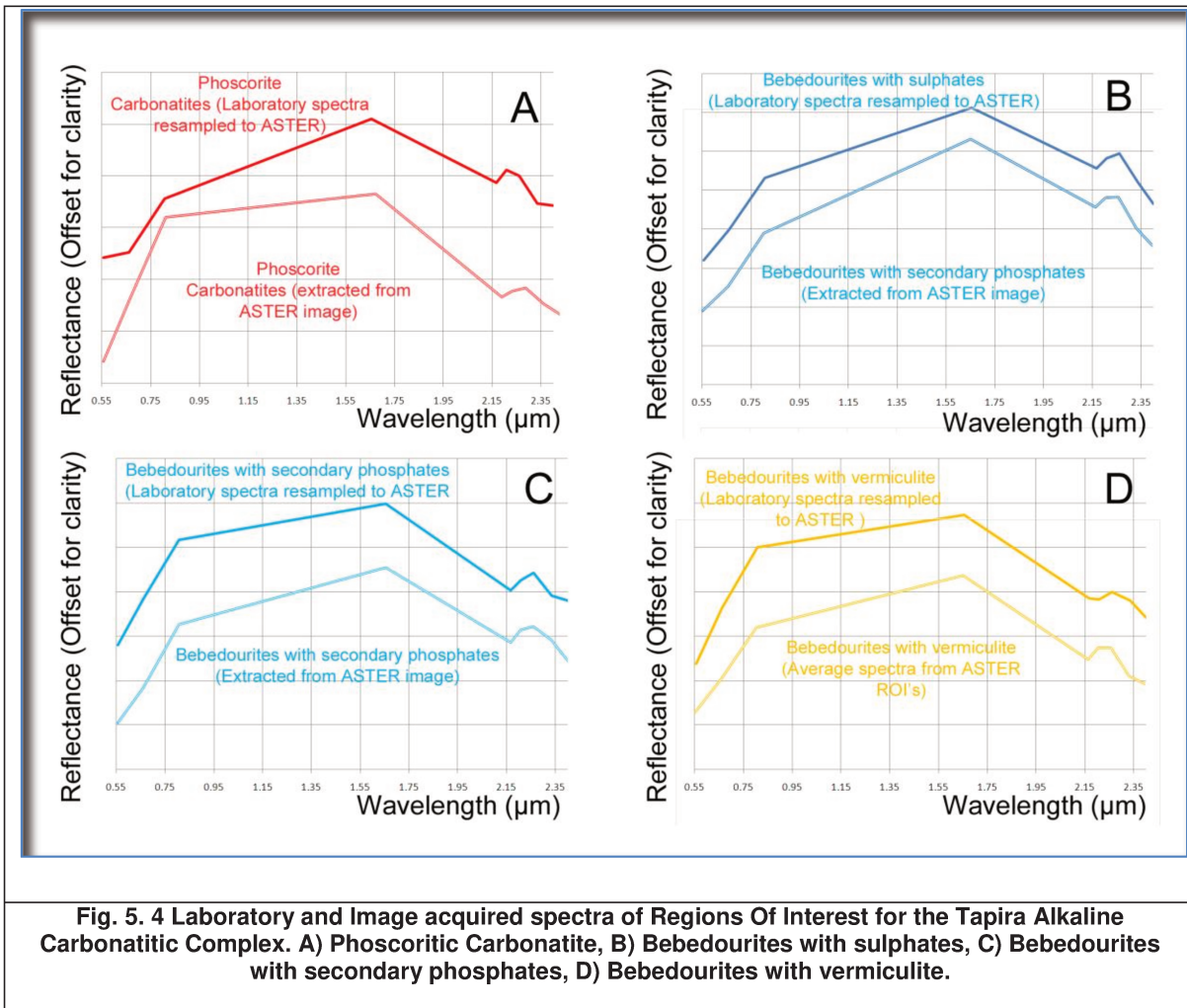


Fig. 5. 3 Average image spectra from the ROI endmembers in the Tapira Alkaline Carbonatitic Complex

When comparing the laboratory endmembers with the spectra that were extracted from the ASTER imagery (Fig. 5.4) at the location of sample extraction, it can be observed that some inconsistency is evident on bands 5 to 9, that can be attributed to deficiencies in the crosstalk correction. Other factors that can be responsible of these changes are: large amount of time in between image acquisition and sample collecting; shortcomings in the atmospheric compensation algorithm and non-representative sampling of the whole material from the ROI.

For this reason, it was not possible to discriminate phosphate minerals directly from image spectra from the ASTER sensor. As such, the mineral assemblages that were looked upon in this research were hosts of phosphate mineralizations but cannot give a direct estimation on phosphate resources, specially on the high variation in ore levels that can exist in weathering profile deposits.



5.3.1.2 Spectral Angle Mapper (SAM):

The endmembers employed for the SAM classification of the ASTER imagery covering the Tapira mine are shown in table 5.3. The spectral library used for the SAM algorithm is displayed in Fig. 5.4 as light lines (marked as Extracted from ASTER Image, Fig. 5.4 A, B, C and D). It is noteworthy that although biotite is abundant in the Tapira complex, the SAM algorithm could not classify it in any imagery pixel (Fig. 5.5).

Tab. 5. 3: SAM classification colors for targets (endmembers) in the Tapira Carbonatitic Alkaline Complex

Unit	Class color
Bebedourites with sulphates	Blue
Bebedourites with vermiculite	Orange
Phoscoritic Carbonatite	Red
Bebedourite with secondary phosphates	Cyan

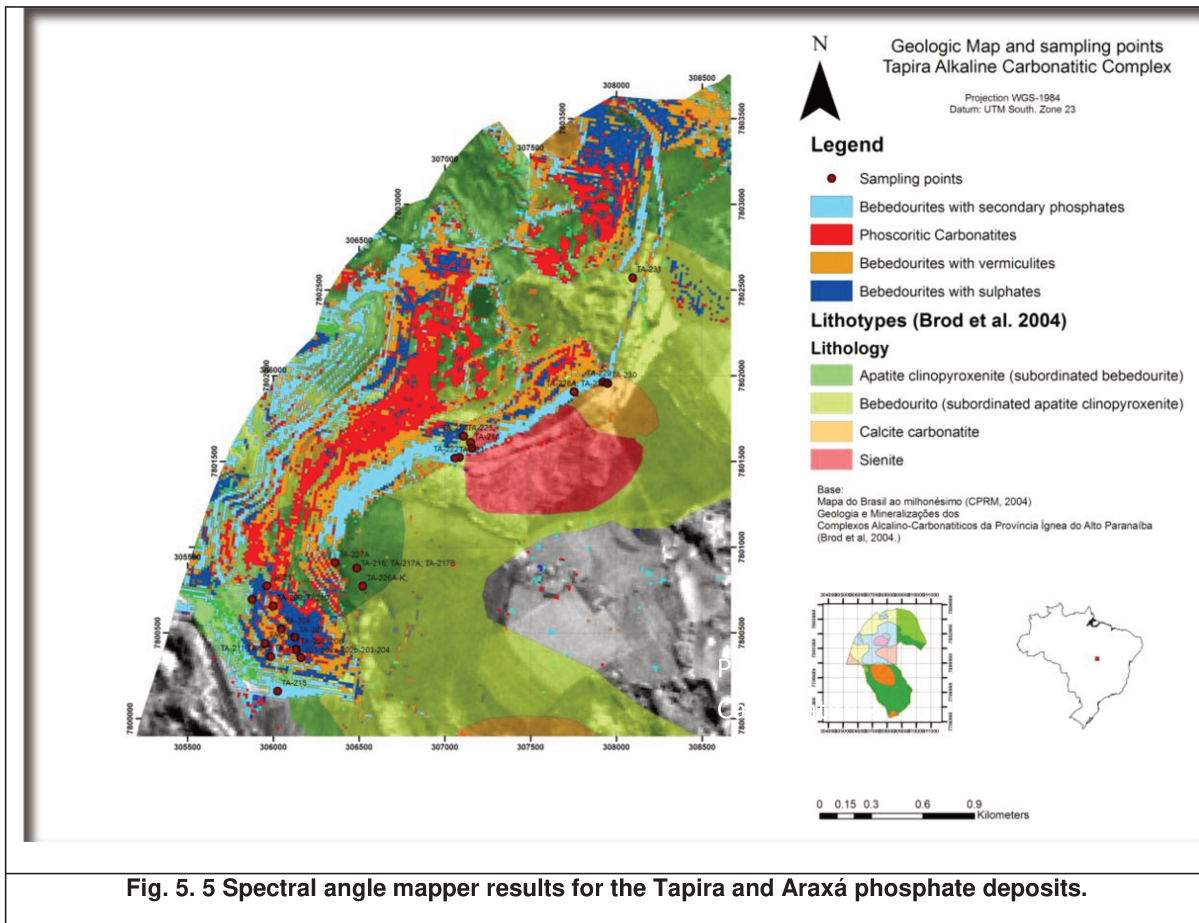


Fig. 5. 5 Spectral angle mapper results for the Tapira and Araxá phosphate deposits.

It is observed in fig. 5.5 that the classification discriminates very well the units that represents bebedourites with secondary phosphates (in cyan) in the Tapira Complex. Several areas in the imagery are depicted as sites containing secondary phosphates. Also, phoscoritic carbonatites take the center of the mine and are surrounded by orange pixels representing vermiculite, almost in the same way as it was observed during the field campaign. Bebedourites bearers of sulphates are also discriminated by the SAM algorithm, concentrating towards the south of the mine (Fig.5.5)

The classification results show that the bebedourites with sulphate mixture comprises 3443 pixels, accounting for 0.676% of the classified pixels. Bebedourites with vermiculite are represented by 10,116 pixels and comprised 1.986% of the mapped pixels. The phoscoritic carbonatite represents 8764 pixels and a total percentage of 1.721% of the classification. Some 476055 pixels were unclassified either by masking of vegetation or lack of spectral likelihood with the chosen endmembers, representing 93.469% of the classified image.

The confusion matrix for the SAM algorithm showed a modest accuracy, in which 41.8605% of the ground truth information collected at the mine site was corresponded. This encourages a more thorough refinement of the spectral data, undefined at the moment, that might turn this algorithm and other geological informations as tools to locate possible new igneous phosphate deposits in the PIAP region. The confusion matrix is presented in tab. 5.4.

Tab. 5. 4: Confusion Matrix for the SAM classification in the Tapira Carbonatitic Complex

Overall	Accuracy	=	(36/86)	41.86%	
Kappa	Coefficient	=	0.2297		
Ground Truth (Pixels)					
Class	Region #4	Region #1	Region #2	Region #3	Total
Unclassified	0	0	0	0	0
Bebedourites w/vermiculite	19	0	3	2	24
Bebedourites w/sulphates	2	0	28	0	30
Phoscoritic Carbonatites	0	15	4	0	19
Bebedourites w/ secondary phosphates	0	0	0	13	13
Total	21	15	35	15	86
Ground Truth(Percent)					
Class	Region #4	Region #1	Region #2	Region #3	Total
Unclassified	0	0	0	0	0
Bebedourites w/vermiculite	90.48	0	8.57	13.33	27.91
Bebedourites w/sulphates	9.52	0	80	0	34.88
Phoscoritic Carbonatites	0	100	11.43	0	22.09
Bebedourites w/ secondary phosphates	0	0	0	86.67	15.12
Total	100	100	100	100	100
	Commission	Omission	Commission	Omission	
Class	(Percent)	(Percent)	(Pixels)	(Pixels)	
Bebedourites w/vermiculite	20.83	9.52	5/24	2/21	
Bebedourites w/sulphates	100	100	30/30	15/15	
Phoscoritic Carbonatites	78.95	88.57	15/19	31/35	

Bebedourites w/ secondary phosphates	0	13.33	0/13	02/15	
	Prod. Acc.	User Acc.	Prod. Acc.	User Acc.	
Class	(Percent)	(Percent)	(Pixels)	(Pixels)	
Bebedourites w/vermiculite	90.48	79.17	19/21	19/24	
Bebedourites w/sulphates	0	0	0/15	0/30	
Phoscoritic Carbonatites	11.43	21.05	4/35	4/19	
Bebedourites w/ secondary phosphates	86.67	100	13/15	13/13	

5.3.1.3 Mixture Tuned Matched Filtering (MTMF)

In order to improve the results obtained by SAM, a Mixture Tuned Matched Filtering algorithm was performed on the Tapira ASTER dataset. For the same reference spectra used for the SAM algorithm, it was possible to pinpoint the location of the original sampling sites and interpolate those pixels in the regions of the cloud where MF scores were high and Infeasibility scores were reasonably low. The only sample that showed high infeasibility values was TA-219 (carbonatite phoscorite picrite). Results are displayed in Fig. 5.8.

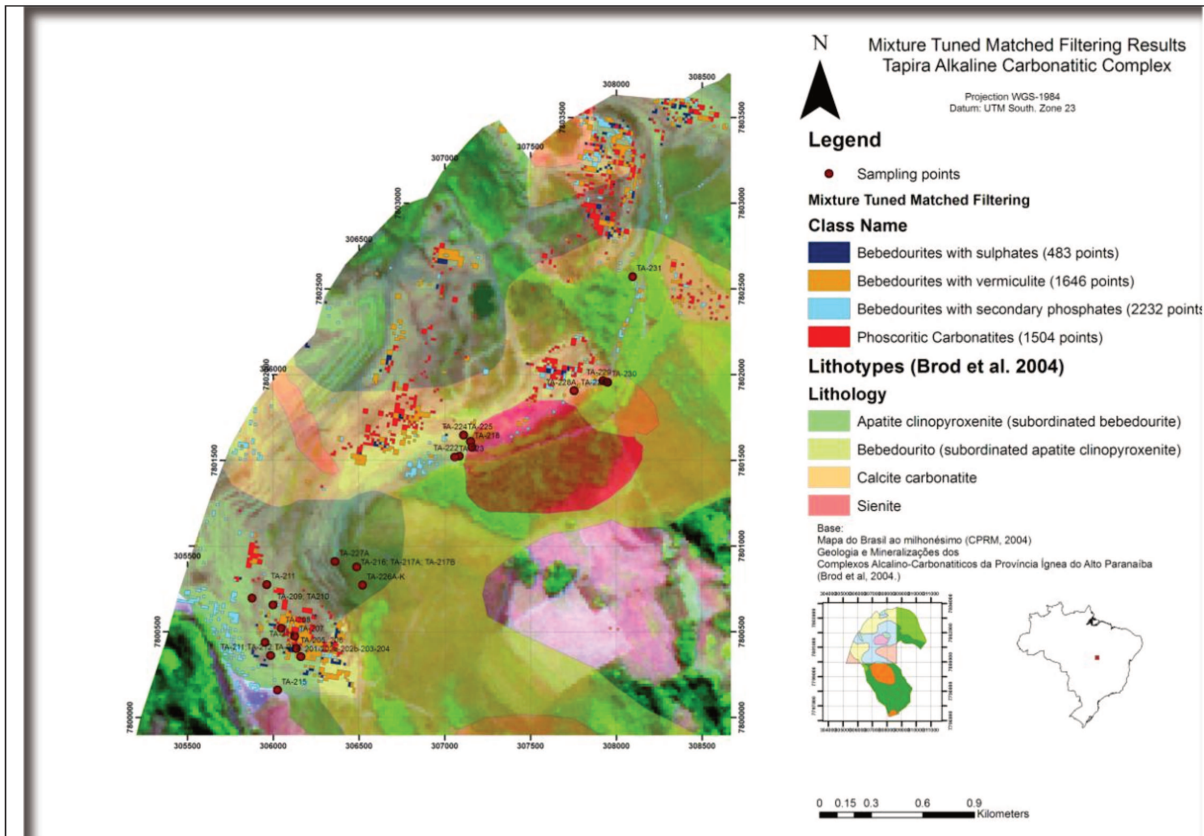
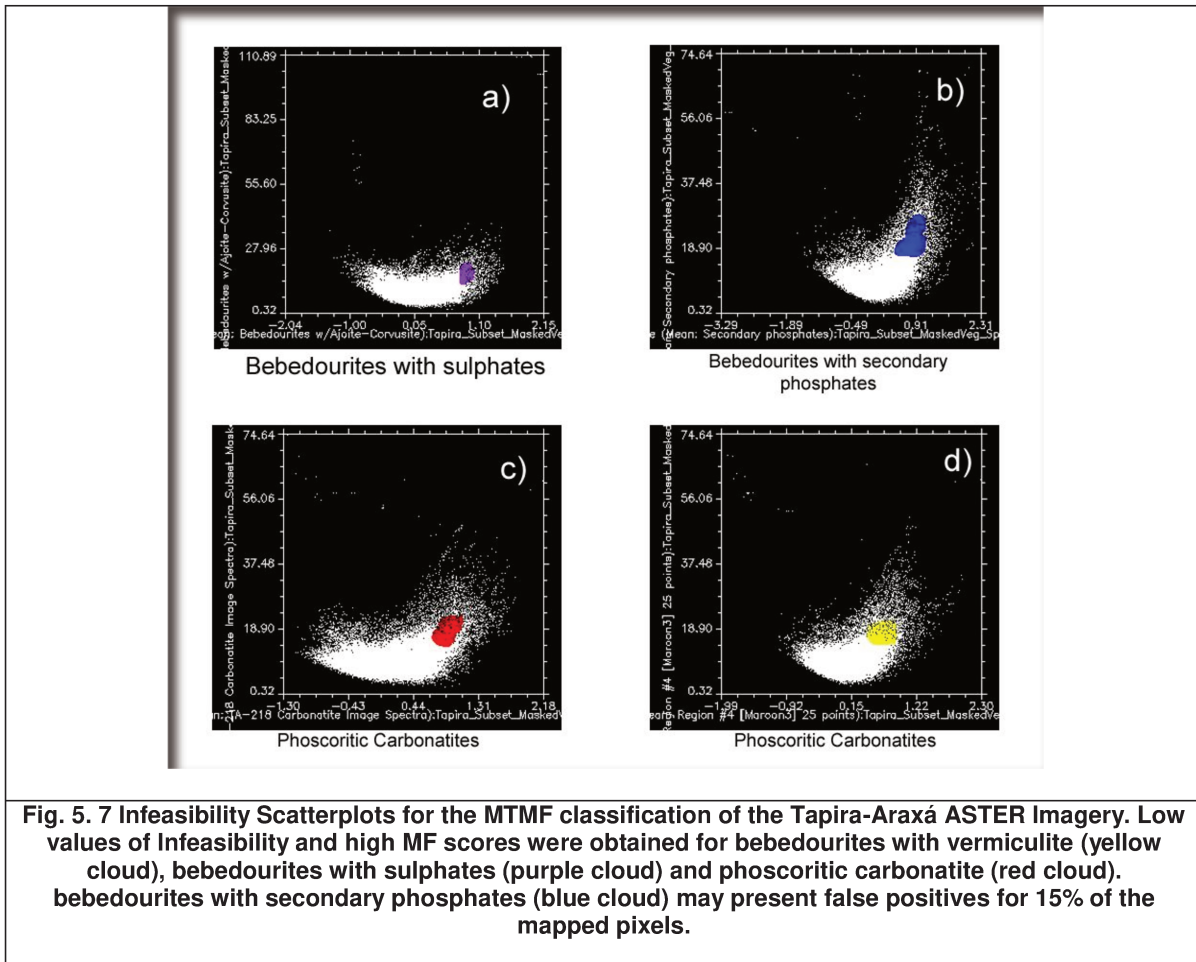


Fig. 5. 6 Mixture Tuned Matched Filtering results for the Tapira Carbonatitic Alkaline Complex.

The MF scores vs infeasibility diagrams (fig. 5.9) for each of the endmembers show that best results in terms of uncertainty and accuracy are with the endmember of secondary phosphate and vermiculite. The carbonatite scatterplot shows that although it keeps a good feasibility value, its MF scores are lower than expected. The most imprecise measurement is the ajoite-apatite endmember that shows unimportant infeasibility and MF scores.



A new confusion matrix was produced for the MTMF classification yielded from the ASTER imagery covering the Tapira Alkaline Carbonatitic Complex. The sites where the samples were collected were used as ground control points. This matrix was compared to see if possible false positives were arising as SAM results. The results are shown in the Table 5.5.

Results show that the MTMF was able to improve SAM results. Comparisons show that the better classified material was the bebedourites with secondary phosphates, which

had the best ratings of matching and was less perceived as a false positive by other classes. The bebedourites with sulphates endmember was highly perceived by the MTMF, while the bebedourites with vermiculite and the phoscoritic carbonatite were perceived and mapped in different classes.

Tab. 5. 5 Confusion Matrix for MTMF Classification. Tapira Alkaline Carbonatitic Complex

Overall Accuracy	(4710/ 5865)	80.31%			
Kappa Coefficient	0.7225				
Ground Truth (Pixels)					
Class	Unclassified	Bebedourite with secondary phosphates	Bebedourite w/sulphates	Phoscoritic Carbonatites	Bebedourites w/vermiculite
Unclassified	0	0	0	0	0
Bebedourite with secondary phosphates	1516	0	0	0	1516
Bebedourite with sulphates	49	243	0	0	292
Phoscoritic Carbonatites	145	62	1305	0	1512
Bebedourites with vermiculite	522	178	199	1646	2545
Total	2232	483	1504	1646	5865
Ground Truth (Percent)					
Class	Unclassified	Bebedourite w/ secondary phosphates	Bebedourite w/sulphates	Phoscoritic Carbonatites	Bebedourites w/vermiculite
Unclassified	0	0	0	0	0
Bebedourite with secondary phosphates	67.92	0	0	0	25.85
Bebedourite with sulphates	2.2	50.31	0	0	4.98
Phoscoritic Carbonatites	6.5	12.84	86.77	0	25.78
Bebedourites with vermiculite	23.39	36.85	13.23	100	43.39
Total	100	100	100	100	100
	Commi ssion	Omission	Commission	Omission	
Class	(Percent t)	(Percent)	(Pixels)	(Pixels)	
Bebedourite with secondary phosphates	0	32.08	0/1516	716/2232	
Bebedourite with sulphates	16.78	49.69	49/292	240/483	
Phoscoritic Carbonatites	13.69	13.23	207/1512	199/1504	
Bebedourites w/vermiculite	35.32	0	899/2545	0/1646	
	Prod. Acc.	User Acc.	Prod. Acc.	User Acc.	
Class	(Percent t)	(Percent)	(Pixels)	(Pixels)	
Bebedourite with secondary phosphates	67.92	100	1516/2232	1516/1516	
Bebedourite with sulphates	50.31	83.22	243/483	243/292	
Phoscoritic Carbonatites	86.77	86.31	1305/1504	1305/1512	
Bebedourites with vermiculite	100	64.68	1646/1646	1646/2545	

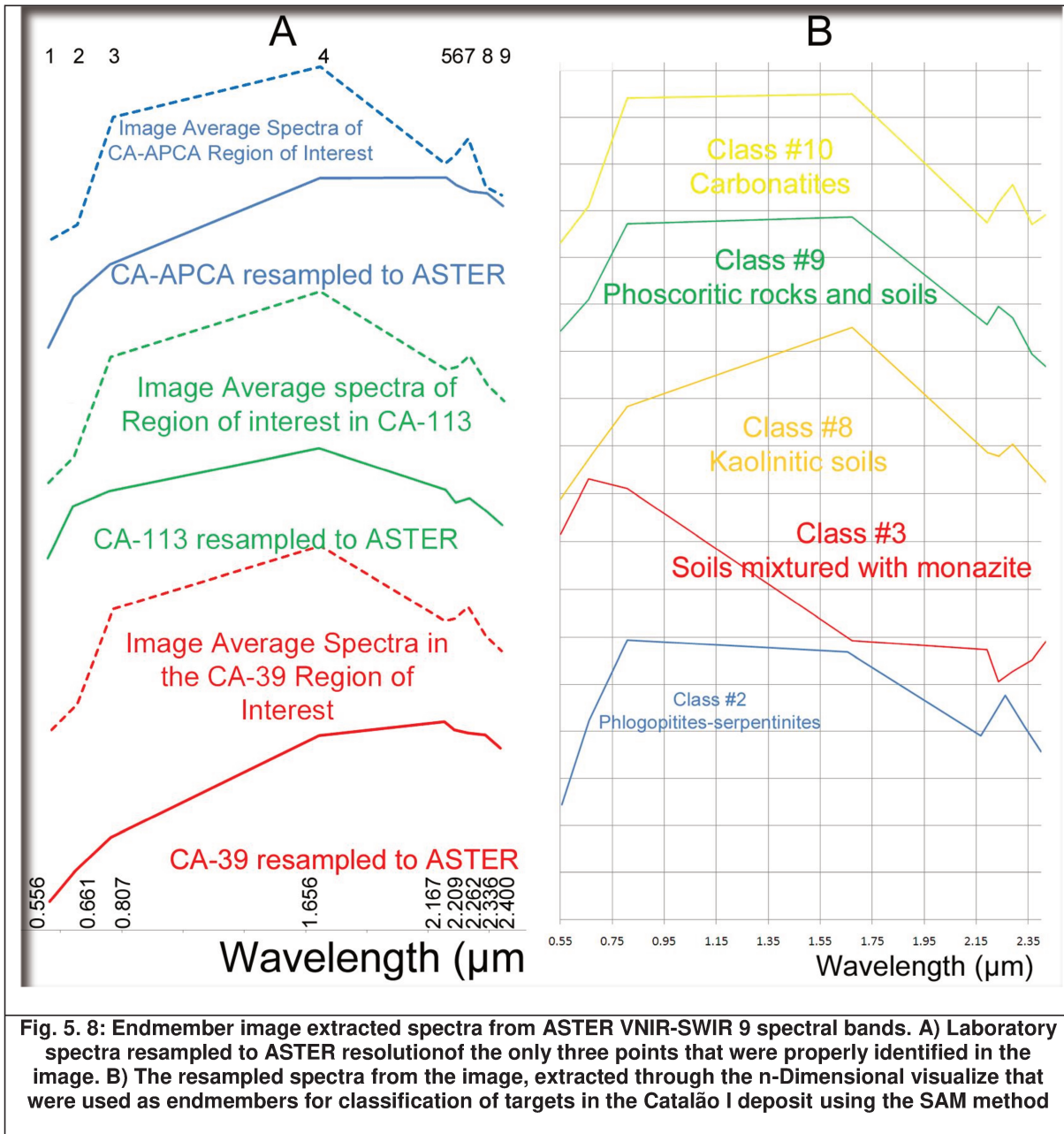
5.3.2 Catalão I Alkaline Carbonatitic Complex:

Rock spectra yielded for Catalão I samples from the ASTER images (Fig.5.10) show absorption features in bands related to Fe^{+3} , CaO and $\text{Al}(\text{OH})$ chemical bonds. Endmembers selected for target recognition were extracted from the n-Dimension visualizer given the fact that most of the samples acquired during field campaign were represented in the ASTER image as vegetated zones. However, the endmembers derived from the image have similarities with spectra obtained in the laboratory. Since vegetation was masked from the ASTER imagery, the classification is focused exclusively in areas where scanty or no vegetation is present.

5.3.2.1 Image endmembers:

Endmembers extracted from the image that were used for SAM algorithm in the Catalão I Carbonatitic Alkaline Complex are shown in Fig.5.8. The spectra had to be extracted directly from the image due to the fact that most of the collected samples when registered with the ASTER dataset were located in areas that had vegetation cover at the time of acquisition (August 27th, 2003).

When compared to laboratory spectra, there are certain issues regarding sensor calibration that were not fully resolved because of spatial and spectral differences. Since the ground truth field campaign started in March 2012, almost nine years passed from the image acquisition time to local sampling. In this sense, laboratory spectroscopy conducted in this research was outdated regarding image spectra, and served only to crosscheck that some of the interesting features in the VNIR-SWIR were present in the image spectra.

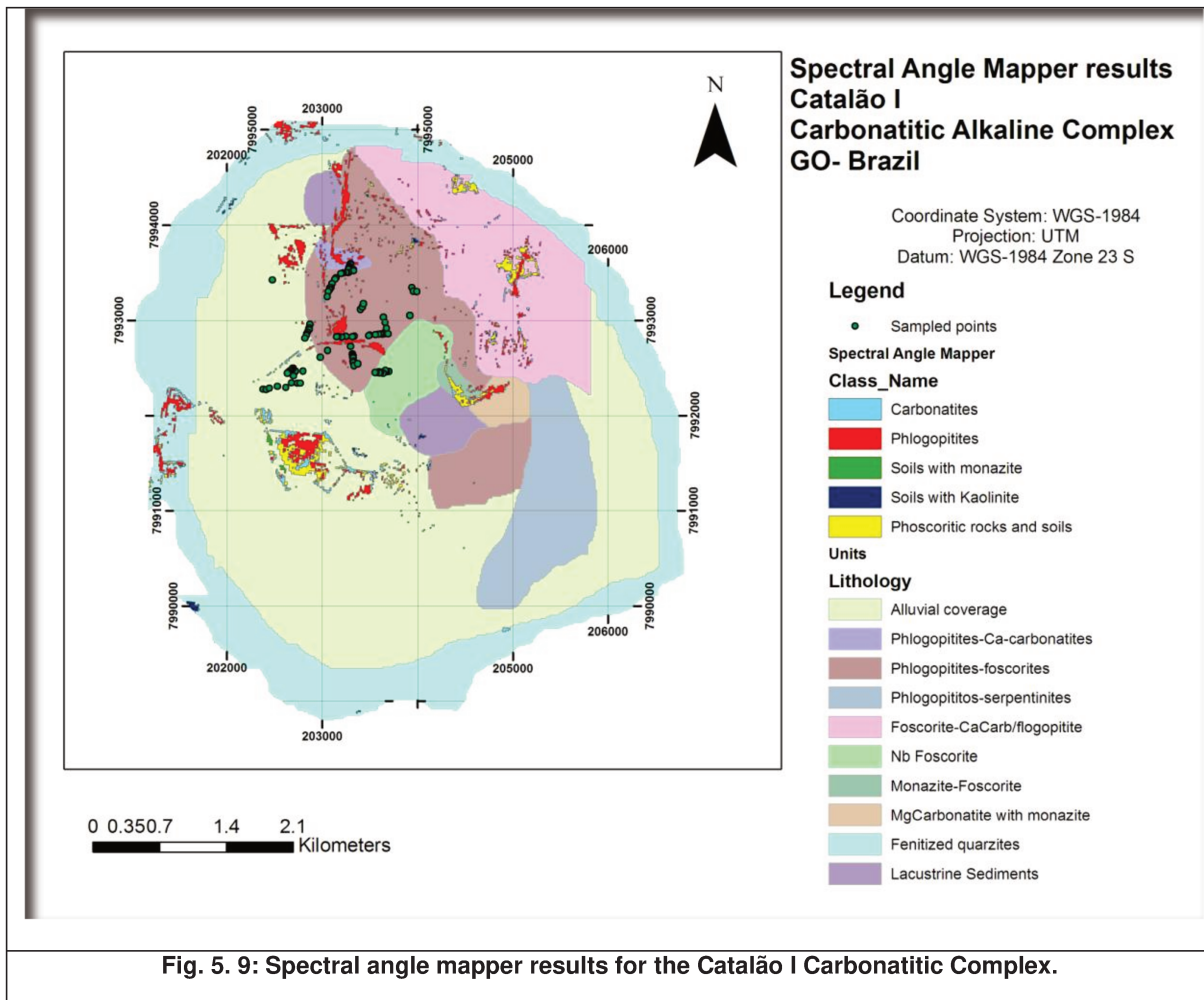


5.3.2.2 Spectral Angle Mapper Results:

Endmembers used for the SAM algorithm as viewed on Fig.5.8B provided results portrayed in fig. 5.9

The SAM classification was able to recognize 2.5% of the pixels for the image subset after all vegetation was masked in the image. The endmember that represented phlogopitites (Class #2, Fig.5.8B) mapped 3343 pixels, representing 1.275% of the classification result. The endmember that represented the monazitic soils (Class #3, Fig. 5.8B) mapped 32 pixels corresponding to 0.01% of the image. Kaolinitic soils mapped

(Class #8, Fig.5.8B) represented the 0.108% for 282 pixels. Phoscoritic soils and rocks (Class #9, Fig. 5.8B) were mapped in 1125 pixels, corresponding to 0.429% of the image and finally, carbonatitic rocks (Class #10) were mapped in 1818 pixels, representing the 0.694% of the classification.



A confusion matrix was calculated to assess the accuracy of the classification for the SAM algorithm. The results are presented in table 5.6. It could be seen that the best endmembers for classification are vermiculite and monazite, followed by the sample of magnetitic phoscorite and the isalteritic soil (poor in phosphates). Although the overall accuracy is quite successful, it has to be acknowledged that samples were collected years after the moment of image acquisition from the sensor and that image spectra used is not completely discernible due to the lack of updated information in the ASTER dataset. The period of time from image acquisition until sampling allowed for land changes that cannot

be updated due to the ASTER problem with the SWIR sensor, which had a permanent failure after May 2008.

Tab. 5. 6. Confusion Matrix for the SAM results obtained in Catalão I.

Overall	Accuracy	=	(4/5)	80.00%	
Kappa Coefficient		=	0.7619		
Class	Phlogopitite	Soils with monazite	Kaolinitic soils	Phoscoritic rocks and soils	Carbonatites
Unclassified	0	0	0	0	1
Phlogopitites	1	0	0	0	0
Soils with monazite	0	1	0	0	0
Kaolinitic soils	0	0	1	0	0
Phoscoritic rocks and soils	0	0	0	1	0
Carbonatites	0	0	0	0	0
Total	1	1	1	1	1
Ground Truth	(Pixels)		Ground Truth	(Percent)	
Class	Total		Class	Total	
Unclassified	1		Unclassified	20	
Phlogopites	1		n-DclassMean#2	20	
Soils with monazite	1		n-DclassMean#3	20	
Kaolinitic soils	1		n-DclassMean#8	20	
Phoscoritic rocks and soils	1		n-DclassMean#9	20	
Carbonatites	0		n-DclassMean#10	0	
Total	5		Total	100	
Ground Truth	(Percent)				
Class	Phlogopites	Soils with monazite	Kaolinitic soils	Phoscoritic rocks and soils	Carbonatites
Unclassified	0	0	0	0	100
Phlogopites	100	0	0	0	0
Soils with monazite	0	100	0	0	0
Kaolinitic soils	0	0	100	0	0
Phoscoritic rocks and soils	0	0	0	100	0
Carbonatites	0	0	0	0	0
Total	100	100	100	100	100
Class	Commission	Omission	Commission	Omission	
(Percent)	(Percent)	(Pixels)	(Pixels)		
Phlogopites	0	0	0/1	0/1	
Soils with monazite	0	0	0/1	0/1	
Kaolinitic soils	0	0	0/1	0/1	
Phoscoritic rocks and soils	0	0	0/1	0/1	
Carbonatites	0	100	0/0	1/1	
	Prod. Acc.	User Acc.	Prod. Acc.	User Acc.	
Class	(Percent)	(Percent)	(Pixels)	(Pixels)	
Phlogopites	100	100	1/1	1/1	
Soils with monazite	100	100	1/1	1/1	
Kaolinitic soils	100	100	1/1	1/1	
Phoscoritic rocks and soils	100	100	1/1	1/1	
Carbonatites	0	0	0/1	0/0	

5.3.3 Lagamar and Rocinha Mines

Lagamar mine rocks that contains P ore levels display a tendency to portray illite or illite-kaolinite mixtures as can be observed in the spectra of samples LG-01H, LG-02A and LG-01B (Fig.5.10a). From averaged image spectra obtained from the regions of interest of the samples in the ASTER dataset it was not possible to discriminate the illite-kaolinite feature directly, given that the initial feature of absorption starts at band 4, going until band 8, showing responses that include clay minerals, Al and Fe-Mg hydroxides of several kinds. There is little correspondence in spectra obtained in the laboratory with image extracted spectra. The visual comparison between laboratory measures and ASTER image spectra is shown on Fig. 5.10.

5.3.3.1 Image endmembers:

The reference endmembers of Rocinha and Lagamar mines for the SAM algorithm are presented in fig. 5.10 and fig.5.11. Spectra are presented in ASTER resolution. There is a strong tendency of features to correspond to alteration clays (illite, kaolinite or both as intimate mixtures) and lack of REEs absorption features. Other minerals recognizable are calcite and hematite/goethite. There is few resemblance from the laboratory spectra to the ASTER image extracted spectra, which is why the SAM algorithm was performed using the spectral library from the image spectra.

5.3.3.2 Spectral Angle Mapper Results

The SAM classification in the Lagamar and Rocinha mines was performed subsetting both mines from the same ASTER image converted to reflectance, using reference endmembers from each mine that matched actual samples. The notion was to verify how reflectance spectra differences were accounted by the algorithm. Given their proximity in the stratigraphic record and their mineralogical likelihood, it was expected that results were close to the rock sample endmembers. The higher detail taken on the Rocinha mine sampling, displayed these endmembers with better data dispersion in the classification than those of Lagamar, in which rock heterogeneity is yet less detailed.

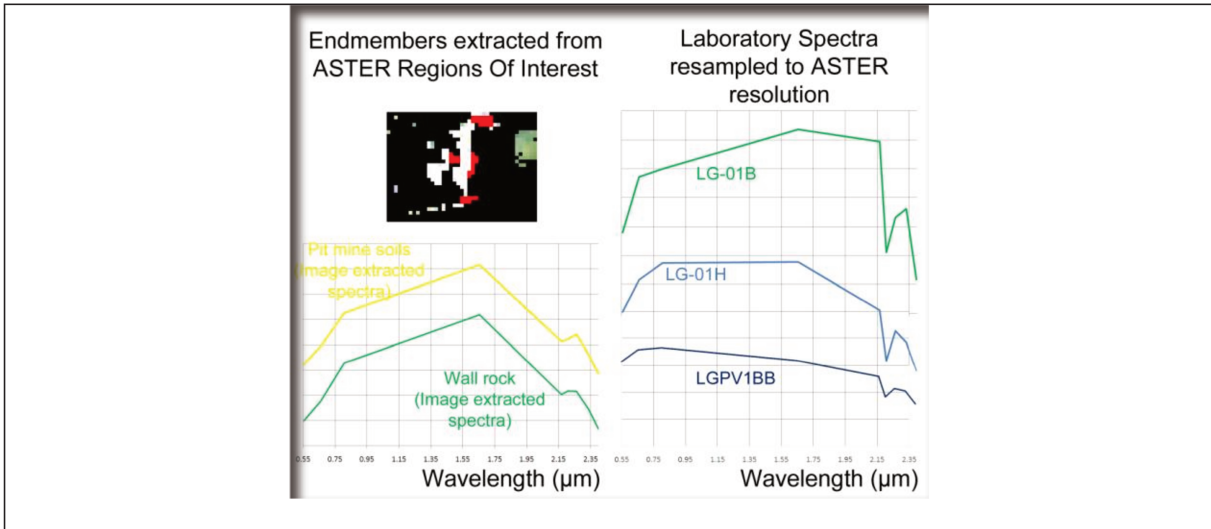


Fig. 5. 10 Spectra (Image extracted and Laboratory) from Lagamar mine

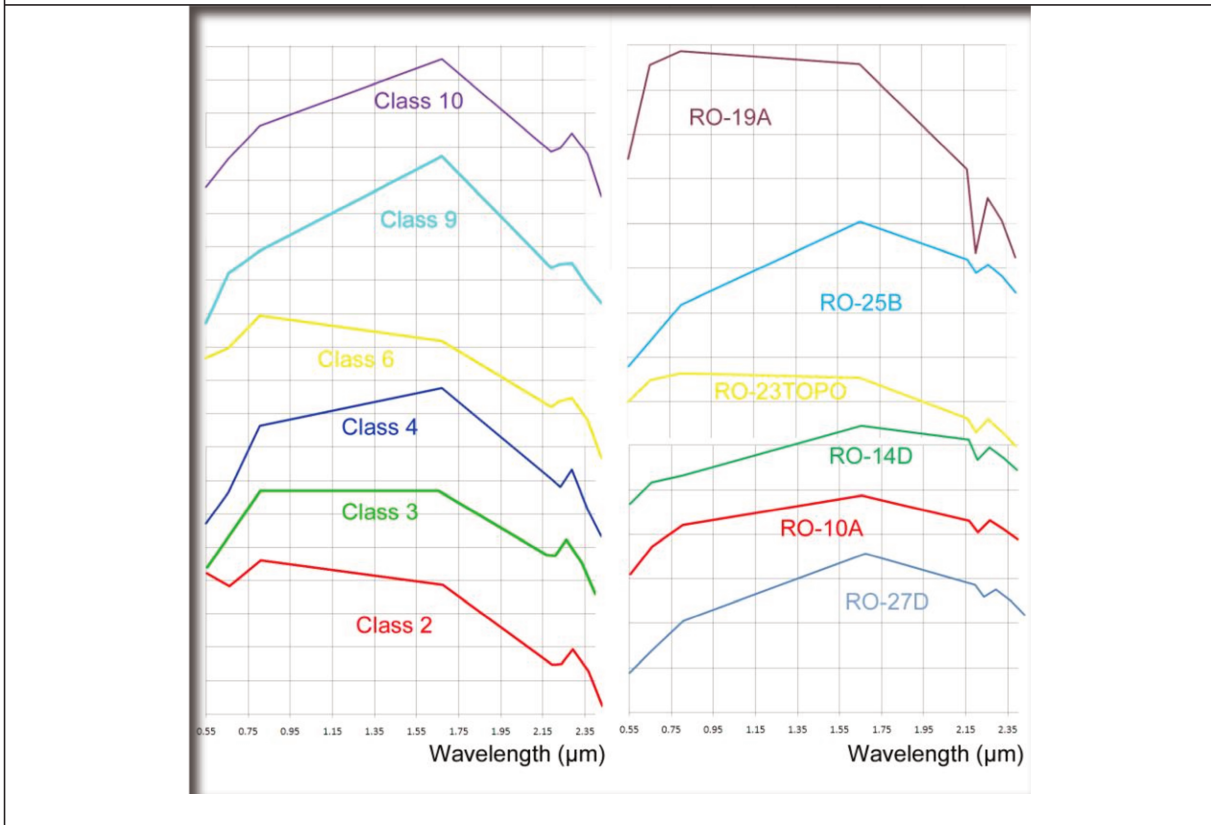
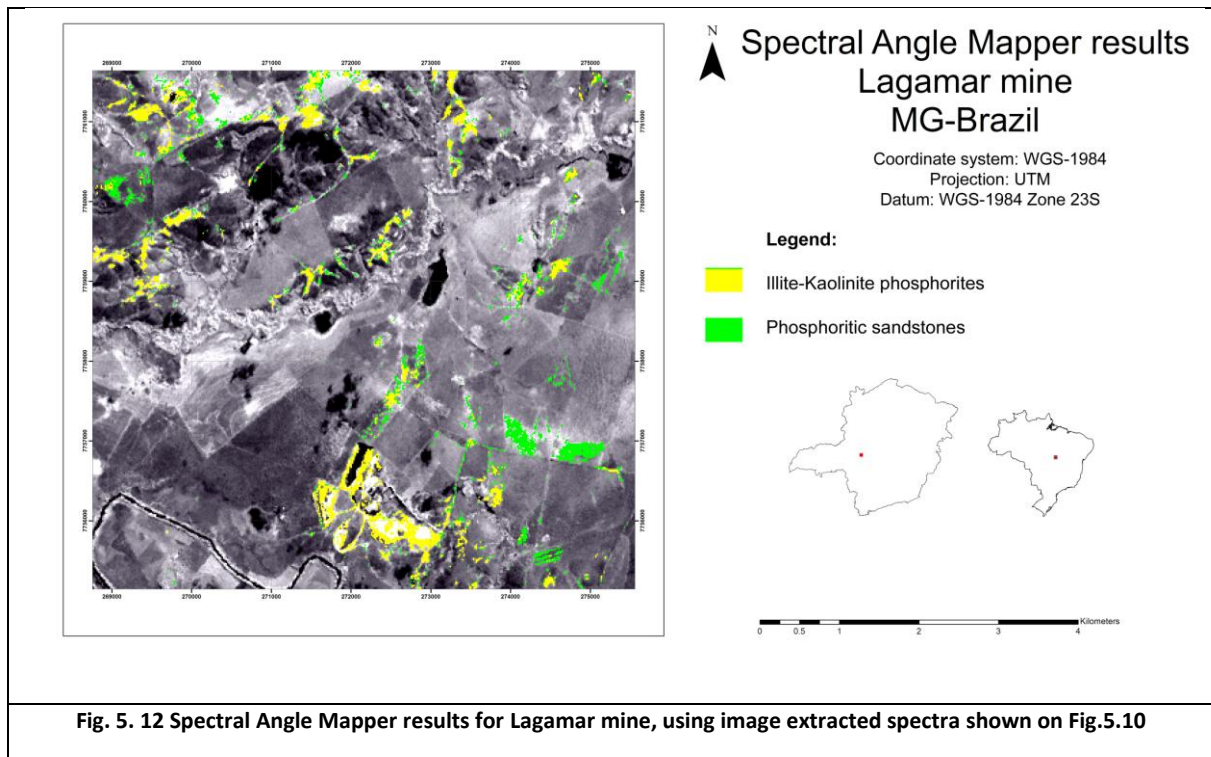


Fig. 5. 11 Endmember spectra (Image extracted and Laboratory) of Rocinha mine.

It can be observed that the SAM algorithm was able to discriminate 2 lithotypes in the Lagamar Mine (fig. 5.12) and 4 lithotypes in the Rocinha mine (fig.5.13). However, when comparing the results of the classification, the Lagamar endmember was more accurate for defining the lithotypes with higher P_2O_5 concentration. Fig. 5.16 shows the

subset of the studied mines using each of the spectral libraries. It is noted that even though lithotypes are similar, Lagamar holds higher illite concentration that reflects on image spectra identification.

The SAM algorithm was able to recognize pixels that seems to correspond to Illite-kaolinite phosphorites displayed in yellow pixels (corresponding to ore material), making 0,56% of the SAM classification results. Pixels that seem to represent phosphoritic sandstones were recognized and are displayed as green, making 3,673% of the classification. The remaining 95.76% represents unclassified pixels.



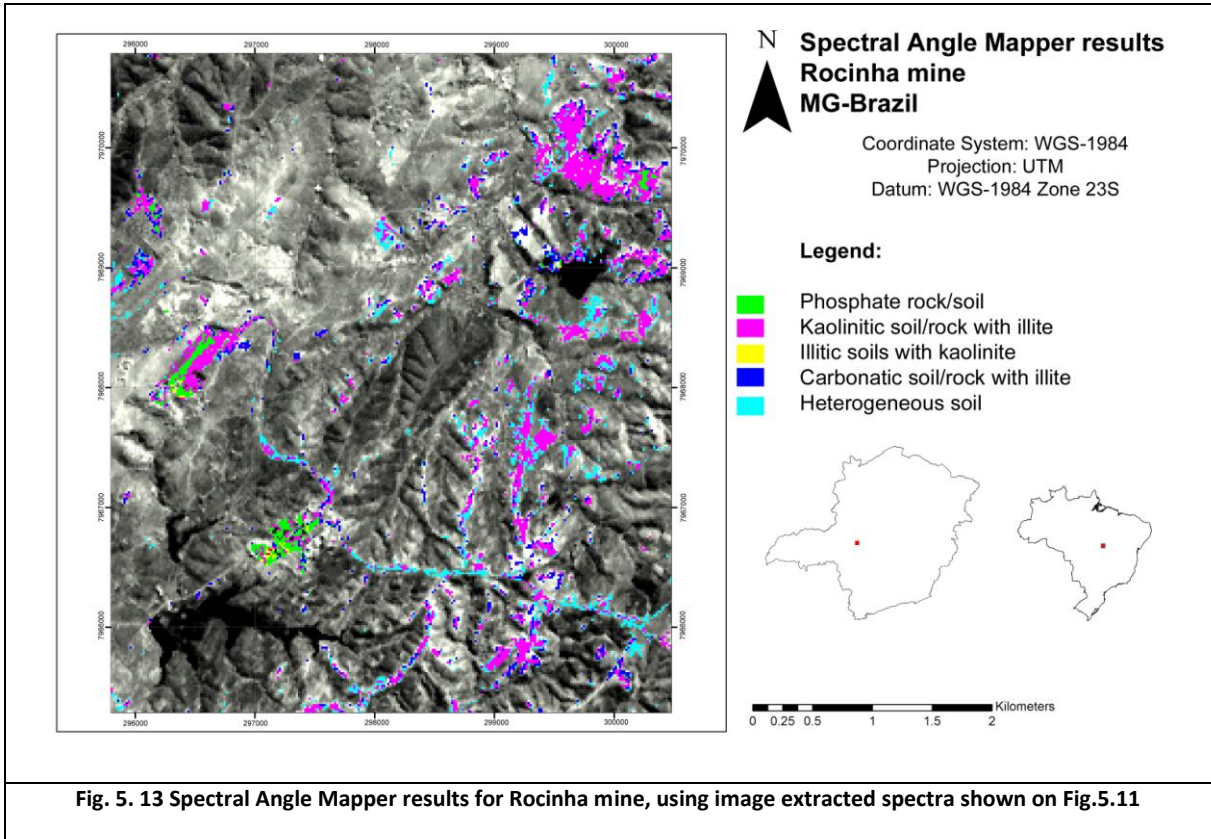


Fig. 5. 13 Spectral Angle Mapper results for Rocinha mine, using image extracted spectra shown on Fig.5.11

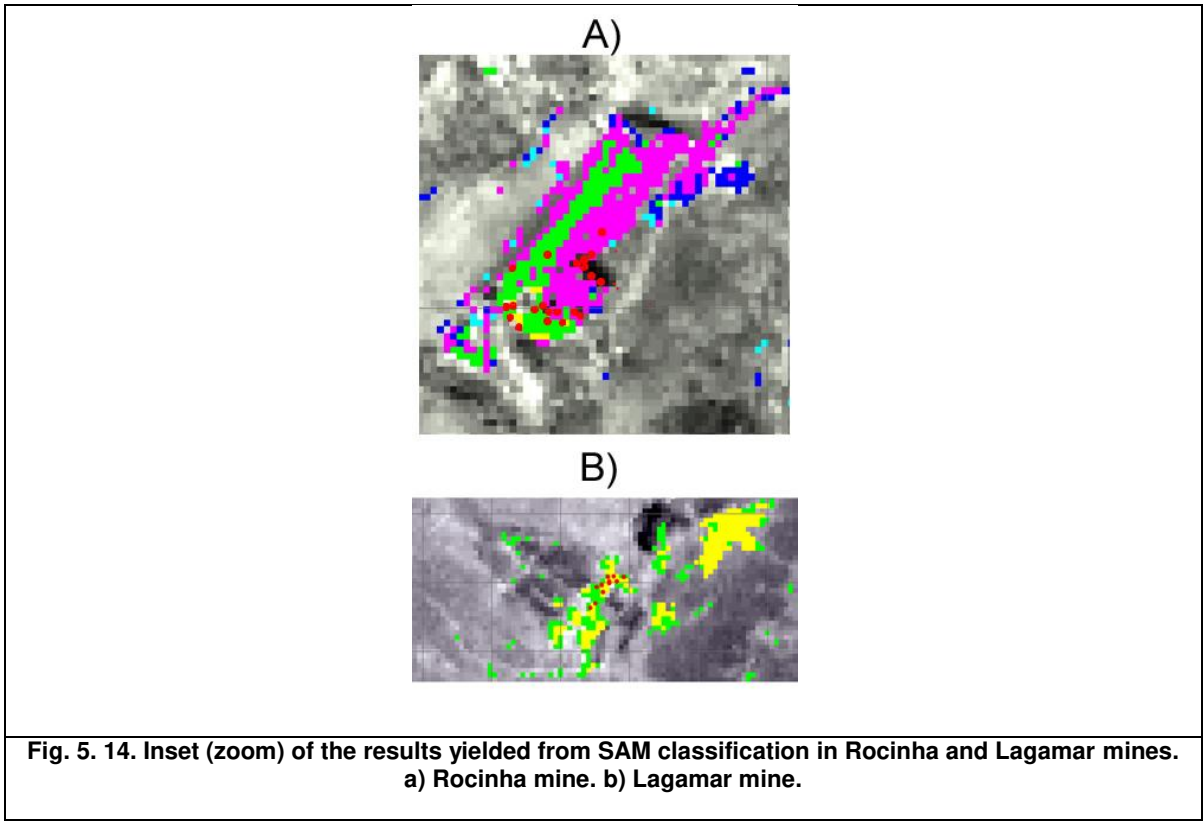


Fig. 5. 14. Inset (zoom) of the results yielded from SAM classification in Rocinha and Lagamar mines. a) Rocinha mine. b) Lagamar mine.

The Rocinha spectral library was able to extract 5 endmembers from image spectra. Phosphate rock/soil class mapped in green accounted for 3271 pixels (1.154%) of the classification. Kaolinitic soil rock with illite accounted for 10152 pixels (3.582%) of the classification. Illitic soils with kaolinite accounted 53 pixels for 0.019% of the classification. Carbonatic soils/rocks accounted for 876 pixels (0.309%). Heterogeneous soils were classified by 7796 pixels (2.751%). 261249 pixels from the subset image (92%) was unclassified due to lack of signatures or vegetation masking.

5.4. Discussion

The remote sensing of phosphates covered in this study has revealed that is possible to identify the lithotypes that bear significant amounts of phosphates within the carbonatites and ultramafic rocks related to them. Sedimentary phosphate-bearing rocks, although lack some key absorption features of their igneous counterparts, can also be distinguished from other lithological units by means of remote sensing techniques, but their phosphate contents are not easily discriminated.

Crystal development and rock preservation are important characteristics to consider when performing remote sensing studies of igneous phosphates. Brazilian igneous phosphates from the Alto Paranaíba Igneous Province are extracted from deep weathering mantles that formed over carbonatitic complexes; several of them also experienced several metasomatic and hydrothermal alterations (e.g. Catalão I and II, Araxá). Tapira experienced less alteration processes, which enabled the weathering mantle to preserve most of the original mineral chemistry of the underlying rocks.

The best explanation of how weathering and tradeoff between rock-soil-environment affects the remote sensing of the igneous phosphates lies in the work produced for the Catalão I Carbonatitic Complex. Although we were able to recover well-preserved rocks from the bottom of the mine, the extension of the aloteritic and isalteritic weathering profiles pose problems for the discrimination of lithotypes that bears P_2O_5 minerals. Also, the strong influence of monazite in the spectra affects the ASTER sensor response at the 15m-pixel scale.

While the spectral classification made on the Catalão I complex was based on nine endmembers, results yielded from the SAM algorithm only provided 5 classes. It was not

possible to discriminate the lithology using the SAM but it was possible to determine the presence of key minerals in lithologic characterization (vermiculite and monazite).

Other key factor that has to be taken into account for detailed mapping is the changes in the surface of mining sites and the collection of samples after the image was obtained. A good part of the collected samples during the field sessions were covered by vegetation or soil when the ASTER image was acquired, giving only spectroscopic information that could not be related directly to the images.

When weathering features are not as overwhelming as they are in the Catalão I Complex, lithological mapping of rock units is possible for the carbonatites, as demonstrated by Rowan *et al* (1995) and Mars and Rowan (2011). In this study, the best approximate to a lithological map is the SAM classification result of the Tapira-Araxá ASTER image, in which was possible to discriminate soils with secondary phosphates, carbonatite dykes and carbonatite-phoscorite-picrite units. Also, an intimate mixture of apatite, corvusite, ajoite and vermiculite (Sample TA-205 Ajoite-Corvusite Possible Monazite) was effectively mapped, giving another prospective guide for the localization of soils and rocks with differentiated P_2O_5 content. Confusion matrices in the Tapira Alkaline Carbonatitic Complex were able to indicate possible SAM and MTMF applications of as aid to exploration programs.

Vermiculite plays an important role in the definition of carbonatitic complexes in the PIAP. Its use as an endmember aided the discrimination of outcrops of carbonatitic related rocks. Although having high portions of Fe that mask the REEs features of phosphates, it tends to associate with rocks/soils that have secondary phosphates, which helps in the identification of future prospects.

When the goal is finding sedimentary phosphates, the direct identification of phosphatic rocks is not possible using multispectral images. Although ASTER spectral resolution in the VIS-NIR-SWIR is good enough to map clays, carbonates and micas, REEs features of the phosphates are masked or lost for the meta-sedimentary phosphates of the Brasilia Folding Belt (BFB). Relying on the presence of illite as a phosphate identifier is not a safe choice, since weathering alteration of the clays will involve the formation of illite at every certain point. However, as a case study, creating data-driven techniques in which remote sensing, structural geology and fuzzy logic search methods are integrated,

there can be a possibility to achieve predictive mapping, as developed for Cu-Au deposits in Philippines and Argentina (CARRANZA & SADEGHI 2010; ROY et al. 2006).

5.5. Conclusions

Phosphate detection using remote sensing is a promising subject for the mineral exploration industry. While some information is known from planetary exploration from the Mars missions (see BISHOP *et al.*, 2005; LANE *et al.*, 2008; LANE *et al.*, 2007a; LANE *et al.*, 2007b), extraterrestrial phosphates are of very rare occurrence on Earth, which makes them of little use for mineral prospection.

The Remote Sensing of igneous phosphates at the moment poses a more optimistic subject, since the present technology allow us to determine carbonatitic related lithotypes and minerals that are either bearers or located where phosphate reserves exist. Mineral assemblages of the mica minerals, clays and REEs absorption features present in the igneous phosphates are known for the PIAP; so methodologies and algorithms can be developed for pinpointing favorable areas for phosphate exploration.

Also, the similarities noted in the REEs patterns and compositions, specifically for the PIAP and their presence along the weathering profile, makes the area very likely to be mapped through remote sensing. If the new areas indicated in this research prove to be true carbonatitic deposits, research exploration programs can be held towards confirming and extending current phosphate, titanium and REEs reserves, with the economic and strategic benefits that the findings will bring to the mining sector.

Remote sensing of sedimentary phosphates has the inconvenience of the possible lack of REEs in the phosphate structure because the geochemical environment allowed the trade of these elements for Ca sites in the apatite structure. In the case of Rocinha and Lagamar, in which the main phosphate is fluorapatite, there is the great problem of the REEs substitution during the geochemical P cycle (FILIPPELLI 2002, 2008). A larger comparison with sedimentary apatites with normalized values of REEs can lead to know if it is possible to map sedimentary phosphates in the VNIR-SWIR region of the EMS.

Other shortage needed to be overcome in the mapping of sedimentary apatites is the SNR of thermal emission spectrometers. At the present moment, only the SEBASS sensor can map with enough spectral and spatial resolution phosphate occurrences, but its use is

only allowed on the United States. ASTER sensor characteristics give several problems at the moment of performing the spectral unmixing of emission signals of phosphate bearing rocks.

The capability of the ASTER sensor for mapping P_2O_5 igneous bearing rocks makes it a great asset in the exploration of igneous reserves in major carbonatitic provinces worldwide. This will create new opportunities for the spectral mapping of terrains for the mineral exploration community.

6. References

- BISHOP, J. L., DARBY DYAR, M., LANE, M. D., & BANFIELD, J. F. (2005). Spectral identification of hydrated sulfates on Mars and comparison with acidic environments on Earth. **International Journal of Astrobiology**, 3(4), 275–285. doi:10.1017/S1473550405002259
- BROD, J. A., GASPAR, J. C., DINIZ-PINTO, H. S., & JUNQUEIRA-BROD, T. C. (2005). Spinel chemistry and petrogenetic processes in the Tapira Alkaline-Carbonatite Complex, Minas Gerais, Brazil. **Revista Brasileira de Geociências**, 35(1), 23–32.
- BROD, JOSÉ A., JUNQUEIRA-BROD, T. C., GASPAR, J. C., GIBSON, S. A., & ROBERT, N. (1999). Ti-rich and Ti-poor garnet from the Tapira Carbonatite Complex, SE Brazil: Fingerprinting fractional crystallisation and liquid immiscibility. In **Proceedings of the 8th International Kimberlite Conference** (pp. 1–5).
- CARRANZA, E. J. M., & SADEGHI, M. (2010). Predictive mapping of prospectivity and quantitative estimation of undiscovered VMS deposits in Skellefte district (Sweden). **Ore Geology Reviews**, 38(3), 219–241. doi:10.1016/j.oregeorev.2010.02.003
- CRÓSTA, A. P., DE SOUZA FILHO, C. R., AZEVEDO, F., & BRODIE, C. (2003). Targeting key alteration minerals in epithermal deposits in Patagonia, Argentina, using ASTER imagery and principal component analysis. **International Journal of Remote Sensing**, 24(21), 4233–4240. doi:10.1080/0143116031000152291
- DAASCH, L., & SMITH, D. (1951). Infrared Spectra of Phosphorus Compounds. **Analytical Chemistry**, 23(6), 853–868. doi:10.1021/ac60054a008
- FILIPPELLI, G. M. (2002). The Global Phosphorus Cycle. In J. Rakovan, J. M. Hughes, & M. J. Kohn (Eds.), **PHOSPHATES Geochemical, geobiological, and materials importance** (pp. 391–425). doi:10.2138/rmg.2002.48.10
- FILIPPELLI, G. M. (2008). The Global Phosphorus Cycle: Past, Present, and Future. **Elements**, 4, 89–95.
- HAIDER, S. Z. (1961). Identification of phosphate anions in Niobium and Tantalum phosphates by means of infra-red spectra. **Analytica Chimica Acta**, 24, 250–253.
- HUNT, G., SALISBURY, J., & LENHOFF, C. (1972). Visible and near-infrared spectra of minerals and rocks. V. Halides, phosphates, arsenates, vanadates, and borates. **Modern Geology**, 3, 121–132. Retrieved from http://www.oato.inaf.it/biblioteca/OLDv3/oato.only/pdf/ModGeo_3_121.pdf
- KRUSE, F. A., LEFKOFF, A. B., BOARDMAN, J. B., HEIDBRECHT, K. B., SHAPIRO, A. T., BARLOON, P. J., & GOETZ, F. H. (1993). The Spectral Image Processing System (SIPS)- Interactive Visualization and Analysis of Imaging spectrometer Data. **Remote Sensing of Environment**, 44, 145–163.
- LANE, M. D., BISHOP, J. L., DARBY DYAR, M., KING, P. L., PARENTE, M., & HYDE, B. C. (2008). Mineralogy of the Paso Robles soils on Mars. **American Mineralogist**, 93(5-6), 728–739. doi:10.2138/am.2008.2757
- LANE, M. D., BISHOP, J. L., DARBY DYAR, M., PARENTE, M., KING, P. L., & HYDE, B. C. (2007). Identifying the phosphate and ferric sulfate minerals in the Paso Robles soils (Gusev Crater, Mars) using an integrated spectral approach. **Lunar and Planetary Science**, XXXVIII, 2–3.
- LANE, M. D., DARBY DYAR, M., & BISHOP, J. L. (2007). Spectra of phosphate minerals as obtained by Visible-Near Infrared Reflectance, Thermal Infrared Emission, and Mössbauer laboratory analyses. **Lunar and Planetary Science**, 4(XXXVIII), 1–2.

- REDDY, B. J., FROST, R. L., & PALMER, S. J. (2008). A near-infrared spectroscopic study of the phosphate mineral pyromorphite $Pb_5(PO_4)_3Cl$. **Spectrochimica acta. Part A, Molecular and biomolecular spectroscopy**, 71(2), 430–5. doi:10.1016/j.saa.2007.12.030
- ROY, R., CASSARD, D., COBBOLD, P. R., ROSSELLO, E. A., BILLA, M., BAILLY, L., & LIPS, A. L. W. (2006). Predictive mapping for copper–gold magmatic-hydrothermal systems in NW Argentina: Use of a regional-scale GIS, application of an expert-guided data-driven approach, and comparison with results from a continental-scale GIS. **Ore Geology Reviews**, 29(3-4), 260–286. doi:10.1016/j.oregeorev.2005.10.002
- TEXEIRA, R. DE A. (2011). **Avaliação espectral de Depósitos de Fosfatos utilizando imagens ASTER nas regiões de Campos Belos e Catalão (GO)**. Dissertação de Mestrado Universidade de Brasília.
- TORRES, M. G. (2008). **Composição química superficial e nanotopográfica da apatita do Proto-minério da Mina do Barreiro**. Tese de Doutorado. Universidade de Brasília.
- UNITED STATES GEOLOGICAL SURVEY (USGS). (2010). **Mineral Commodity Summaries 2010**. *Office report* (p. 193).